nagra
National Cooperative for the
Disposal of Radioactive Waste

TECHNICAL REPORT 99-06

Diffusion and Sorption on Hardened Cement Pastes – Experiments and Modelling Results

August 1999

A. Jakob
F.A. Sarott
P. Spieler

PSI, Würenlingen and Villigen

Hardstrasse 73, CH-5430 Wettingen/Switzerland, Telephone +41-56-437 11 11

nagra
National Cooperative for the
Disposal of Radioactive Waste

TECHNICAL REPORT 99-06

Diffusion and Sorption on Hardened Cement Pastes – Experiments and Modelling Results

August 1999

A. Jakob
F.A. Sarott
P. Spieler

PSI, Würenlingen and Villigen

Hardstrasse 73, CH-5430 Wettingen/Switzerland, Telephone +41-56-437 11 11

This report was prepared on behalf of Nagra. The viewpoints presented and conclusions reached are those of the author(s) and do not necessarily represent those of Nagra.

PREFACE

The Laboratory for Waste Management at the Paul Scherrer Institut is performing work to develop and test models as well as to acquire specific data relevant to performance assessments of planned Swiss nuclear waste repositories. These investigations are undertaken in close co-operation with, and with the financial support of, the National Co-operative for the Disposal of Radioactive Waste (Nagra). The present report is issued simultaneously as a PSI-Bericht and a Nagra Technical Report.

ISSN 1015-2636

Table of contents

List of Figures

List of Tables

Die Wissenschaft lebt vom Widerspruch
(Science springs from contradictions)

Abstract

Large parts of repositories for low and intermediate level radioactive waste consist of cementitious materials. Radionuclides are transported by diffusion in the cement matrix or, in case of fractured or highly permeable cement, by advection and dispersion. In this work we aim at a mechanistic understanding of diffusion processes of some reactive tracers. On the laboratory scale, ten through-diffusion experiments were performed to study these processes for Cl^-, I^-, Cs^+ and Ni^{2+} ions in a Sulphate Resisting Portland Cement (SRPC) equilibrated with an artificial pore water. Some of the experiments continued up to nearly three years with daily measurements. In all the experiments, a cement disk initially saturated with an artificial pore water was exposed on one side to a highly diluted solution containing the species of interest. On the second side, a near-zero concentration boundary was maintained to drive through-diffusion of the tracer. The changes of concentrations on both sides of the samples were monitored, allowing careful mass balances. From these data, values of the diffusive flux and the mass of tracer taken up by the cementitious material were determined as a function of time.

In the subsequent modelling, the time histories of these tracer breakthroughs were fitted using five different models. The simplest model neglects all retarding mechanisms except pure diffusion. More complex models either account for instantaneous equilibrium sorption in form of linear or non-linear (Freundlich) sorption or for first-order sorption kinetics where the forward reaction may be linear or non-linear according to the Freundlich isotherm, while the back-reaction is linear. Hence, the analysis allows the extraction of the diffusion coefficient and parameter values for the sorption isotherm or rate-constants for sorption and desorption. The fits to the experimental data were carried out by an automated Marquardt-Levenberg procedure yielding error estimates of the fit-parameter values, correlation coefficients and also, as a measure of the goodness of the fits, the minimum values for the χ^2-merit function.

Most of the models yielded an excellent agreement between measurements and calculated breakthrough curves but with best-fit values which are inconsistent with independent measurements. K_d -values from modelling through-diffusion experiments may be orders of magnitude smaller than values obtained using batch sorption experiments. The inadequacy of the models became obvious when the predicted tracer uptake based on the preceding best-fit parameter values was compared with measurements. As a rule, the models failed to predict the correct time behaviour of the amount of tracer taken up. Only caesium seems to act as a conservative tracer, because the simplest models approximately reproduce both the breakthrough curves and the experimental data for tracer uptake.

Finally, to obtain further information on the homogeneity of the specimens and retarding mechanisms, for two of the four nickel experiments, the boundary condition at the high-concentration side was changed to measure the out-diffusion of the tracer previously taken up. This was done by quickly replacing the high tracer concentration reservoir by a compartment with artificial pore water. In steady-state the concentration profile across the sample should be a linear function of space, and predictions based on a simple model are possible provided that the porous material is homogeneous. With such an experiment we were able to test this underlying assumption for a homogeneous tracer distribution. The analysis of both experiments, however, clearly demonstrated that such an assumption - for nickel as tracer - must be rejected.

Zusammenfassung

Grosse Teile eines Endlagers für schwach- und mittel-radioaktive Abfälle bestehen aus zementhaltigem Material. Radionuklide werden entweder diffusiv durch die Zementmatrix transportiert oder, im Fall von Spalten oder hoch-durchlässigem Zement, durch Advektion und Dispersion. In dieser Arbeit beabsichtigen wir, ein mechanistisches Verständnis für die diffusiven Prozesse mittels einiger reaktiver Tracer zu gewinnen.

Im Labormassstab wurden zehn Durch-Diffusionsexperimente mit Cl^-, I^-, Cs^+ und Ni^{2+}-Ionen an sulphatresistentem Portlandzement (SRPC) durchgeführt, der im Gleichgewicht mit einem künstlichen Porenwasser war. Einige der Experimente dauerten bis zu drei Jahren mit täglichen Messungen. Bei allen Experimenten wurde eine, vorher mit künstlichem Porenwasser gesättigte, Zementscheibe auf der einen Seite in Kontakt mit einer stark verdünnten Lösung der entsprechenden Spezies gebracht. Auf der anderen Seite wurde näherungsweise eine Konzentration=0 Randbedingung aufrechterhalten, um die Durch-Diffusion des Tracers zu bewirken. Die Messgrössen waren die Konzentrationsänderungen auf beiden Seiten der Probe, was eine sorgfältige Massenbilanz ermöglichte. Daraus wurden Werte für den diffusiven Fluss und für die durch das zementhaltige Material aufgenommene Tracermenge als Funktion der Zeit bestimmt.

In der nachfolgenden Modellierung wurde jeweils der zeitliche Tracerdurchbruch mit Hilfe von fünf verschiedenen Modellen gefittet. Das einfachste Modell vernachlässigt alle retardierenden Mechanismen mit Ausnahme der reinen Diffusion. Komplexere Modelle schliessen instantane Gleichgewichts-Sorption in Form einer linearen oder nicht-linearen (Freundlich) Isotherme ein; oder sie berücksichtigen erste-Ordnung-Kinetik, bei der die Vorwärtsreaktion linear oder nicht-linear, entsprechend der Freundlich-Isotherme, sein kann, während die Rückreaktion linear ist. Deshalb erlaubt die Analyse die Bestimmung von Diffusionskoeffizienten und Parameterwerten für die Sorptionsisothermen oder Raten für die Sorption und Desorption. Die Anpassung an die experimentellen Daten erfolgte mit Hilfe einer automatisierten Marquardt-Levenberg-Prozedur, welche Fehlerabschätzungen der Fitparameterwerte, Korrelationskoeffizienten und - als ein Mass für die Güte der Fits - χ^2-Minimumswerte lieferte.

Die meisten Modelle ergaben eine hervorragende Übereinstimmung von gemessener und gerechneter Durchbruchskurve, aber mit Best-Fit-Werten, die nicht konsistent waren zu solchen unabhängiger Messungen. K_d -Werte, bestimmt aus der Modellierung von Durch-Diffusionsexperimenten, können Grössenordnungen kleiner sein als solche aus Batch-Sorptionsexperimenten. Die Unzulänglichkeit der Modelle wurde offensichtlich, wenn die vorausgesagte Tracer-Deposition, basierend auf den vorangehenden Best-Fit-Parameterwerten, mit den Messungen verglichen wurde. In der Regel waren die Modelle nicht geeignet, die Zeitabhängigkeit der aufgenommenen Tracermenge korrekt vorauszusagen. Nur Cäsium scheint als konservativer Tracer zu wirken, weil die einfachsten Konzepte sowohl die Durchbruchskurven als auch die experimentellen Daten zur Tracerdeposition angenähert reproduzieren.

Schlussendlich, um weitere Information betreffend Homogenität der Proben und retardierende Mechanismen zu erhalten, wurde an zwei der vier Nickel-Experimente eine der beiden Randbedingungen geändert, um die Rückdiffusion des vorher deponierten Tracers zu messen. Dazu wurde das Reservoir mit der hohen Tracerkonzentration schnell ersetzt durch ein mit künstlichem Porenwasser gefülltes Gefäss. Im stationären Zustand sollte das Konzentrationsprofil über die Probe eine lineare Funktion des Ortes sein. Voraussagen auf der Basis eines einfachen Modells sind möglich, vorausgesetzt, dass das poröse Material homogen ist. Mit Hilfe eines solchen Experiments ist man in der Lage, die zugrundeliegende Annahme, eine homogene Tracerverteilung betreffend, zu überprüfen. Die Analyse der beiden Experimente aber hat klar gezeigt, dass eine solche Annahme - mit Nickel als Tracer - verneint werden muss.

Résumé

De grandes parties des sites de stockage à faible ou moyenne activité sont constituées de matériaux à base de ciment. Les radionucléides sont transportés soit par diffusion dans la matrice de ciment, soit par advection dans le cas du ciment fracturé où à haute perméabilité. Dans ce travail on veut obtenir une compréhension mécanistique des processus de diffusion pour quelques traceurs réactifs.

À l'échelle de laboratoire, dix expériences de diffusion ont été effectuées dans des SRPC (Ciment Portland résistant aux sulfates) préalablement équilibrés avec une eau artificielle interstitielle de ciment afin d'étudier la migration des ions Cl^-, I^-, Cs^+ et Ni^{2+}. Certaines de ces expériences ont duré près de trois ans avec des prélèvements journaliers. Dans toutes les expériences, un disque de ciment, préalablement saturé avec une eau interstitielle artificielle, a été mis en contact sur l'une de ces faces avec une solution fortement diluée contenant les espèces chimiques étudiées. La seconde face a été mise en contact avec une solution de concentration quasi-nulle afin d'avoir les conditions favorisant une diffusion des traceurs. Les variations des concentrations des deux solutions ont été enregistrées permettant de faire des bilans de masse précis. Le flux diffusif et la masse de traceurs incorporés par le ciment ont ainsi été déterminés au cours du temps.

Nous avons ensuite essayé de simuler les variations au cours du temps des courbes de libération à l'aide de cinq modèles différents. Le plus simple ne prend en compte que la pure diffusion et néglige tous les phénomènes de retard. Les modèles plus complexes prennent en compte soit la sorption à l'équilibre sans cinétique (réaction instantanée) de manière linéaire ou non-linéaire (Freundlich), soit une cinétique de premier ordre des réactions de sorption : la réaction directe peut-être considérée comme linéaire ou non-linéaire, tandis que la réaction inverse est toujours linéaire. Cet ajustement permet de dériver les coefficients de diffusion, les paramètres intervenant dans les isothermes de sorption, et/ou les constantes cinétiques des réactions de sorption et de désorption. L'ajustement des modèles aux données expérimentales a été effectué à l'aide de la procédure automatisée de Marquardt-Levenberg qui permet non seulement d'estimer les paramètres ajustés, mais aussi de calculer les coefficients de corrélation associés, et la valeur minimale de la fonction χ^2 qui est une mesure de la qualité de l'ajustement.

La plupart des modèles permettent de reproduire parfaitement les courbes de libération mais en utilisant des valeurs pour les paramètres ajustés qui sont incohérentes avec les mesures expérimentales indépendantes. Ainsi, les valeurs de K_d dérivées de ces simulations sont inférieures de plusieurs ordres de grandeur aux valeurs mesurées dans les expériences de sorption en batch. Le décalage entre les modèles et les expériences est encore plus évident pour les courbes d'évolution de la quantité de traceurs incorporés par le ciment. De manière générale, les modèles n'ont permis de simuler de manière satisfaisante l'évolution au cours du temps de la quantité de traceurs incorporés par le ciment. Seul le césium semble se comporter de manière conservative car le modèle le plus simple (diffusion pure) reproduit approximativement l'évolution de la quantité de traceurs incorporés, et les courbes de libération.

Dans un dernier temps, afin d'obtenir de plus amples informations sur l'homogénéité de l'échantillon et les mécanismes de retard, les conditions aux limites de deux des quatre expériences en présence de nickel ont été modifiées en cours d'expérience: le compartiment source contenant la solution concentrée en traceur a été rapidement remplacée par une eau de ciment interstitielle artificielle. Ce changement permet ainsi de mesurer la quantité de traceurs incorporés par le ciment progressivement libérés. A l'équilibre, le profil de concentration au travers l'échantillon doit être linéaire, et des prédictions à partir du modèle le plus simple sont possibles si l'on suppose que l'échantillon est homogène. Une telle expérience nous a permis de tester l'hypothèse d'une distribution homogène du traceur. L'analyse des deux expériences démontre cependant que pour le nickel, une telle hypothèse doit être rejetée.

Riassunto

Molte parti dei depositi per scorie debolmente o mediamente radioattive consistono di materiali cementizi. I radionuclidi vengono transportati per diffusione nella matrice di cemento, o per avvezione e dispersione nel caso di cemento altamente permeabile o fratturato. In questo studio si intende ottenere una comprensione meccanicistica dei processi diffusivi di alcuni traccianti reattivi. Dieci esperimenti di diffusione sono stati effettuati in scala di laboratorio al fine di investigare tali processi per gli ioni Cl^-, I^-, Cs^+ e Ni^{2+} in un cemento SRPC (cemento Portland resistente ai solfati) equilibrato con un acqua interstiziale artificiale. Taluni esperimenti sono durati per quasi tre anni, con misure giornaliere. In tutti gli esperimenti, un disco di cemento, inizialmente saturato con acqua interstiziale artificiale, è stato esposto da un lato a una soluzione molto diluita contenenti le speci summenzionate. Sul secondo lato, è stata mantenuta una concentrazione all'interfaccia quasi nulla, per favorire la diffusione dello ione tracciante. I cambiamenti di concentrazione in entrambi lati del campione sono stati misurati ad intervalli regolari, in modo da permettere bilanci di massa accurati. Partendo da questi dati, si sono potuti determinare sia i flussi diffusivi che le quantità di tracciante assorbito dal materiale cementizio in funzione del tempo.

Nella successiva modellizzazione si è cercato di simulare, con cinque modelli, lo sviluppo nel tempo del rilascio di tracciante. Il modello più semplice trascura tutti i meccanismi ritardanti, eccetto la pura diffusione. I modelli più complessi prendono in considerazione equilibri di assorbimento istantaneo sotto forma di assorbimento lineare o non lineare (Freundlich), oppure una cinetica di primo ordine per l'assorbimento, in cui la reazione diretta può essere lineare o non lineare, secondo l'isoterma di Freundlich, mentre la reazione inversa è sempre lineare. Quindi, questa analisi permette di estrarre il coefficiente di diffusione e i valori parametrici per l'isoterma di assorbimento o le costanti cinetiche di assorbimento e desorbimento. L'aggiustamento ai dati sperimentali è stato effettuato per mezzo della procedura automatizzata di Marquardt-Levenberg, che permette di stimare gli errori dei parametri di aggiustamento e di determinare parametri di correlazione e i minimi della funzione χ^2, che è una misura della qualità dell'aggiustamento.

Benchè la maggior parte dei modelli permette di riprodurre ottimamente le curve di rilascio, i parametri di aggiustamento sono inconciliabili con misure sperimentali indipendenti. I valori K_d derivati dalla modellizzazione delle curve di rottura possono essere ordini di grandezza più piccoli di quelli ottenuti da esperimenti di assorbimento in "batch". L'inadeguatezza dei modelli diventa ovvia quando si confrontano i valori di retenzione del tracciante, calcolati sulla base dei parametri di aggiustamento ottimizzati, con le misure sperimentali. In generale, questi modelli non predicono correttamente le quantità di tracciante fissate dal cemento in funzione del tempo. Solo il cesio pare comportarsi come un tracciante conservativo, poichè il modello più semplice è in grado di riprodurre in modo approssimato sia la curva di rottura, sia i dati sperimentali di assorbimento del tracciante.

Infine, per ottenere ulteriori informazioni sull'omogeneità dei campioni e sui meccanismi ritardanti, la condizione ai limiti di due dei quattro esperimenti effettuati in presenza di nichel è stata modificata sul lato ad alta concentrazione nel corso dell'esperimento, al fine di misurare il rilascio per diffusione del tracciante precedentemente assorbito. Tale modifica è stata realizzata sostituendo rapidamente il serbatoio di acqua ad alta concentrazione di tracciante con una cella contenente acqua interstiziale artificiale. In condizioni stazionarie il profilo di concentrazione del tracciante attraverso il campione dovrebbe risultare lineare, in modo da rendere possibili, a condizione che il campione sia omogeneo, previsioni basate su modelli semplici. Grazie a tali esperimenti abbiamo potuto controllare l'ipotesi della distribuzione omogenea del tracciante. L'analisi di entrambi gli esperimenti ha tuttavia confutato tale ipotesi nel caso del nichel.

Samenvatting

Grote hoeveelheden cementhoudende materialen worden benodigd in een opbergingsplaats voor laag en middel radioactief afval. Radionucliden kunnen door de cementmatrix via diffusieve processen of, in het geval van gebarsten of hoog doorlatend cement, via advektieve en dispersieve processen getransporteerd worden. In deze studie word getracht het mechanisme van de diffusieve processen te begrijpen door experimenten met reactieve tracers.

Op laboratorium schaal werden tien diffusie-experimenten met Cl^-, I^-, Cs^+ en Ni^{2+} ionen in een sulfaatresistente Portlandcement (SRPC) doorgevoerd. In deze experimenten werd een cementschijf, die vooraf met een kunstmatige poriënvloeistof verzadigd was, aan één zijde in contact gebracht met een sterk verdunde oplossing van het ion van interesse. Aan de andere zijde werd een "nulconcentratie" randvoorwaarde opgelegd om de diffusie van de radiotracer te bewerkstelligen. De concentratieverandering aan beide zijden van de cementschijf werd gemeten zodat een nauwkeurige massabalans kon worden opgesteld. Aan de hand van deze gegevens werden waarden voor de diffusieve flux en voor de hoeveelheid opgenomen tracer, in functie van de tijd bepaald.
De tijdsafhankelijke doorbraakcurven van de tracers werden met behulp van vijf verschillende modellen gefit. Het eenvoudigste model verwaarloost, met uitzondering van zuivere diffusie, alle retardatiemechanismen. De meer complexe modellen houden rekening met onmiddellijke evenwichtsadsorptie door middel van een lineaire of niet-lineaire (Freundlich) adsorptie-isotherm; of onderstellen een eerste-orde-kinetica, waarbij de voorwaartse reactie lineair of niet-lineair kan zijn, in overeenstemming met de Freundlich-isotherm, en waarbij de terugwaartse reactie lineair is. Zo een analyse laat de bepaling van diffusiecoëfficiënten toe, alsook van de parameterwaarden voor de adsorptie-isotherm of de reactiesnelheden voor adsorptie en/of desorptie. De aanpassing aan de experimentele gegevens werd uitgevoerd met behulp van een geautomatiseerde Marquardt-Levenberg procedure. Deze procedure levert een foutschatting van de fitparameters, correlatiecoëfficiënten en, als maat voor de juistheid van de simulatie, de minimawaarden voor de χ^2-merit functie.
De meeste modellen gaven een zeer goede overeenstemming tussen gemeten waarden en de berekende doorbraakcurven. De bestfit waarden zijn echter niet consistent met onafhankelijke metingen: K_d waarden afgeleid uit de modellering van de diffusie-experimenten waren orden van grootte kleiner als zulke gemeten in batch adsorptie-experimenten. De ontoereikendheid van de gebruikte modellen werd vooral duidelijk wanneer de voorspelde traceropname, gebaseerd op de bestfit parameters, vergeleken werd met de meetresultaten. In de regel falen alle modellen wanneer de tijdsafhankelijkheid van de opgenomen hoeveelheid tracer voorspeld wordt. Alleen voor cesium als conservatieve tracer bleek het eenvoudigste model zowel de doorbraakcurven alsook de experimentele gegevens voor tracerdepositie te kunnen reproduceren.
Om bijkomende informatie in verband met de homogeniteit en de retardatiemechanismen te krijgen, werd in twee van de vier nikkel experimenten één van beide randvoorwaarden gewijzigd om de terugdiffusie van de eerder opgenomen tracer te meten. Om dit te bewerkstelligen werd het reservoir met de hoge tracerconcentratie vervangen door een reservoir gevuld met enkel een kunstmatige poriënvloeistof. In stationaire toestand zou het concentratieprofiel door het proefmonster een lineaire functie zijn van de plaats. Voorspellingen met behulp van een eenvoudig model zijn mogelijk indien het poreus materiaal homogeen is. Met dit soort van experimenten waren we in staat om de aanname van een homogene tracerverdeling te testen. Een analyse van beide experimenten toonde echter duidelijk aan dat deze aanname - tenminste voor de nikkeltracer - onjuist is.

1. Introduction and motivation

Materials containing cement, e.g., concrete, will play a central rôle in the construction of a Swiss repository for short-lived low- and intermediate level and for long lived intermediate level radioactive waste. Concrete will be used as backfill material for the radioactive waste in the drums, as backfill material in the containers and as backfill material for the spaces both between the containers themselves and the containers and the tunnel wall. In addition, concrete will be used in the actual construction of the repository as such and therefore will be present in large quantities. Though materials containing cement show disadvantageous qualities such as, e.g., high leaching rates, they nevertheless have different practical advantages like, e.g., low costs, easy processing, thermal stability and alkaline qualities which prevent the rusting of the reinforcement of concrete and steel containments. Cementitious materials will initially act as a mechanical barrier preventing advective water flow through the waste for a long time and thus will contribute to the retardation of dissolved radionuclides by the combination of physical and chemical interactions. Most chemical species in aqueous solutions will undergo some kind of (chemical) interactions with any solids of the cementitious material. Hence, transport through a porous medium such as cement is a combination of physical transport and chemical interactions. The chemical interactions may retard mobile radionuclides and lower transport rates. Therefore, it is of great importance to develop a quantitative understanding of the chemical processes involved and to strictly differentiate between physical and chemical aspects of radionuclide transport through such materials.

Radionuclides can only leave such a repository if they succeed in overcoming all these cementitious barriers. An imaginable way of doing this would be that of diffusive transport under water-saturated conditions.

Such a scenario is the reason for the great interest - both theoretical and experimental - in the study of diffusive transport of radionuclides through cementitious, water-saturated materials [1], [2], [3]. It is also conceivable that results from such investigations can have a great impact on other areas like, e.g., the transport of oxygen and chloride ions in concrete in road or underwater constructions leading, in the long run, to the corrosion of the reinforcement and, finally, mechanical destruction of the concrete.

An important question is the long-term behaviour of a cementitious barrier; this means the question of mechanical and chemical changes with time which could strongly influence the mobility of radionuclides. It is obvious that such a question is directly coupled with the degradation of cementitious material, a process which is determined by the exchange of pore-water solution with fresh groundwater by diffusion and causing the dissolution of cement and other concrete forming materials of the barrier.

Most of the mobile chemical species will interact with constituents of the cementitious material in one way or another while diffusively overcoming the barrier. Therefore, such transport cannot be considered as a purely physical phenomenon only; a great variety of chemical processes is also involved so that an adequate description necessarily has to combine physical transport and chemical interaction of the mobile radionuclides with the components of the solid phase or the solute. Above all, chemical interactions lead to an essential retardation of mobile radionuclides. Therefore, in order to obtain a realistic model for the transport, it is important to know the characteristics of the relevant mechanisms and to quantitatively evaluate their effects on the mobility of the radionuclides. Then, more realistic predictions can be made concerning the long-term behaviour and barrier effect of a repository

for low- and intermediate level radioactive waste. Under certain conditions this may even lead to a change of the repository design in order to obtain a better barrier effect.
Relevant mechanisms could be the long-term adsorption of radionuclides onto the solid phase, possible permeability changes due to chemical reactions and cracking, and diffusion. Other processes which might have a somewhat lesser influence on the mobility of radionuclides are, e.g., surface precipitation or up-take of radionuclides by the CSH-gel.
For a better understanding of the system of dissolved radionuclides/cementitious material it is mandatory to conduct experiments; these should serve a double aim: to ascertain the mechanisms controlling the transport behaviour of radionuclides and to determine the values of parameters characterising the processes in the models. Therefore, in theoretical work, models have to be developed containing **measurable** parameters for transport mechanisms and allowing - within the framework of safety analyses - reliable, quantitative predictions about the barrier effects and the long-term behaviour of a repository. However, performance assessments are not intended to be a detailed prediction of the evolution of the repository system. In addition, for efficiency and/or due to lack of appropriate data, reasonable model simplifications and approximations have to be done. But in order to make the correct simplifications and approximations and to estimate the effects of the approximations an excellent understanding of the most important mechanisms and processes is essential. For that it is necessary to develop sophisticated models which are able to describe with high precision **all** available observations and to perform predictions based on those underlying assumptions, and values for the model parameters, that can be tested in new experiments.

In the first part of this report, some of the experiments being carried out at the PSI are presented in detail. The aim of all these long-term experiments, some of which went on for years with daily measurements, is to provide information on the time evolution of transport and sorption properties of hardened cement pastes (HCP) as a function of the degree of degradation. For these experiments, previously a number of matured HCP's was produced; their production was documented in [4]. The artificial degradation to different degrees of HCP's, and also of crushed material, was carried out in a special equipment, an in-house development for this purpose, by pressing large volumes of water through the samples under near-to-equilibrium conditions. These experiments were performed under controlled conditions and in a practically CO_2-free atmosphere in glove boxes preventing precipitation of calcium carbonate in the pores [5]. The main objective of these experiments was primarily the artificial "ageing" of cementitious material. In addition, other important information, such as values for the hydraulic conductivity of the material, its chemical composition and the colloid content of the permeated water, is obtained. These diffusion experiments we are going to present are made - as a first step - using unaltered HCP's. However, it is planned in the future to also apply artificially altered cementitious material in order to thoroughly investigate the transport properties for the second and third degradation phase. The apparatus is described in detail in [6], details of the measurements and data evaluation are given in [7] and the experimental data are compiled in detail in [8], [9], [10], [11] and [12]. In addition the chemical data are evaluated and interpreted with the help of an appropriate cement degradation model [13] in order to provide the basis for a more comprehensive chemical understanding of cement degradation [14].

Sorption is dependent on nuclides; thus, the following nuclides were used so far as tracers for batch sorption experiments: ^{36}Cl, ^{63}Ni, ^{125}I, ^{241}Am. It is intended to proceed with these experiments using tritium, Na, Cs, Se, Sr, Eu and Th as tracers in the near future. The choice of these nuclides represents the basic chemistry of the broad variety of nuclides in a repository

for low- and intermediate level radioactive waste. In these experiments distribution coefficients are determined through the conventional equilibrium method. In addition, we get information about the sorption isotherms, as well as rates for the kinetics of sorption and desorption for some nuclides, respectively. Especially, the influence of organic ligands on the sorption behaviour resulting from organic degradation products is investigated [15]. However, in our diffusion experiments organic ligands do not affect the immobilisation potential of the cement because the preparation of the HCP's was done in the absence of any cement additives [16]. The experimental data hitherto obtained in (static) batch experiments are summarised in [17]. In contrast to the long-term dynamic diffusion experiments lasting - as a rule - hundreds of days, the static batch sorption experiments have to be considered as alternative experiments for the determination of sorption qualities. The former are described in this report in detail. At this point the question also arises whether values for the distribution ratio obtained from batch experiments on crushed material can be compared to sorption data gained from long-term diffusion experiments. Therefore, in this report such types of data are compared systematically; their consistency is tested and possible differences are identified and discussed.

Diffusion of a tracer through a sample can take place in many different ways depending both on the initial or the boundary conditions involved. So far, such diffusion experiments were mostly performed in the way that the sample was initially free of tracer and the diffusion was driven across the sample by the application of a constant concentration gradient. Then, after reaching the steady-state, i.e. after reaching a constant nuclide flux over the boundary of the low-concentration side, parameter values for diffusion and sorption were deduced with the help of an appropriate model. However, a sample conditioned in this way can also be used to perform a so-called out-diffusion experiment. For this, the solution at the reservoir side (high-concentration side) is quickly replaced by (tracer-free) equilibrated cement-pore water, and on this side, too - as on the low-concentration side -, the concentration is maintained, as far as possible, at $C_{tracer} = 0$. By such a procedure the cement matrix slowly drains and, from the shape of the curve of both nuclide fluxes, we are able to check the initial tracer distribution in the steady-state phase. We can also try to examine whether sorption is reversible on the time-scale of diffusion. For these reasons, after several hundred days the diffusion process was stopped for two experiments and the out-diffusion started as outlined above.

Survey of contents

Following this introduction, in chapter 2, the experiments are described in detail. In 2.1., the apparatus, the preparation of the samples and the experimental conditions are explained. In the sub-section 2.2. the experimental data for chlorine, iodine and caesium diffusion are given; in 2.3., those for four nickel experiments [1] are compiled and - where necessary - are commented from the point of view of the experimentator. In 2.4., the apparatus for the out-diffusion experiments is introduced and in 2.5., the experimental data gained from nickel out-diffusion experiments nos. 5 and 7 are presented.

---

[1] For practical purposes we adopt the experimentalist's notation, i.e., there are, e.g., two diffusion experiments (with Cl^- as tracer) and these are identified as no.3 and no. 4, respectively. We refrain from renumbering the experiments to avoid confusion with the experimentalist's laboratory journal. Of course, there were also experiments with numbers 1 and 2; however, they were excluded from the modelling due to experimental deficiencies (e.g. wrong calibration of the β-counter) which would have made modelling extremely difficult and questionable.

In chapter 3, the concept for the modelling of diffusion and out-diffusion is outlined and the experimental facts are interpreted in the framework of different approaches. In sub-section 3.1., the formalism for the diffusion is developed and, in sub-section 3.2., the results of the modelling for the through-diffusion experiments are presented. In 3.2.1., those for chloride, in 3.2.2. those for iodide, in 3.2.3. those for caesium, and in 3.2.4. the results of the inverse modelling for nickel diffusion of experiments nos. 5 - 8 are listed. In sub-section 3.3., the formalism for the out-diffusion is developed; the blind-predictions in the frame of a simple linear sorption/diffusion model for the experiments nos. 5 and 7 are presented and compared with measurements.
Finally, in chapter 4, an overall-conclusion is drawn. The consequences for future work, both experimental and theoretical, are considered and recommendations given for further investigations.

2. The experiments

The experimental techniques for the diffusion experiments were widely used in the past and are therefore well-established. Similar equipment was used for diffusion experiments on materials such as biotite gneiss [18], sandstone, anhydrite, limestone [19], or on Darley Dale sandstone; the latter experiments were the basis for an earlier PSI modelling work [20].
All the experiments described in this paper were performed with fresh, i.e. non-degraded cement pastes and were carried out in glove boxes under a controlled nitrogen atmosphere. Further information will be found in sub-section 2.1.1.

2.1. The apparatus and the experimental set-up for through-diffusion

The whole apparatus (see the figure below) is constructed modularly and consists of transparent polystyrene allowing an easy check of the height of the solutions. The exterior measurements are about ($l \times w \times h$) $20 \times 15 \times 12$ cm. The larger cavity is the reservoir for the source concentration, its total volume being about 540 ml. With the help of a membrane pump (Alldos membrane pump, Type 201/40145A) a smaller part of the reservoir side (volume≈ 45 - 50 ml) is continuously supplied with “fresh” solution from the larger part of the cavity. The pipes consist of PTFE, have a total length of about 0.7 m and an inner diameter of about 4 mm; the wetted parts of the pump are covered with PVDF, and the pump rate is about 12 - 15 ml/min, i.e. about 50 % of the maximum performance. The surplus of solution flows off an overflow back to the lower lying reservoir part of the cell. With such an arrangement a constant solution head is guaranteed.

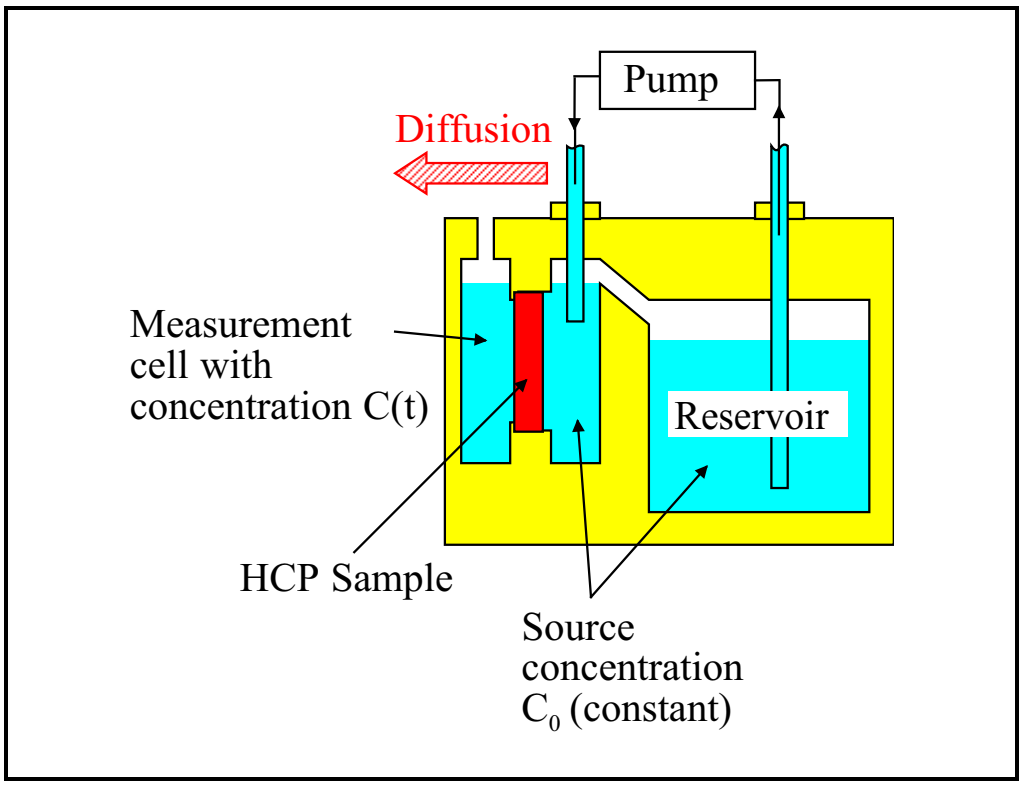

Figure 2.1.-1: Sketch of the apparatus for the through-diffusion experiment.

Due to the great amount of traced solution of the reservoir side the concentration on this side is kept nearly constant over a longer time span. Below the measurement cell there is a magnetic stirrer continuously mixing the solution in the measurement cell with the help of a small (Teflon covered) magnet. The temperature measured in the source solution changed in the interval of 26 - 33 °C [2], depending on the season.

Quantity	Symbol	Unit	Value
Volume of the measurement cell	V	$\cdot 10^6$ [m^3]	47.0 ± 0.3
Volume of the reservoir side	V_0	$\cdot 10^6$ [m^3]	540 ± 30

Table 2.1.-1: Some geometrical aspects of the apparatus. (Values are given with one standard deviation.)

At the beginning of the experiments sorption of the tracer occurred at the walls of the diffusion cell and onto inner surfaces of pipes and pump. Therefore, daily and, later on, weekly checks of the reservoir concentration were performed by taking out 1 or 2 ml samples. Necessary corrections were made with the help of pre-calculated higher concentrated tracer solutions. Especially for some nickel experiments the astonishing observation could be made that the time span to reach the expectation value was from days up to several weeks. With the nickel experiment no. 5 the expectation value was reached first after several weeks and than even exceeded by about 25 %, because in the mean time too much tracer was added for correction. However, we have no explanation for such a long relaxation time of the nickel diffusion system. Except for this experiment, deviations from the expectation value on the reservoir side were always less than ± 10 %.

The height of the liquid in the measurement cell had always to be at the same level as that of the reservoir side to avoid an additional driving force for diffusion due to a pressure gradient. The controlling and re-adjustment of this level after the sampling was done 'just by eye'[3]. The volume of the measurement cell was determined to be 47.0 ml with an uncertainty of about 0.3 ml (0.6 % relative error).

---

[2] According to the Stokes-Einstein equation, the diffusion coefficient D is linked with the (absolute) temperature and the temperature dependent viscosity η of the solution:

$$\frac{D(T_2)}{D(T_1)} = \frac{\eta(T_1)\cdot T_2}{\eta(T_2)\cdot T_1} \quad .$$

The viscosity η for different temperatures in the pore water and, thus, in relatively dilute solutions, can be found, e.g., in CRC Handbook of chemistry and physics. A temperature change from 26 to 33 °C corresponds to an increased value for the diffusivity by approximately 25%.

[3] A possible difference in the heights of the liquid in the reservoir and the measurement cell was always smaller than Δh = 1 mm. Such a small difference will cause an additional advective tracer flux j_{adv} [mol/(m^2s)] through the sample which is:

$$j_{adv} = v_f\, C_0 = \frac{v_D}{\varepsilon} C_0 = -\frac{K}{\varepsilon}\frac{\Delta h}{L} C_0 \quad .$$

v_f [m/s] is the water velocity through the sample; v_D [m/s] the specific discharge; ε [-] the samples porosity and C_0 [mol/m^3] the concentration in the reservoir; K [m/s] is the hydraulic conductivity and L [m] the sample thickness. Assuming reasonable values for the hydraulic conductivity (see sub-section 2.1.1.) and the tracer concentration (see sub-section 2.1.2.) we arrive at an additional tracer flux of the order of $j_{adv} \approx 2 \cdot 10^{-11}$ moles/(m^2s) for chlorine and 2 - 4 $\cdot$ 10^{-14} moles/(m^2s) for all the other tracers. When compared to the steady-state values for the diffusive flux, which is at least more than an order of magnitude larger it is evident that such additional fluxes can play a definite role only in the very early part of the tracer breakthrough curve.

An ideal boundary condition at the low concentration side would have been an exact zero concentration condition which only was fulfilled at the very beginning of the experiments. For practical reasons in maximum a concentration of 1 % of that of the reservoir concentration side was accepted resulting in daily sampling, hence replacing of the whole liquid volume of the measurement side. However, in the (near) steady-state phase the concentration could periodically exceed this 1 % level of C_0, yet only in the two days absence of the experimentalists during the weekends. After the weekends the maximum concentration in the measurement cell could be a few percent, but it was always well below 5 % of C_0.

2.1.1. The preparation of the hardened cement pastes (HCP)

To obtain a relatively high permeability a high water-cement ratio (W/C=1.3) was chosen. For the manufacturing procedure [4] a sulphate-resistant Portland cement of the type CPA 55 HTS Lafarge (France) [21] and de-ionised water were used. In plexiglas forms cylindrically formed samples of a diameter of 4.1 cm and a height of 10 cm were cast which were then hydrated at a relative humidity of 100 % under CO_2-free conditions for about 6 months. The time history of the permeability shows that the hydration had nearly come to an end after about three months.

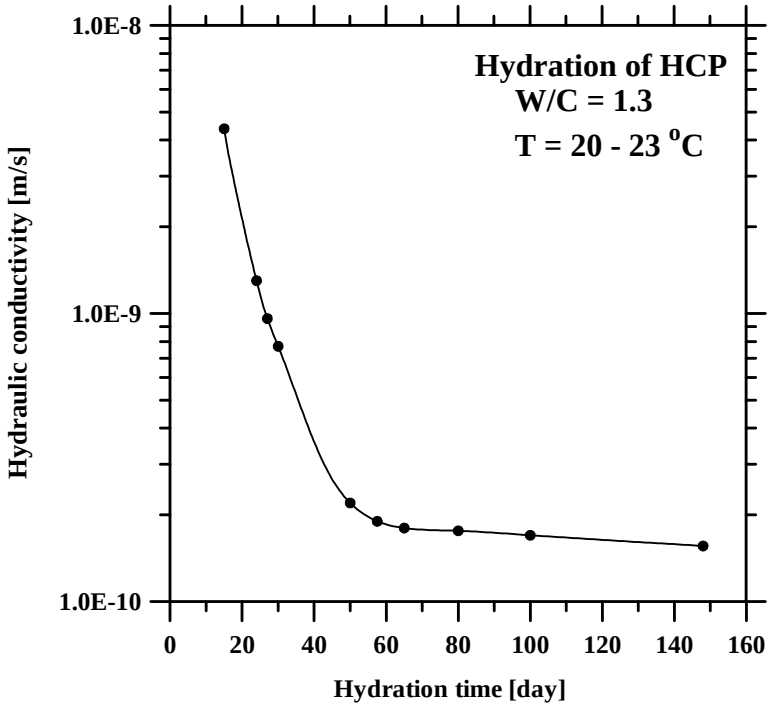

Figure 2.1.1.-1: Time history of the hydraulic conductivity for a sample with a W/C of 1.3. As can be seen the permeability of the HCP strongly decreases during the first two months and subsequently reaches nearly a constant value. Subsequent measurements several months or even years after the production show the same constant value of about $1\text{-}2\cdot10^{-10}$ m/s for the hydraulic conductivity.

Under CO_2-free conditions and with the help of a diamond wire - or better a diamond saw - several disc-like specimens were cut with a thickness of 0.50 and 1.00 cm [4] and an uncertainty in the last digit. A single disk was glued [5] into a sample holder made of polystyrene which itself was part of the diffusion apparatus.

The disk-like samples had a density of (1475 ± 10) kg / m^3 determined by the ratio of the weight of the water-saturated sample and its geometrical volume [4]. With the help of the mercury high-pressure method a value for the connected porosity of 63.3 % was determined; the total porosity was - with a value of 65.4 % - only 2.1 % larger[6]. Further investigations

[4] Values determined with the help of a micrometer.

[5] Two-component glue, type Rivalplan, MBT, Meynadier AG, Zürich, Switzerland.

[6] There is no further information concerning the isolated pore space being not accessible to water. Therefore we will neglect this small difference in the porosity for the following, well knowing that in other cases we would have to account for it.

showed that all samples were fissure-free and thus were considered being homogeneous concerning porosity, capillarity and hydration [22]. In the table below are compiled the values of the most relevant quantities together with their standard deviations.

Quantity	Symbol	Unit	Value	Source
Sample diameter	$2r$	$\cdot 10^2$ [m]	4.1 ± 0.1	[4]
Sample thickness	L	$\cdot 10^2$ [m]	(0.50/1.00)± 0.01 [7]	---
Cross-sectional area accessible for diffusion	F	$\cdot 10^4$ [m^2]	13.2 ± 0.1	[4]
Dry bulk density $(1-\varepsilon)\rho$	$\overline{\rho}$	$\cdot 10^{-3}$ [kg/m^3]	0.777 ± 0.010	[22]
Sample (connected) porosity [8]	ε	[-]	0.63 ± 0.05	[22]

Table 2.1.1.-1: Some geometrical aspects of the HCP and values for the dry bulk density and the porosity. (Values are given with one standard deviation.)

Cement is carbonated through the presence of CO_2 in the air. The precipitated $CaCO_3$ closes the pore space resulting in a much lower porosity in domains close to the surface [23]. Consequently, decreasing rates for diffusion and the hydraulic conductivity were observed in former experiments [6]. Therefore, special care was taken at all times to prevent the HCP from getting into contact with CO_2 of the air. This was achieved with the help of technical devices like preservation in closed vessels, application of CO_2-traps, and rinsing of the equipment with nitrogen. The diffusion experiments were consequently carried out in glove boxes under a controlled nitrogen atmosphere (≤ 5 ppm CO_2, ≤ 5 ppm O_2).

2.1.2. The aqueous solutions

The preparation of the solutions was consequently performed under controlled atmosphere conditions within a glove box. In order to prevent any degradation of the fresh HCP discs [24], an artificial cement pore water solution was used which consisted of $180 \cdot 10^{-3}$ mol/l KOH, $114 \cdot 10^{-3}$ mol/l NaOH, and $1.2 \cdot 10^{-3}$ mol/l $Ca(OH)_2$ and had a pH value of 13.3. Such a solution is considered to be in chemical equilibrium with the HCP sample. The de-ionised water with a specific electrical resistance of ≥ 18 mΩcm still contained some CO_2 with a maximum value of $2.2 \cdot 10^{-6}$ mol/l. However, such a concentration can be neglected when compared to the carbonate concentration of about $1.3 \cdot 10^{-3}$ mol/l due to the preparation of the solution using the mentioned hydroxides. The dissolution of the hydroxides was done in portions of 2 litres with the help of a measuring flask. The solution was then filtered within 2 - 3 hours using a polysulfon filter (Gelman Acrodisc, 0.2 µm and Gelman Criticap 0.1 µm) in order to partially remove colloidal particles, precipitated calcite, or portlandite. Unfiltered the solution typically showed about $8.7 \cdot 10^9$ particles/l; after filtration through the 0.1 µm filter there were still about $5.0 \cdot 10^9$ particles/l using a single particle counter. (The in-situ particle counting in liquids is based on the principle of light scattering on particles [25].) The solution prepared this way was not analysed after filtration (the calculated maximum CO_3^{2-}-

[7] For the nickel experiments only the sample thickness was always 0.5 cm.

[8] Total porosity is $\varepsilon_{tot} = 0.65 \pm 0.05$.

content is about 1 - 2 · 10^{-4} mole/l [26]) and stored for further use within PE-flasks and within the glove box.

The diffusion experiments were performed with a mixture of active and inactive tracer substance. Due to the short half-live of ^{125}I a labelled solution with only 1 per-mille of active tracer was used; all the other tracers were used "carrier free" as specified in the following Table 2.1.2.-2. All of the tracers were bought from Amersham International Plc. (England).

Nuclide	**^{36}Cl**	**^{125}I**	**^{134}Cs**	**^{63}Ni**
Chemical form	NaCl	NaI	CsCl	$NiCl_2$
Isotopic purity (active/total)	0.4-0.5	≤ 0.90	≤ 0.005	0.25
Decay	β^-	e^-, γ	β^-	β^-
Half-live	3.0 · 10^5 y	60.14 d	2.06 y	100 y

Table 2.1.2.-2: Tracer specific data for all four nuclides (e^- … emission of conversion electrons).

A few remarks concerning the stability of the traced solutions:

For chlorine, iodine and caesium a limiting concentration is considered as unlikely in the concentration range up to 10^{-4} mol/l. However, there could be hydrated calcium-aluminates which could well act as a sink for such ions.
According to NAGRA's thermodynamical data base [27] nickel is dissolved in the artificial cement pore water up to 10^{-4} moles/l due to anionic complexes formed. This was the underlying hypothesis for the nickel diffusion experiments. However, only recently, there are strong experimental indications that such a solution (saturated with portlandite and calcite) is not stable meaning that above 10^{-9} moles/l precipitation may occur and indicating that presently used thermodynamic data need some revision [28]. In addition, we mention two relevant references on nickel solubility at high pH [29], [30] [9].

[9] Pilkington and Stone measured the solubility in a range of cement-equilibrated waters at approximately pH 12 and studied the pH dependence in BFS/OPC- and BFS/OPC/Limestone-equilibrated waters. In these a minimum solubility of approximately 3 · 10^{-8} mol/l was measured at about pH 12, with the solubility increasing to lower and higher pH values. Similar data were obtained by Mattigod et al. although their measurements above pH 11 are at or below a rising detection limit. On the basis of these two references, the nickel concentration used in the through-diffusion experiments was at the solubility limit. This may lead to localised precipitation and could be the explanation for the nickel behaviour observed in the blank experiments described in sub-section 2.1.5.

Tracer	Experiment no.	pH of the source solution	Source concentration of total tracer	Concentration of the measurement cell
		$[^{10}\log(\text{mol/l})]$	C_0 [mol/l]	$C(t) / C_0$ [-]
Cl^-	3	13.3 ± 0.1	$(2.79 \pm 0.09) \cdot 10^{-5}$	<1%
	4		$(2.81 \pm 0.16) \cdot 10^{-5}$	
I^-	5		$(3.61 \pm 0.17) \cdot 10^{-8}$	
	6		$(3.71 \pm 0.17) \cdot 10^{-8}$	
Cs^+	7		$(3.82 \pm 0.15) \cdot 10^{-8}$	
	8		$(3.83 \pm 0.17) \cdot 10^{-8}$	
Ni^{2+}	5		$(6.39 \pm 0.47) \cdot 10^{-8}$	
	6		$(3.67 \pm 0.42) \cdot 10^{-8}$	
	7		$(3.85 \pm 0.27) \cdot 10^{-8}$	
	8		$(3.63 \pm 0.33) \cdot 10^{-8}$	

Table 2.1.2.-3: Some averaged values for the solution at the reservoir as well as at the measurement side for all of the tracer used. (Values are given with one standard deviation.)

2.1.3. Activity measurements, total diffused mass and flux

The observables are the activity of the reservoir A_{res} as well as of the measurement cell A_{meas}, both a function of (the parameter) time *t*.
To a given time point t_n several aliquots of the solution were pipetted with a total volume $V_{pr,n}$. To 2 ml of the aliquot another 2 ml of the scintillation liquid Instagel™ (Canberra Packard) were added and mixed in 5 ml vials. This solution was then used to measure, within 10 - 30 minutes, the activity *A* (in counts per minute and milli-litre - Cpm/ml) of the sample using a β-counter (model Tri-Carb 2200 CA, Canberra Packard) in the energy interval of 0 - 500 keV for chlorine and caesium, 0 - 70 keV for iodine, and 4 - 70 keV for nickel. With the help of a conversion factor which transforms the tracer activity into moles the total tracer concentration C_n in the measurement cell was calculated.

Tracer	Conversion factor f [mol l^{-1} / Cpm ml^{-1}]
Cl^-	$(7.787 \pm 0.390) \cdot 10^{-10}$
I^-	$(5.165 \pm 0.104) \cdot 10^{-13}$
Cs^+	$(6.533 \pm 0.131) \cdot 10^{-13}$
Ni^{2+}	$(1.262 \pm 0.038) \cdot 10^{-12}$

Table 2.1.3.-1: Table of the conversion factors with one-standard deviation errors for all four nuclides.

The pipetted amount of aliquots was replaced by the same amount of fresh cement pore water resulting in a dilution of the solution in the measurement cell. The dilution factor after pipettting the n-th aliquot is simply given by

$$\beta_n = \frac{V_{tot} - V_{pr,n}}{V_{tot}} \quad , \tag{2.1.3.1}$$

where V_{tot} is the volume of the solution in the measurement cell. Hence, after the sampling, the remaining concentration C_n' of total tracer in the measurement cell is given by $C_n' = C_n \beta_n$. The concentration in the measurement reservoir C_n', reduces the driving force for diffusion. By multiplying the concentration C_n with the volume of the solution in the measurement cell the total tracer mass is obtained. Considering the dilution caused by the (n-1)-th sampling we are able to calculate the total amount of diffused mass in the interval $(t_{n-1},\ t_n]$ which is $\Delta m_{n-1,n} = m_n - m_{n-1}^{'}$.
Schematically:

Sampling time	$t = t_0 = 0$	$t = t_1$	$t = t_2$	...	$t = t_n$
Concentration in the measurement cell	0	C_1	C_2	...	C_n
Total tracer mass in the measurement cell	0	$m_1 = C_1 V_{tot}$	$m_2 = C_2 V_{tot}$	...	$m_n = C_n V_{tot}$
Remaining concentration after sampling	0	$C_1^{'} = C_1 \beta_1$	$C_2^{'} = C_2 \beta_2$	...	$C_n^{'} = C_n \beta_n$
Remaining total tracer mass after sampling	0	$m_1^{'} = C_1^{'} V_{tot}$	$m_2^{'} = C_2^{'} V_{tot}$	...	$m_n^{'} = C_n^{'} V_{tot}$
Total diffused tracer mass in the time interval	0	$\Delta m_{0,1} = m_1$	$\Delta m_{1,2} = m_2 - m_1^{'}$	...	$\Delta m_{n-1,n} = m_n - m_{n-1}^{'}$

For the $\Delta m_{n-1,n}$ we therefore can write:

$$\begin{aligned} \Delta m_{n-1,n} &= m_n - m_{n-1}^{'} = (C_n - C_{n-1}^{'})V_{tot} = (C_n - C_{n-1}\beta_{n-1})V_{tot} \\ &= (C_n - C_{n-1})V_{tot} + C_{n-1}V_{pr,n-1} \quad . \end{aligned} \tag{2.1.3.2}$$

In practice this relationship is used for the first few weeks where the concentration in the measurement cell always is well below the (artificial) limiting value of 1 % C_0. However, when later on the concentration reached this value, the whole volume of the measurement cell was replaced by fresh cement pore water (meaning that $V_{pr,n} = V_{tot}$ holds) to achieve a zero concentration boundary condition again. The total accumulated (diffused) tracer mass on the secondary side is simply given by the sum of the Δm_i [mol]:

$$m_{tot}(t_N) = \sum_{i=1}^{N} \Delta m_{i-1,i} \quad . \tag{2.1.3.3}$$

The averaged flux $\bar{j}$ in the time interval $(t_n, t_{n-1}]$ is given by:

$$\bar{j} = j\left(\frac{t_n - t_{n-1}}{2}\right) = \frac{\Delta m_{n-1,n}}{F(t_n - t_{n-1})} \quad , \tag{2.1.3.4}$$

where *F* is the cross-sectional area of the sample. As the corresponding time point for the flux $\bar{j}$ [10] we define the arithmetic mean of the time interval limits.

2.1.4. Error analysis

In this sub-section we consider some important aspects concerning data evaluation.

All observations are subject to errors of various kinds. Even with well-posed experiments, meaning, despite all the care and precautions taken with the measurements, more or less uncertainty occur in their results caused by errors which can be conceptionally divided into two categories - systematical and statistical measurement errors. Systematical measurement errors are due to, e.g., wrong calibration of an equipment or arise due to a principal lack of theoretical comprehension of the process of measurement (e.g. measurement of the pressure *p(V)* of a gas as a function of its volume where changes in the temperature due to volume changes are not considered). Systematical errors cannot be handled with the help of a formal treatment. Such a type of errors can only be discovered by independent measurements and results in a corresponding shift of the final result. Moreover, there is no general rule to avoid systematical errors[11]. Statistical errors, however, are caused by fluctuations and uncertainties of the measurement equipment or are due to the statistical character of the physical quantity being measured and can be quantified by a suitable formalism. More measurements increase the precision of the result, hence decrease its errors or uncertainty. In contrast to this, systematical errors cannot be decreased by an increased number of measurements (a ruler being too short will always result in too large distances independent of the number of measurements). Therefore, we can say that systematic errors affect the accuracy of the final result while statistical errors affect the precision of the result.

It is commonplace to take the average or arithmetic mean $\bar{x}$ as a better estimate of a physical quantity than any of a series of *n* observations (measurements) $\{x_i\}$

$$\bar{x} = \frac{1}{n}\sum_{i=1}^{n} x_i \quad . \tag{2.1.4.1}$$

The standard deviation σ_x of the measurements is given by

$$\sigma_x = \sqrt{\frac{1}{n-1}\sum_{i=1}^{n}(x_i - \bar{x})^2} \quad [12]. \tag{2.1.4.2}$$

The underlying idea of (2.1.4.1) is that 1) the average minimises the variance σ_x^2 and 2) the sum of the residuals $(x_i - \bar{x})$ is zero.
However, the standard deviation of the mean is

$$\sigma_{\bar{x}} = \frac{\sigma_x}{\sqrt{n}} = \sqrt{\frac{1}{n(n-1)}\sum_{i=1}^{n}(x_i - \bar{x})^2} \quad . \tag{2.1.4.3}$$

---

[10] For simplicity's sake we will omit the "bar" on top of *j* for the rest of the report.

[11] We already mentioned that some of the experiments were excluded from modelling due to systematic errors and because they hardly could have been taken into account satisfactorily.

[12] Dividing by the factor *(n*-1*)* gives an unbiased estimator.

For more and more measurements σ_x does not change much, but $\sigma_{\bar{x}}$ slowly decreases approaching zero with increased *n*. With the help of more observations the final result becomes more reliable.
σ_x taken as such does not say anything about the quality of the result. But, with the help of the confidence interval of the measurements *T* where $T = t\,\sigma_x$ (*t* = Student factor, dependent on the degree of freedom $f = (n - 1)$ and the statistical probability p %) a justification can be made. The meaning of *T* is that p % of all measurements are located within the interval $(x \pm T)$. The corresponding confidence interval $T_{\bar{x}}$ of the mean is simply given by

$$T_{\bar{x}} = \frac{T}{\sqrt{n}} = t\,\sigma_{\bar{x}} \quad . \tag{2.1.4.4}$$

The Student factor takes care that the standard deviations of the mean (or of the measurements) becomes larger due to an insufficient number of single measurements.

For all the diffusion/out-diffusion experiments two samples were taken from the measurement cell (or from the reservoir side) for the activity measurements providing the basis for the average and standard deviation of the mean according to the equations (2.1.4.1) and (2.1.4.3). Therefore, for the Student factor *t* the degree of freedom is $n = 1$; in addition an (arbitrary) error probability of 5 % was assumed. The numerical value of *t* is [31]

$$t\,(1,\ 95\ \%) = 12.71 \quad .$$

Normally for the final result such as flux, etc. we have to evaluate the error of a (non-) linear combination of physical quantities with means $\{\ \bar{x}_i\ \}$ subject to error. In this case we have to make the assumption that

1) the fluctuations $\sigma_{\bar{x}_i}$ are small with regard to the (means of the) measurements themselves, hence $\left|\sigma_{\bar{x}_i} / \bar{x}_i\right| << 1$. The reason for doing this is that we have to linearise the function $f(\bar{x}_1, \bar{x}_2, \ldots, \bar{x}_N)$ by means of a truncated Taylor series, and the truncation will only be valid, if the errors are small;
2) all the observations as well as their fluctuations are uncorrelated.

With these two assumptions we can calculate the error of the quantity *f* according to the following expression

$$\sigma_f\,(\bar{x}_1, \bar{x}_2, \ldots, \bar{x}_N) \cong \sqrt{\sum_{i=1}^{N} \left(\frac{\partial f}{\partial \bar{x}_i}\right)^2 \sigma_{\bar{x}_i}{}^2} \quad . \tag{2.1.4.5}$$

For the data evaluation we assumed all measured quantities as being uncorrelated, so that an additional covariance term in equation (2.1.4.5) could be omitted. Fluctuations in the time were mostly much less than a quarter of an hour; uncertainties in the other physical quantities (such as volume of the measurement cell, volume of the pipette, etc.) being relevant for the calculation of the diffusive flux and the total accumulated mass in the measurement cell, were estimated and determined in series of independent measurements and specified in the text and tables, respectively.

2.1.5. Blank value measurements

For the determination of some blank values the same equipment as for the diffusion experiments was used but without the cementitious diffusion barrier. In this case the total volume of the compartment was about (686 ± 10) ml being about 5 % larger than for the through-diffusion experiments. The handling was the same as for the real experiments: Some 617 ml of a defined tracer solution were filled into the cell and circulated by a membrane pump. The experiments were performed under the same controlled conditions within a glove box and are described in more detail in the previous sub-sections. Periodically two 1 ml samples were drawn to measure the activity as described in sub-section 2.1.3. Occasionally some concentrated tracer solution was added for re-adjustment of the concentration level to the expectation value due to marked tracer deposition onto the cell surfaces.

For chlorine, iodine and caesium no appreciable tracer up-take by the surfaces of the polystyrene diffusion cell could be recognised. However, the results looked completely different for nickel and will be discussed in the following in more detail.
The experiment continued for about 445 days, and at 100 dates activity measurements were performed. In the next figure the normalised nickel amount in the mobile phase as a function of time is shown.

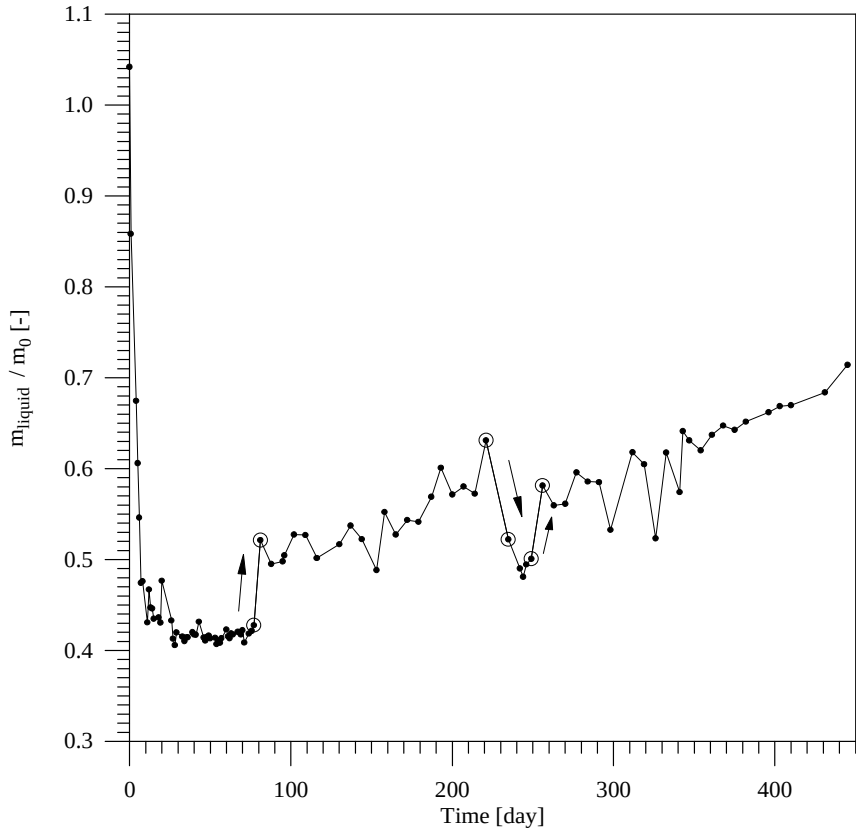

Figure 2.1.5.-1: The ratio of nickel in the mobile phase m_{liquid} and total nickel m_0 as a function of time. In a first phase the tracer amount of the mobile phase dropped due to nickel deposition onto the cell surfaces. Therefore during the experiment three times concentrated tracer was added for the adjustment indicated in the figure by intervals bounded by open circles. The arrows emphasise the response of the system on traced mass increase.

Shortly after the beginning the amount of nickel in the liquid dropped to about 40 % of the original value within about 10 days and remained on this low level for another 70 days. For the adjustment some higher concentrated tracer solution was added followed by a certain increase of the nickel mass in the mobile phase. However, the expectation value of about $2.34 \cdot 10^{-8}$ moles was not reached, because some added nickel was immediately taken up by the surfaces. In the next phase which continued about 160 days slow nickel release could be recognised. After 231 days again some concentrated tracer solution was added resulting in a fast - and surprising - decrease of the tracer amount in the liquid. Therefore in a third attempt more concentrated tracer was added to the system answered by a moderate increase of the tracer mass in the liquid. However, the expectation value was still not reached at all. Until the termination of the experiment slow nickel release could be detected.
In order to estimate a range for nickel deposition onto the polystyrene surfaces of the diffusion cell we consider the following figure where the amount of nickel taken up by the equipment is plotted versus the nickel concentration of the mobile phase.

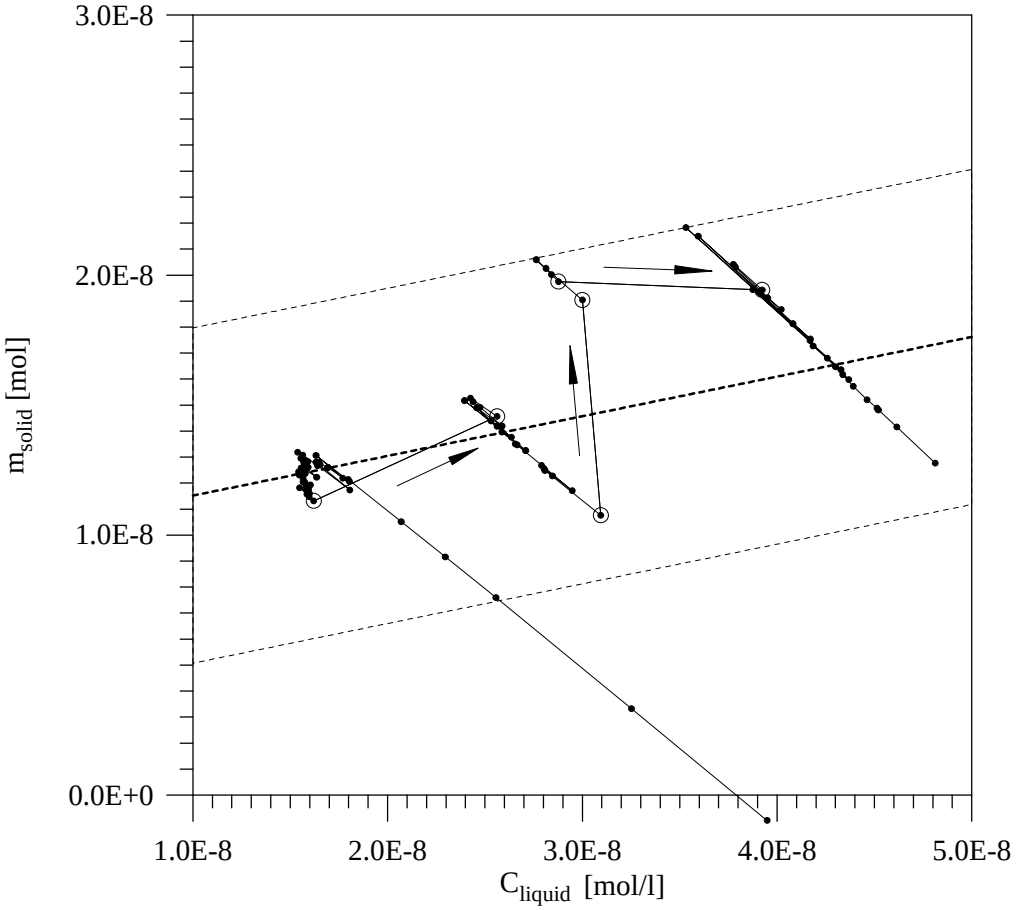

Figure 2.1.5.-2: The amount of deposited nickel m_{solid} as a function of the compartment concentration C_{liquid}. The intervals bounded by open circles indicate that concentrated tracer was added to the system; the arrows show the direction of the response of the system. As can be seen from the figure the deposited tracer amount is - except at the very beginning - of the order of $(1-2) \cdot 10^{-8}$ moles when varying the nickel concentration of the liquid in the range of $(1-5) \cdot 10^{-8}$ moles/l. The dashed line (bold) represents a linear regression curve of all the data; its parallels limit its error range.

When varying the concentration of the liquid in the range of $(1-5)\cdot 10^{-8}$ moles/l the deposited nickel amount is of the order of $(1-2)\cdot 10^{-8}$ moles. An analysis of the data however indicates, that there is a slight tendency for an increased deposition for an increased concentration of the solution. (The slope of a linear regression curve has a value of 0.153 [litre], and its constant is $1.00 \cdot 10^{-8}$ [mole].) As an average of the blank measurements a value of about $\overline{m}_{\text{solid}} \pm \Delta m_{\text{solid}} = (1.39 \pm 0.65)\cdot 10^{-8}$ moles was determined for an 'averaged' nickel concentration in solution of about $\overline{C}_{liquid} \pm \Delta \overline{C}_{liquid}$ = (2.56 ± 0.11) · 10^{-8} moles/l. To avoid a systematic error in the data evaluation for nickel diffusion we will have to account for this blank value, especially when discussing mass balances. However, we know very well that this blind value is based on only one experiment and that we neglected both time- and concentration-dependent effects of unspecified nickel deposition processes which can be recognised in the existing data set.

With the help of a roughly estimated value of the wetted surface area of about $F_{\text{solid}} \pm \Delta F_{\text{solid}} = (3.69 \pm 1.23)\cdot 10^{-2}$ m^2 we can determine according to

$$S_F = K_a \cdot C_{\text{liquid}} \qquad (2.1.5.1)$$

with units [mol/m^2] a value for the surface-based sorption coefficient K_a for nickel onto polystyrene for a pH of the solution of 13.6

$$K_a \pm \Delta K_a = 15 \pm 9 \text{ m.}$$

To our knowledge there is no other value known, therefore, we are not able to make further comments and considerations.

2.2. Experiments with chlorine, iodine and caesium

In this section we will describe some initial experiments performed with ^{36}Cl, ^{125}I and ^{134}Cs as tracers. Chlorine is an activation product, iodine as well as caesium are fission products; all of them are considered as safety-relevant nuclides for a Swiss repository for low and intermediate radioactive waste [32]. Expecting that chlorine and iodine, both being anions, would only show little sorption on cement, hence short duration of the experiments and fast steady-state were assumed. Caesium is strongly competed by sodium and potassium of the artificial cement pore water (see also sub-section 2.1.2.); together, both are by a factor of 10^5 more concentrated in solution than caesium. Therefore also for caesium only small retardation was assumed.

2.2.1. Chloride through-diffusion - Experiment no. 3

The experiment was started on June 29th, 1990, and was terminated on December 21st, 1990, after about 175 days. As mentioned above, chlorine was assumed to act as a conservative tracer fast reaching steady-state. In the following figure the measured diffusive flux as a function of time together with its error bars [13] representing a 95 % confidence interval is shown.

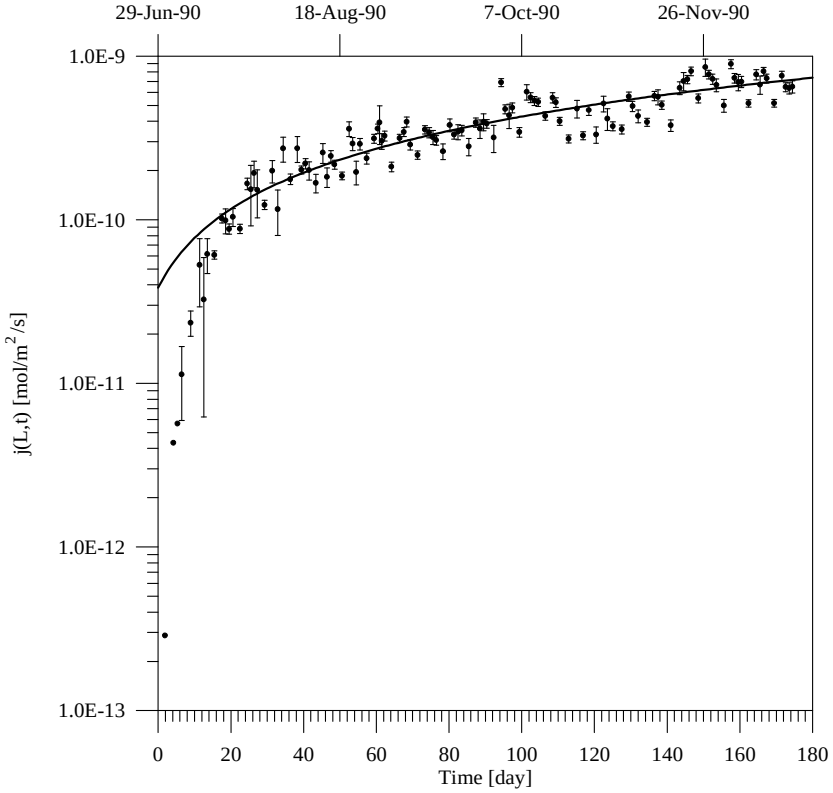

Figure 2.2.1.-1: A semi-log plot of the measured diffusive flux for chlorine and experiment no. 3 as a function of time with corresponding error bars representing a 95 % confidence interval. For illustration purposes a linear regression curve (solid line) fitted on all the data beyond 80 days is also shown indicating that steady-state is not yet reached.

[13] Unfortunately the plot software is not able to draw the error bars of such data points the limits of which are beyond the plot window. Hence, for these data only the values without error bars are drawn.

During the first 80 days a fast increase of the diffusive flux can be recognised, after that it evolves practically linearly when neglecting short time fluctuations indicating that the system is not in a steady-state phase even after 175 days.
If considering the accumulated diffused chlorine mass as a function of time instead of the flux we would rather assume a stationary state of the system after at least 140 days. This can be seen in the following figure.

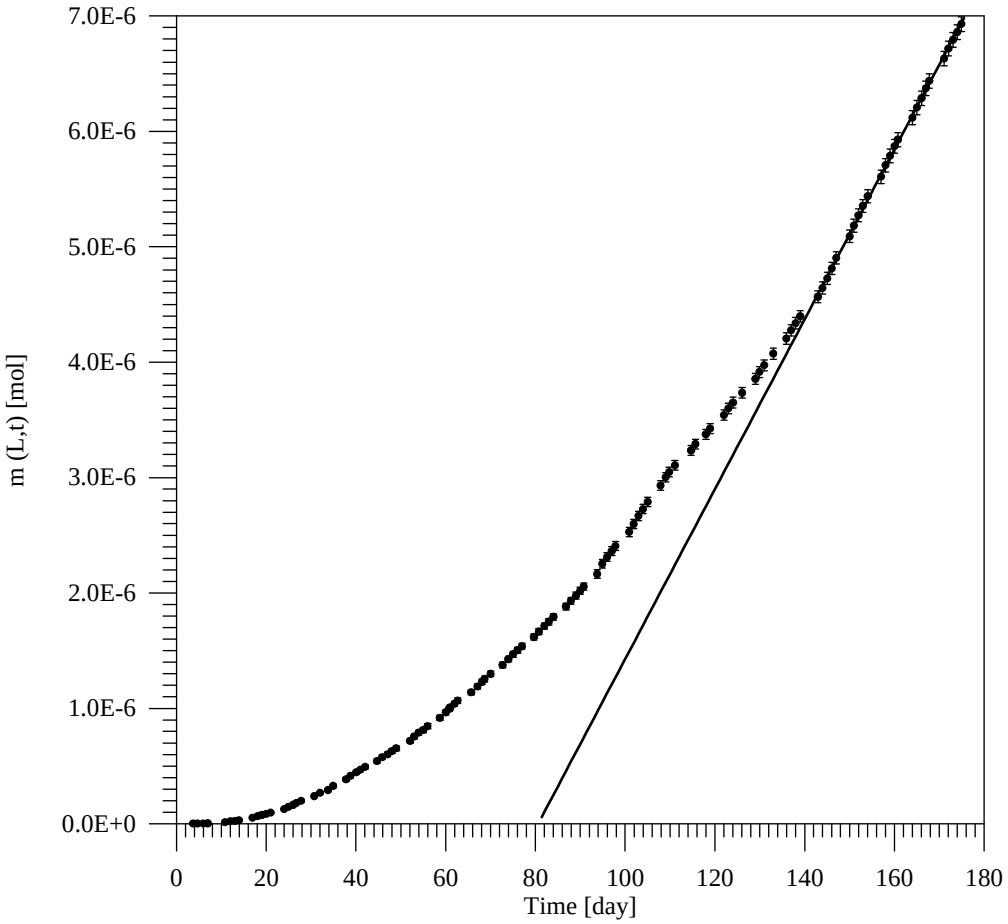

Figure 2.2.1.-2: Plot of the accumulated diffused chlorine mass for experiment no. 3 as a function of time together with the error bars which represent a 95 % confidence interval. At first view steady-state for diffusion could be assumed beyond 140 days. However, from the previous figure we know that this is not the case.

Therefore, for a provisional judgement of the experimental data we clearly prefer the *j(t)* instead of the *m(t)* representation avoiding - by the way - problems which arise due to the accumulation of measurement errors in the latter case.
In the following plot the fluctuations in the reservoir concentration $C_0(t)$ are shown. Nevertheless, of a total chlorine content of the reservoir compartment of roughly $1.6 \cdot 10^{-5}$ moles, fluctuations occurred due to the tracer up-take of the HCP as well as due to diffusion. Therefore the reservoir concentration was periodically adjusted with the help of additions of concentrated tracer solution. However, in this experiment these fluctuations in $C_0(t)$ were always less than ± 10 % of the mean $\overline{C}_0$ which was determined to be $\overline{C}_0 \pm \Delta C_0$ = $(2.79 \pm 0.09) \cdot 10^{-5}$ mole/l.

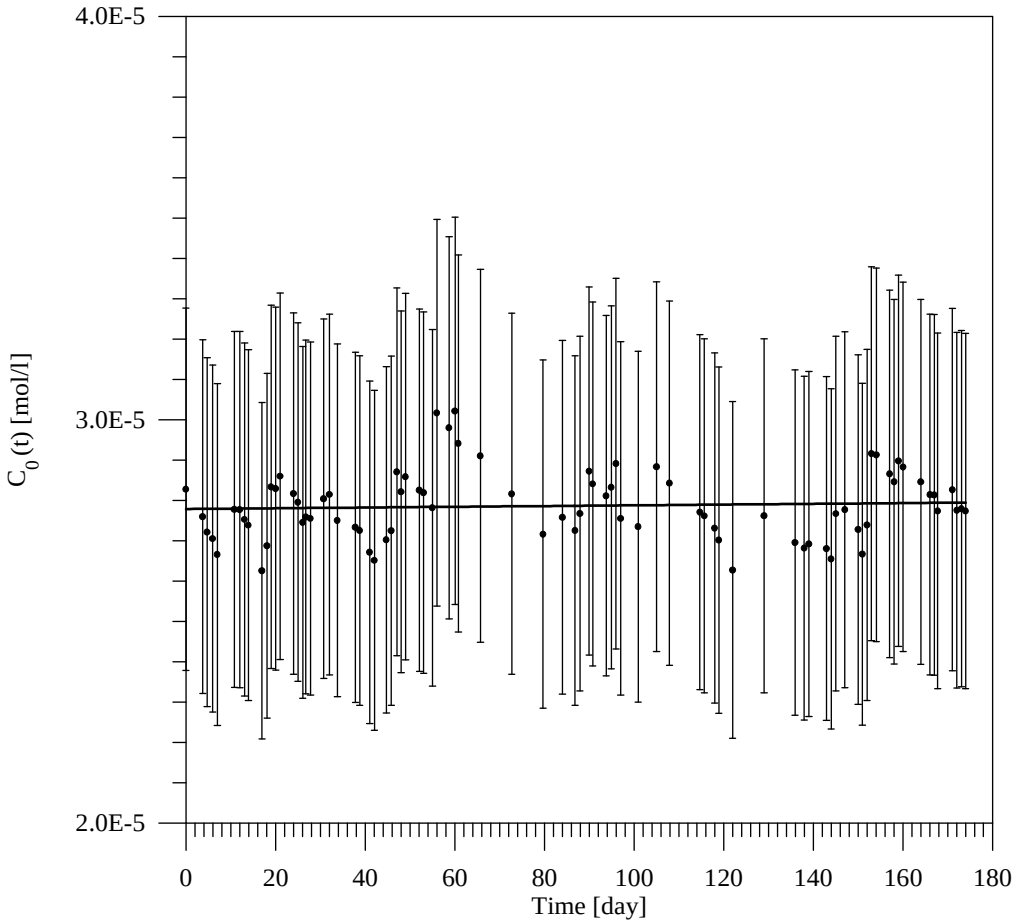

Figure 2.2.1.-3: The reservoir concentration $C_0(t)$ of chlorine and experiment no. 3. As can be seen, fluctuations were always less than ± 10 % during the whole period of the experiment. The error bars represent a 95 % confidence interval based on two single measurements. The solid line represents a linear regression of all data which practically coincides with the averaged value of about $(2.79 \pm 0.09) \cdot 10^{-5}$ mol/l.

From a careful mass balance we can estimate the amount of chlorine which was taken up by the hardened cement paste. This may be an interesting quantity giving further information on the processes being involved such as, e.g., sorption kinetics etc. These values can also be compared with corresponding data obtained in independent batch sorption experiments thus allowing a consistency check.

From the following Figure 2.2.1.-4 we can see, that the chlorine up-take has reached its maximum after about 80 -140 days when the tracer slowly becomes released again. However, without additional information it is not possible to make reasonable (temporarily) assumptions about the mechanisms being involved.

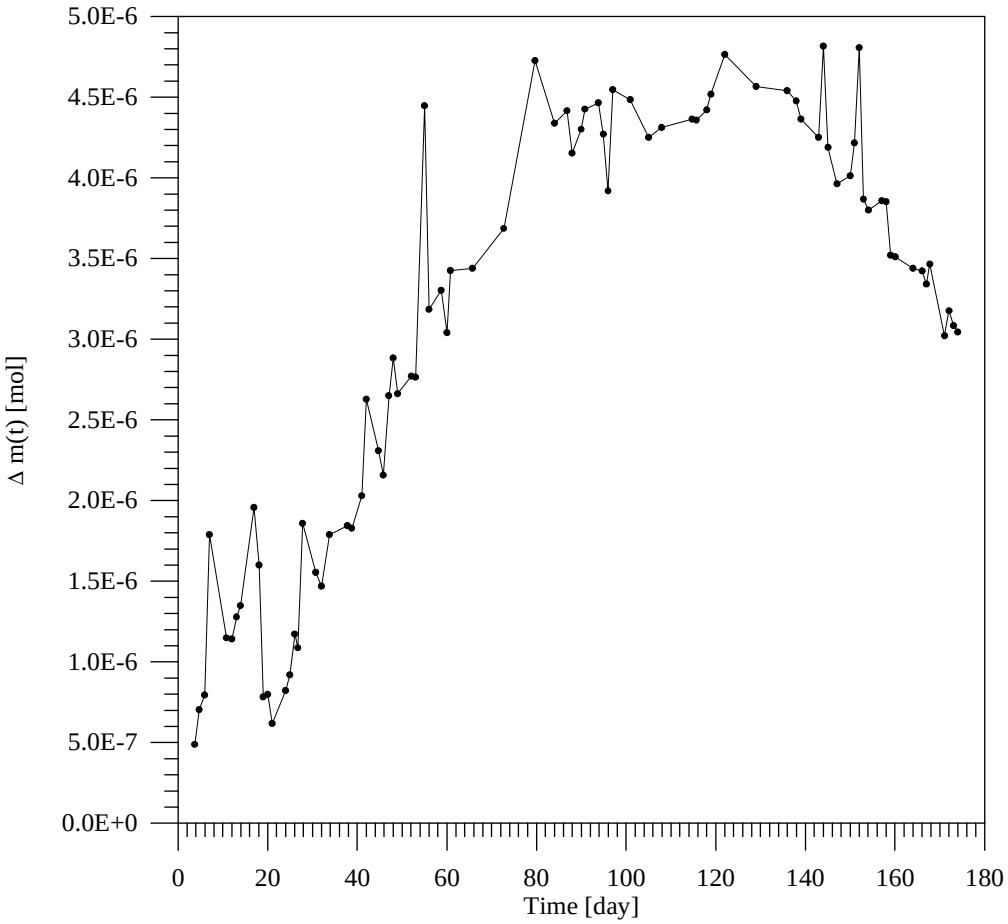

Figure 2.2.1.-4: Mass *Δ m(t)* of chlorine of experiment no.3 deposited within the HCP and - possibly - also onto the walls of the equipment as a function of time. The data are based on a mass balance and show an increased up-take of chlorine for the first 80 days; there is a tendency for a plateau for another 40 - 50 days followed by a slow decrease. Such an evolution also supports the assumption that the system has not reached a steady-state phase.

2.2.2. Chloride through-diffusion - Experiment no. 4

The experiment was started - like the previous experiment no. 3 - on June 29th, 1990, and was terminated on December 21st, 1990, after about 175 days. To recall: chlorine as an anion was assumed to act as a conservative tracer fast reaching steady-state. In the following figure the measured diffusive flux as function of time together with its error bars representing a 95 % confidence interval is shown.

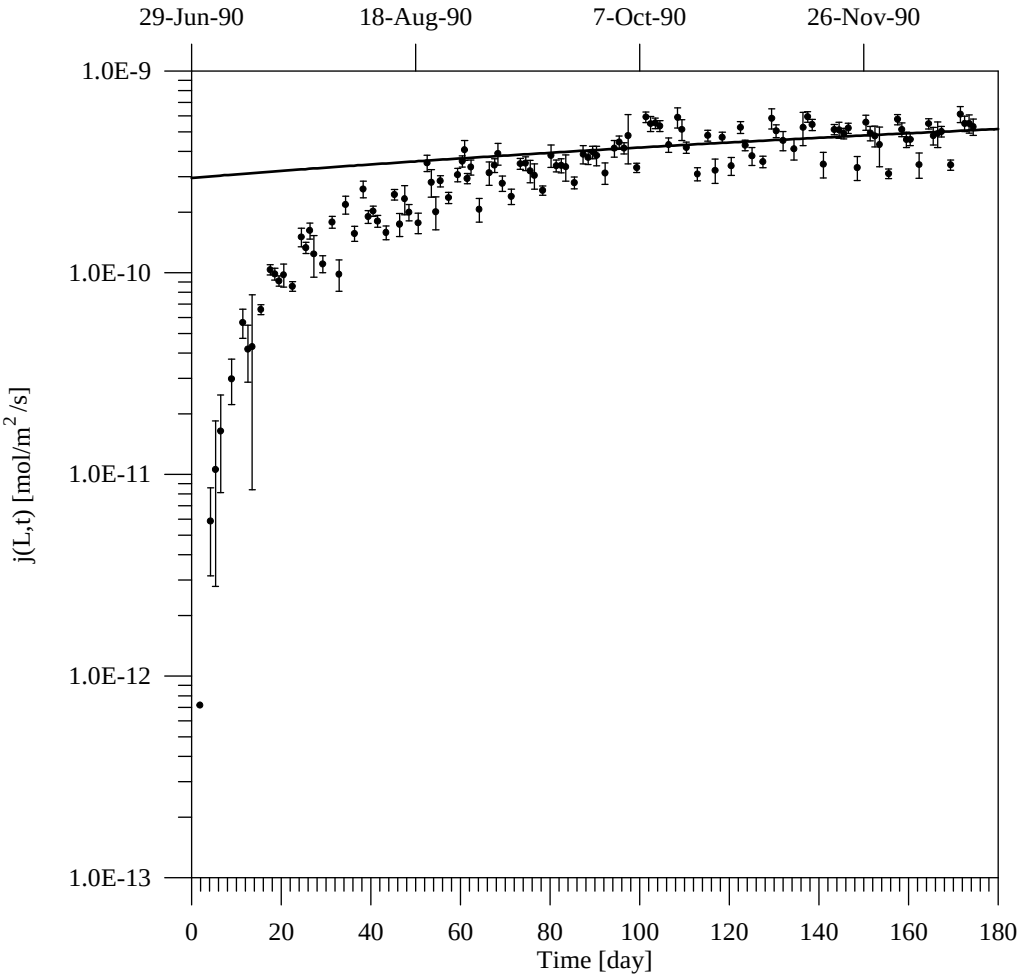

Figure 2.2.2.-1: A semi-log plot of the measured diffusive flux for chlorine and experiment no. 4 as a function of time with corresponding error bars representing a 95 % confidence interval. For illustration purposes a linear regression curve (solid line) fitted on all the data beyond 80 days is also shown indicating that steady-state is not yet reached.

As for experiment no. 3, the flux was evolving all the time, and a steady-state was never reached. A linear regression of the measurements beyond 80 days confirms this fact. However, if plotting the accumulated diffused chlorine mass as a function of time, one easily could conclude that the system is in a stationary phase with constant flux. This fact can be seen in the following figure where, in addition and for the purpose of demonstration, the linear regression curve is also drawn. The solid line matches the measurements for $t > 85$ days nearly perfectly.

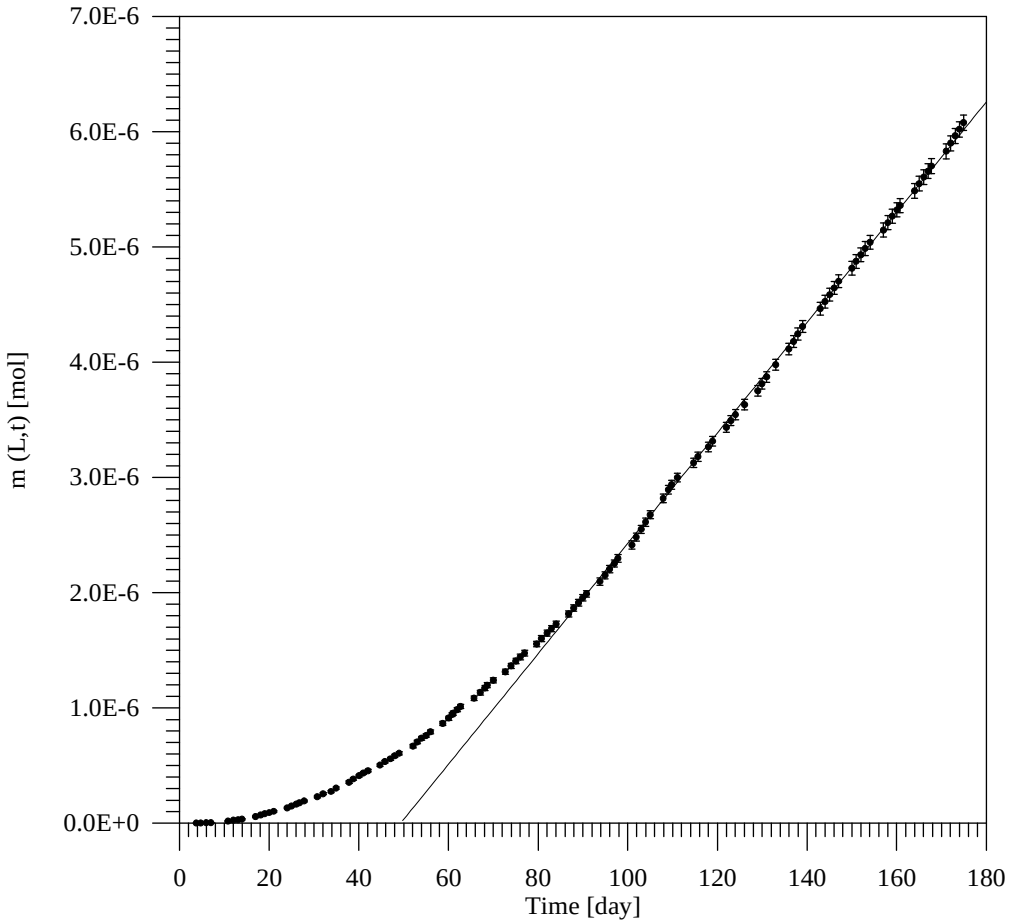

Figure 2.2.2.-2 Plot of the accumulated diffused chlorine mass of experiment no. 4 as a function of time together with the error bars which represent a 95 % confidence interval. At first view steady-state for diffusion could be assumed beyond 85 days, which is supported by the linear regression (solid) line. However, the previous figure indicates a slow evolution of the diffusive flux.

The next figure shows the time history of the reservoir concentration $C_0(t)$. The expectation value was assumed to be $2.92 \cdot 10^{-5}$ mol/l; however, fluctuations due to chlorine up-take of the sample and the equipment disturbed the expectation value resulting in a time-dependent boundary condition. For the adjustment periodically some concentrated tracer solution was added. As a mean a value of about $\overline{C_0} \pm \Delta C_0 = (2.81 \pm 0.16) \cdot 10^{-5}$ mol/l can be determined which is less than 4 % smaller than the expectation value.

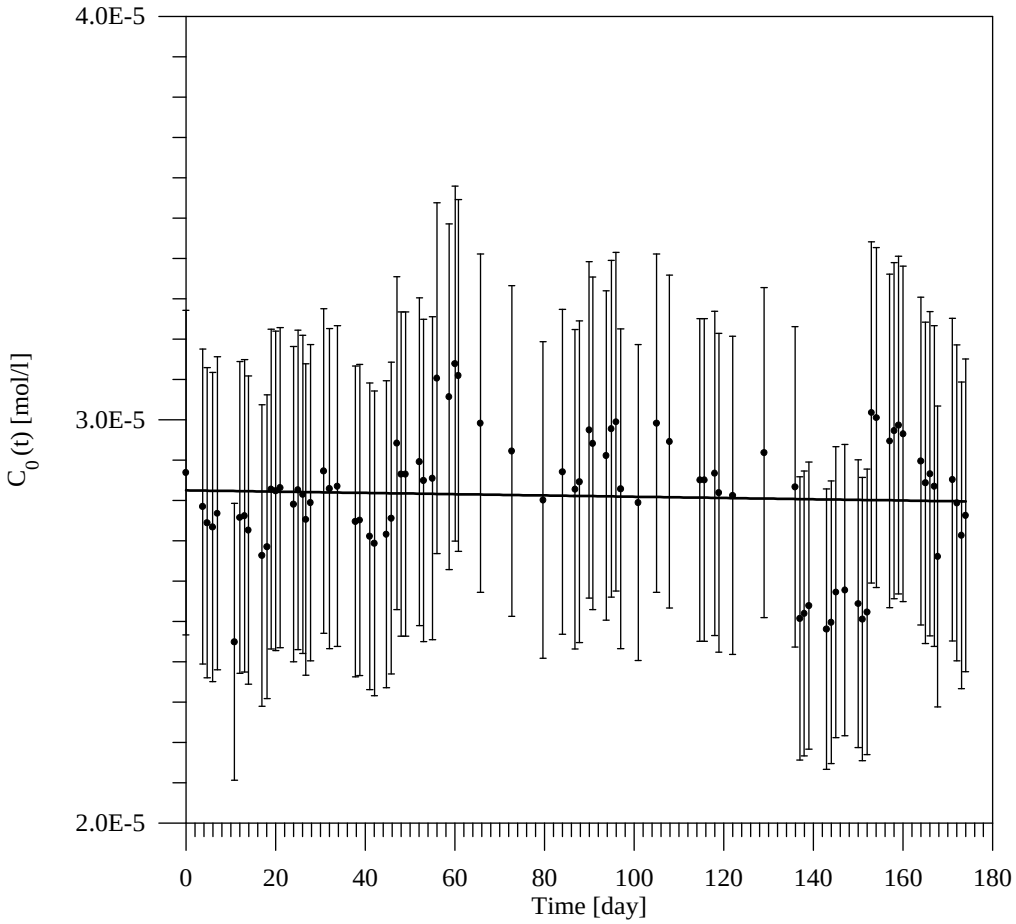

Figure 2.2.2.-3: The reservoir concentration $C_0(t)$ of chlorine and experiment no. 4. As can be seen fluctuations were mostly less than ± 10 % of the mean $\overline{C}_0$ during the whole period of the experiment. The solid line represents a linear regression of all the measurements which nearly coincides with the mean value of about $2.81 \cdot 10^{-5}$ mol/l.

Last, we consider the results of a careful mass balance. In the following figure the amount of chlorine $\Delta m(t)$ taken up by the HCP and - possibly - the equipment is plotted versus time. As can be seen, neglecting short time fluctuations which are considered being measurement artefacts, $\Delta m(t)$ increases with time. In contrast to the previously presented experiment no. 3, where a maximum for $\Delta m(t)$ occurred followed by a slow decrease, such a behaviour cannot be recognised. Because both experiments were performed under the same experimental conditions we have no reasonable explanation for these marked differences in the mass-balance and in the breakthrough curves *m(L,t)*.

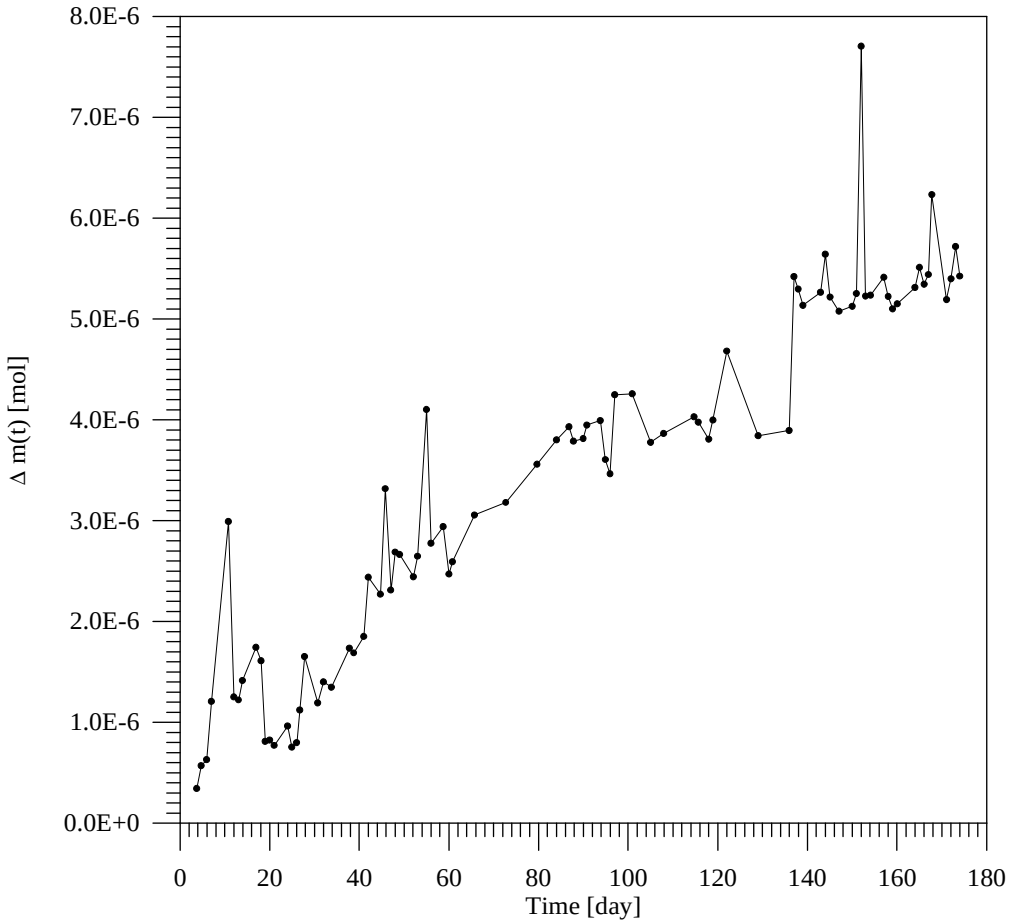

Figure 2.2.2.-4: Mass *Δ m(t)* of chlorine deposited within the HCP and - possibly - also onto the walls of the equipment as a function of time. The data are based on a mass-balance and show a continuously increased up-take during the experiment. It is an open question whether after 180 days the system had reached a stationary state.

2.2.3. Iodide through-diffusion - Experiment no. 5

The experiment was started on September 28th, 1990, and was terminated on December 21st, 1990, after about only 84 days. As mentioned above, iodine - as a safety-relevant fission product - was assumed to act as a conservative tracer, hence reaching fast steady-state. In the following figure the measured diffusive flux as a function of time together with the error bars representing a 95 % confidence interval is shown.

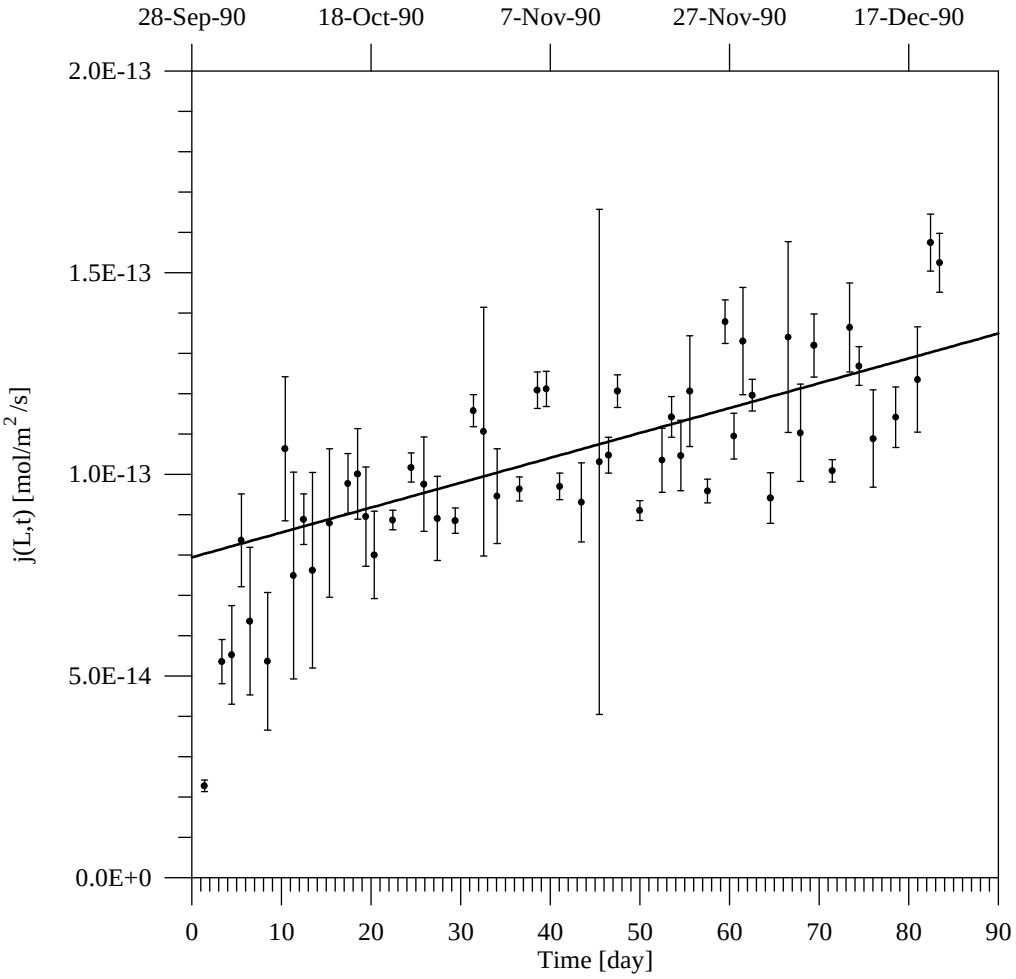

Figure 2.2.3.-1: A semi-log plot of the measured diffusive flux for iodide and experiment no. 5 as a function of time with corresponding error bars representing a 95 % confidence interval. For illustration purposes a linear regression curve (solid line) fitted on all the data beyond 30 days is also shown indicating that steady-state is not yet reached.

From the figure we can see that the flux is rapidly increasing for the first 20 to 30 days and then evolves further only slowly until the termination of the experiment. It is obvious that the system never reached a stationary phase with constant diffusive flux across the boundary. Indeed, a linear regression of the data for $t > 30$ days also confirms an increase in the flux values. Comparing these 30 days for terminating the first period of fast evolution of the diffusion system with the 85 days for chloride (see sub-sections 2.2.1. and 2.2.2) we conclude that retardation effects of iodide must play a much smaller rôle than that of the other halogen.

If the diffusive flux would have been considered as constant, a value for the effective diffusion constant could be determined according to Fick's first law

$$j(L,t) = -D_e \left.\frac{\partial C}{\partial x}\right|_{x=L} = \text{const.} \quad . \tag{2.2.1}$$

Nevertheless, with the help of the time history of the total diffused tracer mass such a value can be determined, even if the system has not reached a stationary state, as will be shown in the modelling part of the report (see section 3). However, a representation of the total diffused iodine mass as a function of time would imply that the system had reached a steady state at least after about 30 days, as can be seen in the following Figure 2.2.3.-2.

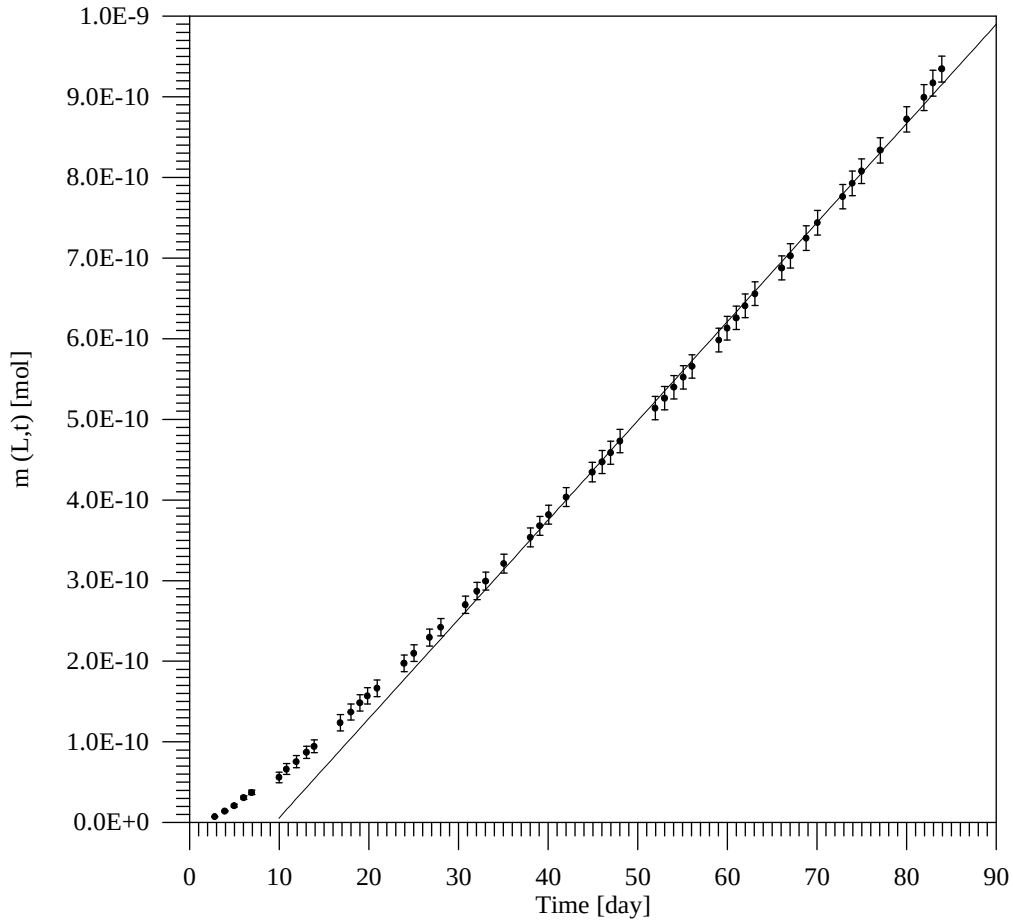

Figure 2.2.3.-2: Plot of the accumulated diffused iodine mass of experiment no. 5 as a function of time together with the error bars which represent a 95 % confidence interval. At first view, steady-state for diffusion could be assumed beyond 30 days, and as it is supported by a linear regression of all the data with t > 30 days (solid line). However, from the previous figure we know that this is not the case.

The next Figure 2.2.3.-3 shows the variation of the reservoir concentration $C_0(t)$. Due to diffusion and up-take C_0 had to be adjusted periodically to guarantee a - more or less - constant boundary condition. As can be seen the fluctuations in general were less than ± 10 % of the mean concentration being $\overline{C_0} \pm \Delta C_0 = (3.61 \pm 0.17) \cdot 10^{-8}$ mol/l (the uncertainty is one standard deviation).

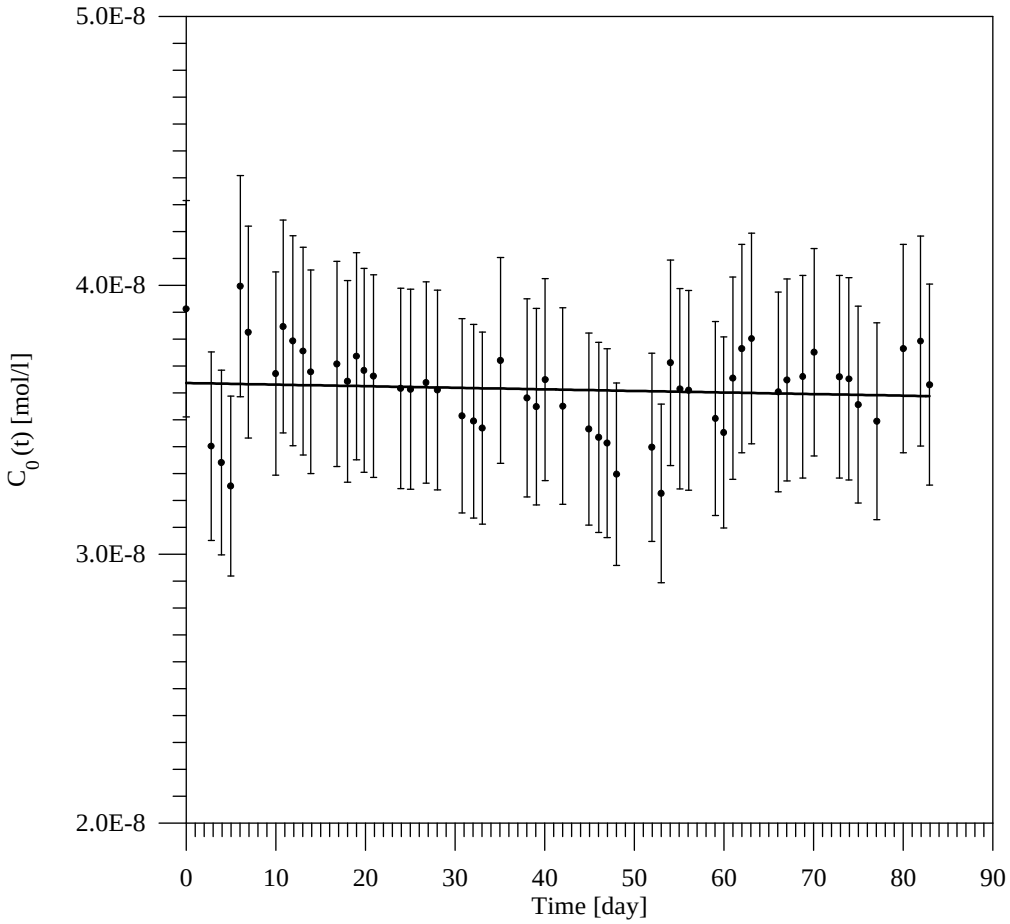

Figure 2.2.3.-3: The reservoir concentration $C_0(t)$ of iodine and experiment no. 5. The error bars are based on two single measurements respectively and correspond to a 95 % confidence interval. As can be seen fluctuations were mostly less than ± 10 % of the mean $\overline{C}_0$ during the whole period of the experiment. The solid line represents a linear regression of all the measurements which nearly coincides with the mean value of about $3.61 \cdot 10^{-8}$ mol/l.

In the following Figure 2.2.3.-4 the deposited iodine mass $\Delta m(t)$ is plotted versus time. With deposited mass we mean the total up-take of iodine of the HCP as well as - possibly - the equipment. As can be seen in the figure, deposition is increasing monotonically when neglecting short term variations, and it does not reach a maximum value during the period of experimentation. Such a behaviour indicates, too, that the system had never reached a stationary state.

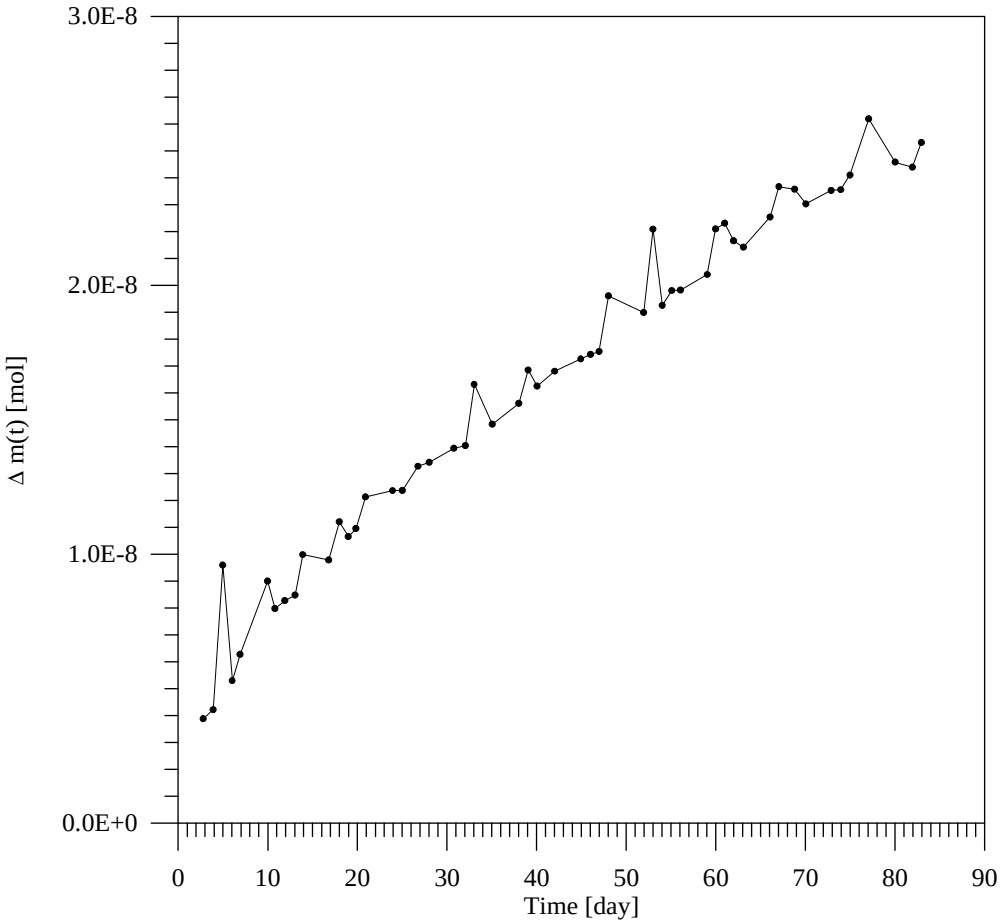

Figure 2.2.3.-4: Mass *Δ m(t)* of iodine and experiment no. 5 deposited within the HCP and - possibly - also onto the walls of the equipment as a function of time. The data are based on a mass balance and - neglecting short time fluctuations - show a continuously increased up-take until the termination of the experiment.

2.2.4. Iodide through-diffusion - Experiment no. 6

The experiment was started simultaneously with experiment no. 5 on September 28th, 1990, and was terminated on December 21st, 1990, after about only 84 days. In the following figure the measured diffusive flux as function of time together with its error bars representing a 95 % confidence interval is shown.

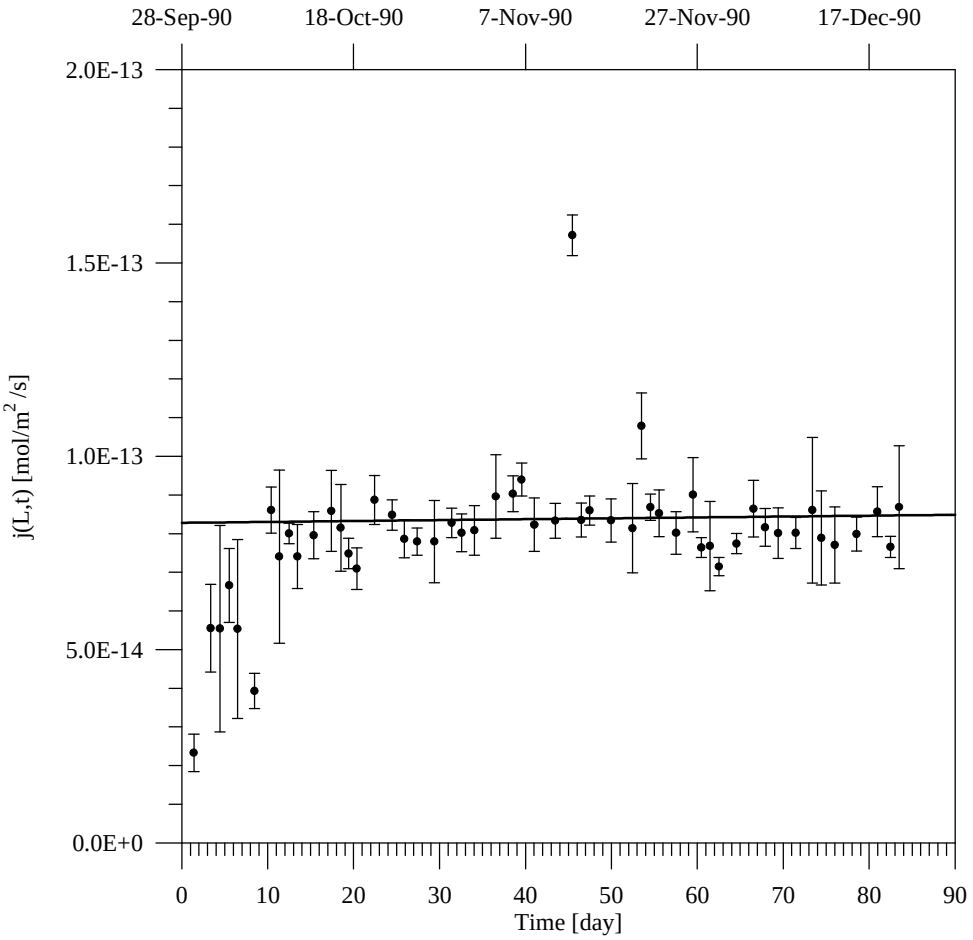

Figure 2.2.4.-1: A semi-log plot of the measured diffusive flux for iodide and experiment no. 6 as a function of time with corresponding error bars representing a 95 % confidence interval. For illustration purposes a linear regression curve (solid line) fitted on all the data beyond 10 days is also shown indicating that nearly a steady-state is reached.

For this experiment, too, the first period of about 10 to 20 days shows a fast increase in the flux values; after that the system is nearly in a steady-state. Such a behaviour is in contradiction to experiment no. 5 where the diffusive flux is always evolving leisurely.

Figure 2.2.4.-2 shows the cumulated diffused iodine mass versus time. There is no problem with achieving an excellent representation of the data by a linear regression curve excluding only the first 6 measurement values for $t < 10$ days which clearly represent a (fast) transient phase of the system. However, the time history of the total diffused mass is not a suitable quantity to determine the time point when a diffusion system has reached a steady-state, because measurement errors enter the quantity cumulatively, a fact which makes long-term modelling based on such a quantity a questionable issue.

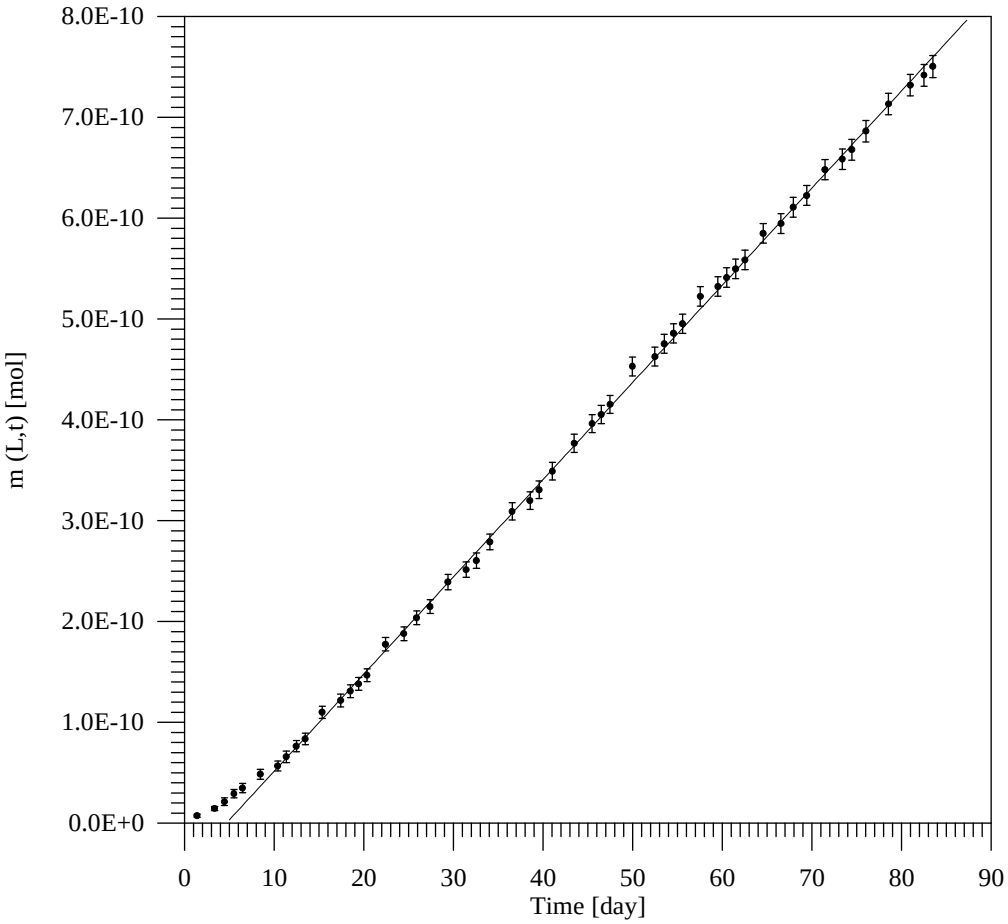

Figure 2.2.4.-2: Plot of the accumulated diffused iodine mass of experiment no. 6 as a function of time together with the error bars which represent a 95 % confidence interval. Steady-state for diffusion could be assumed beyond 10 days, and as it is supported by a linear regression curve (solid line).

Figure 2.2.4.-3 shows the fluctuations in the reservoir concentration $C_0(t)$. For the mean $\overline{C}_0$ a value of about $\overline{C}_0 \pm \Delta C_0 = (3.71 \pm 0.17) \cdot 10^{-8}$ mol/l can be determined (the uncertainty is one standard deviation). Most of the variations are less than ± 10 % of the mean and are caused by the diffusion and up-take of the tracer. Periodically the level was adjusted by adding some concentrated tracer solution to achieve a - more or less - constant boundary condition on the reservoir side.

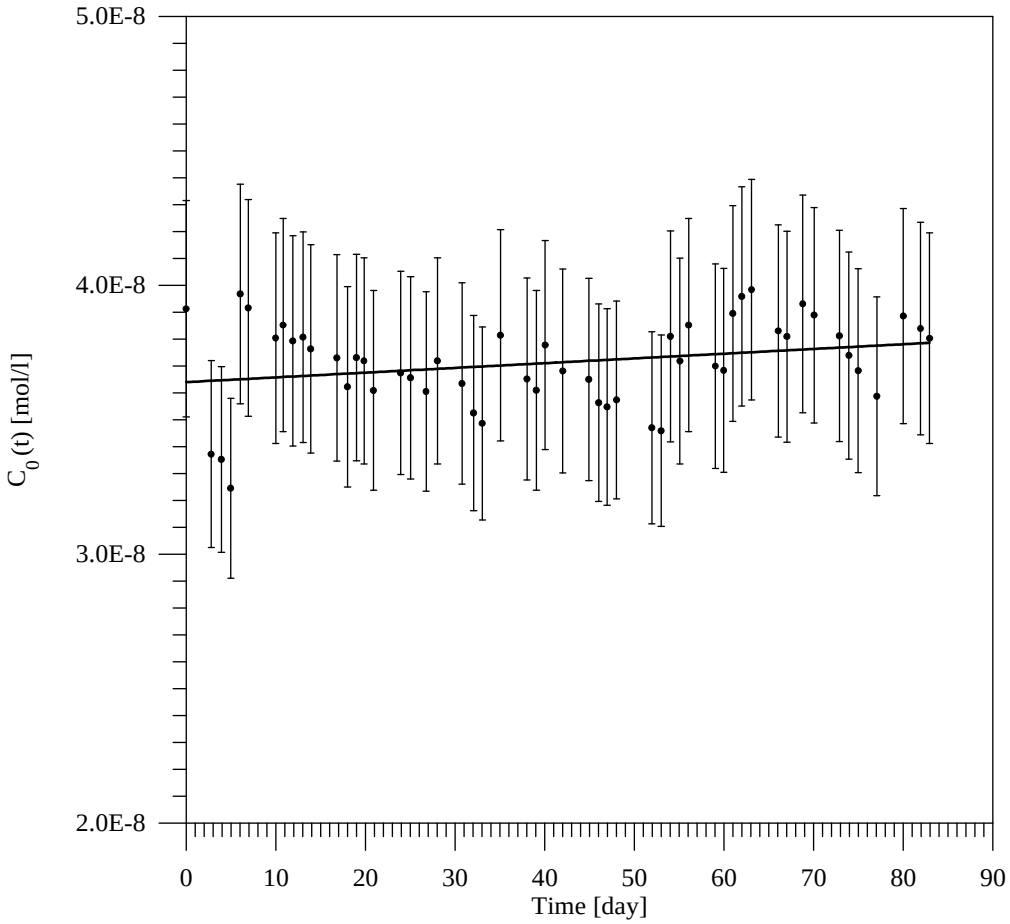

Figure 2.2.4.-3: Plot of the reservoir concentration $C_0\,(t)$ of iodine and experiment no. 6. The error bars are based on two single measurements respectively and correspond to a 95 % confidence interval. As can be seen, fluctuations were mostly less than ± 10 % of the mean $\overline{C}_0$ during the whole period of the experiment. The solid line represents a linear regression of all the measurements which nearly coincides with the mean value of about $3.71 \cdot 10^{-8}$ mol/l.

In the following Figure 2.2.4.-4 the deposited iodine mass $\Delta m(t)$ is plotted versus time. It is evident that deposition is increasing monotonically when neglecting short term variations and does not reach a maximum value during the period of experimentation. Such a behaviour is practically identical to that of the previously described iodine experiment no. 5. For this experiment, too, we consider this as an indication that the system never reached a stationary state and was still slowly evolving after a period of about 84 days.

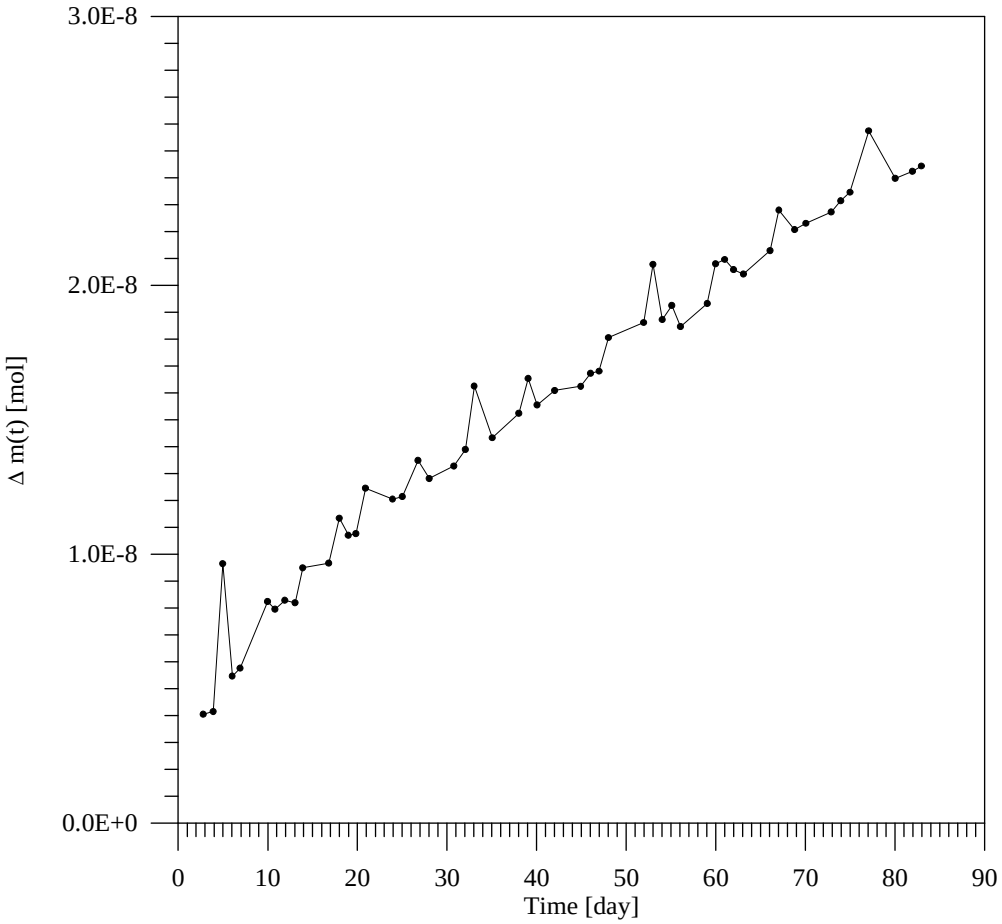

Figure 2.2.4.-4: Mass *Δ m(t)* of iodine and experiment no. 6 deposited within the HCP and - possibly - also onto the walls of the equipment as a function of time. The data are based on a mass balance and - neglecting short time fluctuations - show a continuously increasing up-take until the termination of the experiment.

2.2.5. Caesium through-diffusion - Experiment no. 7

The experiment was started on September 25th, 1990, and was terminated on December 21st, 1990, after about 87 days. In the following figure the measured diffusive flux as a function of time together with the error bars representing a 95 % confidence interval is shown. A total of 57 data pairs are available for the measurement side; for each of those pairs two samples were drawn and evaluated according to the procedure described in the sub-sections (2.1.3) and (2.1.4).

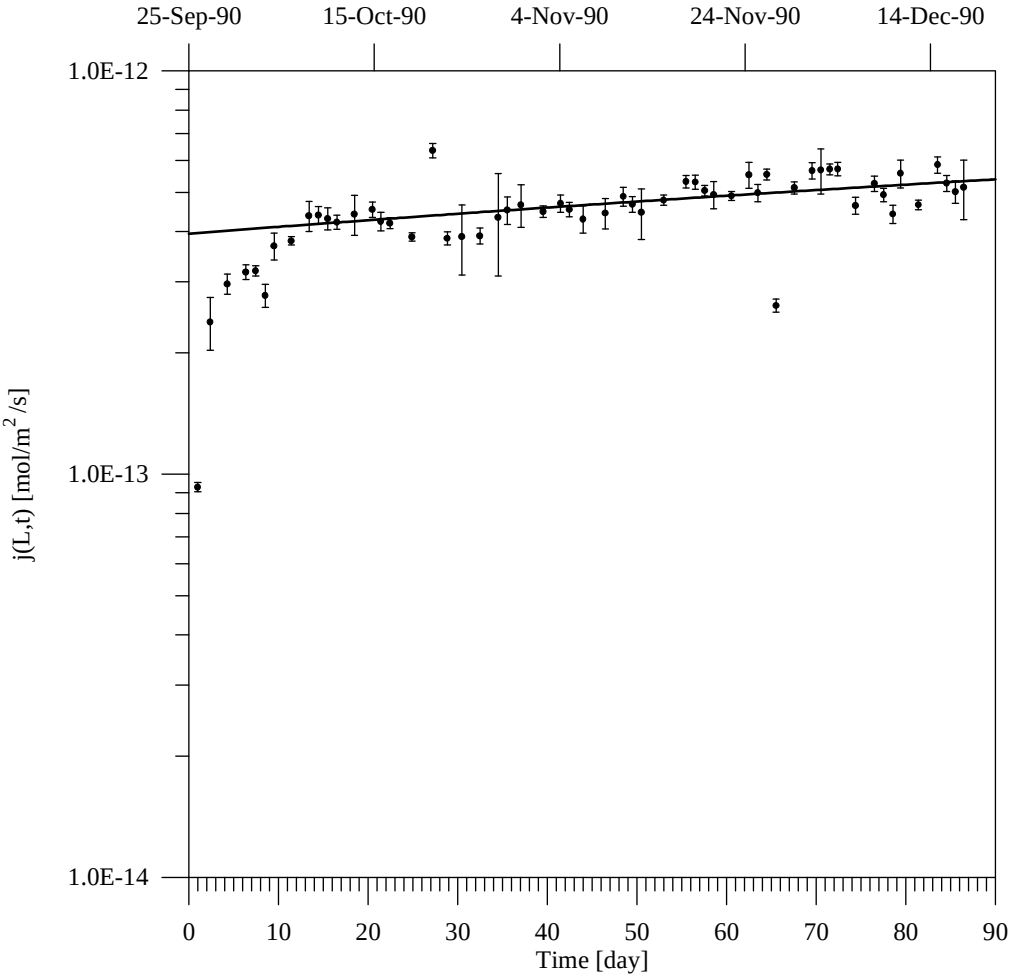

Figure 2.2.5.-1: A semi-log plot of the measured diffusive flux for caesium of experiment no. 7 as a function of time with corresponding error bars representing a 95 % confidence interval. For illustration purposes a linear regression curve (solid line) fitted on all the data beyond 20 days is also shown indicating that steady-state is not yet reached.

The first period of about 20 days shows a fast change in the flux values; after that the system evolves only leisurely. However, the diffusive flux never became constant - a fact which is also supported by a linear regression of the data for $t > 20$ days. From the time history of the flux we conclude that retarding mechanisms such as sorption - as assumed before the experiment - only play a minor rôle.

Figure 2.2.5.-2 shows the accumulated diffused caesium mass versus time. In a series of subsequent linear regressions for the fits we used measured data beyond 20, 30 and 60 days

after the start of the experiment. While the values of the slope of the straight line did not change significantly, its constant became smaller and smaller, also indicating that the system had not reached a stationary state. However, from the small value of t_0 - the intersect of the linear regression curve and the time axis - we expect only little retention of the diffusing caesium. But a more careful evaluation will be the aim of the modelling work, explained in the theory section 3 of this report.

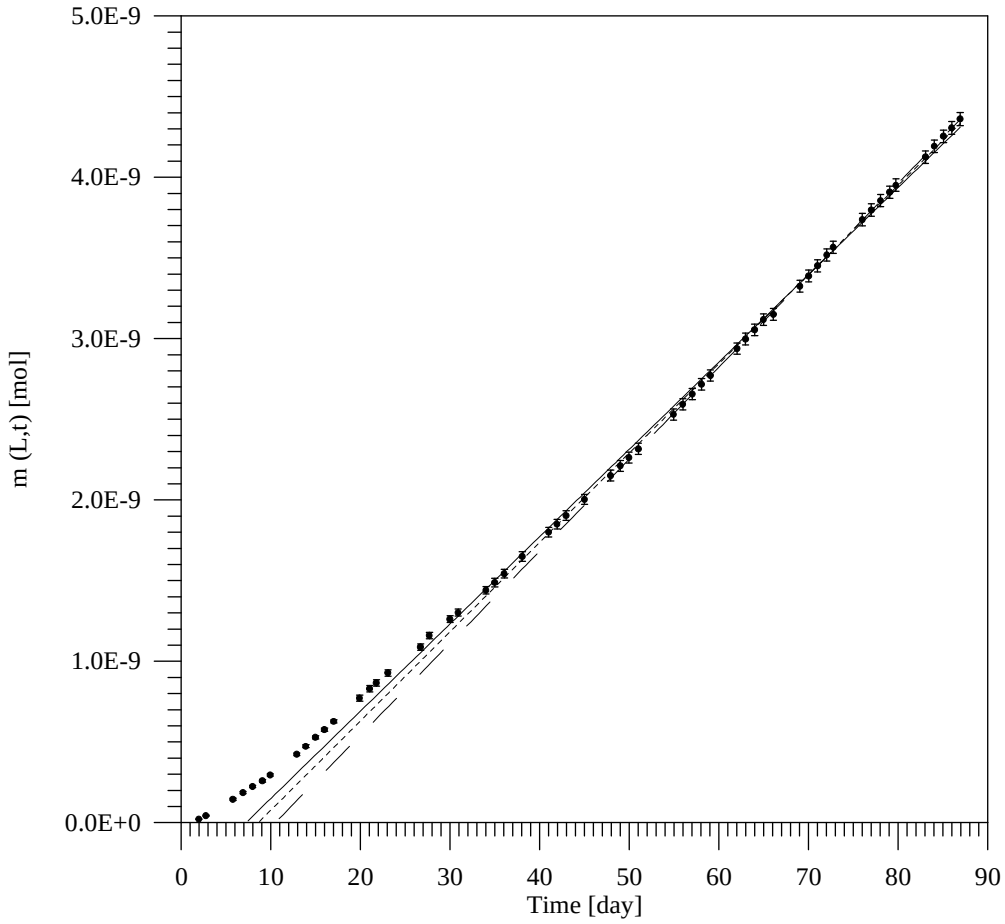

Figure 2.2.5.-2: Plot of the accumulated diffused caesium mass of experiment no. 7 as a function of time together with the error bars which represent a 95 % confidence interval. Drawn are also three linear regression curves using data beyond 20 (solid line), 30 (dashed line) and 60 (broken line) days indicating that caesium diffusion did not reach a stationary state, as we already supposed from the interpretation of the previous figure.

Figure 2.2.5.-3 shows the fluctuations in the reservoir concentration $C_0(t)$. For the mean $\overline{C}_0$ a value of about $\overline{C}_0 \pm \Delta C_0 = (3.82 \pm 0.15) \cdot 10^{-8}$ mol/l can be determined (the uncertainty is one standard deviation). The variations are always less than ± 10 % of the mean and are caused by the diffusion and up-take of the tracer. Periodically the level was adjusted by adding some concentrated tracer solution to achieve a - more or less - constant boundary condition at the reservoir side.

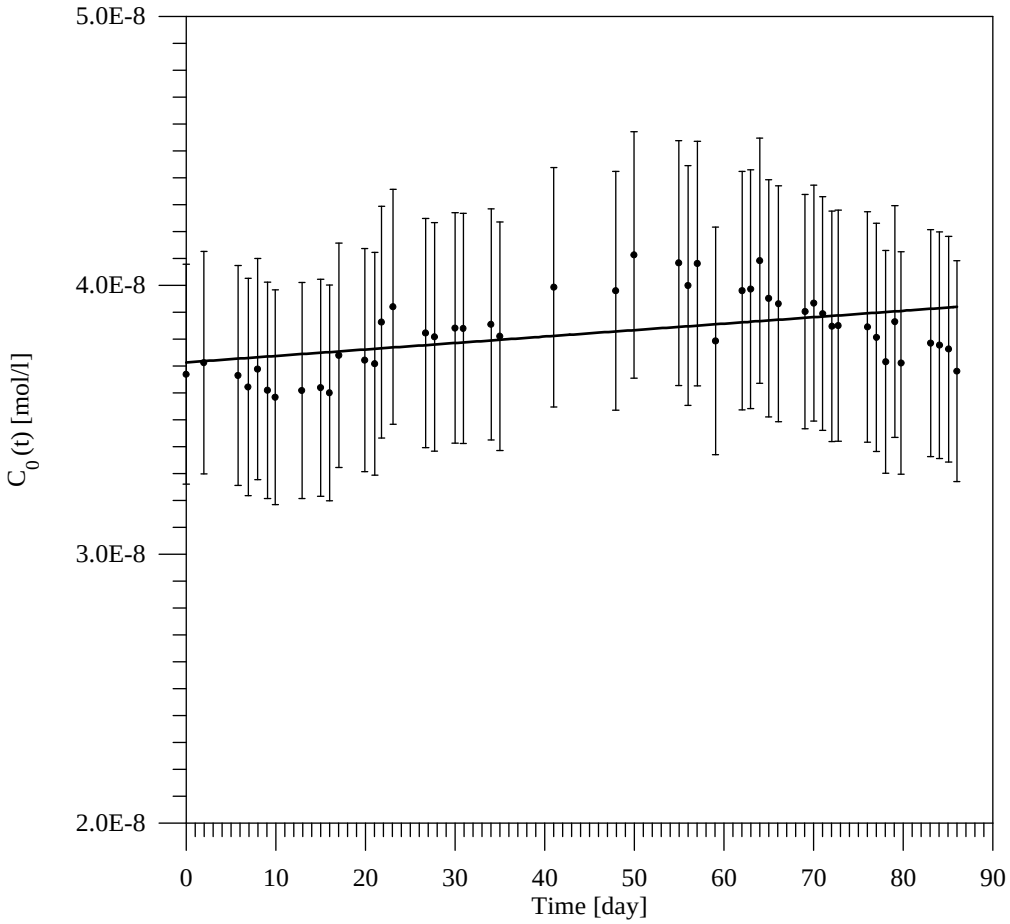

Figure 2.2.5.-3: Plot of the reservoir concentration $C_0(t)$ of caesium and experiment no. 7. The error bars are based on two single measurements to a given time point respectively and correspond to a 95 % confidence interval. As can be seen, fluctuations were always less than ± 10 % of the mean $\overline{C}_0$ during the whole period of the experiment. The solid line represents a linear regression of all measurements. The mean value is about $3.82 \cdot 10^{-8}$ mol/l.

In the last Figure 2.2.5.-4 of this sub-section the deposited caesium mass $\Delta m(t)$ is plotted versus time. Deposition may occur - in principle - in the HCP and/or onto surfaces of the cell and tubes of the diffusion equipment. In contrast to the other experiments with chloride and iodide as tracers no significant caesium deposition can be recognised. The fluctuations are considered as measurement artefacts. The values are always at least an order of magnitude smaller when compared with those, e.g., from iodine diffusion which had - by the way - a comparable reservoir concentration.

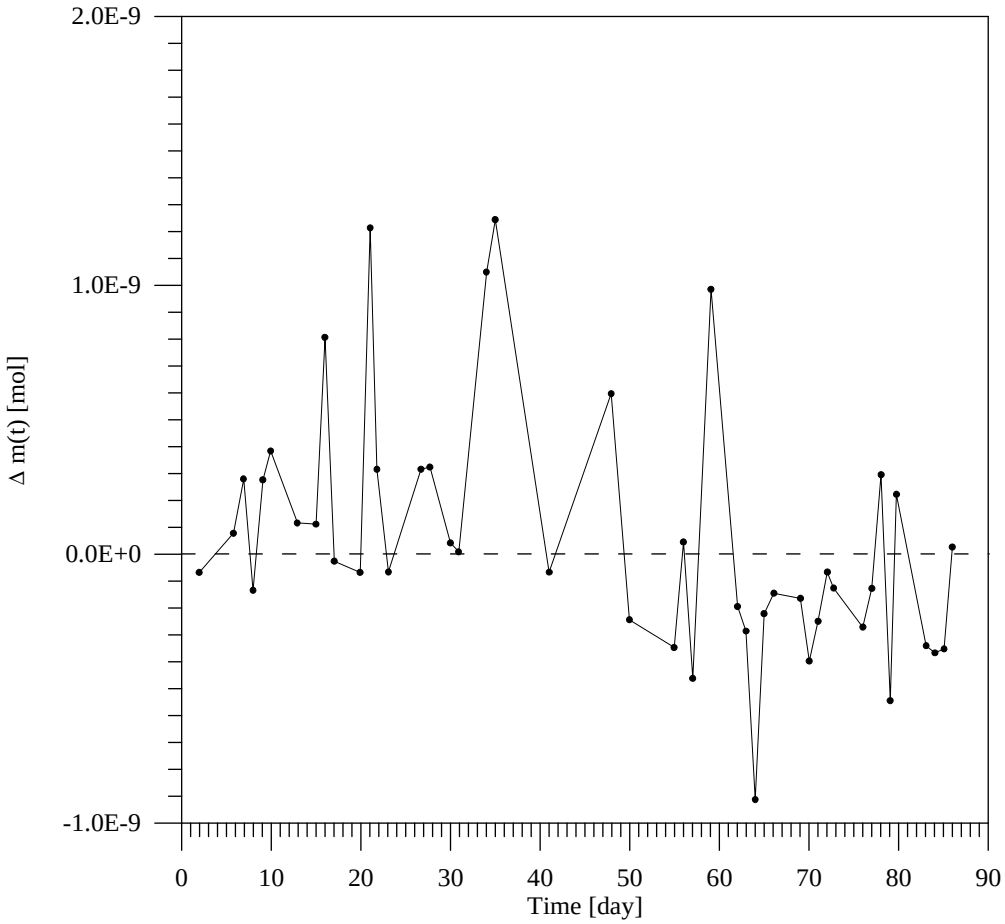

Figure 2.2.5.-4: Mass $\Delta m(t)$ of caesium and experiment no. 7 deposited within the HCP and - possibly - also onto the walls of the equipment as a function of time. The data are based on a mass balance and show - neglecting short time fluctuations - no significant up-take of caesium. (The dashed line represents the zero line.)

2.2.6. Caesium through-diffusion - Experiment no. 8

The experiment was also started on September 25th, 1990, and terminated on December 21st, 1990, after about 87 days. In the following figure the measured diffusive flux as a function of time together with the error bars representing a 95 % confidence interval is shown. As for the other caesium experiment, a total of 57 data pairs are available for the measurement side; for each of those pairs two samples were drawn and evaluated according to the procedure described in the sub-sections (2.1.3) and (2.1.4).

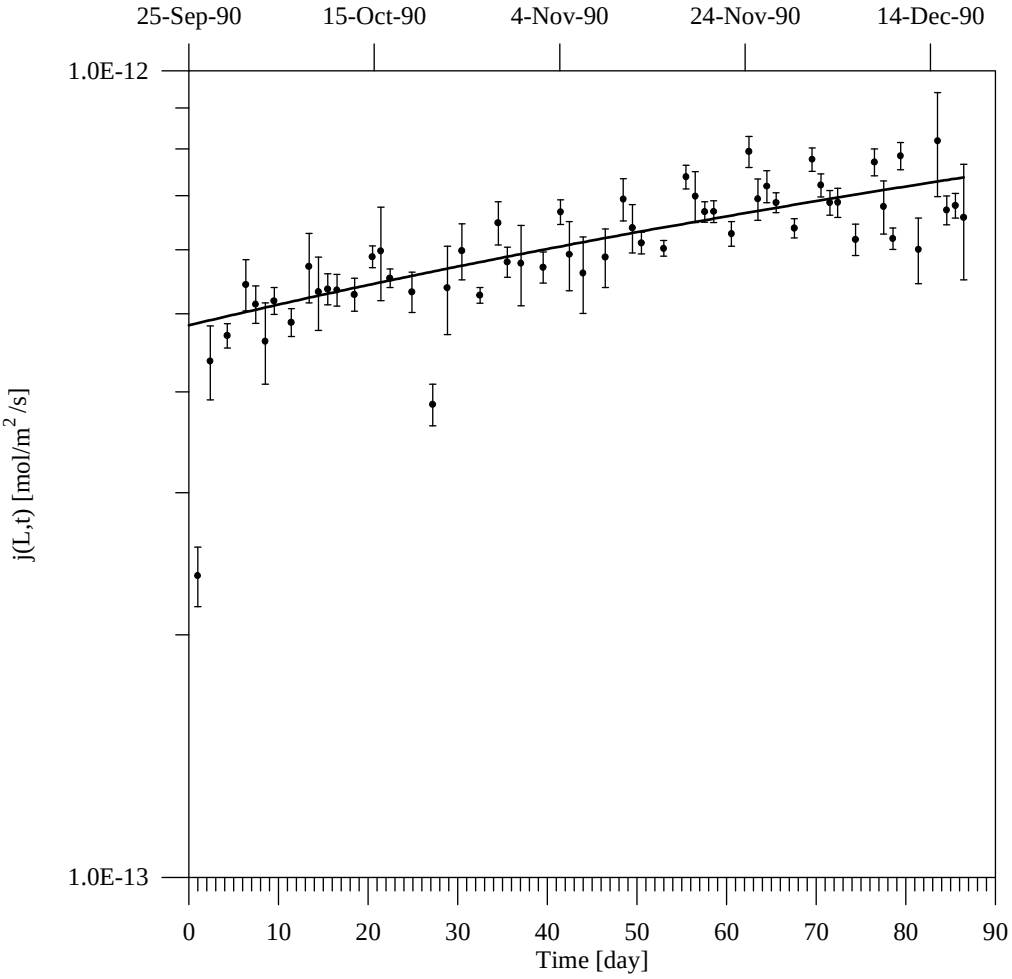

Figure 2.2.6.-1: A semi-log plot of the measured diffusive flux for caesium and experiment no. 8 as a function of time with corresponding error bars representing a 95 % confidence interval. For illustration purposes a linear regression curve (solid line) fitted on all the data beyond 20 days is also shown indicating that steady-state is not yet reached.

Also for this experiment the first period of a few days shows a fast increase in the flux values; after that the system evolves only leisurely until the end of the experiment. However, the diffusive flux never became constant - a fact which is also supported by a linear regression of the data for $t > 20$ days. From the flux evolution in the starting phase (rising edge) we conclude that retarding mechanisms, such as, e.g., sorption, only play a minor rôle.

Figure 2.2.6.-2 shows the accumulated diffused caesium mass versus time. For a series of subsequent linear regressions we only used the measured data beyond 20, 30 and 60 days

respectively. While the value of the slope of the straight line did not change significantly, its constant became smaller and smaller indicating, too, that the system had not reached a stationary state. However, from the small value of t_0 (6.7, 8.3 and 10.6 days) - the intersect of the asymptotic (linear regression) curve and the time axis - we expect only little retention of the diffusing caesium when compared with those values for t_0 extracted from the chloride diffusion profiles. But a more careful evaluation of the measurements will be the aim of the modelling work explained in the theory section 3 of this report.

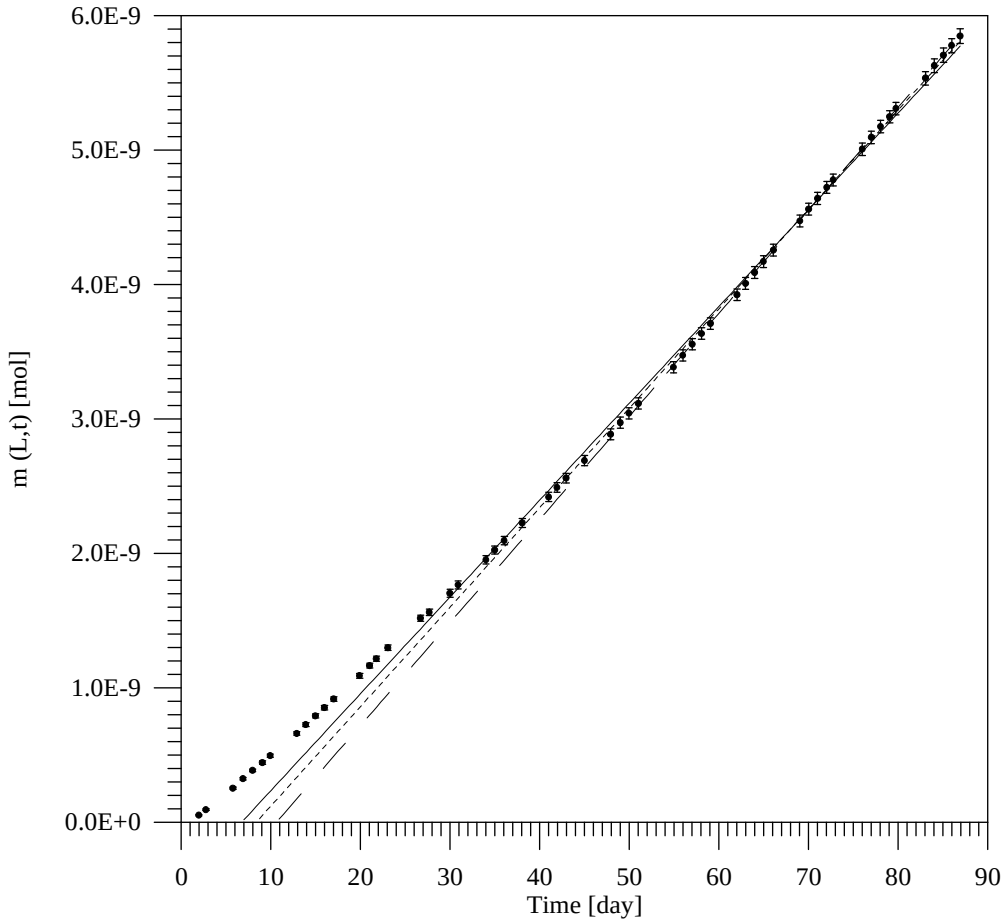

Figure 2.2.6.-2: Plot of the accumulated diffused caesium mass of experiment no. 8 as a function of time together with the error bars which represent a 95 % confidence interval. Drawn are also three linear regression curves using data beyond 20 (solid line), 30 (dashed line) and 60 (broken line) days indicating that caesium diffusion did not reach a stationary state as we already supposed from the interpretation of the previous figure.

Figure 2.2.6.-3 shows the fluctuations in the reservoir concentration $C_0(t)$. For the mean $\overline{C_0}$ a value of about $\overline{C_0} \pm \Delta C_0 = (3.83 \pm 0.17) \cdot 10^{-8}$ mol/l can be determined (the uncertainty is one standard deviation). The variations are always less than ± 10 % of the mean and are caused by the diffusion and up-take of the tracer. Periodically the level was adjusted by adding some concentrated tracer solution to achieve a - more or less - constant boundary condition on the reservoir side.

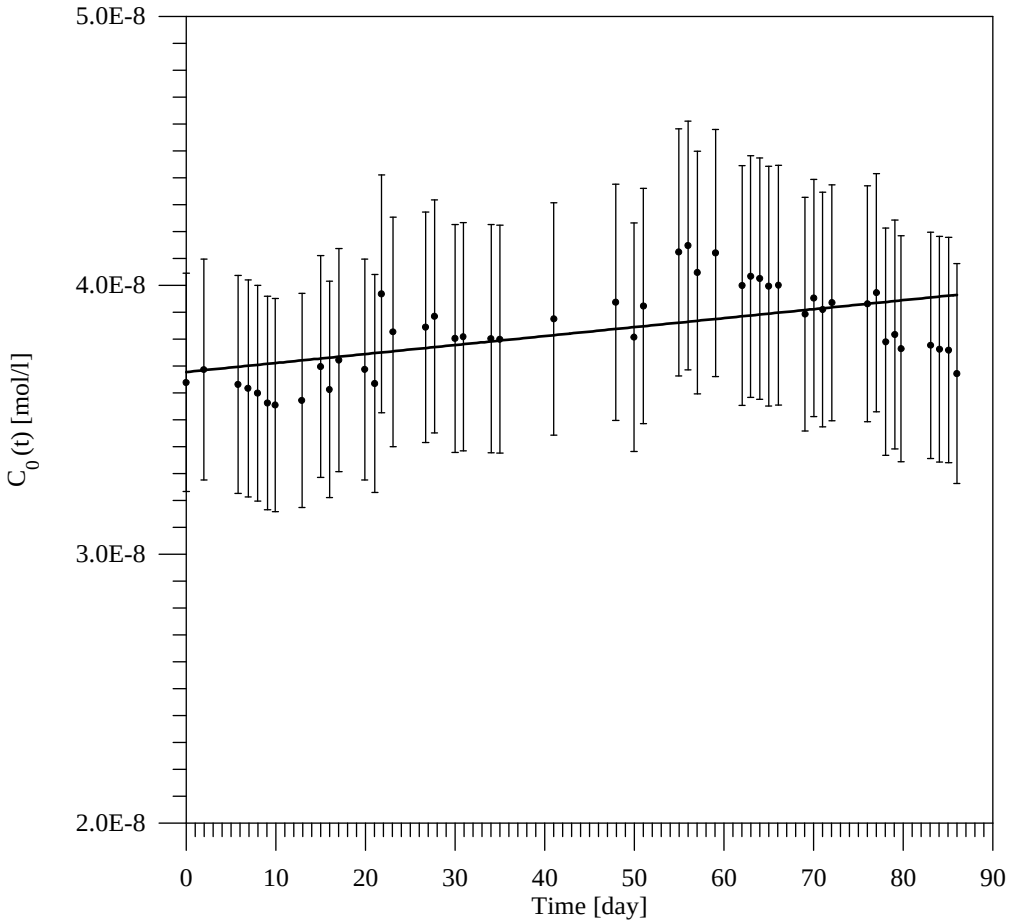

Figure 2.2.6.-3: Plot of the reservoir concentration $C_0(t)$ of caesium and experiment no. 8. The error bars are based on two single measurements to a given time point respectively and correspond to a 95 % confidence interval. As can be seen, fluctuations were always less than ± 10 % of the mean $\overline{C_0}$ during the whole period of the experiment. The mean value $\overline{C_0}$ is about $3.83 \cdot 10^{-8}$ mol/l, and the solid line represents a linear regression of all the measurements.

In the last Figure 2.2.6.-4 the deposited caesium mass $\Delta m(t)$ is plotted versus time. Deposition might occur - in principle - in the HCP and/or onto surfaces of the cell and tubes of the equipment. In contrast to the other experiments with chlorine and iodine as tracers, but in good agreement with the results obtained from the former caesium experiment no. 7, no significant caesium deposition can be recognised. The fluctuations and especially the negative values are considered as due to the uncertainties in the different measurements for achieving $\Delta m(t)$, hence as artefacts. Again, as for experiment no. 7, the range of the values is always at least an order of magnitude smaller when compared with that, e.g., of iodine diffusion.

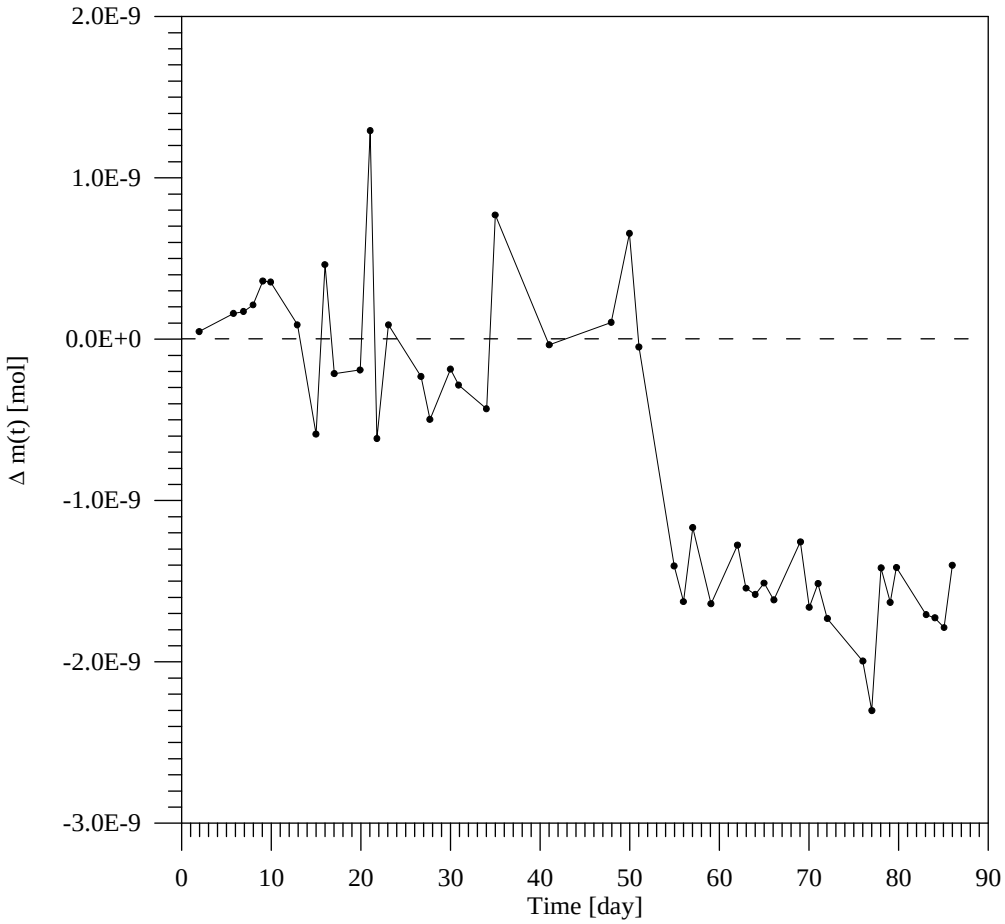

Figure 2.2.6.-4: Mass $\Delta m(t)$ of caesium and experiment no. 8 deposited within the HCP and - possibly - also onto the walls of the equipment as a function of time. The data are based on a mass balance and - neglecting short time fluctuations - show no significant up-take of caesium. (The dashed line represents the zero Δm-line.)

2.3. Experiments with nickel

2.3.1. Data obtained from experiment no. 5

The experiment was started on February 16th, 1993, and terminated on May 3rd, 1994. In the Figure 2.3.1.-1 below, based on totally 291 data pairs, the measured diffusive flux of nickel as a function of time across the boundary at $x = L$ is shown. After about 140 - 150 days nearly steady-state is reached with an approximate value of about $3 \cdot 10^{-13}$ moles / (m^2s) for the diffusive flux. There is no reasonable explanation for the two prominent dips in the steady-state phase after 200 and 320 days.

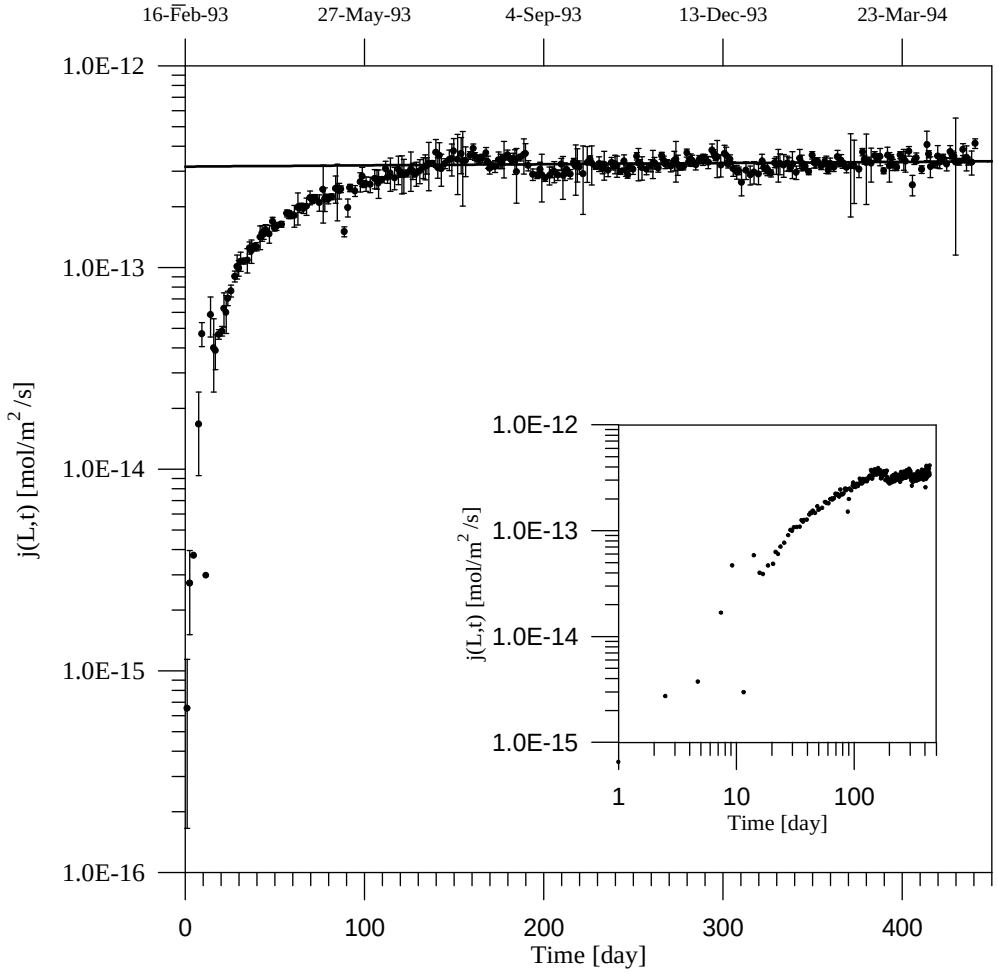

Figure 2.3.1.-1: Measured diffusive flux of nickel (for experiment no. 5), together with the 95 % confidence intervals, across the boundary at $x = L$ as a function of time. As can be seen, nearly steady state is reached after about 140-150 days. This is supported by a linear regression of the measured data above 150 days. The regression curve for the flux (solid line) increases only about 3.7 % in the interval 150 - 440.6 days. In addition, in the lower right corner a log-log representation of the measurements is given.

Using measured data of the “plateau region” above 150 days for a simple linear regression, according to $j(L,t) = a\,t + b$, for the two constants we find:

$$a \pm \Delta a = (4.39 \pm 2.08) \cdot 10^{-17} \ \frac{\text{moles}}{\text{m}^2 \, \text{s} \, \text{day}},$$

$$b \pm \Delta b = (3.17 \pm 0.07) \cdot 10^{-13} \ \frac{\text{moles}}{\text{m}^2 \, \text{s}} \quad ;$$

with an averaged (measured) flux of

$$\bar{j} \pm \Delta j = (3.30 \pm 0.25) \cdot 10^{-13} \ \frac{\text{moles}}{\text{m}^2 \, \text{s}}$$

and

$$\bar{j} \pm \Delta \bar{j} = (3.30 \pm 0.02) \cdot 10^{-13} \ \frac{\text{moles}}{\text{m}^2 \, \text{s}}$$

respectively; hence, in the interval from 150 to 440.6 days the increase is only 3.7 % indicating that the diffusive flux can be considered as constant for practical purposes. To make a rough estimation of the effective diffusion constant we assume a linear concentration profile across the hardened cement paste:

$$C(x)_{\text{steady-state}} = \overline{C}_0 \left(1 - \frac{x}{L} \right) \tag{2.3.1}$$

with mean reservoir concentration $\overline{C}_0$ and with constant (Fickian) flux across the boundary

$$\left. \frac{\partial C}{\partial x} \right|_{x=L} = -\frac{\overline{C}_0}{L} \quad .$$

Inserting the numerical values for C_0 and L and performing an error estimation, we find from

$$D_e = \frac{\bar{j}}{-\left. \frac{\partial C}{\partial x} \right|_{x=L}} = \frac{\bar{j} \, L}{\overline{C}_0} \tag{2.3.2}$$

a value of

$$D_e \pm \Delta D_e = (2.58 \pm 0.20) \cdot 10^{-11} \ \frac{\text{m}^2}{\text{s}} \quad ,$$

which seems reasonable when being compared with literature data [6] and [34]. The largest contribution to the uncertainty (one standard deviation) in D_e stems from the fluctuations of the reservoir concentration around the mean $\overline{C}_0$. The modelling will show whether such a primitive value has to be changed essentially when considering retarding mechanisms which can account strongly for the shape of the transient part of the breakthrough curve.

In the next figure the total diffused nickel mass *m(L,t)* is shown as a function of time. The error bars correspond to a 95 % confidence interval, and each of them is based on two single measurements. After about 100 days *m(L,t)* evolves practically linearly as it would if flux would be constant in time. This assumption is also supported by a linear regression (solid line in the figure) which matches the measurements nearly perfectly. For the fit all the data beyond 80 days were used. Using data beyond 90, 100, ... days did not change the fit-parameter values essentially indicating that the diffusive flux had become nearly constant.

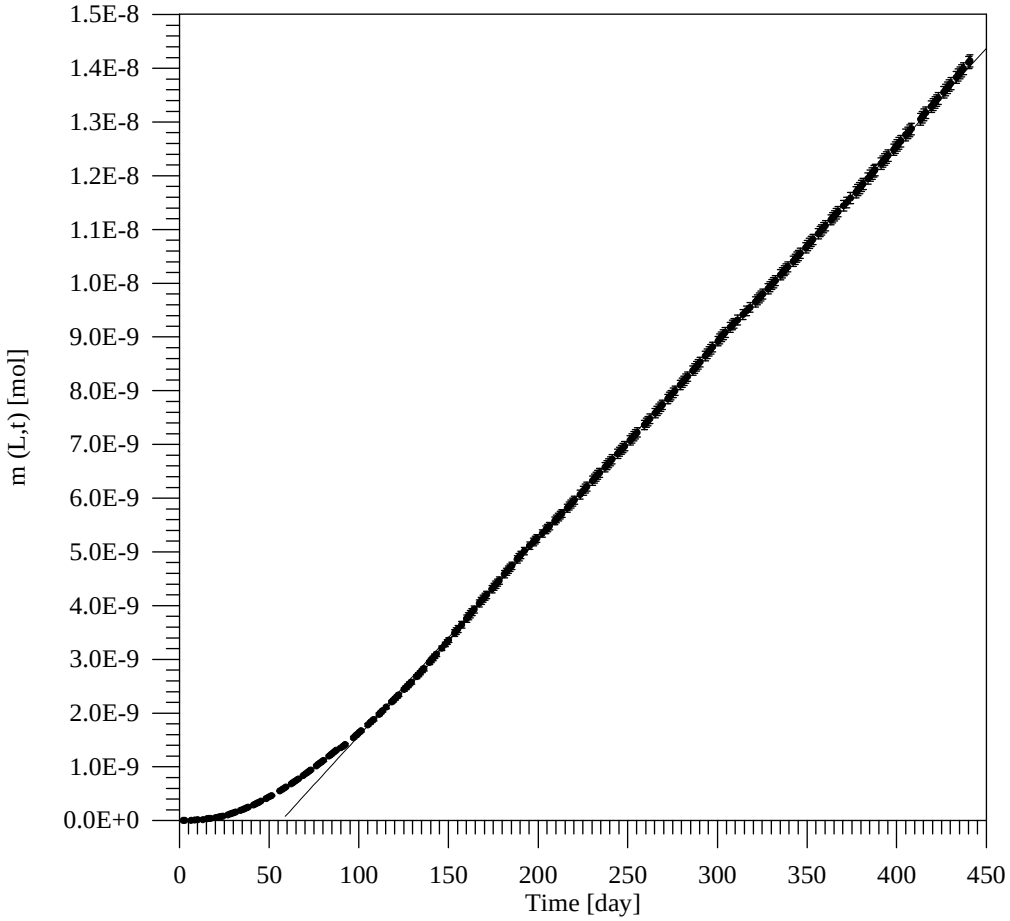

Figure 2.3.1.-2: Total diffused nickel mass *m(L,t)* of experiment no. 5 as a function of time. The error bars represent a 95 % confidence interval, the solid line a linear regression of the measurements beyond 80 days. The excellent agreement of fit and data in the asymptotic limit is considered as an indication that the system has nearly reached a steady-state after about 100 - 150 days.

Although the reservoir had a volume of about 540 ml containing the tracer with a concentration of about 10^{-8} moles/l, the concentration was not constant during the experiment. The evolution of the concentration in the reservoir compartment was followed as a function of time by taking daily samples and measuring the activity. If the concentration had sunk some concentrated tracer was added for adjustment. In the Figure 2.3.1.-3 the time history of the reservoir concentration is shown. It can be recognised that first a fast decrease in the concentration occurred due to tracer up-take of the equipment and the HCP as well as due to the beginning diffusion. The solid line represents a linear regression of the measurements above 80 days which yields a mean value $\overline{C_0} \pm \Delta C_0 = (6.39 \pm 0.47) \cdot 10^{-8}$ moles/l (the uncertainty in the measurements corresponds to one standard deviation).

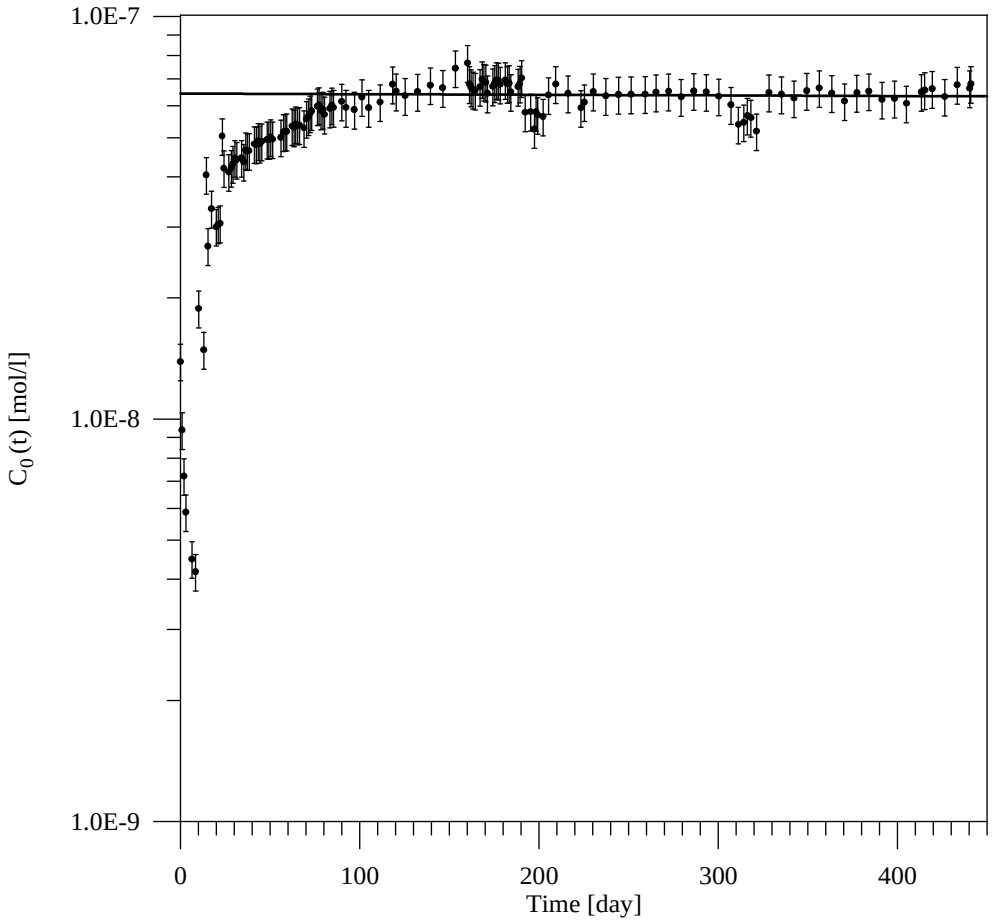

Figure 2.3.1.-3: Time history of the nickel reservoir concentration C_0 *(t)* for experiment no. 5. After the start of the experiment the concentration decreased rapidly by a factor of roughly two due to tracer up-take of the HCP, the walls of the reservoir cell and the tubes and due to the starting diffusion. By some additional (concentrated) tracer the concentration was adjusted. Drawn are also the uncertainties in C_0 which were estimated to be less than ± 10.4 % in maximum. The solid line is a linear regression curve for the data beyond 80 days which coincides well with the mean $\overline{C_0}$ of $6.39 \cdot 10^{-8}$ moles/l.

A mass balance shows that totally $11.5 \cdot 10^{-8}$ moles nickel were applied to the experiment; $5.1 \cdot 10^{-8}$ moles remained on the reservoir side; another $1.4 \cdot 10^{-8}$ moles were diffused through the HCP to the measurement cell hence; $\Delta m(t) = 5.0 \cdot 10^{-8}$ moles were taken up by the HCP and the equipment.

There is no simple functional relationship between time and the up-taken amount of nickel as can be seen in the following Figure 2.3.1.-4. The plot clearly shows a subsequent tracer release for about 150 days after reaching a (global?) maximum after about 30 days. However, there is no reasonable explanation for such a slow tracer release. After this interval of altogether 180 days and when compared to the maximum value, the total amount of up-taken nickel remained on a 30 % lower level, being - more or less - constant for another 260 days, until the termination of the experiment; however, with a slight tendency to greater values of Δm. A simple linear regression of the data for $t > 150$ days supports this assumption but stays in contradiction with the conclusion, drawn from the evaluation of the flux data, that the system has reached a near steady-state phase.

Whether tracer was also released from the equipment, especially from the walls on the reservoir side of the diffusion cell, can hardly be ascertained because several times concentrated tracer was added by the experimentalists for the adjustment of the reservoir concentration.

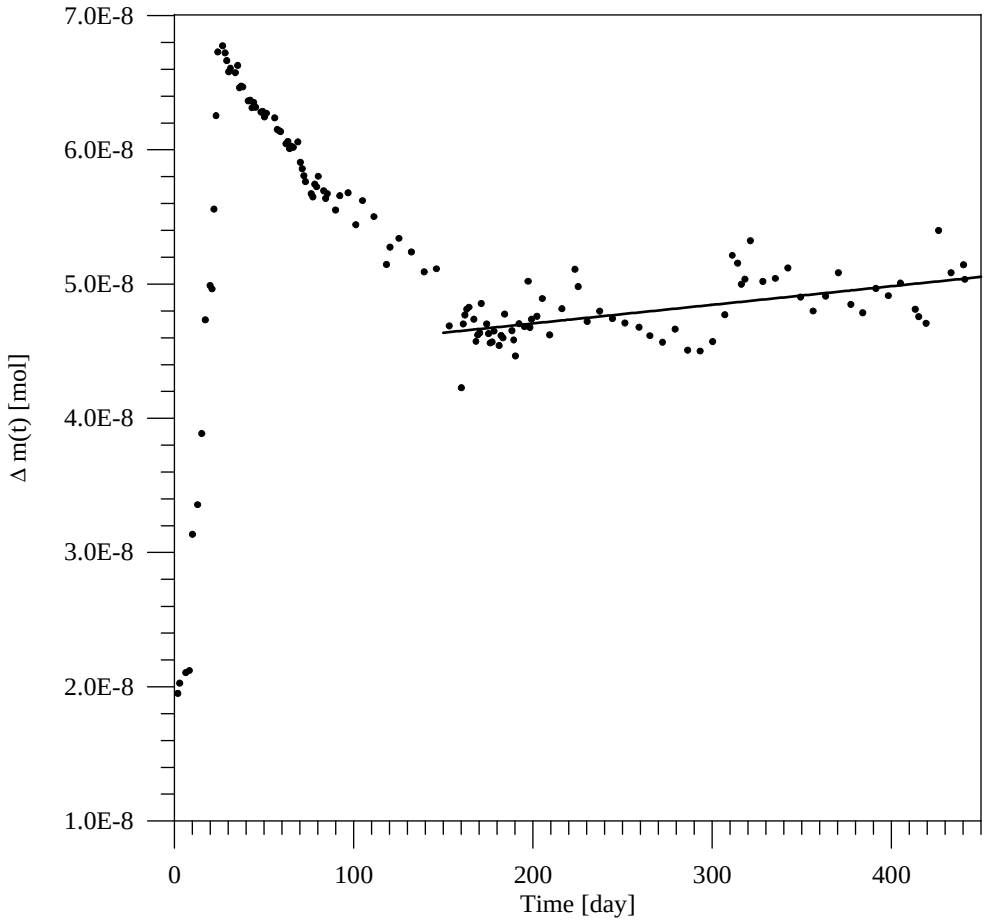

Figure 2.3.1.-4: The total amount of nickel $\Delta m(t)$ of the HCP and the equipment as a function of time based on a mass balance for experiment no. 5. Shortly after the beginning of the experiment the total nickel quantity reaches a maximum followed by a slow decrease. After about 150 days an averaged value of about $4.8 \cdot 10^{-8}$ mole is reached with a slight shift towards greater values. This is supported by a linear regression of all the data for $t > 150$ days which is represented in the figure by the straight line.

2.3.2. Data obtained from experiment no. 6

The experiment was started on February 16th, 1993 and terminated on November 10th, 1995. In the Figure 2.3.2.-1 below, based on totally 430 data pairs, the measured diffusive flux of nickel as a function of time across the boundary at $x = L$ is shown. After about 120 - 130 days an asymptotic phase is reached with an averaged value for the flux of about $1.8 \cdot 10^{-13}$ moles$/(m^2 s)$. However, there can be seen in the plot that the flux is still slightly increasing. Compared to the steady-state value of experiment no. 5 the values of *j(L,t)* of experiment no. 6 are about 40% smaller and correspond to the lower reservoir concentration.

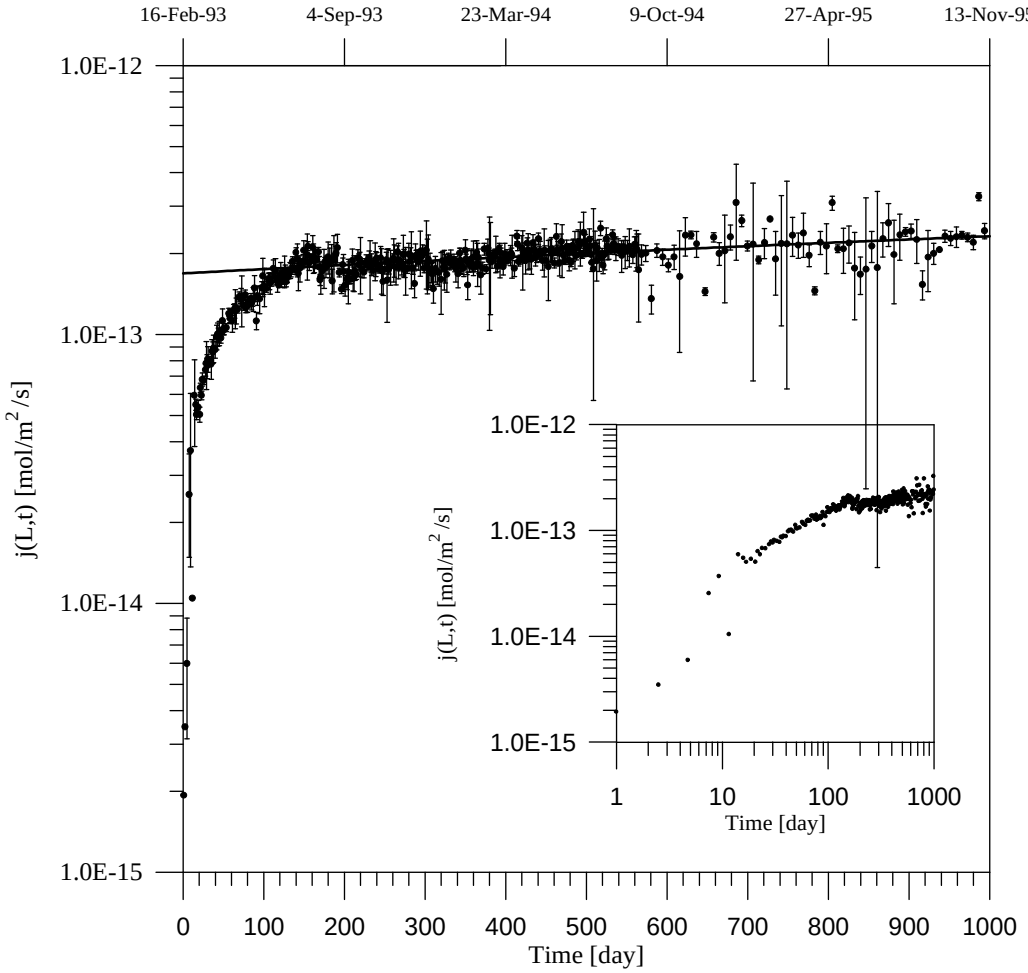

Figure 2.3.2.-1: Measured diffusive flux of nickel of experiment no. 6, together with the 95 % confidence intervals, across the boundary at $x = L$ as a function of time. As can be seen, nearly steady-state is reached after about 140-150 days, but with a shift to increased flux. The assumption of a systematic shift of the measured flux values is supported by a simple linear regression of the measured data above 150 days. The regression curve for the flux (solid line) increases indeed by about 30.3 % in the interval between 150 and 993.8 days. In addition, in the lower right corner a log-log representation of the measured data is given.

Using measured data of the "plateau region" above 150 days for a simple linear regression according to $j(L,t) = a\,t + b$ for the two constants we find:

$$a \pm \Delta a = (6.32 \pm 0.53) \cdot 10^{-17} \frac{\text{moles}}{\text{m}^2\,\text{s}\,\text{day}},$$

$$b \pm \Delta b = (1.69 \pm 0.03) \cdot 10^{-13} \frac{\text{moles}}{\text{m}^2\,\text{s}} \quad .$$

Such a value for *a* (the slope of the regression curve) is roughly a factor of 1.5 larger when compared with that for experiment 5. For the diffusive flux at *t* = 150 and 993.8 days, respectively we find:

$$j(L,150) \cong 1.78 \cdot 10^{-13} \frac{\text{moles}}{\text{m}^2\,\text{s}} \quad ,$$

and

$$j(L,993.8) \cong 2.32 \cdot 10^{-13} \frac{\text{moles}}{\text{m}^2\,\text{s}} \quad ;$$

hence, the difference is about 30.3 % indicating that the diffusive flux cannot be considered as constant for practical purposes in the interval from 150 to 993.8 days. Consequently, we do not estimate a value for the effective diffusion constant according to equation (2.3.2); this will be the goal of the subsequent modelling work.

Both experiments, no. 5 and no. 6, were started simultaneously and in the same glove-box. Therefore it seems reasonable to assume the same experimental conditions for both experiments, if we explicitly exclude handling errors or a systematic change of the boundary conditions being involved. It seems obvious to interpret the continuous shift in the diffusive flux as a result of sample heterogeneities and/or kinetics of a further transport mechanism such as sorption or (surface) precipitation, etc. However, it is mysterious why the mechanisms should be different for the two experiments.

Figure 2.3.2.-2 shows the time history of the total diffused nickel mass *m(L,t)* based on 430 data pairs. Neglecting a short transient phase of about 200 days, *m(L,t)* seems to increase practically linearly. However, using data beyond 150, 300 and 500 days for a series of linear regressions clearly shows that the system had not reached a stationary phase. The intersection of the linear regression curves with the time axis moves from 74.2 to 90.9 and further to 108.3 days, indicating that the system was always slowly evolving.

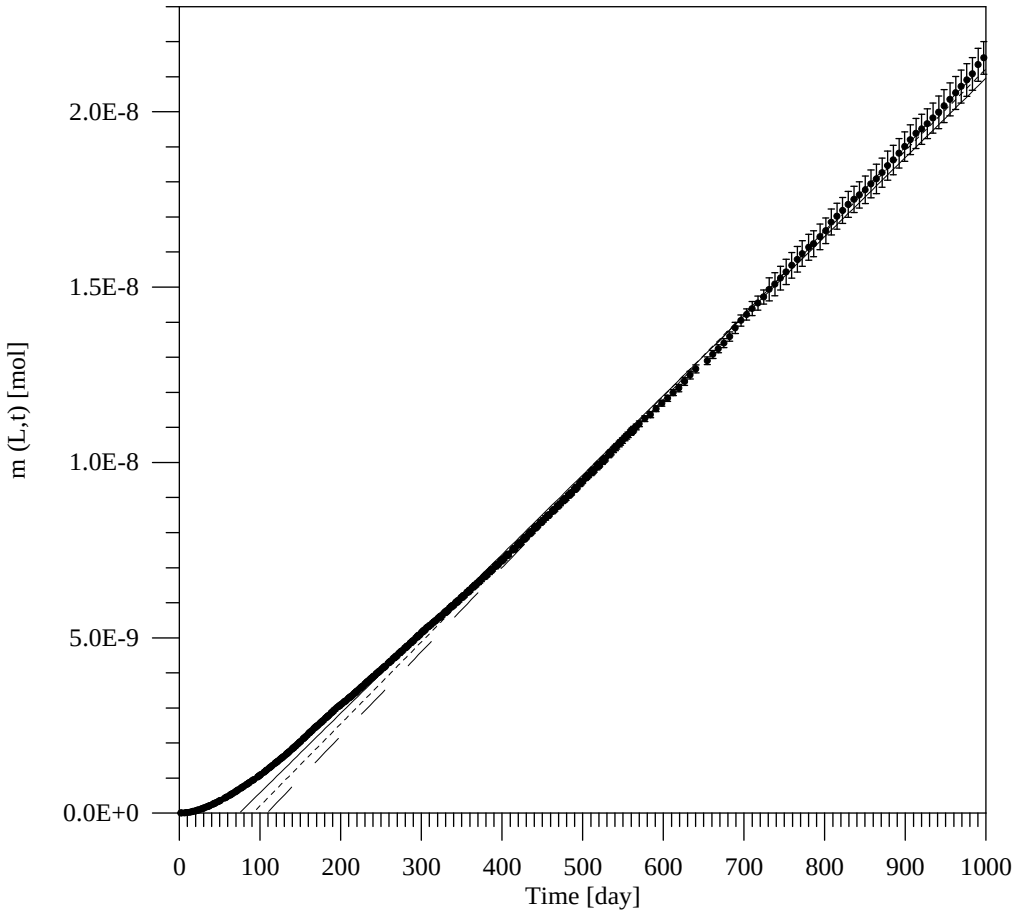

Figure 2.3.2.-2: Time history of the total diffused nickel mass *m(L,t)* for experiment no. 6. After a transient phase of about roughly 200 days the system seems to be in steady-state because *m(L,t)* increases practically linearly with time. However, a series of subsequent linear regressions of the data beyond 150 (solid line), 300 (dashed line) and 500 days (broken line) clearly demonstrate that this assumption is too hasty, because the intersection of the linear regression curve with the time axis continuously moves to greater times again indicating that the diffusive flux must be slowly increasing.

For completeness we also present the reservoir concentration $C_0(t)$ which consists of 216 data pairs. Similar to the profile of co-experiment no. 5 we can see that here, too, the concentration drops to about 1/4 of the initial concentration shortly after the beginning of the experiment indicating that some nickel had been taken up by the equipment and the HCP. During the experiment the reservoir concentration was adjusted several times by adding some concentrated tracer solution resulting in smooth ups and downs around the mean. With the help of a linear regression of all the data pairs for the mean $\overline{C_0}$ a value of $\overline{C_0} \pm \Delta C_0 = (3.67 \pm 0.42) \cdot 10^{-8}$ mol/l was determined. The uncertainty in the measurements corresponds to one standard deviation.

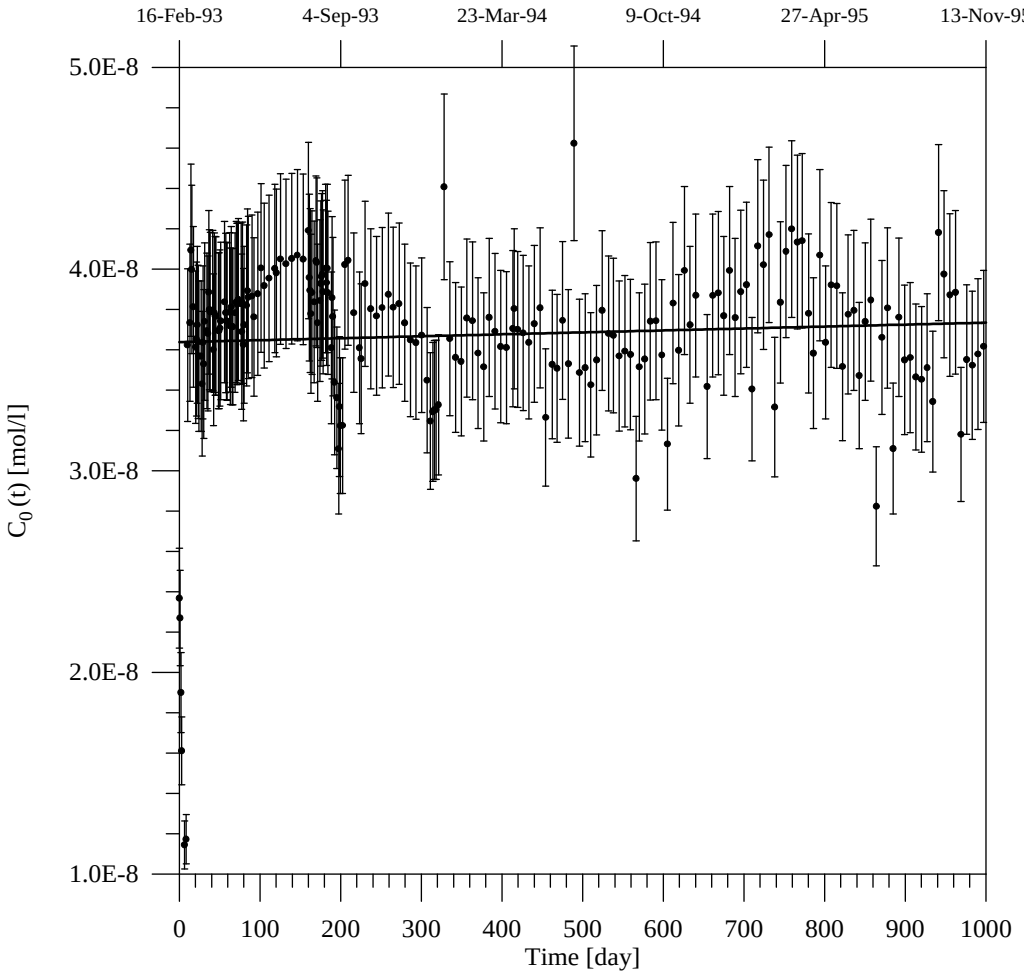

Figure 2.3.2.-3: Time history of the nickel reservoir concentration C_0 *(t)* for experiment no. 6. After the start of the experiment the concentration decreased rapidly by a factor of roughly four due to tracer up-take of the HCP, the walls of the reservoir cell and the tubes and due to starting diffusion. By some additional (concentrated) tracer the concentration was adjusted. Drawn is also the uncertainty in C_0 which was estimated to be ± 10.4 %. The solid line represents a linear regression curve of all the data practically coinciding with the mean $\overline{C_0} = 3.67 \cdot 10^{-8}$ mol/l.

Finally, in Figure 2.3.2.-4 we present the results of a careful mass-balance based on totally 216 data pairs. The total applied nickel mass on the reservoir side was about $8.44 \cdot 10^{-8}$ moles; $3.38 \cdot 10^{-8}$ moles or 40.0 % remained on the reservoir side (or were partially removed by drawing samples), and another $2.15 \cdot 10^{-8}$ moles or 25.5 % were diffused through the cement paste, hence $\Delta m(t) = 2.90 \cdot 10^{-8}$ moles or 34.4 % were taken up by the equipment and the HCP. As can be seen in the figure there is again no simple functional relationship for the time history of the nickel deposition. A fast up-take can be recognised shortly after the beginning of the experiment reaching a local maximum after about 70 days. For another 130 days - and when neglecting short time variations - some nickel becomes mobile again followed by a slow increase of $\Delta m(t)$ until the end of the experiment. The question, whether the nickel deposition has finally come to an end, cannot be answered, in view of the existing data on up-taken tracer. However, from the previous and preliminary discussion concerning flux and total diffused mass measurements we know that this can hardly be the case.

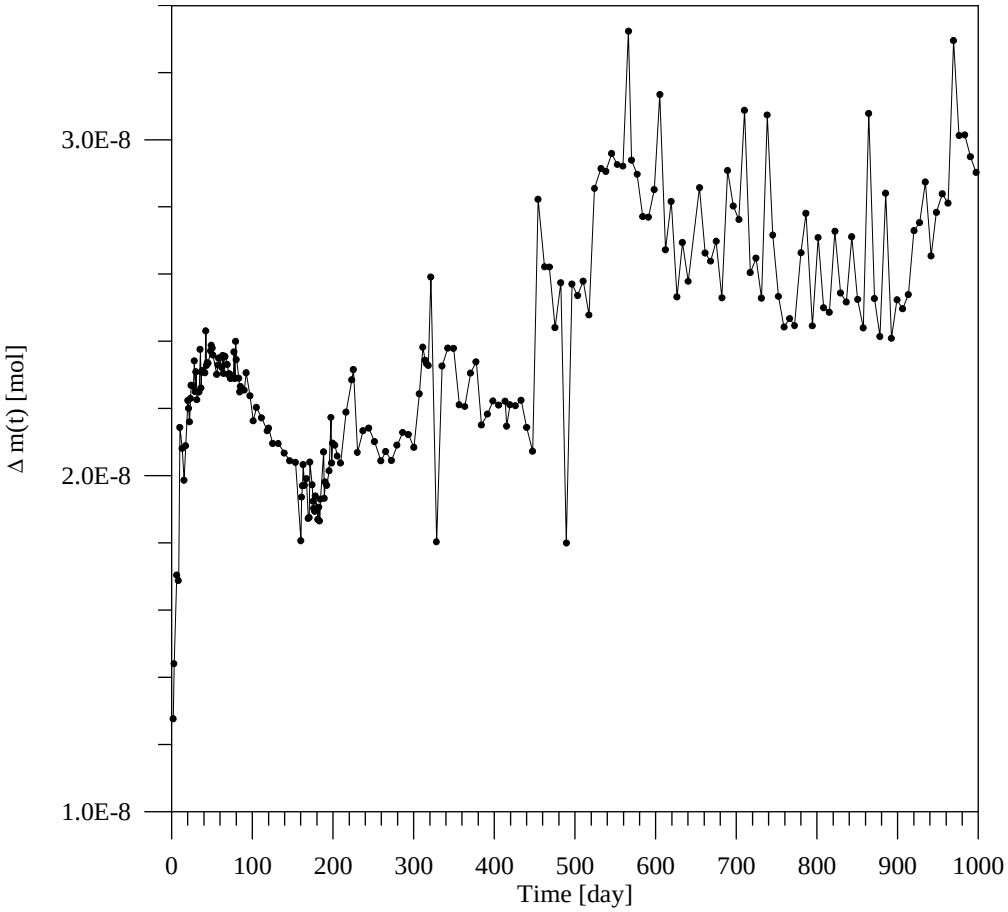

Figure 2.3.2.-4: The total amount of nickel of the HCP and the equipment as a function of time based on a mass balance for experiment no. 6. Shortly after the beginning of the experiment the deposited nickel quantity reaches a local maximum at about 70 days followed by a slow decrease. After this period the up-taken amount of nickel increases again when neglecting short time variations. However, based on these data it is difficult to decide, even in the last phase of the experiment, whether the process of nickel deposition has reached a stationary state.

Both nickel experiments no. 5 and 6 show the same qualitative behaviour for $\Delta m(t)$ for the first 450 days. However, for experiment no. 6 the data are, in general, too low even when taking into account that the reservoir concentration is 40% smaller. There is, so far, no reasonable explanation for the differences in the measurements between these two equivalent experiments which were performed simultaneously in the same glove-box.

Finally, after a duration of 994 days, a value of the nickel deposition onto surfaces of the equipment was extracted. First an (averaged) concentration of both the reservoir and the measurement side was determined yielding a value of $\overline{C} = (3.33 \pm 0.44) \cdot 10^{-8}$ moles/l (one standard deviation error). Then the diffusion barrier and the liquid in both cavities were removed. To mobilise the nickel 200 ml of 0.1N hydrochloric acid were filled into the diffusion apparatus and continuously pumped through the equipment. To measure the activity of the solution after about two days nine samples were drawn. Then this flushing procedure was repeated once more. The measurements in the β-counter yielded (one standard deviation errors):

Dissolved nickel in the first flushing	$(9.78 \pm 0.10) \cdot 10^{-9}$ moles
Dissolved nickel in the second flushing	$(0.294 \pm 0.012) \cdot 10^{-9}$ moles
Total dissolved nickel	$(1.01 \pm 0.02) \cdot 10^{-8}$ moles.

Comparing this data pair with the estimation for nickel deposition onto poly-styrene described in sub-section 2.1.5 concerning blank values we recognise that the data are in good agreement with our former considerations.

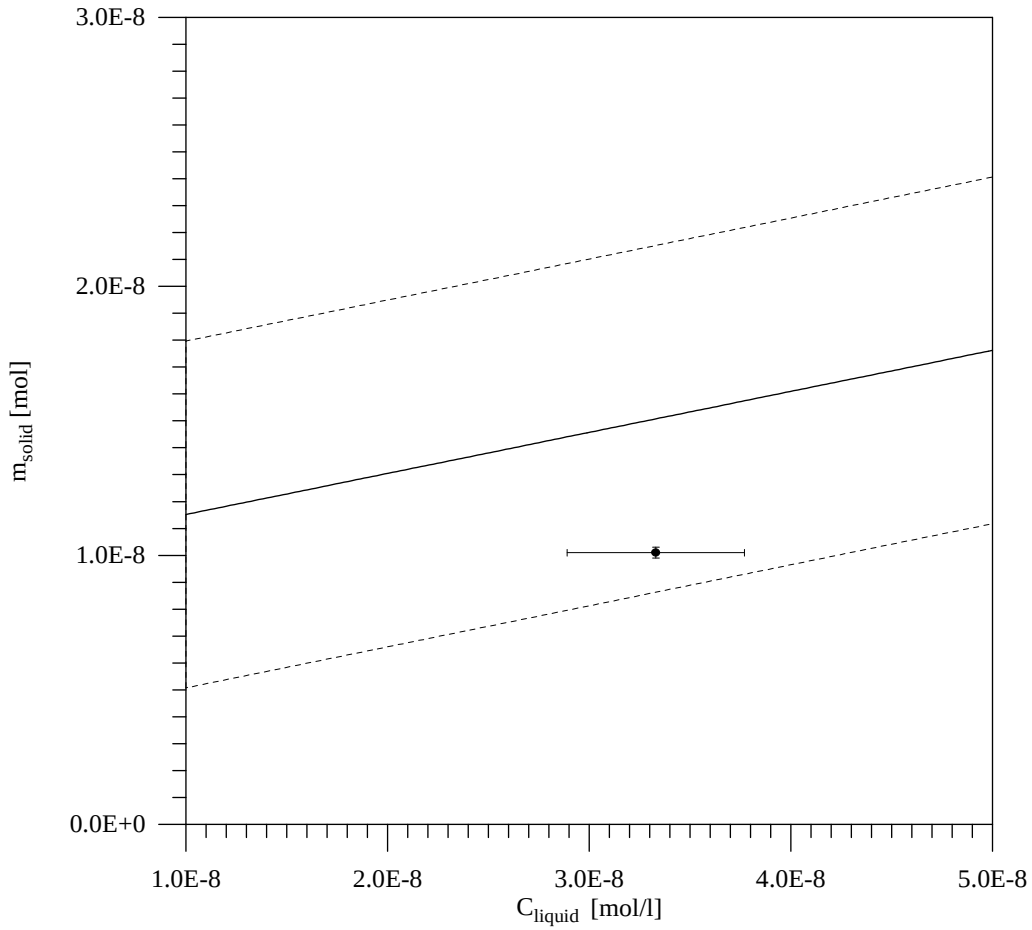

Figure 2.3.2.-5: The deposited nickel mass onto surfaces of the equipment versus the averaged concentration of the liquid at the end of the diffusion experiment no. 6. The solid line represents the linear functional relationship derived in subsection 2.1.5. together with its error range limited by the two dashed lines. The extracted value with one standard deviation error seems to be comparable with our former considerations concerning nickel up-take by the poly-styrene equipment.

At last the hardened cement past was frozen for further investigations. For that, within the CO_2 and O_2-free atmosphere of the glove box the liquid on both sides of the HCP was sucked off and the adhering solution onto the sample holder was dabbed. Then, the HCP in the sample holder was packed into a poly-ethylene bag, enclosed up-right standing in a plastic vessel and frozen in a freezer at -18° C.

2.3.3. Data obtained from experiment no. 7

The experiment was started on July 26th, 1993, and terminated on September 5th, 1994. In Figure 2.3.3.-1 below, based on 266 data pairs, the measured diffusive flux of nickel as a function of time across the boundary at $x = L$ is shown. After about 70 - 80 days the temporal change in the flux is decreasing rapidly, but a “steady-state phase” is never reached. In the plot there can be seen that the flux is still increasing, and compared to the flux of experiment no. 6 this increase is even more pronounced. There is no explanation for the dips between 160 - 210 days.

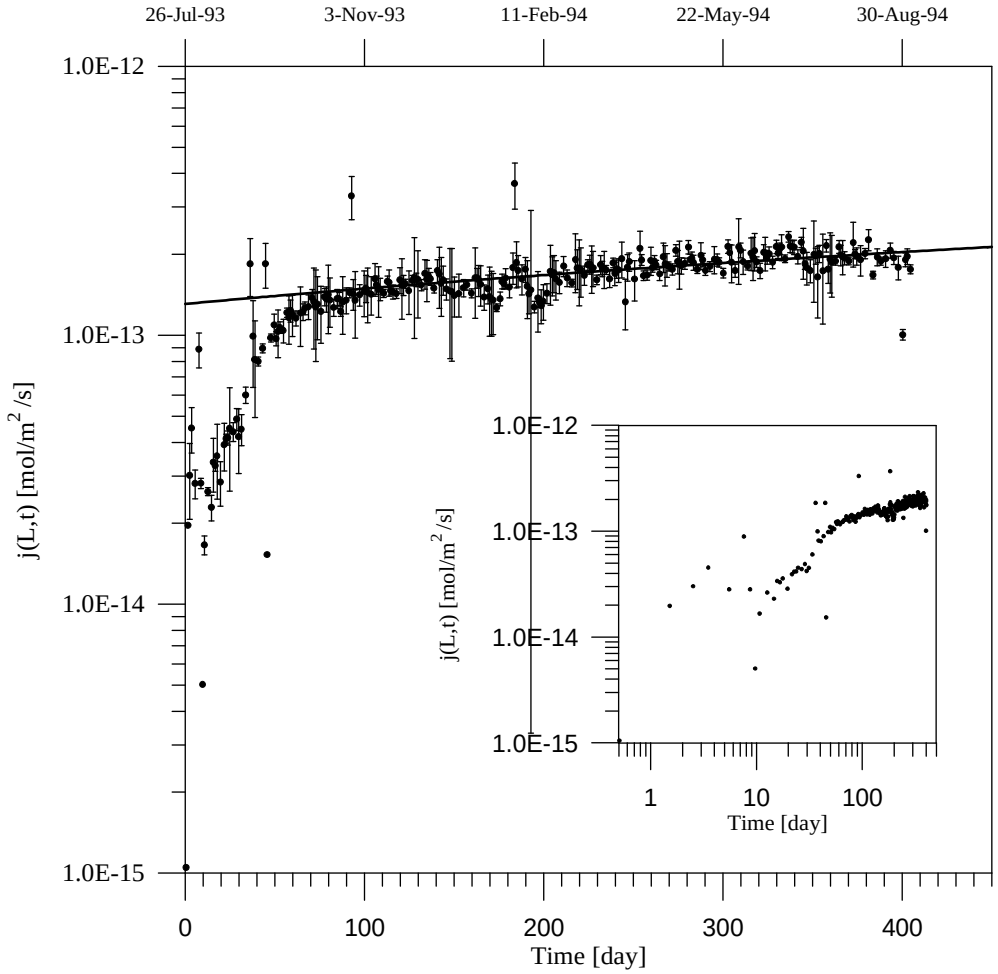

Figure 2.3.3.-1: The measured diffusive flux of nickel (for experiment no. 7), together with the error bars each of them representing a 95 % confidence interval, across the boundary at $x = L$ as a function of time. In contradiction to the results obtained from experiment no. 5 the flux does not become constant, however is strongly reduced after about 80 days, indicating that the system as such never reaches a steady state. This is also supported by a simple linear regression of the measured data above 100 days. The regression curve (solid line) increases indeed by about 37.6 % in the interval from 100 up to 404.6 days. In addition, in the lower right corner a log-log representation of the measurements is shown.

Using measured data beyond 100 days for a simple linear regression according to $j(L,t) = a\,t + b$ for the two constants we find:

$$a \pm \Delta a = (18.3 \pm 1.8) \cdot 10^{-17}\ \frac{\text{moles}}{\text{m}^2\,\text{s}\,\text{day}} \quad ,$$

$$b \pm \Delta b = (1.31 \pm 0.05) \cdot 10^{-13}\ \frac{\text{moles}}{\text{m}^2\,\text{s}} \quad ,$$

with

$$j(L,100) \cong 1.49 \cdot 10^{-13}\ \frac{\text{moles}}{\text{m}^2\,\text{s}} \quad ,$$

and

$$j(L,404.6) \cong 2.05 \cdot 10^{-13}\ \frac{\text{moles}}{\text{m}^2\,\text{s}} \quad ;$$

hence, the difference is about 37.6 % so that the diffusive flux can never be considered as constant in the measurement interval. Consequently, we also do not estimate a value for the effective diffusion constant according to equation (2.3.2).

The next figure illustrates the time history of the total diffused nickel mass.

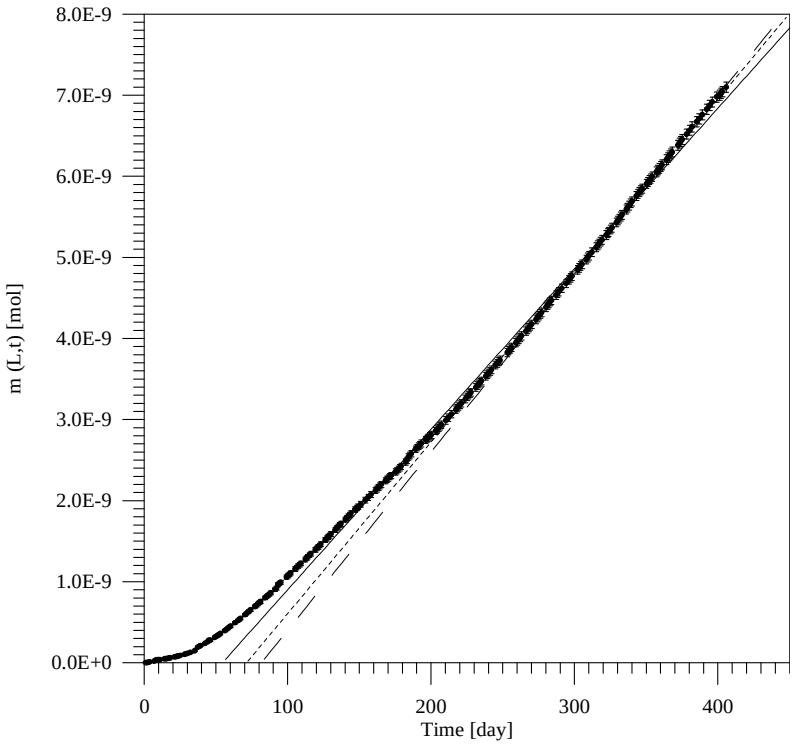

Figure 2.3.3.-2: Time history of the total diffused nickel mass *m(L,t)* for experiment no. 7. During the first 100 - 150 days the system evolves rapidly, after this period only quite moderately. That the system had not reached a stationary state with constant flux can be seen by the drawn straight lines. They represent a series of subsequent linear regression calculations using only data beyond 100 (solid line), 200 (dashed line) and 300 days (broken line). The intersect of the regression curves with the time axis moves continuously to greater times (54.5, 71.3 and 81.7 days).

With the help of a series of linear regression calculations we also see for *m(L,t)* that a stationary state was never reached. If using only data for t > 100, 200 and 300 days the slope of the regression straight line increases only weakly, however, the intersect of the fit curve with the time axis significantly moves towards larger times as specified in the figure caption above.

As for the previous experiments we also present a figure of the time-dependent reservoir concentration. Again, after the beginning of the experiment the concentrations dropped by a factor of about 3 by the nickel up-take of the equipment and HCP. After the re-adjustment by several subsequent adds of concentrated nickel solution an averaged value of about $\overline{C}_0 \pm \Delta C_0 = (3.85 \pm 0.27) \cdot 10^{-8}$ mol/l was reached where the uncertainty correspond to one standard deviation.

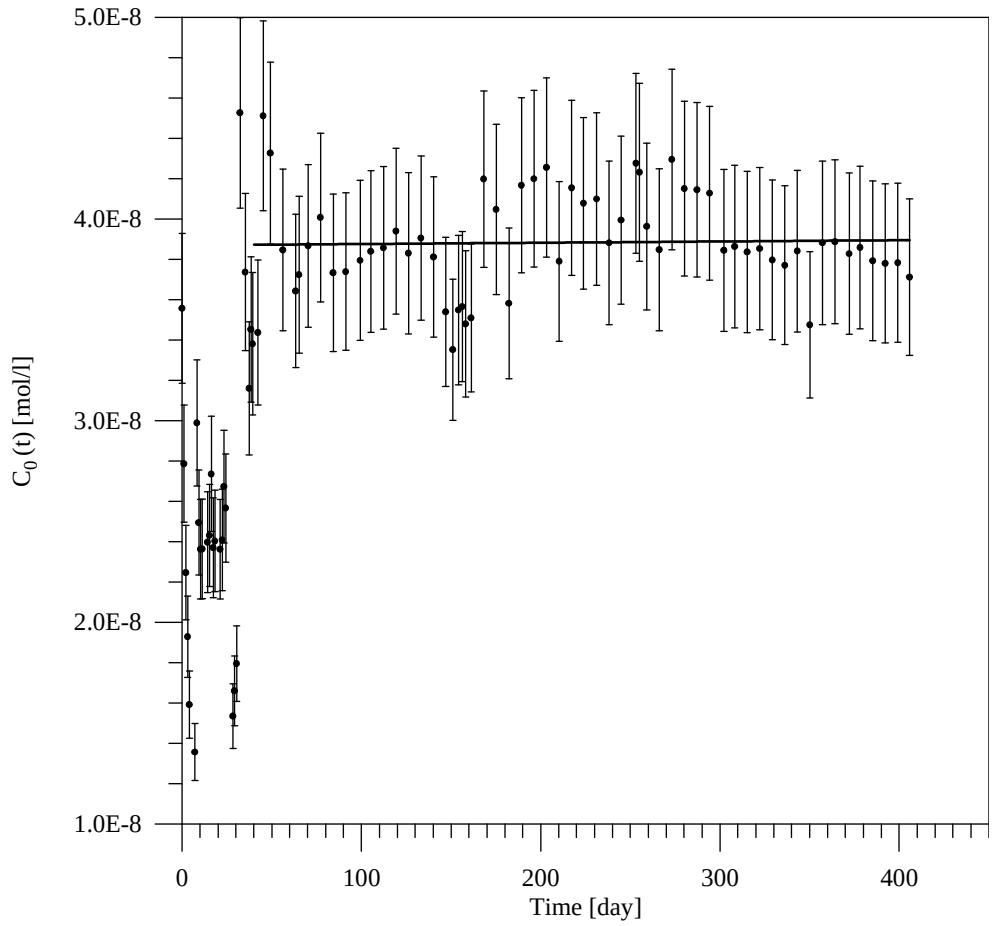

Figure 2.3.3.-3: Time history of the reservoir concentration $C_0(t)$ for nickel and experiment no. 7. After the start of the experiment the concentration rapidly decreased by a factor of more than three due to tracer up-take of the HCP, walls of the reservoir cell and tubes and due to starting diffusion. By some additional (concentrated) tracer the concentration was adjusted. Drawn are also the uncertainties in C_0 which were estimated to be ± 10.4 % (95% confidence interval). The solid line represents a linear regression of all the measurements beyond 40 days.

Finally, in Figure 2.3.3.-4 we show a graph of the totally deposited nickel mass as a function of time, based on 85 data pairs of a mass balance. A total of $6.43 \cdot 10^{-8}$ mol nickel was applied for the experiment, $0.71 \cdot 10^{-8}$ mol (11.0 %) were diffused through the cementitious sample, $2.57 \cdot 10^{-8}$ or 40.0 % remained on the reservoir side; hence, $3.15 \cdot 10^{-8}$ mol or 49.0 % were deposited either onto the surfaces of the diffusion cell and tubes or onto the surfaces of the HCP and within the liquid phase of the pore space.

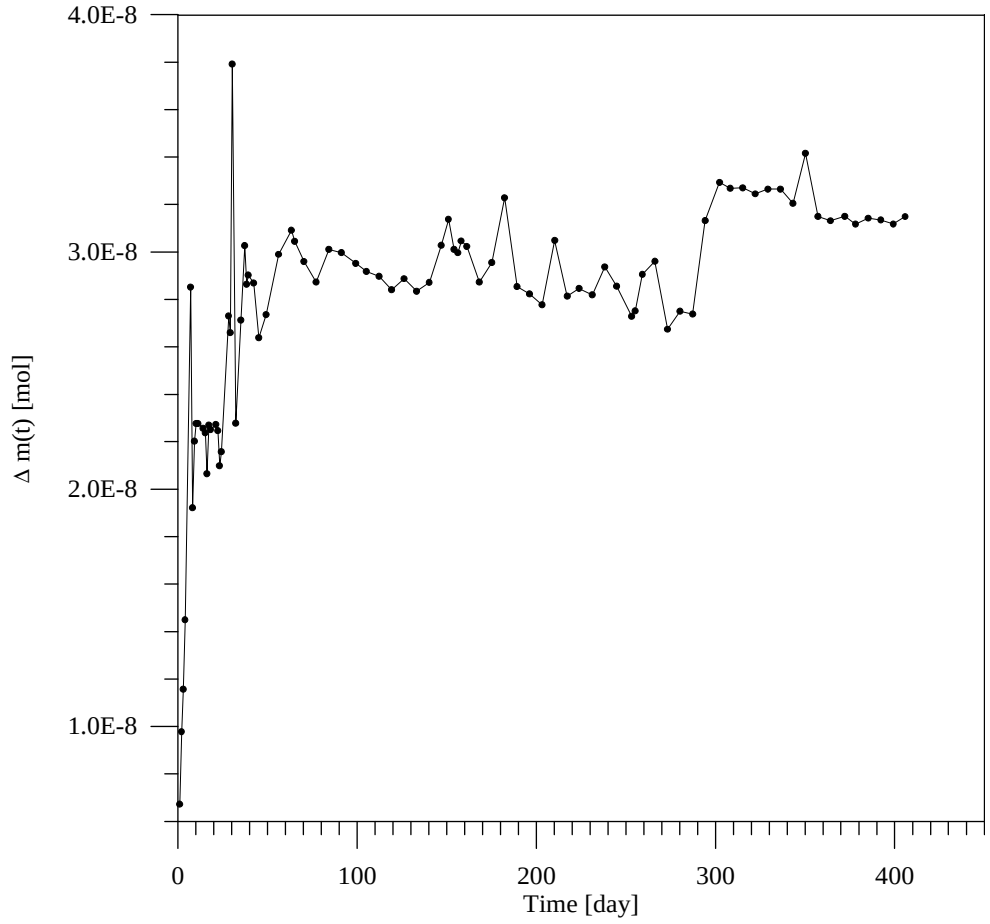

Figure 2.3.3.-4: The total amount of nickel of the HCP and the equipment as a function of time based on a mass balance for experiment no. 7. After the first 80 days of the experiment and when neglecting short time variations the deposited nickel quantity reaches a local maximum followed by a slow decrease. After about 300 days a sudden additional up-take can be recognised again followed by a slow decrease of the data.

After a first fast up-take of nickel for about 20 days the system only moderately evolves to a maximum value followed by a period of more than 250 days characterised by a slight tendency for nickel release. After about 300 days deposition increases briefly, followed again by a phase of weak tracer release. This event coincides with a corresponding decrease of the reservoir concentration; the underlying mechanism, however, is not known.

2.3.4. Data obtained from experiment no. 8

The experiment was started on July 26th, 1993, and terminated on November 10th, 1995. In Figure 2.3.4.-1 below, based on 328 measurements, the diffusive flux of nickel as a function of time across the boundary at $x = L$ is shown. After about 70 days the temporal change of the diffusive flux decreases rapidly. However, there can be seen that after these first 80 days the flux is still increasing slightly. As for experiment no. 7, there is a prominent dip at around 160 days, but there is no reasonable explanation for this.

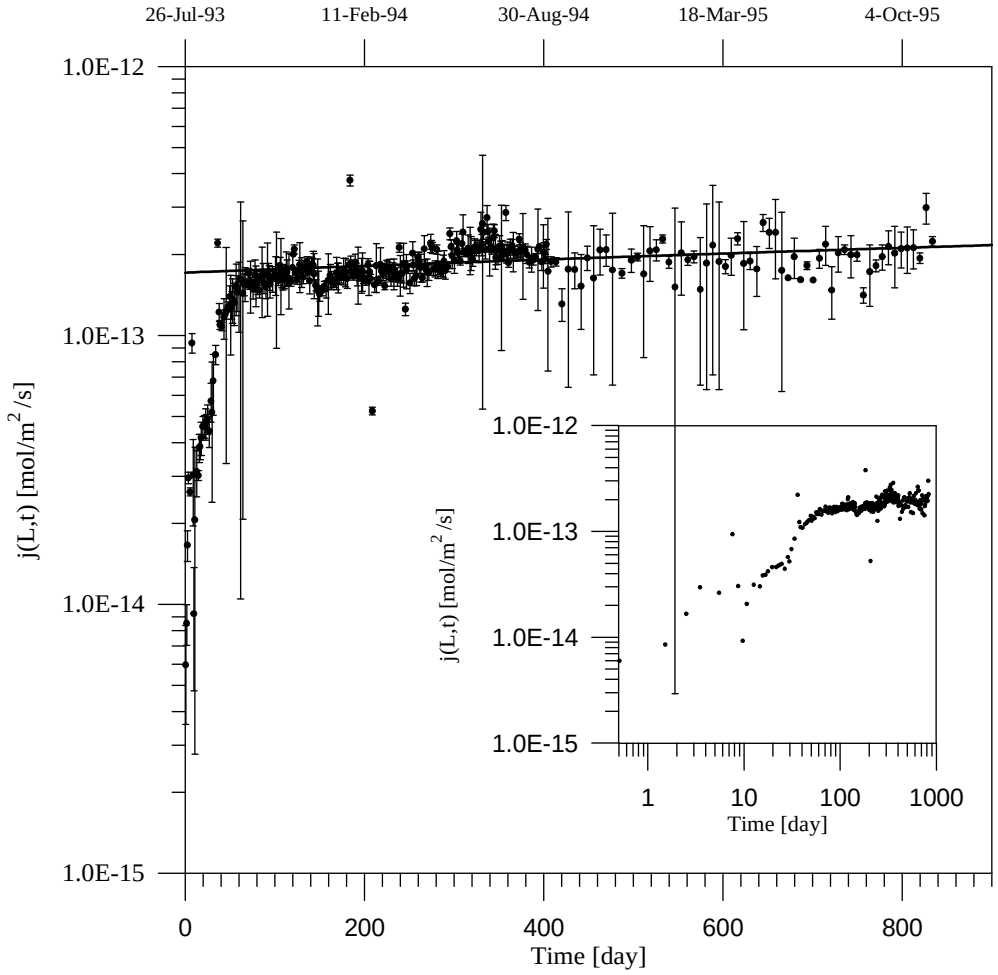

Figure 2.3.4.-1: The measured diffusive flux of nickel of experiment no. 8, together with the 95 % confidence intervals, across the boundary at $x = L$ as a function of time. At first sight we suppose that after about 70 days the flux has reached a (first) constant value for about another 130 days. However, analysing the breakthrough curve with the help of a simple linear regression model it turns out that the flux is still slightly increasing. A linear regression curve for the measured data beyond 100 days (solid line) increases by about 21.0 % in the interval between 100 and 833.7 days.

Using measured data beyond 100 days for a simple linear regression according to $j(L,t) = a\,t + b$, for the two constants we find:

$$a \pm \Delta a = (5.06 \pm 0.95) \cdot 10^{-17} \, \frac{\text{moles}}{\text{m}^2 \, \text{s} \, \text{day}} \quad ,$$

$$b \pm \Delta b = (1.71 \pm 0.04) \cdot 10^{-13} \frac{\text{moles}}{\text{m}^2\,\text{s}} \quad ,$$

with

$$j(L,100) \cong 1.76 \cdot 10^{-13} \frac{\text{moles}}{\text{m}^2\,\text{s}} \quad ,$$

and

$$j(L,833.7) \cong 2.13 \cdot 10^{-13} \frac{\text{moles}}{\text{m}^2\,\text{s}} \quad ;$$

hence, the difference is about 21.0 % so that the diffusive flux can never be considered as constant in the measurement interval. Consequently, we also do not estimate a value for the effective diffusion constant according to equation (2.3.2).

Figure 2.3.4.-2 illustrates the time history of the total diffused nickel mass *m(L,t)* together with the accumulated errors. The uncertainties correspond to a 95 % confidence limit.

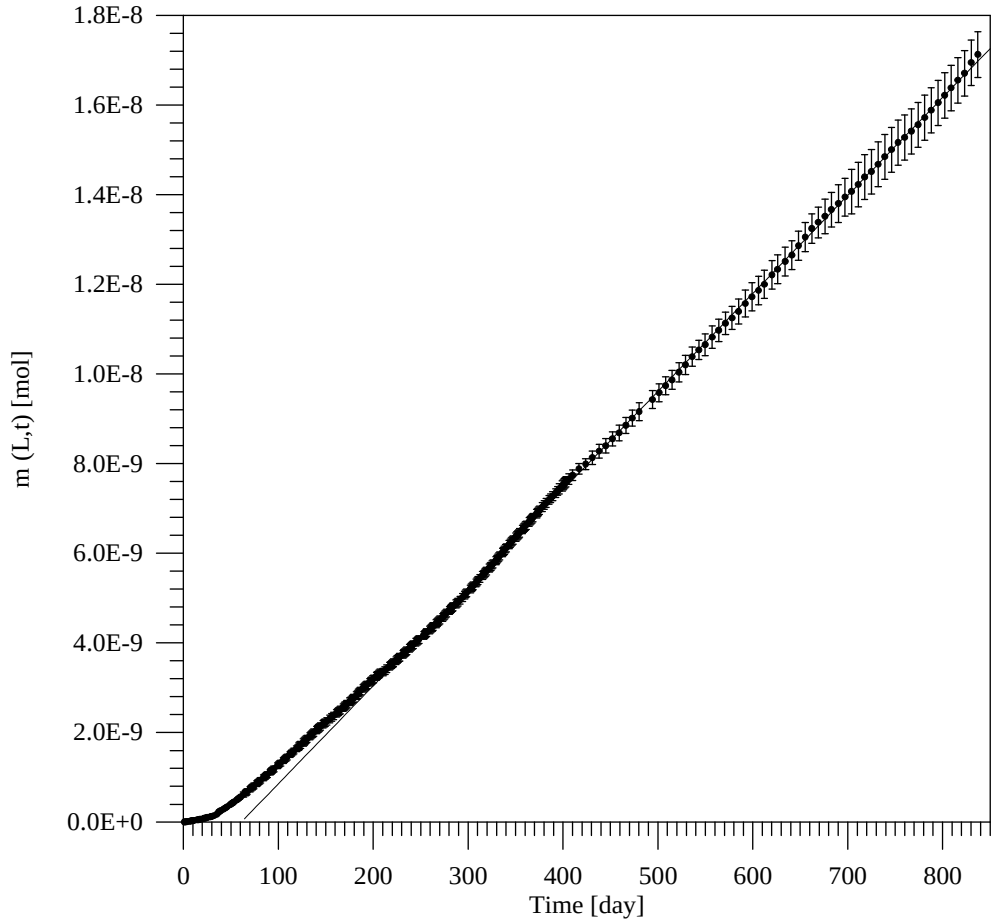

Figure 2.3.4.-2: Time history of the total diffused nickel mass *m(L,t)* for experiment no. 8. The error bars correspond to a 95 % confidence interval. It can be seen from the figure that there is a transient phase for at least 200 days, after this period the system seems to be in a steady state. The solid line represents a linear regression calculation of all the data beyond 200 days. The regression (straight) line matches the measurements nearly perfectly.

A series of linear regression calculations implies that the system has reached a stationary state after about 200 days, meaning that the parameters of the regression curve (slope and intersect with the time axis) do not change their values significantly. However, from the previous discussion concerning the flux evolution we know that the system still evolves, even after several hundreds of days.

The next figure presents the time-dependent reservoir concentration $C_0(t)$. The figure is based on 144 measurements, and the error bars correspond to a 95 % confidence interval.

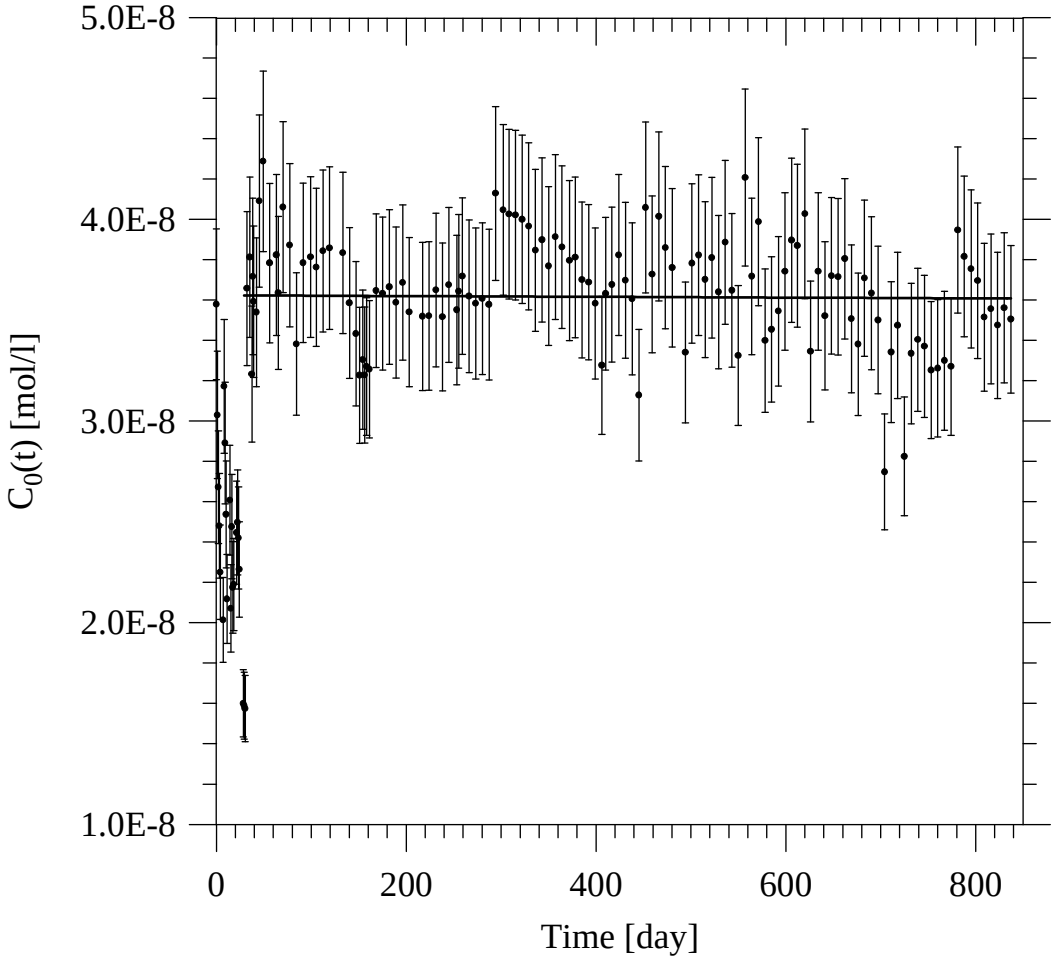

Figure 2.3.4.-3: Time history of the nickel reservoir concentration $C_0(t)$ for experiment no. 8. After the start the concentration decreased rapidly by a factor of more than two due to tracer up-take of the HCP, walls of the reservoir cell and tubes and due to starting diffusion. By some additional (concentrated) tracer the concentration was adjusted. Drawn are also the uncertainties (95 % confidence interval) in C_0 which were estimated to be ± 10.4 %. The solid line represents a linear regression of all data beyond 29 days.

Again, as for the other experiments a first and fast up-take of nickel by the equipment and the HCP reduced the tracer concentration in the reservoir compartment to about 60 % of the initial value. Consequently, the expectation value had to be re-adjusted by adding high concentrated tracer solution several times. For the mean reservoir concentration we determine a value of $\overline{C_0} \pm \Delta C_0 = (3.63 \pm 0.33) \cdot 10^{-8}$ mol/l where the uncertainty corresponds to one standard deviation.

At last we present a graph of the total deposited nickel mass as a function of time and based on totally 144 measurements. For the experiment $7.03 \cdot 10^{-8}$ moles of nickel were applied: $1.71 \cdot 10^{-8}$ moles or 24.4 % were diffused through the cementitious barrier, $2.55 \cdot 10^{-8}$ moles or 36.3 % remained in the reservoir compartment (or were removed from the reservoir by drawing samples for measurement purposes); hence, $2.76 \cdot 10^{-8}$ moles (39.3 %) were deposited onto the surfaces of the equipment and the hardened cement paste.

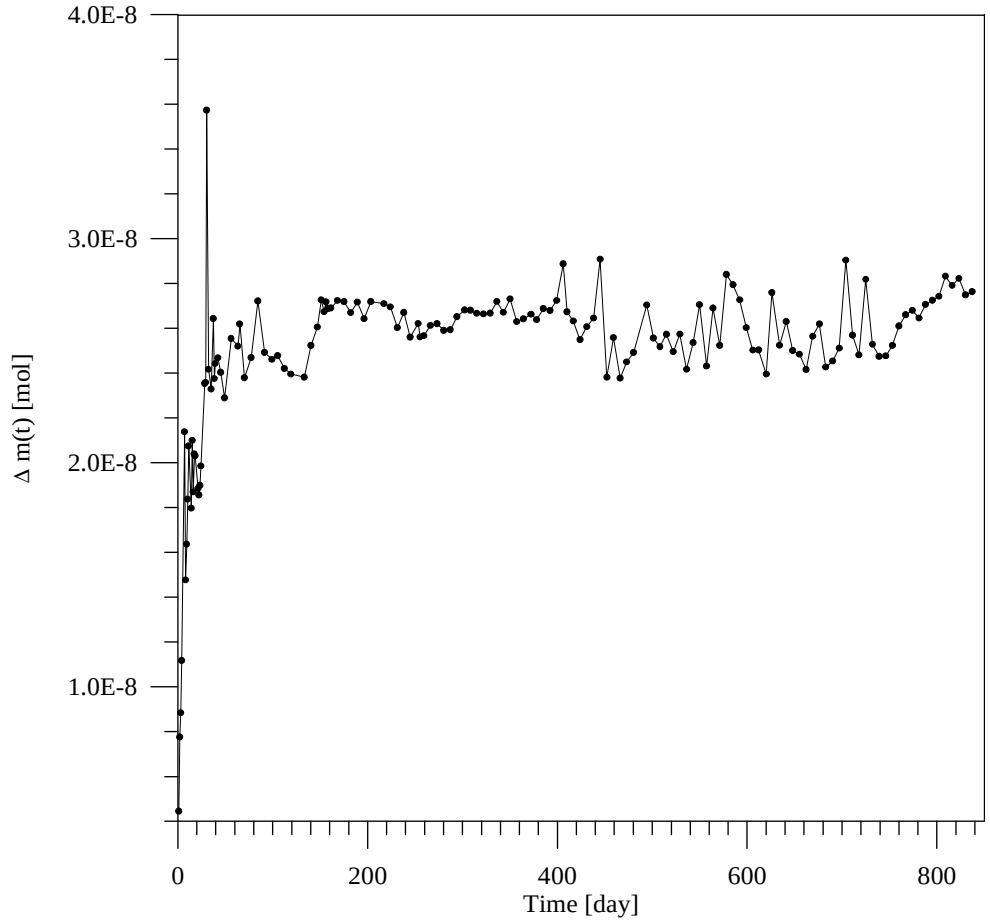

Figure 2.3.4.-4: The total amount of nickel of the HCP and the equipment as a function of time based on a mass-balance for experiment no. 8. After a relatively short transient phase of about 40 days where deposition mainly occurs, further tracer up-take seems to be negligible when neglecting short time fluctuations.

A relatively short period of only about 40 days is characterised by the deposition of nickel. After that a further nickel up-take cannot be recognised in the data when neglecting short time variations.

Again, as for experiment no. 6, and as described in more detail on page 77 at the end of the experiment, after about 834 days a value for the adhering nickel onto the poly-styrene of the diffusion cell was determined. As an averaged concentration of both the solutions of the reservoir and of the measurement side we determine a value of $\overline{C} = (3.23 \pm 0.42) \cdot 10^{-8}$ moles/l (one standard deviation error). The activity measurements yielded, with the help of the β-counter, for the flushing solutions (one standard deviation errors):

Dissolved nickel in the first flushing	$(9.44 \pm 0.53) \cdot 10^{-9}$ moles
Dissolved nickel in the second flushing	$(0.226 \pm 0.006) \cdot 10^{-9}$ moles
Total dissolved nickel	$(9.67 \pm 0.54) \cdot 10^{-9}$ moles.

Comparing this data pair with the estimation for nickel deposition onto poly-styrene described in sub-section 2.1.5 concerning blank values we recognise that the data are also in good agreement with our former considerations.

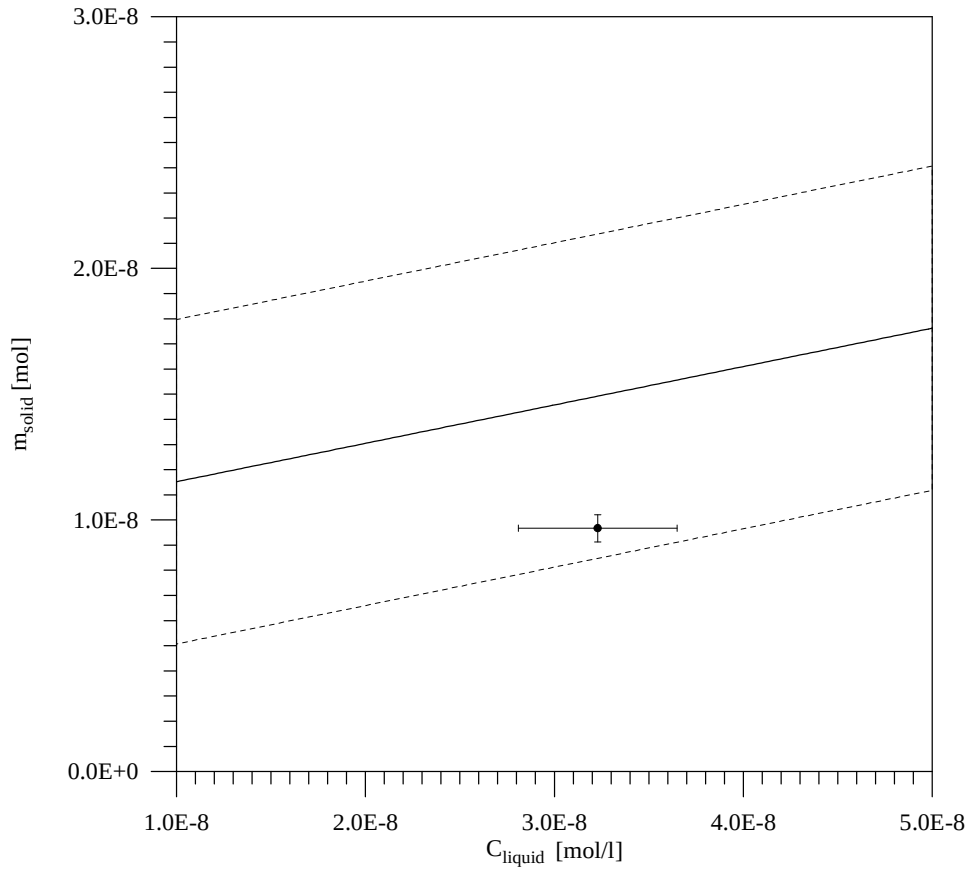

Figure 2.3.4.-5: The deposited nickel mass onto surfaces of the equipment versus the averaged concentration of the liquid at the end of the diffusion experiment no. 8. The solid line represents the linear functional relationship derived in subsection 2.1.5. together with its error range limited by the two dashed lines. The extracted value (value with one standard deviation error) seems to be comparable with our former considerations concerning nickel up-take by the poly-styrene equipment of the diffusion cell; it is practically identical with the value for experiment no. 6.

Finally, the hardened cement paste was frozen for further investigations. For that, within the CO_2 and O_2-free atmosphere of the glove box the liquid on both sides of the hardened cement paste was sucked off and the adhering solution onto the sample holder was dabbed. Then, the HCP in the sample holder was packed into a poly-ethylene bag, enclosed standing up-right in a plastic vessel and frozen in a freezer at -18° C.

2.4. The apparatus and the experimental set-up for out-diffusion

As for the diffusion experiments the out-diffusion experiments, too, were made in glove boxes under the same controlled nitrogen atmosphere as described before. For the experiments the following apparatus was used. The sample holder as well as the compartment of one side were the same as for the previous through-diffusion experiments. In contrast to those experiments the reservoir on the other side of the HCP sample was replaced by another small cavity similar to the measurement cell but with a slightly larger volume $V' = 56.0 \pm 0.3$ ml.

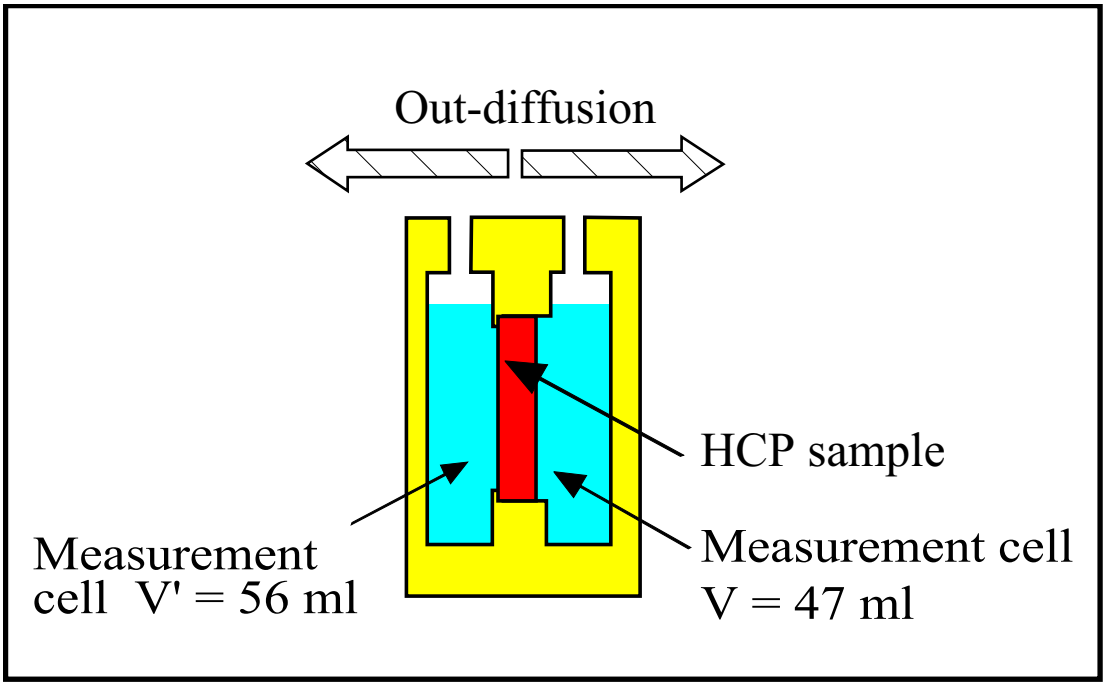

Figure 2.4.-1: Sketch of the apparatus for the out-diffusion experiments.

After the termination of the diffusion experiment the sample was installed quickly in such an equipment and both cavities filled up to the same level with artificial cement pore water (for the preparation of this pore water see also sub-section 2.1.2.). Immediately 2 - 3 quick water changes were made to remove adhering traced water from the surfaces of the HCP, especially from the ex high-concentration side, and to arrive at zero concentration boundary conditions. The exposure time of the cement interfaces to the fresh cement pore water was only of the order of 10 - 20 seconds. For subsequent mass balances also the activities of these volumes had to be measured in the β-counter. For good mixing of the liquid in both cavities there were installed small PTFE-covered magnets which were driven by a magnetic stirrer below the apparatus.

The activity measurements were performed according to the procedure described in sub-section 2.1.3 and according to the data evaluation in 2.1.4. Due to technical limitations of the measurement equipment a minimal tracer concentration of about 10^{-13} moles/ml had to be secured. With the help of theoretical consideration (more details can be found in sub-section 3.3.) we estimated a period of about 7 hours for the right measurement cell (ex low-concentration side) for the first out-diffusion time interval. For the left measurement side (ex high-concentration or reservoir side) a duration of about only 20 minutes for reaching a

concentration of approximately 10^{-12} moles/ml was determined. Of course, when continuing with the experiment these two out-diffusion intervals had to be expanded continuously to keep the maximum concentration well above the detection limit. After about one year the period between two (artificial cement pore) water changes was already extended up to one week. Two of the four nickel experiments were used for out-diffusion. Because experiment no. 5 was considered to be nearly in steady state, it was used first. Later on, as a second experiment, no. 7 was used.

Finally, after the termination of the experiments, both HCP's were conserved for further investigations. Within the CO_2 and O_2-free atmosphere of the glove box the liquid on both sides of the HCP was sucked off, and the adhering solution onto the sample holder was dabbed. Then, the HCP in the sample holder was packed into a poly-ethylene bag, enclosed up-right standing in a plastic vessel and then frozen in a freezer at -18° C.

2.5. Experiments with nickel

2.5.1. Data obtained from experiment no. 5

The out-diffusion experiment based on the nickel through-diffusion experiment no. 5 was started on May 3rd 1994 and was terminated on November 10th 1995 after about 556 days of nickel out-diffusion. There are 104 data points for the flux and total diffused nickel mass available for the ex low-concentration side at $x = L$ as well as 110 data points for the ex high-concentration side at $x = 0$. In Figure 2.5.1.-1 the values for the diffusive fluxes together with their error bars across both boundaries are shown.

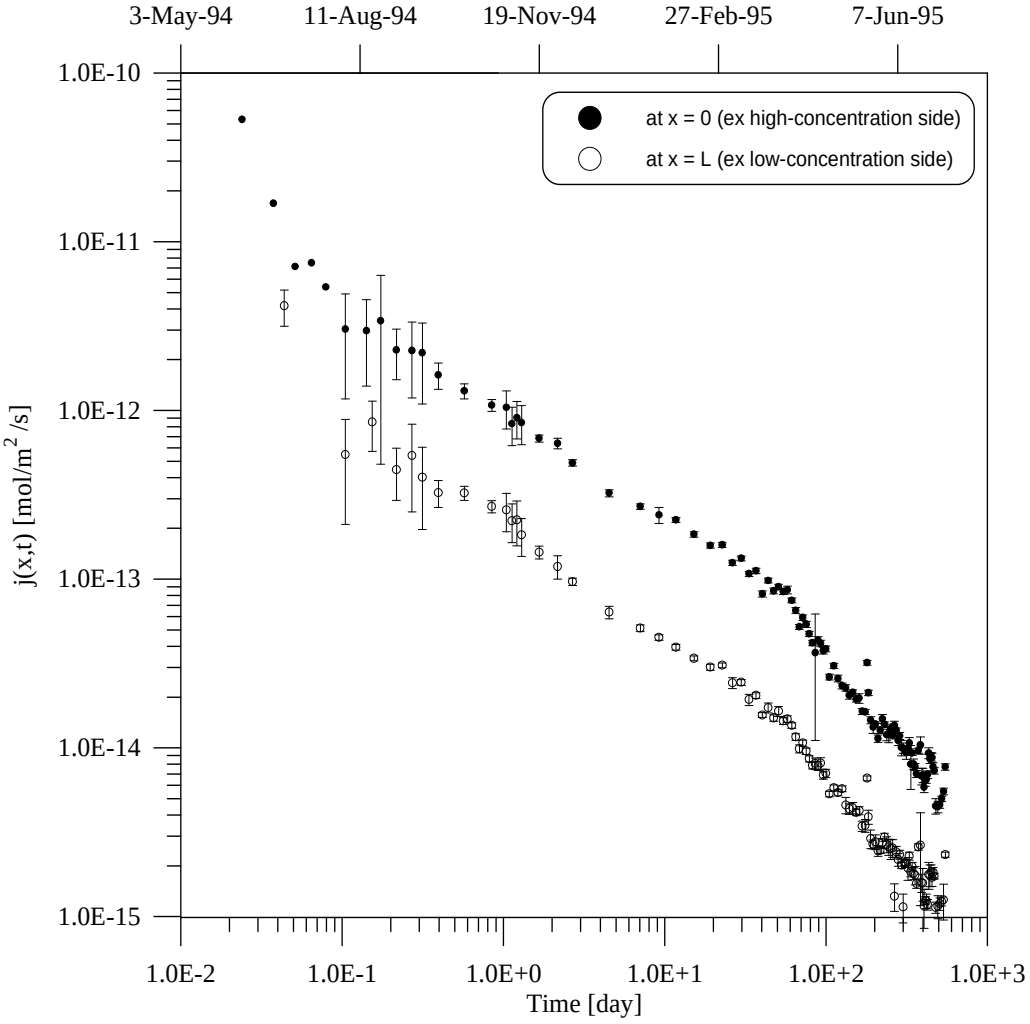

Figure 2.5.1.-1: Measured nickel fluxes across both boundaries as a function of time and as indicated in the legend. The data are those from experiment no. 5, and the error bars[14] correspond to a 95% confidence interval.

At the end of the through-diffusion experiment the high concentration boundary condition at $x = 0$ was quickly replaced by a zero concentration boundary condition. To remove adhering traced water 2 - 3 quick water changes were made and to also release adhering air onto the

[14] If an error bar is missing in the figure, this is due to a technical flaw of the plot software which is unable to draw error bars in a (semi-) log representation where the error bars are larger than the measurement value itself.

surfaces of the HCP the whole equipment was shaken thus probably inducing a further driving force for diffusing nickel. Therefore, the first 2 - 3 measurements on the ex high-concentration side and at least the first measurement on the ex low-concentration side at $x = L$ are considered as unreliable.

After about 50 - 60 days an enhanced decline in both fluxes can be recognised. The next figure shows the time history of the total diffused nickel mass.

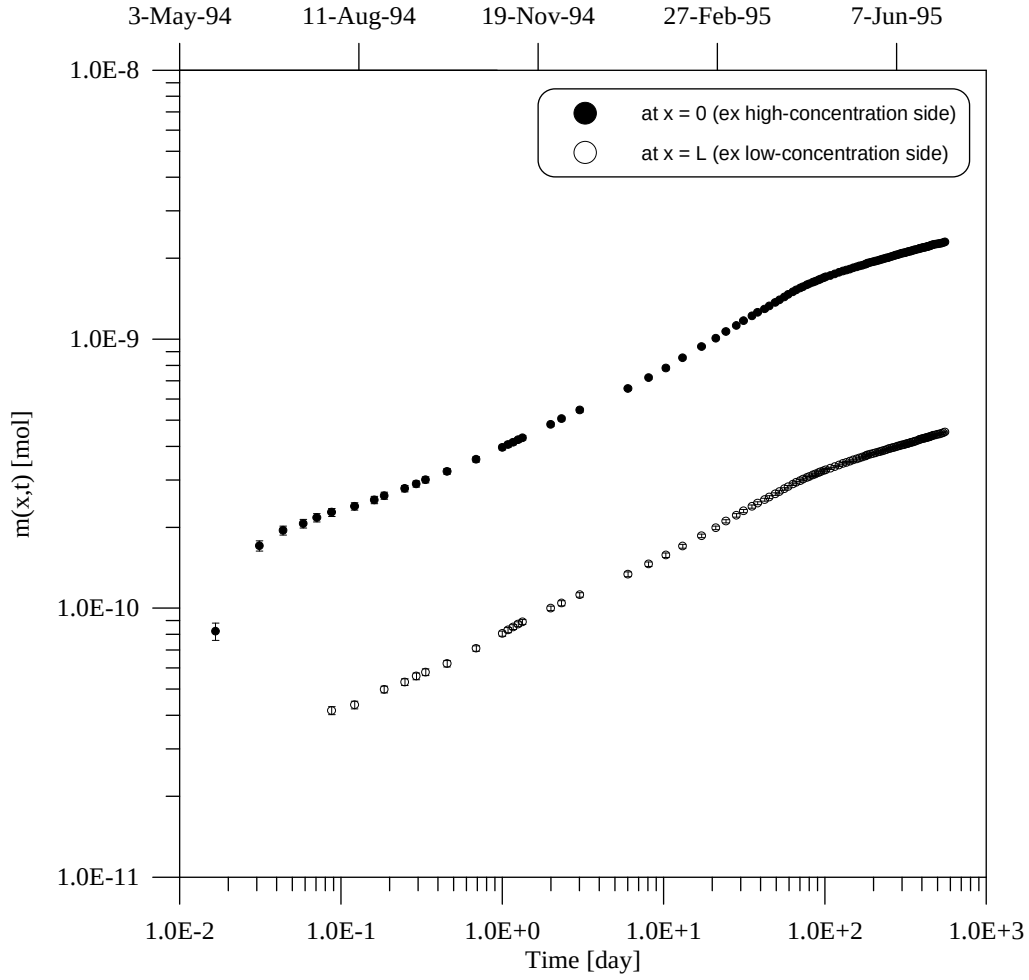

Figure 2.5.1.-2: Cumulated diffused nickel mass across both boundaries as indicated in the legend. The data are those from experiment no. 5, and the error bars correspond to a 95% confidence interval.

Comparing the underlying values of this plot with those from page 70 concerning the deposited nickel mass based on a careful mass balance and taking into account that about $1.4 \cdot 10^{-8}$ moles nickel were deposited onto the poly-styrene of the equipment we can conclude that after about 556 days of out-diffusion only about 10 % of the total nickel has left the HCP. From a safety assessment point of view such a behaviour of a cementitious barrier for out-diffusing nickel is certainly highly appreciated.

Finally, the hardened cement paste was frozen for further investigations as described on page 78.

2.5.2. Data obtained from experiment no. 7

A further out-diffusion experiment was performed for both the purpose of comparison and in order to exclude the deficiencies of experiment no. 5. This second experiment was started on September 5th, 1994 and was terminated on November 10th, 1995 after about 431 days of nickel out-diffusion. There are available 127 data points for both the flux and the total diffused nickel mass for the ex low-concentration side at $x = L$ as well as 140 data points for the ex high-concentration side at $x = 0$. In the Figure 2.5.2.-1 below the diffusive fluxes across both boundaries are shown.

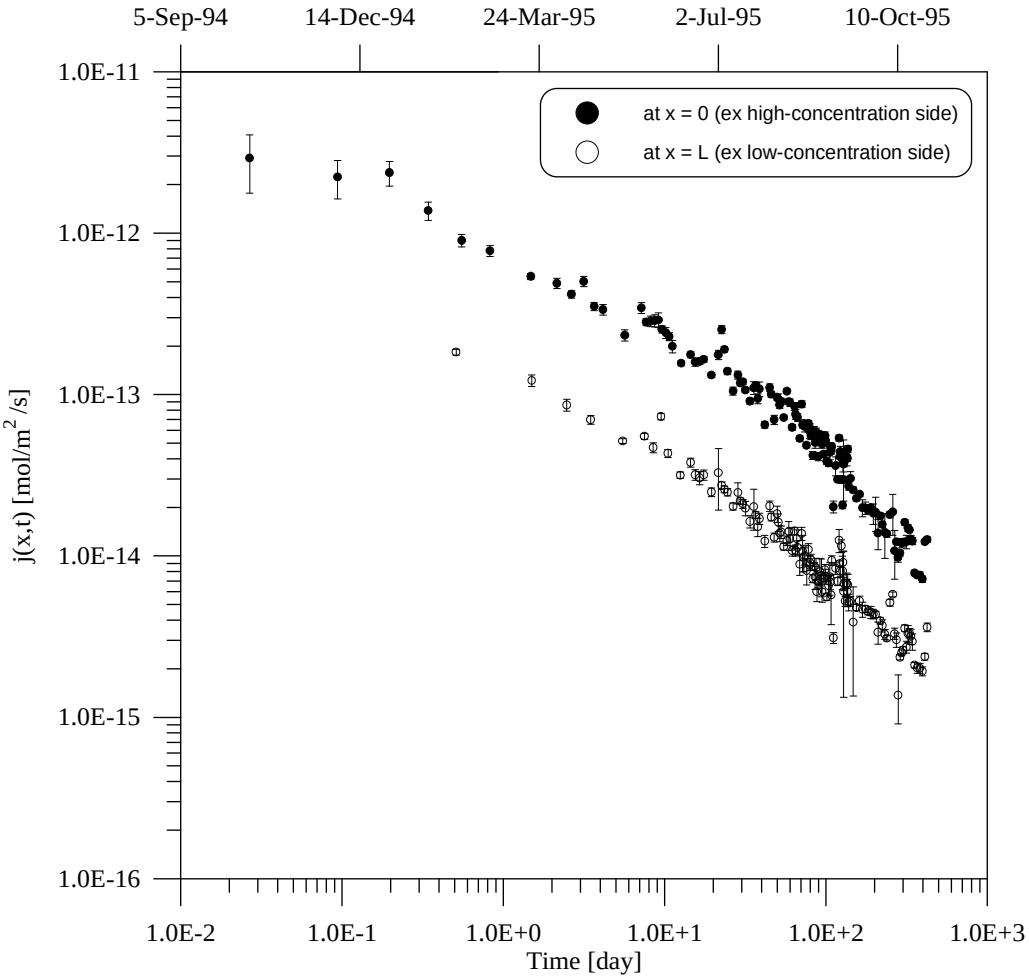

Figure 2.5.2.-1: Measured nickel fluxes across both boundaries as a function of time and as indicated in the legend. The data are those from experiment no. 7, and the error bars correspond to a 95% confidence interval.

In contrast to experiment no. 5 the measurements are more scattered, and also the marked declined fluxes after about 50 - 60 days of experiment no. 5 cannot be recognised any longer. In the next figure the time history of total diffused mass is plotted.

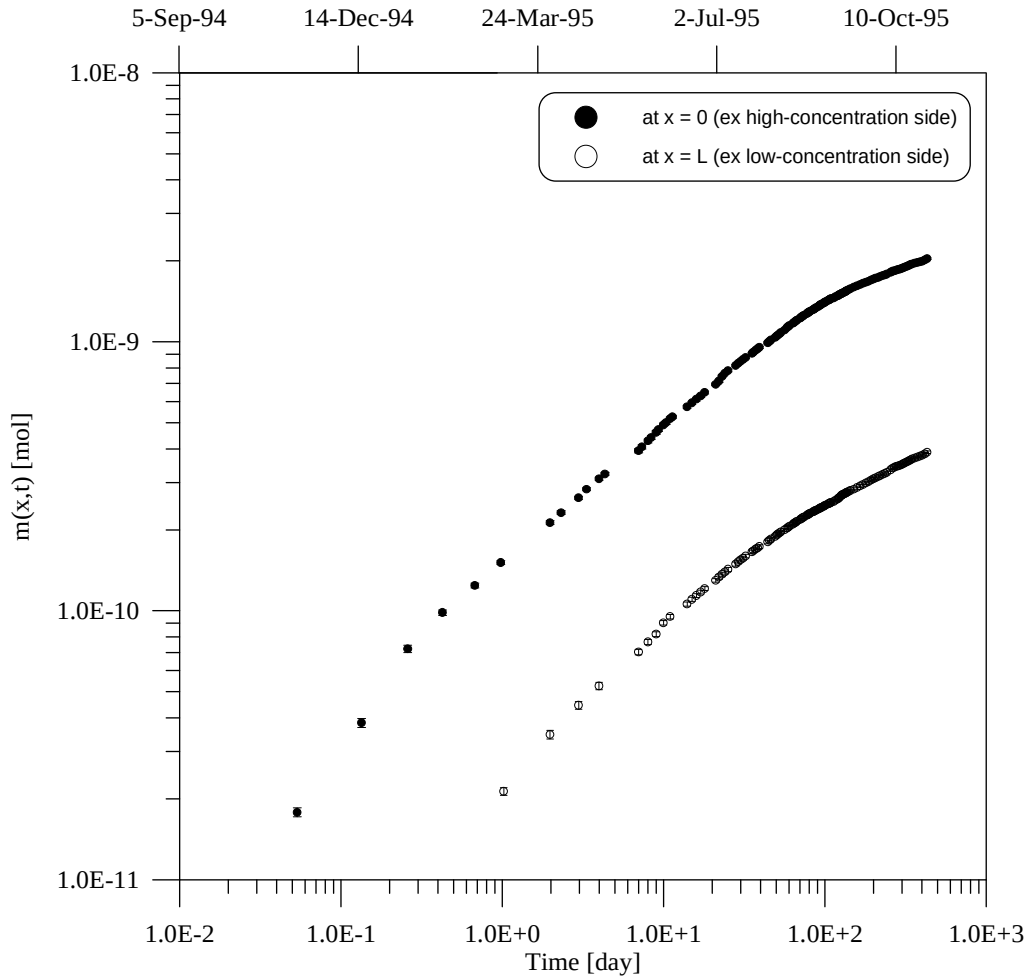

Figure 2.5.2.-2: Cumulated diffused nickel mass across both boundaries as indicated in the legend. The data are those from experiment no. 7, and the error bars correspond to a 95% confidence interval.

Finally, also this hardened cement paste was frozen for further investigations as described on page 78.

3. The modelling

3.1. The governing equations for through-diffusion

Most chemical species in aqueous solutions will interact with the solid phases. Therefore, transport through a porous medium will be governed by both physical and chemical processes. Chemical processes may have an important impact on the transport rates and on the retardation of migrating solutes, so it is essential to separate physical and chemical mechanisms in order to characterise them properly and to account for them correctly in predictive models. The chemical mechanisms are very varied. There might be changes in the solid phases, the formation of new phases, precipitation and dissolution of such new compounds may occur, ion-exchange reactions may play an important role, and the kinetics of all these mechanisms might be fast or slow with respect to simple diffusion rates. The most simple chemical interaction is the reversible, instantaneous equilibrium surface adsorption described in terms of a linear isotherm, meaning that the concentration of the species adsorbed onto the solid phases is proportional to its concentration in the mobile phase. However, there are solutes which clearly show a non-linear adsorption characteristics. They may be more appropriately described by non-linear expressions such as the Freundlich or the Langmuir isotherm. Other solutes may show even more complex adsorption behaviour where, e.g., kinetics may be of importance.
For the modelling of the through-diffusion experiments we assume that an appropriate description may be based on a one-dimensional single-porosity medium in which the water diffusion coefficient D [m^2/s] is considered as constant in space and time. Based on mass balance for a stable tracer, diffusion is expressed by Fick's second law:

$$\frac{\partial}{\partial t}\left[C+\frac{1-\varepsilon}{\varepsilon}\rho S\right]=D\frac{\partial^2 C}{\partial x^2} \quad [15]. \tag{3.1.1}$$

In this equation t [s] is time, C [mol/m^3] the concentration of the solution, ε [-] the connected porosity of the sample, ρ [kg/m^3] the solid density, S [mol/kg] the amount of solute absorbed onto the solid phase per unit mass of solid phase, and x [m] the spatial co-ordinate. For simplicity it is assumed that the diffusion and chemical parameters neither will change with time nor are a function of the tracer concentration.

For the sorption processes we assume, in a first case, an instantaneous, reversible, non-linear sorption equilibrium which may be described by a Freundlich isotherm:

$$S=K_p C^{N_p} \quad , \tag{3.1.2}$$

where K_p [$\mathrm{mol}^{1-N_p}\,\mathrm{m}^{3N_p}/\mathrm{kg}$] is the Freundlich coefficient and N_p [-] is the Freundlich exponent, both being constant in space and time. If the Freundlich exponent is unity, the linear isotherm is described with $K_p \equiv K_d$ [m^3/kg], where K_d is the linear sorption equilibrium distribution coefficient.
An alternative description is a reversible, first-order non-linear, kinetic equation:

$$\frac{dS}{dt}=\frac{\varepsilon}{(1-\varepsilon)\rho}k_s C^{N_s}-k_r S \quad . \tag{3.1.3}$$

[15] In subsection 2.1.1 we mentioned that we will neglect the small difference in connected and total porosity. Otherwise the dry bulk density $(1-\varepsilon)\rho$ would have do be changed to $(1-\varepsilon_{tot})\rho$.

This equality describes sorption processes where the forward reaction may be either linear or non-linear and where the backward reaction is linear [16]. k_s [$\mathrm{mol}^{1-N_s}\,\mathrm{m}^{3(N_s-1)}/\mathrm{s}$] and k_r [s^{-1}] are rate coefficients, and N_s is a dimensionless quantity.
The distribution ratio R_D is defined as the ratio of S and C and, in the case of the Freundlich isotherm, is given by:

$$R_D = \frac{S}{C} = K_p C^{N_p - 1} \quad . \tag{3.1.4}$$

For equation we now get:
If we substitute in equation (3.1.1) for the expression in the bracket:

$$\left[1 + \frac{1-\varepsilon}{\varepsilon}\rho\frac{dS}{dC}\right] = \left[1 + \frac{1-\varepsilon}{\varepsilon}\rho K_p N_p C^{N_p - 1}\right] = R(C) \tag{3.1.5}$$

the concentration dependent retardation function $R(C)$ [-], or alternatively:

$$\left[\varepsilon + (1-\varepsilon)\rho\frac{dS}{dC}\right] = \left[\varepsilon + (1-\varepsilon)\rho K_p N_p C^{N_p - 1}\right] = \alpha(C) \quad , \tag{3.1.6}$$

where $\alpha(C)$ [-] is the concentration dependent rock capacity factor and $D_e = \varepsilon D$ [m^2/s] the effective diffusion constant, we get:

$$\frac{\partial C}{\partial t} = \frac{D}{R(C)}\frac{\partial^2 C}{\partial x^2} = \frac{D_e}{\alpha(C)}\frac{\partial^2 C}{\partial x^2} \quad , \tag{3.1.7}$$

For $N_p \equiv 1$ and $K_p \equiv K_d \equiv R_D$ the widely used linear retardation constant and rock capacity factor are obtained:

$$R_{lin.} = 1 + \frac{1-\varepsilon}{\varepsilon}\rho K_d \quad , \tag{3.1.8}$$

$$\alpha_{lin.} = \varepsilon + (1-\varepsilon)\rho K_d \quad . \tag{3.1.9}$$

Accounting for sorption-kinetics of the form of equation (3.1.3) does not result any longer in analytical expressions for the retardation function of the form (3.1.8) and (3.1.9), respectively.

The transport equation (3.1.7) or the system of transport equations (3.1.1) and (3.1.3) has to be solved with appropriate initial and boundary conditions.

a) The initial condition is:

$$C(x,t) = 0 \qquad ; \forall x, \quad t \le 0 \quad , \tag{3.1.10}$$

meaning that the cement paste is originally free of tracer.

b) Suitable boundary conditions are the following:

at the high-concentration side: $C(0,t) = C_0 = \text{const.} \quad ; \; t > 0 \quad ,$ (3.1.11)

at the low-concentration side: $C(L,t) = 0 \quad ; \; t > 0 \quad ,$ (3.1.12)

[16] For the following we will denote some of the diffusion/sorption model either as “linear/linear” or as “non-linear/linear” depending on the value of the exponent N_s in equation (3.1.3.). In principle the backward reaction might be non-linear, too, but we believe including this would lead to unnecessary complexity.

where L [m] is the thickness of the cement paste. These boundary conditions are chosen for their simplicity, although small variations at both boundaries can be recognised (see also chapter 2). However, it is assumed that such small variations in the concentration are damped to a negligible effect due to diffusion.
Appendix 1 outlines the method used to obtain an analytical solution of the transport problem (3.1.7) in the case of a linear sorption isotherm. For more complicated sorption isotherms only numerical solutions can be obtained. For illustration purposes from appendix 1 we adopt the analytical solution for the case when nuclides sorb linearly:

$$\frac{C(x,t)}{C_0} = 1 - \frac{x}{L} - \frac{2}{\pi}\sum_{n=1}^{\infty}\frac{1}{n}\exp\left(-\pi^2 n^2 \frac{D_e}{\alpha L^2} t\right)\sin\left(n\pi\frac{x}{L}\right) \quad . \qquad (3.1.13)$$

The flux $j\left[\frac{\text{mole}}{\text{m}^2\text{s}}\right]$ across the boundary at the low-concentration side at $x = L$ is given by:

$$j(L,t) = -\varepsilon D \left.\frac{\partial C}{\partial x}\right|_{x=L} = \frac{C_0 D_e}{L}\left[1 + 2\sum_{n=1}^{\infty}(-)^n \exp\left(-\pi^2 n^2 \frac{D_e}{\alpha L^2} t\right)\right] \quad . \qquad (3.1.14)$$

At short times there is a transient behaviour of the system while the porosity is filled with the diffusing solute and while the concentrations in the liquid and on the solid come into equilibrium. Later, a linear concentration gradient becomes established according to the first derivative of the leading terms of equation (3.1.13) in the sample, and the diffusion is in steady-state with a constant flux j_L equal to $\frac{C_0 D_e}{L}$; this latter quantity is independent of retarding mechanisms such as sorption. From an inverse modelling point of view using only data from a steady-state flux region, values for the effective diffusion constant D_e can be fitted uniquely. Then, using the measurements from the transient region of the breakthrough curve which is influenced by mechanisms such as sorption additional parameters accounting for retardation can be fixed without having correlation to D_e. However, the attainment of steady-state in the experiment would be a necessary condition for such a procedure. Otherwise D_e and the parameters for retardation have to be adjusted simultaneously and more or less correlation between these parameters can be expected. Integrating the flux with respect to time and multiplying it by the cross-sectional area F [m^2] of the cement paste yields the total diffused mass of tracer in the linear sorption case:

$$m(L,t) = F\int_0^t j(L,t')\,dt' = C_0\frac{D_e F}{L}\left[t - \frac{\alpha L^2}{6 D_e} - 2\frac{\alpha L^2}{\pi^2 D_e}\sum_{n=1}^{\infty}(-)^n \frac{1}{n^2}\exp\left(-\pi^2 n^2 \frac{D_e}{\alpha L^2} t\right)\right]. \qquad (3.1.15)$$

For practical reasons, instead of the expression above, we consider the quantity

$$\frac{m(L,t)\,L}{C_0 F} = D_e t\left\{1 - \frac{\alpha L^2}{6 D_e t}\left[1 + \frac{12}{\pi^2}\sum_{n=1}^{\infty}(-)^n \frac{1}{n^2}\exp\left(-\pi^2 n^2 \frac{D_e}{\alpha L^2} t\right)\right]\right\} \quad , \qquad (3.1.16)$$

with units [m^2]. For large times, $t \to \infty$, every term of the series vanishes and hence, the asymptotic (linear) limit solution is given by:

$$\lim_{t \to \infty} \frac{m(L,t)\,L}{C_0\,F} = D_e\,t - \frac{\alpha L^2}{6} \quad , \tag{3.1.17}$$

from which values for the effective diffusion constant D_e and the rock capacity factor α can be obtained. D_e can be determined from the slope and α from the intercept of the backward extrapolated linear relationship with the time axis, t_0:

$$\alpha = \frac{6 D_e\,t_0}{L^2} \quad . \tag{3.1.18}$$

Thus, t_0 is a measure of the time required to reach a steady-state. For a conservative - i.e. non-sorbing - tracer the rock capacity factor is equal to the porosity of the HCP accessible to the tracer flux. Hence, a third parameter value can be determined.

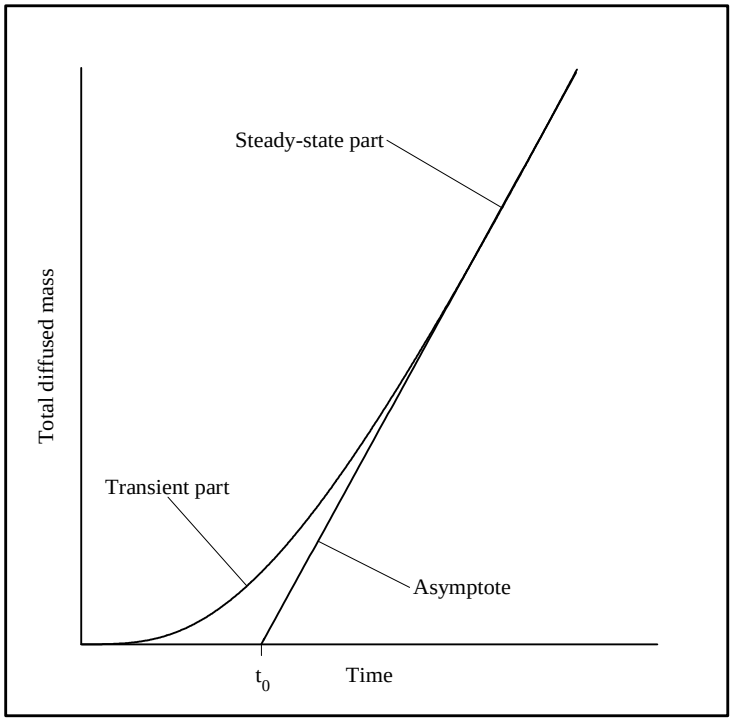

Figure 3.1.-1: The time history of the total diffused mass *m(L,t)* according to equation (3.1.16). Indicated is also the asymptotic limit solution (3.1.17). From the slope of this linear relationship a value for the effective diffusion constant D_e and from the intercept with the time axis (t_0) a value for the rock capacity factor α can be determined. For non-sorbing (conservative) tracers the rock capacity factor is equal to the porosity of the diffusion barrier.

Equation (3.1.7), or alternatively the system of differential equations (3.1.1) and (3.1.2.) or (3.1.3) respectively, has been solved with the help of the subroutine “MOLCH/DMOLCH” of the IMSL/MATH-library [33]. With “MOLCH/DMOLCH” a system of coupled second-order partial differential equations can be solved with an arbitrary initial condition and mixed vonNeumann/Dirichlet boundary conditions using the method of lines. In this package cubic Hermite polynomials are used for the spatial approximation and Gear’s stiff method for the time integration. The output of “MOLCH/DMOLCH” represents the time-history of the flux

$j(x = L, t)$. This is substituted into equation (3.1.15) and numerically integrated with the help of the simple Simpson's rule to arrive at $m(L,t)$ according to the left hand side of equation (3.1.15). However, $j(L,t))$ is used as the basis for a regression algorithm for the measured flux data with either (D_e, K_d), or (D_e, K_p, N_p), or (D_e, k_s, N_s, k_r) as regression parameters [17]. In practice we have taken the parameters as such neglecting the fact that they have not the same order of magnitude. To avoid this we could have used logarithms; however, we did not investigate the effect on the best-fit values of the parameters. Assuming that a particular model represents the most relevant physical processes quite well, for the fitting procedure the modified Levenberg-Marquardt method is used by minimising of the χ^2-merit function with the help of the IMSL/STAT-library function "RNLIN/DRNLIN".
The χ^2-merit function is defined by

$$\chi^2 = \sum_{i=1}^{M} \left[\frac{j(L,t_i) - j_i}{\sigma_i} \right]^2 \tag{3.1.19}$$

where j_i is the time history of the diffusive flux measured at M time points t_i = 1, 2, ..., M. Each of these data is associated with a total statistical error[18] characterised by the standard deviation σ_i. $j(L,t_i)$ is the tracer flux at the down-stream side of the HCP at $z = L$ calculated from equations (3.1.1) and (3.1.3) or (3.1.7), respectively. The variance of the fit s^2 is given by

$$s^2 = \frac{\chi^2 \overline{\sigma^2}}{\nu} = \chi_\nu^2 \overline{\sigma^2} \tag{3.1.20}$$

where the factor $\nu = (M - n)$ is the number of degrees of freedom of the fit and n is the number of freely adjustable parameters of a particular model.

$$\overline{\sigma^2} = \frac{1}{\frac{1}{M} \sum_{i=1}^{M} \frac{1}{\sigma_i^2}} \tag{3.1.21}$$

is the weighted average of the individual variances σ_i^2 of the measurements, and χ_ν^2 is the reduced chi-square. χ_ν^2 or s^2 respectively, is characteristic for both the dispersion of the data around the mean and the accuracy of the fit. If the fitting function is an appropriate representation of the measurements, then χ_ν^2 should be approximately unity; if the fitting function is not appropriate, then χ_ν^2 will be significantly greater than 1. However, a comparison of the χ_ν^2-values only yields a measure of the relative goodness-of-fit of competing models based - of course - on the same set of experimental data.

The Hessian matrix $\boldsymbol{A}$ is defined by

---

[17] In principle in fitting the breakthrough curve, the time history of the tracer mass taken up by the specimen could be fitted and then the breakthrough curve used as a test for the given model. However, such a procedure is not appropriate because the process of tracer deposition may also include precipitation and dissolution reactions which are certainly not part of our formalism. In addition, the deposited tracer mass is a cumulative quantity (proportional to the difference of the time-integrals over the diffusive flux at both boundaries) covering finer details of the deposition process.

[18] All the measurement errors are considered to be independent as well as random and are normally distributed around the expectation value.

$$A_{ij} = \frac{\partial^2 \chi^2}{\partial p_i \, \partial p_j} \quad , i, j = 1, 2, \ldots, n \quad , \tag{3.1.22}$$

which is the second derivative matrix of the χ^2-merit function at any $\vec{p}$, where $\vec{p}$ is a vector containing the n fit-parameters of the model. The inverse of $\boldsymbol{A}$ is proportional to $\boldsymbol{C}$, the covariance matrix of the standard errors in the fitted parameters $\vec{p}$, hence

$$\boldsymbol{C} = 2\,\boldsymbol{A}^{-1} \quad . \tag{3.1.23}$$

The standard errors σ_{p_i} of the regression parameters are related to the diagonal elements of $\boldsymbol{C}$ by

$$\sigma_{p_i} = \sqrt{C_{ii}\,\chi^2_\nu} \quad , i = 1, 2, \ldots, n \quad , \tag{3.1.24}$$

and the correlation matrix $\boldsymbol{R}$ is then given by

$$R_{ij} = \frac{C_{ij}}{\sqrt{C_{ii} C_{jj}}} \quad , i, j = 1, 2, \ldots, n \quad . \tag{3.1.25}$$

R_{ij} - with numbers between -1 and 1 - is the correlation coefficient expressing the degree of association between the uncertainties of two regression parameters. If both parameters are independent, then their covariance is zero; hence, R_{ij} is also zero. A positive value for R_{ij} indicates that both errors of the parameters p_i and p_j are correlated and have the same sign; a negative value indicates that the errors of the parameters are anti-correlated and have opposite sign.

It is important to apply the fitting-procedure several (20 - 50 - 100 - …) times using different starting values for the fit-parameters in order to ensure that the global minimum of the χ^2-merit function has finally been located.

3.2. Modelling results

3.2.1. Modelling results for the chloride experiments no. 3 and 4

3.2.1.1. No sorption case

The breakthrough curves were fitted to the left hand side of equation (3.1.14) using the procedure outlined in sub-section (3.1).

In a series of fits in which sorption was completely neglected, the only free parameter, the effective diffusivity, was adjusted to the flux profiles using the measured data from the first 50, 100, 150 and 175 days. The quality of the fits in general is very poor: the slopes do not match the data, and the transient parts of the diffusion curves especially are crudely reproduced.

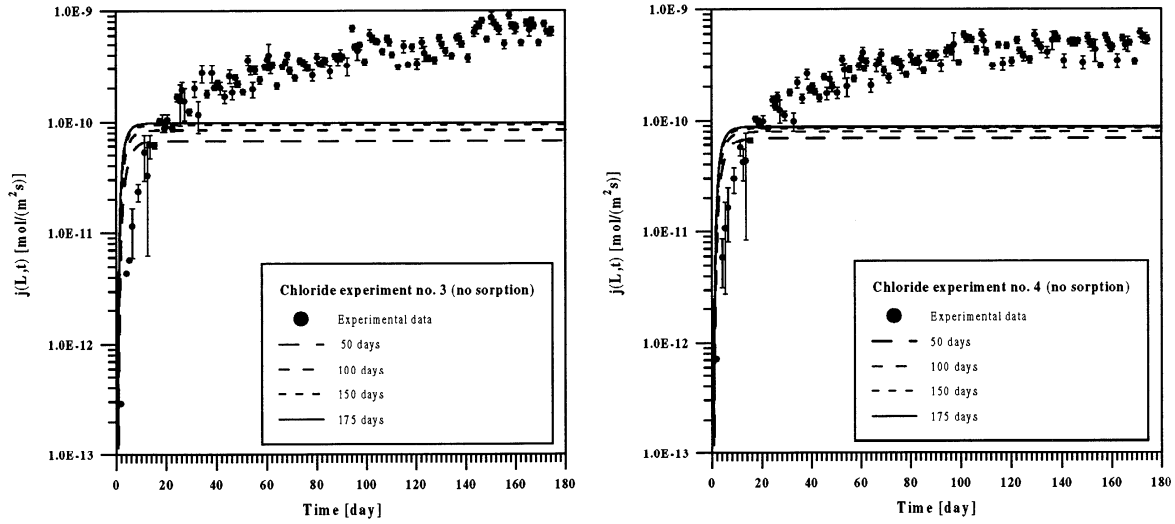

Figure 3.2.1.1.-1: Plots of the experimental data and theoretical breakthrough curves for chloride of experiments no. 3 and 4 and when neglecting sorption at all. Shown are the best-fit curves using experimental measurements from the first 50, 100, … etc. days as indicated in the legends.

In the following table the best-fit parameter values for both chloride experiments are compiled; within one standard deviation corresponding values coincide with each other.

An obvious conclusion from this exercise is the following: Having fixed the sample's porosity and adjusted the only free fit-parameter - the effective diffusion constant D_e - it is impossible to reproduce the measured data, meaning that **at least a further transport mechanism which accounts for chloride retardation, such as e.g. sorption, is necessary if we want to arrive at an acceptable description for the chloride-diffusion profile.**

Best-fit values for chloride through-diffusion - no-sorption case					
		Experiment no. 3		Experiment no. 4	
Δt	N	$D_e \cdot 10^{10}$	χ^2_ν	$D_e \cdot 10^{10}$	χ^2_ν
[day]	[-]	[m^2/s]	[-]	[m^2/s]	[-]
0 - 50	33	0.244 ± 0.029	152	0.247 ± 0.025	161
0 - 100	70	0.303 ± 0.033	287	0.284 ± 0.028	265
0 - 150	100	0.336 ± 0.034	361	0.303 ± 0.029	322
0 - 175	118	0.350 ± 0.035	399	0.313 ± 0.028	337

Table 3.2.1.1.-1: Compilation of the best-fit values[19] for the effective diffusivity D_e together with their one standard deviation errors for chloride through-diffusion and both experiments. For the adjustments N data triplets were used measured in the interval Δt. For comparison purposes the minimal values of the reduced χ^2_ν are given.

[19] Here, and in the rest of the report, fitted parameter values are given to three digits in order to be able to reproduce the calculations. However, this does not imply that the three digits are significant.

3.2.1.2. Linear sorption case

In a further step, linear, instantaneous equilibrium sorption onto the inner surfaces of the HCP was taken into account. In the procedure, a further fit-parameter - the linear equilibrium sorption distribution coefficient K_d - could now be varied. As before, in a series of subsequent fits both parameters were adjusted to the flux profiles using measured data from the first 50, 100, 150 and 175 days. The calculated breakthrough curves now lay much closer to the experimental data than when sorption was neglected.

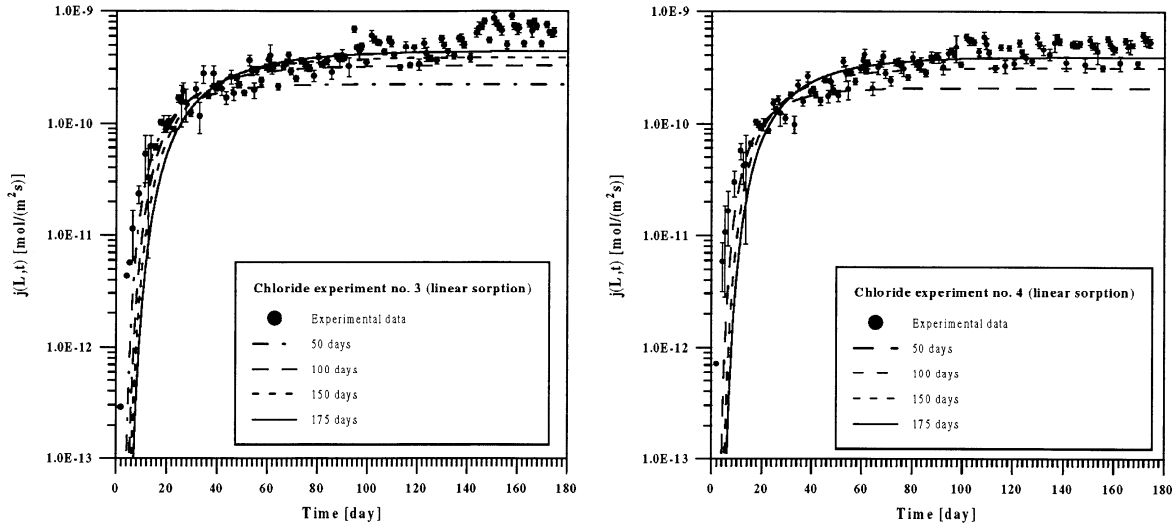

Figure 3.2.1.2.-1: Plots of the experimental data and theoretical breakthrough curves for chloride of experiments no. 3 and 4 assuming linear sorption. The best-fit curves are shown using experimental measurements from the first 50, 100, … etc. days as indicated in the legends.

Compared to the former exercise where sorption was entirely neglected, the improvement of the fits is obvious. However, as more and more measurements are taken into account the reproduction of the data in the plateau region improves, whereas the coincidence of measured data and theory in the rising edge simultaneously becomes worse. There, the model predicts a significantly lower diffusive flux due to too small sorption of the tracer onto the solid phase. Fitting the data for the first 50 days led to a rather strong correlation between D_e and K_d (R_{12} (50 days) = 0.963 [20] for experiment no. 3 and R_{12} (50 days) = 0.970 for experiment no. 4, respectively); using more and more data for the procedure lowered this value to about 0.89 for both experiments.

When inspecting the best-fit parameter values of Table 3.2.1.2.-1 we can recognise that for experiment no. 3 - although the experiments continued for about half a year - a steady state was never reached. Consequently, the values for the effective diffusion constant increase monotonically as the diffusive flux becomes larger. This is because in experiment no. 3 the diffusive flux is enhanced after about 140 days as a consequence of slow chloride release from the HCP, an effect which can be clearly seen in the following figure (left plot). Note that such an effect cannot be recognised for experiment no. 4. The tendency for monotonically increasing best-fit parameter values and increasing discrepancies in the rising edge between model and measurements when using more and more data for the fitting procedure indicates the essential deficiency or inadequacy of the model.

[20] Subscript "12" in R_{12} denotes the first and second parameter.

		Best-fit values for chloride through-diffusion - linear sorption case					
		Experiment no. 3			Experiment no. 4		
Δt	N	$D_e \cdot 10^{10}$	$K_d \cdot 10^3$	χ^2_ν	$D_e \cdot 10^{10}$	$K_d \cdot 10^3$	χ^2_ν
[day]	[-]	[m^2/s]	[m^3/kg]	[-]	[m^2/s]	[m^3/kg]	[-]
0 - 50	33	0.793 ± 0.048	13.1 ± 1.6	13.67	0.735 ± 0.053	11.4 ± 1.7	20.15
0 - 100	70	1.16 ± 0.05	26.2 ± 2.3	32.56	1.11 ± 0.05	24.3 ± 2.1	32.01
0 - 150	100	1.38 ± 0.06	36.9 ± 3.1	46.49	1.33 ± 0.05	34.3 ± 2.6	41.67
0 - 175	118	1.56 ± 0.07	48.8 ± 4.4	60.80	1.38 ± 0.05	37.0 ± 2.5	41.68

Table 3.2.1.2.-1: Compilation of the best-fit values for the effective diffusivity D_e and the volume-based sorption equilibrium distribution coefficient K_d together with their one-standard deviation errors for chloride through-diffusion and for both experiments. For the adjustments N data triplets were used measured in the interval Δt. For comparison purposes the minimal values of the reduced χ^2_ν are given.

For experiment no. 4 however, inspection of the series of best-fit parameter values, suggests the experiment may be nearly in steady-state after about 150 days. The best-fit parameter values for D_e and K_d are constant within one standard deviation using more than 100 data. In the following figure the calculated total deposited tracer mass in the HCP as a function of time is compared with measurements.

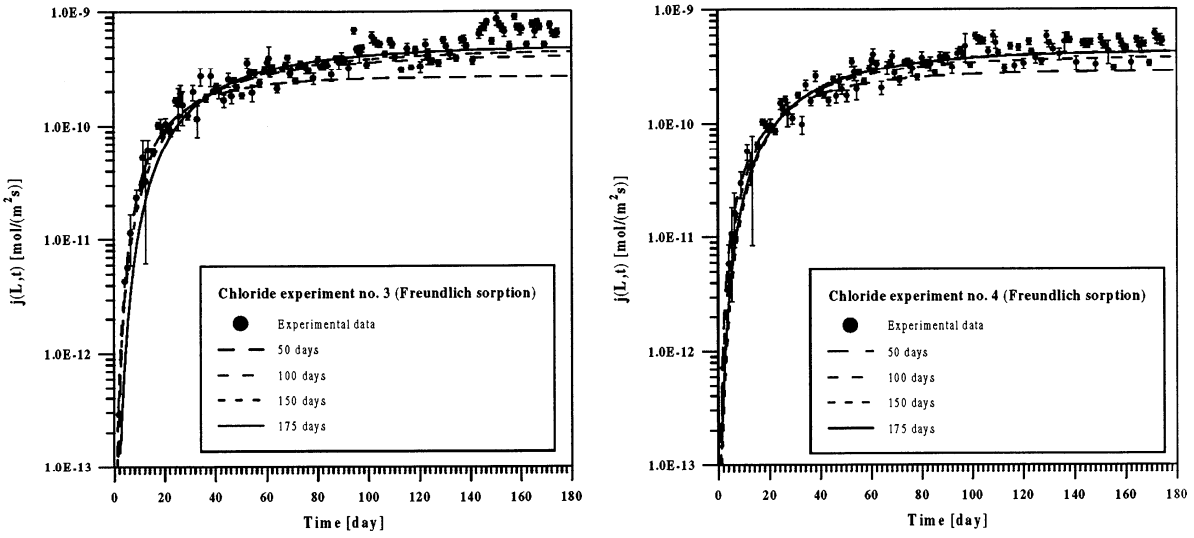

Figure 3.2.1.2.-2: Comparison of the time history of the measured deposited tracer mass $\Delta m(t)$ in the HCP for chloride of experiments no. 3 and 4 with theoretical curves. The curves correspond to best-fits of the diffusive flux assuming a linear isotherm for sorption and using experimental data from the first 50, 100, … etc. days as indicated in the legends.

For no combination of the extracted best-fit parameter-values do the calculated profiles for the amount of deposited tracer mass $\Delta m(t)$ correspond to those of the measurements. This is considered a serious indication that the simple 1D-diffusion model even assuming linear sorption of the tracer is not able to successfully describe the processes involved.
There are other studies for the diffusion of chloride ions through water-saturated cementitious materials. Page et al. [34] measured the diffusion of 1M NaCl solution through cementitious disk-like specimens of various compositions and for several water/cement ratios (W/C) in the temperature range 7 - 47 °C. In the table below we have compiled those averaged value for D_e performed at a temperature T = 25 °C using Ordinary Portland Cement (OPC) or a Sulphate Resistant Portland Cement (SRPC)[21].
Lambert et al. [35] studied the effects of diffusion kinetics on chloride ions in mature hydrated pastes of pure alite ($C_{54}S_{16}AM$) over the temperature range 7 - 45 °C.
Another study was performed by Johnston et al. [2] using an SRCP grout. In the following table we have compiled - for comparison purposes - the values from these studies.
Both chloride experiments were modelled 1992 by Sarott et al. [6]. They evaluated them by fitting the time history of the accumulated diffused chloride mass $m(t)$ neglecting the individual errors of the measurements. If $m(t)$ is used as the basis for a regression algorithm, short term fluctuations in the diffusive flux are damped out especially at large times, and the breakthrough curve becomes strongly smoothed. Hence, it appears the diffusion process is in steady-state although the system is still slowly evolving. Therefore we consider the method of modelling the flux $j(t)$ rather than $m(t)$ to be more appropriate, because every data point is independent and unavoidable measurement errors are not accumulated as they are when using $m(t)$.

	$D_e \cdot 10^{12}$ [m^2 /s]						$K_d \cdot 10^3$ [m^3 /kg]		
W/C [-]	OPC	Ref.	SRPC	Ref.	Alite	Ref.	SRPC	Ref.	
0.25			0.773 / 0.397	[2]					
0.35			1.25 / 1.35	[2]					
0.4	2.60	[34]							
0.5	4.47	[34]	10.00	[34]					
0.6	12.35	[34]			6.67	[35]			
1.3			160 - 200 150 - 170	[6]			26 - 40 27 - 29	[6]	
1.3			156 ± 7 138 ± 5	this study			48.4 ± 4.4 37.0 ± 2.5	this study	
1.3							24	[17]	Batch

Table 3.2.1.2.-2: Reported values for the effective diffusion coefficient D_e and the distribution coefficient K_d for chloride at various water/cement ratios (W/C) and measured at about 25 °C (Reference [2]: 21 °C). For the investigations Ordinary Portland Cement (OPC) as well as Sulphate-Resistant Portland Cement (SRPC) were used. One study was done using a single phase (alite) of OPC and SRPC. For comparison purposes also one K_d value originating from batch sorption experiments is included.

[21] Sulphate-resistant Portland cement (SRPC) contains more iron and less aluminium than OPC resulting in a C_3A content roughly an order of magnitude lower than that of OPC (≈ 15% C_3A for OPC and ≈ 1.5% C_3A for SRCP).

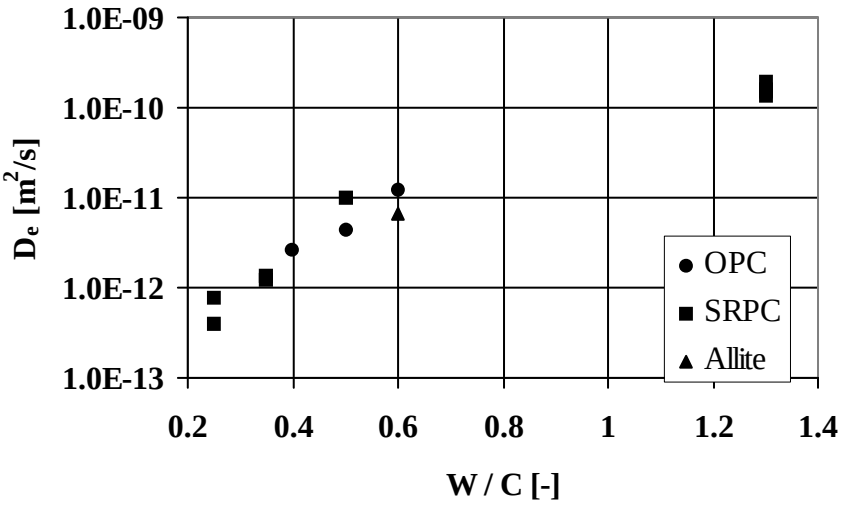

Figure 3.2.1.2.-3: Reported values for the effective diffusion coefficient D_e for chloride as a function of the water/cement ratio (W/C). The temperature was 25 or 21 °C respectively.

From figure 3.2.1.2.-3 and the underlying data of table 3.2.1.2.-2 we see that values for D_e increase monotonically with increasing values of the water/cement ratio. An exponential relationship may prevail at small W/C ratios, especially when taking into account data obtained on SRPC only. But when considering all data and higher water/cement ratios the measurements no longer appear to follow an exponential function. Since the porosity not only changes with the W/C ratio but is also related to the times for hydration we cannot discuss the geometry factor any longer.
The best-fit values for K_d are roughly a factor of 1.5 higher than values from the former study performed by Sarott et al. [5] and also those from batch sorption experiments. These too high K_d values are consistent with the fact that the calculated tracer deposition is higher than the measured data and is a result of the fitting procedure to match the asymptotic flux data.

Reasonable conclusions which can be drawn are:

- Compared with the first fit (see section 3.2.1.1.) where sorption was entirely excluded, accounting for linear sorption considerably improves the quality of the fit. However, when using more and more data for the adjustment the reproduction of the rising edge constantly becomes worse.
- The parameter values extracted for the effective diffusion constant and the distribution coefficient are not unreasonable a priori. But, when taking into account further information from independent experiments, especially the values for K_d seem to be too high by a factor of about 1.5 - 2.
- The measured tracer deposition data are only very crudely reproduced by the model. The shape of the rising edge especially has not much to do with the data. The plateau region in the model is already reached after about 20 days, whereas the measurements show slow tracer deposition for at least 100 - 120 days.
- All these deficiencies lead to the evident conclusion that this concept for diffusion including linear sorption is not sufficient or not appropriate to successfully model the measurements of chloride through-diffusion.

3.2.1.3. Non-linear (Freundlich) sorption case

Again, a series of fits was carried out using only data from the first 50, 100, ... etc. days. The freely adjustable parameters are now the effective diffusion coefficient D_e, the Freundlich coefficient K_p [$\mathrm{mol}^{1-N_p}\mathrm{m}^{3N_p}\mathrm{kg}^{-1}$], and the exponent N_p [-], i.e., one more than in the linear sorption case.

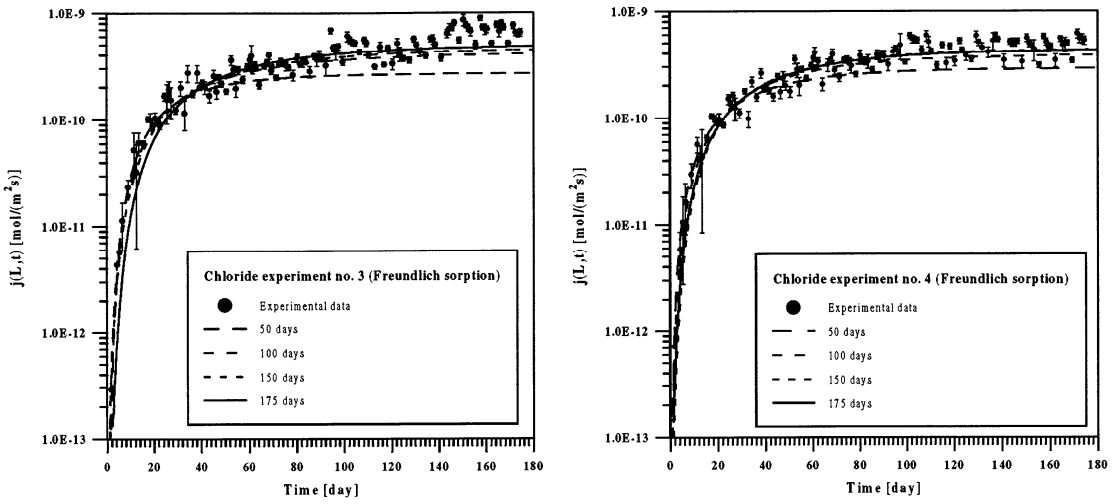

Figure 3.2.1.3.-1: Comparative plot of the experimental data and theoretical breakthrough curves for chloride (experiment no. 3 left plot and experiment no. 4 right) assuming non-linear Freundlich sorption behaviour of the tracer. The best-fit curves using experimental data from the first 50, 100, etc. days are shown as indicated in the legends.

Adjusting a third parameter requires more calculational effort to find the global χ^2_v-minimum. Different sets of starting values do not cogently result in the same best-fit parameter values. Therefore, considerably more calculations were performed than in the linear sorption case to ensure that the global χ^2_v-minimum was reached. When fitting data for the first 50 and 150 days strong (anti-)correlations between the two Freundlich parameters were obtained indicating that the model may be over-parametrised. The correlation coefficients for experiment no. 3 are R_{23}(50 days) = 0.951 and R_{23}(150 days) = 0.971 and for experiment no. 4 R_{13}(50 days) = -0.993 and R_{23}(150 days) = 0.986. According to [36] the Freundlich exponent has to be smaller than unity assuming that the surface being considered heterogeneous for exchange and that each class of exchange sites individually absorbs according to the Langmuir isotherm. However, the values of the Freundlich exponent are always significantly larger than unity (see also the following Table 3.2.1.3.-1) which can be interpreted as precipitation [37]. A former analysis of the two experiments by Sarott et al. also found that the best-fit values for the Freundlich exponent are always larger than unity,
Improvement of the fits is only moderate compared to those models using a linear sorption isotherm for the cement/nuclide interaction. The Freundlich concept, too, especially for experiment no. 3, is not able to reproduce the data with high precision both in the rising edge and in the plateau region.

Best-fit values for chloride through-diffusion - non-linear (Freundlich) sorption case				
Δt [day]	N [-]	Parameter	Experiment no. 3	Experiment no. 4
0 - 50	33	$D_e \cdot 10^{10}$ [m^2/s]	0.963 ± 0.046	1.04 ± 0.09
		$K_p \cdot 10^3$ [mol$^{1-N_p}$m^{3N_p}kg^{-1}]	68.0 ± 5.2	179 ± 12
		N_p [-]	1.26 ± 0.04	1.43 ± 0.05
		χ^2_ν [-]	11.73	16.62
0 - 100	70	$D_e \cdot 10^{10}$ [m^2/s]	1.50 ± 0.06	1.39 ± 0.06
		$K_p \cdot 10^3$ [mol$^{1-N_p}$m^{3N_p}kg^{-1}]	271 ± 28	236 ± 5
		N_p [-]	1.37 ± 0.03	1.37 ± 0.02
		χ^2_ν [-]	21.85	20.57
0 - 150	100	$D_e \cdot 10^{10}$ [m^2/s]	1.65 ± 0.04	1.57 ± 0.04
		$K_p \cdot 10^3$ [mol$^{1-N_p}$m^{3N_p}kg^{-1}]	275 ± 37	181 ± 38
		N_p [-]	1.33 ± 0.04	1.27 ± 0.04
		χ^2_ν [-]	31.04	27.07
0 - 175	118	$D_e \cdot 10^{10}$ [m^2/s]	1.78 ± 0.07	1.56 ± 0.04
		$K_p \cdot 10^3$ [mol$^{1-N_p}$m^{3N_p}kg^{-1}]	189 ± 14	223 ± 15
		N_p [-]	1.22 ± 0.02	1.31 ± 0.03
		χ^2_ν [-]	44.29	26.76

Table 3.2.1.3.-1: Compilation of the best-fit values for the effective diffusivity, the Freundlich coefficient and the exponent together with their one-standard deviation errors for chloride through-diffusion experiments no. 3 and 4. For the adjustments, N data triplets were used measured in the interval Δt. For comparison purposes the minimal values of the reduced χ^2_ν are given.

The best-fit values for D_e are 10 - 30% larger than those found when assuming linear sorption for the tracer. While the Freundlich exponent is more or less constant, the coefficient tends towards high values (with large error bars) enforcing the retardation of the tracer.
Considering further information about deposition of the tracer within the HCP clearly shows the principal deficiencies of the concept for both experiments. This is illustrated in the following figure that shows the time history of calculated and measured total deposited mass in the HCP for both experiments.

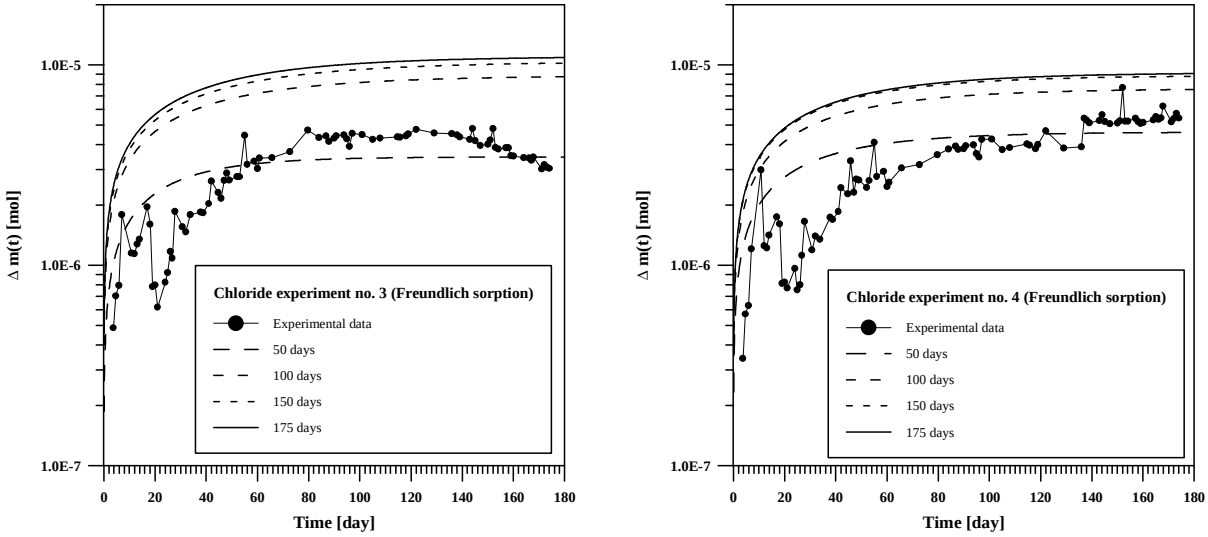

Figure 3.2.1.3.-2: Comparison of the time history of the measured tracer mass $\Delta m(t)$ deposited in the HCP for chloride of experiments no. 3 and 4 and theoretical curves. The curves correspond to best-fits of the diffusive flux assuming a non-linear (Freundlich) isotherm for sorption and using experimental data from the first 50, 100, … etc. days as indicated in the legend.

As can be seen from the figure, with the exception of the first calculation that uses only data from the first 50 days for the fitting procedure, all the calculations show too much tracer deposition in the HCP. In addition, the increasing part of the measured deposition 'curve' is only poorly reproduced thus supporting the assumption that the concept is not appropriate to model the experiment successfully.
The next figure illustrates the partitioning of the total deposited tracer mass in the HCP for experiment no. 3.

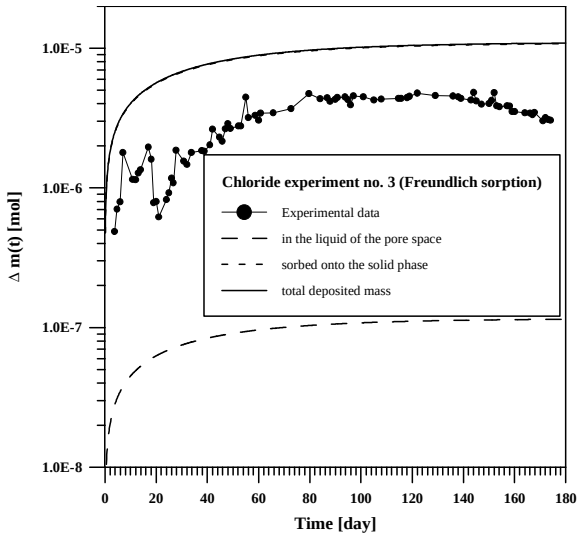

Figure 3.2.1.3.-3: Partitioning of the calculated total deposited mass between that which is in the liquid of the connected pore space and which is sorbed onto the solid phase of the HCP. The calculation is performed for chloride (experiment no. 3), assuming non-linear (Freundlich) sorption. The parameter values originate from the best-fit using all experimental data for the fitting procedure.

Some 90 % of the tracer is sorbed onto inner surfaces of the connected pore space and only 10 % is within the liquid phase. This is also illustrated in the following figure where the time history of the partition coefficient $\Delta m(t)_{solid} / \Delta m(t)_{liquid}$ is plotted.

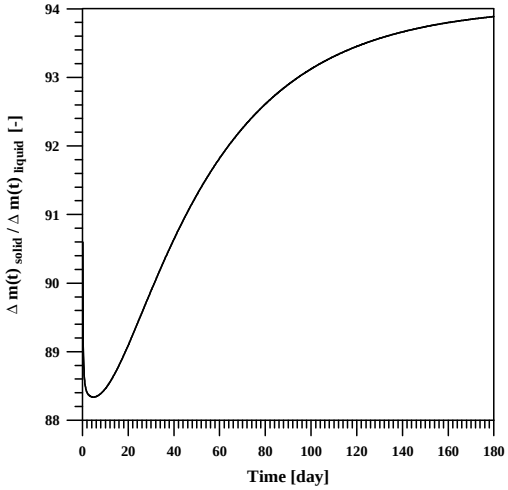

Figure 3.2.1.3.-4: Calculated partition coefficient versus time for chloride and experiment no. 3. The underlying best-fit parameter values for the calculation are those where all available measurements (0 - 175 days) were taken into account. After about 5 days the quantity reaches a global minimum indicating that the migrating nuclides have reached the zero-concentration (down-stream) boundary.

Because the Freundlich exponent is larger than unity, the isotherm is convex with higher partition coefficients at higher contaminant concentrations. At higher concentrations the partition coefficient increases resulting in a front-smeared breakthrough curve because the lower concentration part of the breakthrough curve propagates faster than the high concentration part. Hence, at the beginning the tracer is diluted in the HCP, and the partition coefficient decreases from its starting value. When the weakly retarded nuclides arrive at the zero-concentration down-stream boundary they are removed quickly, and the dilution effect reaches its maximum. Now, due to the slow propagation of the more strongly retarded nuclides, the amount of sorbed tracer increases continuously until steady-state is reached. Assuming a linear concentration profile across the sample at steady-state according to

$$C(x,t) = C_0 \, (1 - \frac{x}{L}) \tag{3.2.1}$$

we can estimate the asymptotic value for the partition coefficient:

$$\frac{\Delta m_{solid}}{\Delta m_{liquid}} = \frac{F \rho (1-\varepsilon) \int_0^L S(x,t)\, dx}{F \varepsilon \int_0^L C(x,t)\, dx} = \frac{\rho(1-\varepsilon)}{\varepsilon} \frac{2}{N_p + 1} K_p \, C_0^{N_p - 1} \tag{3.2.2}$$

in which the symbols are those of sub-section (3.1).

For experiment no. 3 the asymptotic value for the partition coefficient is about 95.6; the maximum number value at the beginning of the experiment based on

$$\frac{\Delta m_{solid}}{\Delta m_{liquid}} = \frac{\rho(1-\varepsilon)}{\varepsilon} K_p C_0^{N_p-1} \qquad (3.2.3)$$

is of the order of 106. For experiment no. 4 these values are 78.8 for the asymptote and 90.9 at the beginning.

3.2.1.4. First-order sorption kinetics - linear/linear case

In a further step we investigated the effect of first-order sorption kinetics according to equations (3.1.1) and (3.1.3) on the diffusion-sorption profile. In our concept sorption, may in principle be non-linear and desorption linear; however, at first to avoid a further free fit-parameter, we fixed the exponent to unity, so that both the forward and the backward reaction are linear relationships. The fit-parameters were the effective diffusivity D_e, the rate for sorption k_s and the rate for desorption k_r. In a series of subsequent fits using data from the first 50, 100, ... etc. days the parameters were adjusted by minimising the χ^2-merit function.

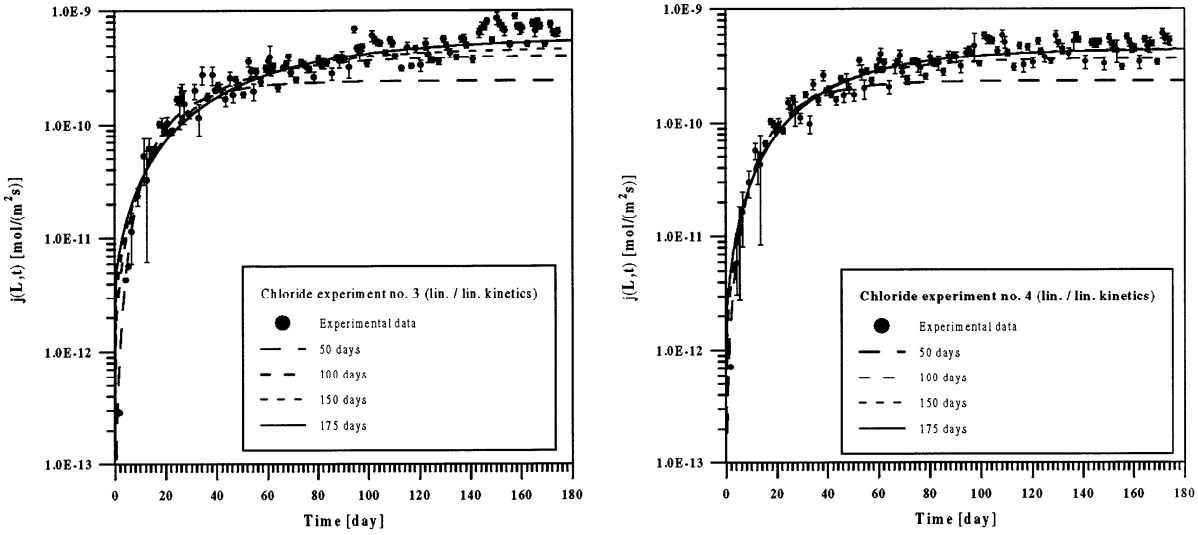

Figure 3.2.1.4.-1: Comparative plot of the experimental data and theoretical breakthrough curves for chloride in experiment no. 3 and 4 assuming first-order sorption kinetics. The best-fit curves using experimental data from the first 50, 100, etc. days are shown as indicated in the legends.

Reproductions of the flux profiles by this model are similar to those for the non-linear (Freundlich) case. However, when using more and more measurements for the adjustment, the model predicts too high a diffusive flux at the beginning. Although the concept has three fit-parameters as has the non-linear (Freundlich) model, there are no longer strong correlations between these parameters. The best-fit values, together with their standard deviations, are compiled in the next table.

Best-fit values for chloride through-diffusion - first-order sorption kinetics (linear/linear)				
Δt [day]	N [-]	Parameter	Experiment no. 3	Experiment no. 4
0 - 50	33	$D_e \cdot 10^{10}$ [m^2/s]	0.871 ± 0.082	0.835 ± 0.090
		$k_s \cdot 10^4$ [s^{-1}]	1.75 ± 1.29	1.25 ± 0.49
		$k_r \cdot 10^6$ [s^{-1}]	8.66 ± 7.73	6.60 ± 3.25
		χ^2_ν [-]	11.83	17.32
		$K_d \cdot 10^3$ [m^3/kg]	16.4 ± 19.1	15.4 ± 9.8
0 - 100	70	$D_e \cdot 10^{10}$ [m^2/s]	1.46 ± 0.11	1.33 ± 0.09
		$k_s \cdot 10^4$ [s^{-1}]	1.62 ± 0.23	1.53 ± 0.21
		$k_r \cdot 10^6$ [s^{-1}]	2.75 ± 0.67	3.15 ± 0.67
		χ^2_ν [-]	23.08	21.96
		$K_d \cdot 10^3$ [m^3/kg]	47.8 ± 14.1	39.4 ± 10.5
0 - 150	100	$D_e \cdot 10^{10}$ [m^2/s]	1.71 ± 0.10	1.63 ± 0.08
		$k_s \cdot 10^4$ [s^{-1}]	1.70 ± 0.22	1.66 ± 0.17
		$k_r \cdot 10^6$ [s^{-1}]	2.01 ± 0.36	2.22 ± 0.35
		χ^2_ν [-]	30.89	25.12
		$K_d \cdot 10^3$ [m^3/kg]	68.6 ± 16.1	60.6 ± 12.4
0 - 175	118	$D_e \cdot 10^{10}$ [m^2/s]	2.10 ± 0.13	1.61 ± 0.06
		$k_s \cdot 10^4$ [s^{-1}]	1.90 ± 0.19	1.66 ± 0.17
		$k_r \cdot 10^6$ [s^{-1}]	1.42 ± 0.22	2.28 ± 0.33
		χ^2_ν [-]	36.90	26.28
		$K_d \cdot 10^3$ [m^3/kg]	108 ± 22	59.0 ± 11.5

Table 3.2.1.4.-1: Compilation of the best-fit values for the effective diffusivity, the rates for sorption k_s and desorption k_r together with their one-standard deviation errors for chloride through-diffusion and both experiments. In addition the calculated values for the volume-based sorption equilibrium constant K_d in the asymptotic steady-state limit are presented (see text). For the adjustments N data triplets were used measured in the interval Δt. For comparison purposes the minimum values of the reduced χ^2_ν are given.

Compared to the former case which assumed non-linear (Freundlich) sorption for the tracer retardation, the best-fit values for D_e are the same within 2σ's. Both concepts have the same degree of freedom of the fit, and the minimum values for the χ^2-merit function can be compared. According to this quantity the non-linear sorption case reproduces the rising edge

slightly better; however, when the data from the plateau region are also taken into account the first-order sorption kinetics model fits the data better. Hence, we conclude that the third concept only moderately improves the overall quality of the fit.

In the near steady-state where $dS / dt \cong 0$, with S [mole/kg] the amount of tracer sorbed on the solid phase, we can calculate a value for the volume-based sorption equilibrium constant K_d [m^3/kg] from the two rate constants for sorption k_s [s^{-1}] and desorption k_r [s^{-1}] of the reversible first-order kinetics sorption equation (3.1.3) with $N_s = 1$ according to:

$$K_d := \frac{\varepsilon}{(1-\varepsilon)\,\rho}\,\frac{k_s}{k_r} \quad . \tag{3.2.4}$$

In Table 3.2.1.4.-1 above we compiled the values for K_d in the steady-state limit. Considering more and more data for the fit increases the values for the K_d. Most of the values seem unrealistically high when compared with data from batch sorption experiments [17]. These experiments suggest a value for chloride of the order of $K_d \approx 24 \cdot 10^{-3}$ m^3/kg. Such a disagreement is considered an additional indication that this concept fails to reproduce the measurements successfully. In batch experiments, ground cementitious material with a well defined upper grain size is used. By such grinding, new sites will be made available for sorption; hence, a higher K_d-value is expected rather from batch than from diffusion experiments.
Finally, with the help of the following figure let us compare the measured time history of the deposited tracer mass in the specimen with the model results for both experiments.

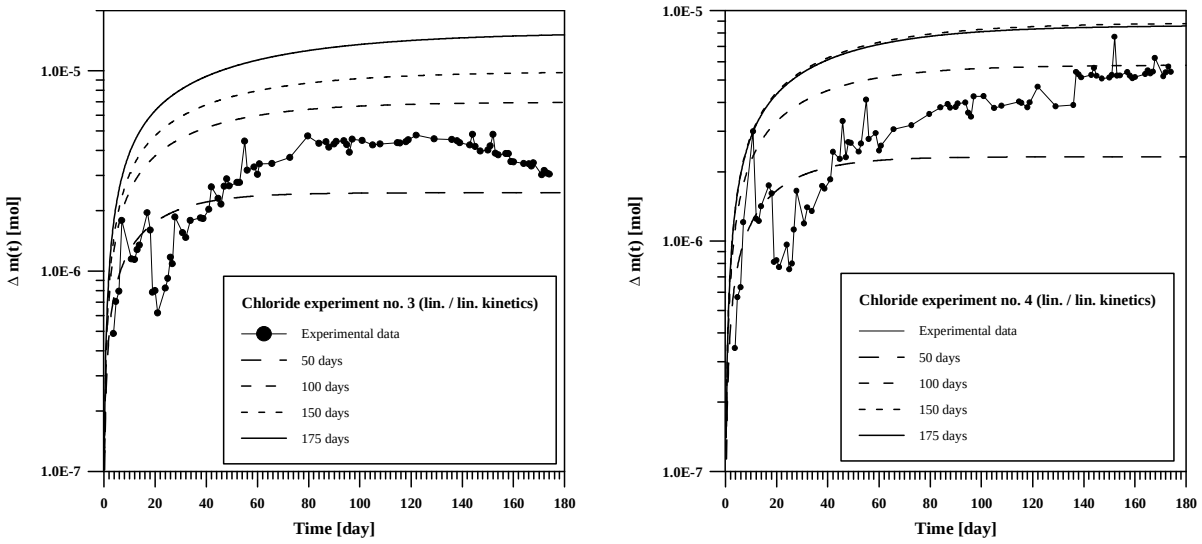

Figure 3.2.1.4.-2: Comparison of the time history of the measured deposited tracer mass $\Delta m(t)$ in the HCP for chloride of experiments no. 3 and 4 with theoretical curves. The curves correspond to best-fits of the diffusive flux assuming first-order sorption kinetics and using experimental data from the first 50, 100, … etc. days as indicated in the legends.

As in the previous cases, using the best-fit parameter values from modelling the breakthrough curve, the present model completely fails to reproduce the measured deposition data. Both shapes and magnitudes of the calculated deposition curves are wrongly reproduced. Only the first calculation using experimental breakthrough data from the first 50 days for the adjustment approximately reproduces roughly the data for both experiments. However, from

the considerations above we know that the model together with the extracted best-fit parameter values has only little predictive capability.
The most obvious conclusion which can be drawn is that this concept, too, is not able to reproduce all the measurements of this diffusion/sorption experiment with high quality. Therefore, at least another - either transport or chemical - mechanism must be included to arrive at a satisfactory description of the observations. Moreover we have difficulties deciding whether the sorption processes for chloride on cementitious material are modelled more correctly either by a linear or non-linear sorption approach or even by a first-order sorption kinetics equation.

3.2.1.5. First-order sorption kinetics - non-linear/linear case

For the sake of completeness, we investigated the effect of sorption kinetics using a non-linear equation (3.1.3) on the diffusion-sorption profile. This equation describes a fully reversible adsorption mechanism where the forward reaction is non-linear according to a Freundlich isotherm and the backward reaction is linear. This ansatz should account for both a better reproduction of the rising edge as for the concept using a Freundlich sorption isotherm and the benefit of the former linear sorption kinetics concept. In this equation k_s [$mol^{1-N_s}m^{3(N_s-1)}s^{-1}$] and k_r [s^{-1}] are the forward and backward adsorption rate coefficients respectively.

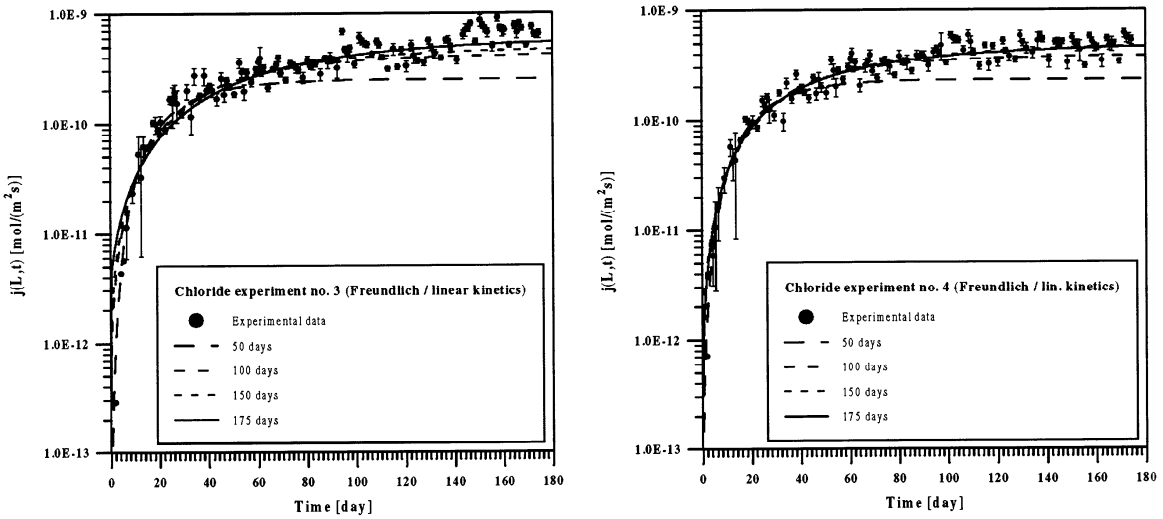

Figure 3.2.1.5.-1: Comparative plot of the experimental data and theoretical breakthrough curves for chloride in experiments no. 3 and 4 assuming a reversible non-linear sorption kinetics model. The best-fit curves using experimental data from the first 50, 100, etc. days are shown as indicated in the legends.

The figure looks practically identical to that from the linear kinetics model, although a further freely adjustable parameter N_s was available. As before, the diffusive flux is too high for the first 10 days, but the overall behaviour of the fit is still acceptable, especially when using the full dataset. However, when inspecting the best-fit parameter values, the essential deficiencies of the model become obvious.

Best-fit values for chloride through-diffusion - first-order sorption kinetics (non-linear (Freundlich) / linear)				
Δt [day]	N [-]	Parameter	Experiment no. 3	Experiment no. 4
0 - 50	33	$D_e \cdot 10^{10}$ [m^2/s]	0.905 ± 0.103	0.830 ± 0.097
		$k_s \cdot 10^4$ [mol$^{1-N_s}$m$^{3(N_s-1)}$s^{-1}]	6.28 ± 4.36	2.07 ± 3.04
		N_s [-]	1.11 ± 0.07	1.05 ± 0.10
		$k_r \cdot 10^6$ [s^{-1}]	16.9 ± 14.3	8.9 ± 11.0
		χ^2_ν [-]	12.20	17.84
0 - 100	70	$D_e \cdot 10^{10}$ [m^2/s]	1.55 ± 0.17	1.38 ± 0.09
		$k_s \cdot 10^4$ [mol$^{1-N_s}$m$^{3(N_s-1)}$s^{-1}]	13.0 ± 12.4	7.81 ± 4.97
		N_s [-]	1.23 ± 0.08	1.18 ± 0.08
		$k_r \cdot 10^6$ [s^{-1}]	6.83 ± 3.99	6.52 ± 2.35
		χ^2_ν [-]	22.56	21.59
0 - 150	100	$D_e \cdot 10^{10}$ [m^2/s]	1.77 ± 0.15	1.74 ± 0.11
		$k_s \cdot 10^4$ [mol$^{1-N_s}$m$^{3(N_s-1)}$s^{-1}]	13.4 ± 17.4	18.0 ± 14.3
		N_s [-]	1.23 ± 0.13	1.27 ± 0.10
		$k_r \cdot 10^6$ [s^{-1}]	5.10 ± 3.33	6.11 ± 2.56
		χ^2_ν [-]	30.23	23.75
0 - 175	118	$D_e \cdot 10^{10}$ [m^2/s]	2.15 ± 0.25	1.74 ± 0.10
		$k_s \cdot 10^4$ [mol$^{1-N_s}$m$^{3(N_s-1)}$s^{-1}]	5.5 ± 17.4	98.0 ± 27.9
		N_s [-]	1.13 ± 0.38	1.42 ± 0.04
		$k_r \cdot 10^6$ [s^{-1}]	2.11 ± 2.66	16.5 ± 6.1
		χ^2_ν [-]	36.54	24.41

Table 3.2.1.5.-1: Compilation of the best-fit values for the effective diffusivity, the exponent N_s, the rates for sorption k_s and desorption k_r together with their one-standard deviation errors for chloride through-diffusion and experiments no. 3 and 4. For the adjustments N data triplets were used measured in the time interval Δt. For comparison purposes the minimum values of the reduced χ^2_ν are given.

Again, the Freundlich exponent is always larger than unity indicating that the forward reaction is inconsistent with a simple exchange process. Moreover, the first two fits using data only from the first 50 and 100 days, seem not to be optimised, because the χ^2 values are even larger than those of the concept with a Freundlich isotherm. Compared to the linear sorption kinetics case, the values for k_s are between a factor of 3 to 8 larger and those for k_r larger by a factor of

1.5 to 2.5. However, all fits are slightly better than in the linear sorption kinetics case, but this is considered an effect of the fourth fit-parameter only.

The suspicion that also this concept fails in adequately modelling the observations is confirmed when comparing the calculated tracer deposition with measurements (see the following figure). Again, the model (used with the best-fit parameter values from fitting the breakthrough curve) deposits too much tracer onto inner surfaces of the cementitious disk. The shape of the calculated curve increases too fast at the beginning - the diffusive flux across the down-stream boundary is too high - hence, does not reproduce the data. Whereas the modelled deposition is a strictly monotonically increasing function with time, the measured data for experiment no. 3 show a global deposition maximum and slow tracer release after about 100 days. Therefore we conclude that this model also lacks an important mechanism. Accounting for non-linear sorption kinetics only slightly improves the fit, but the concept remains completely inadequate to reproduce the measured deposited tracer mass in the HCP.

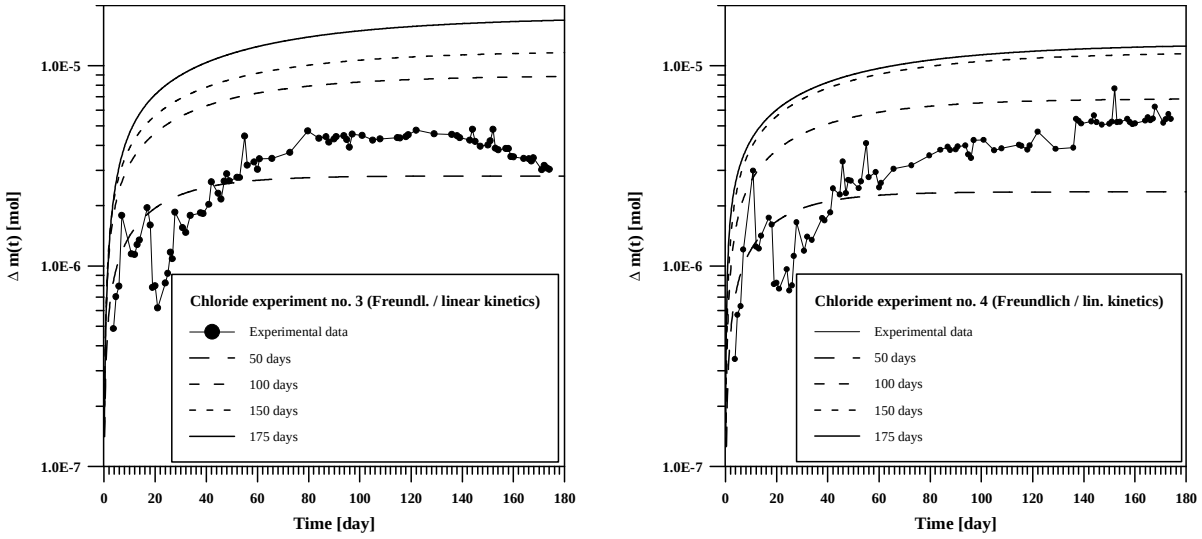

Figure 3.2.1.5.-2: Comparison of the time history of the measured deposited tracer mass $\Delta m(t)$ in the HCP for chloride for both experiments and theoretical curves based on the non-linear / linear sorption kinetics model. The curves correspond to best-fits of the diffusive flux when using experimental data from the first 50, 100, … etc. days as indicated in the legends.

3.2.1.6. Conclusions for chloride

Conclusions based on these modelling results for chloride through-diffusion and experiments no. 3 and 4 are the following:

- It is not possible to model the measured breakthrough curve with the effective diffusion coefficient D_e as the only free fit parameter. Hence, neglecting retarding mechanisms such as sorption is completely inadequate.
- Including linear sorption improves the quality of the fit to the breakthrough curve. The extracted value for K_d seems - with regard to values of table 3.2.1.2.-2 on page 102 - too high by a factor of two compared to values based on batch sorption experiments on crushed cementitious material. Moreover, the rising edge of the measured tracer deposition 'function' is only very roughly reproduced indicating that the linear sorption ansatz may not be appropriate.
- Using a model including non-linear (Freundlich) sorption does not improve the situation substantially. The fits look slightly better compared to the linear sorption case; however, the Freundlich parameter values extracted both for the coefficient and for the exponent are too high. The exponent is significantly larger than unity, in contradiction to the basic assumptions of an exchange process. This concept also overestimates the deposited tracer mass in the specimen, and the shape of the curve is far off agreement.
- Expanding the model to include first-order sorption kinetics results in only a slight improvement of the fit. A nearly steady-state value for K_d can be determined from the two rate constants of the sorption kinetic equation. However, such a K_d-value is by a factor of four too high, compared to those obtained from batch sorption experiments. Furthermore, the model again predicts too much tracer deposition within the HCP.
- A reversible non-linear sorption kinetics model also does not solve the problem. Introducing a fourth fit parameter slightly improves the quality of the fitted breakthrough curve. However, the extracted best-fit parameter values for the sorption processes are much too high, and the exponent is again - as for the Freundlich sorption case - larger than unity. Therefore, also this concept fails to model the measured deposition behaviour of chloride in the HCP successfully.
- Starting with really simple concepts and after ascertaining their deficiencies, proceeding to more sophisticated models leads to none that are able to model all available data with consistent parameter values. Although it was possible to obtain quite good-looking fits of the measured breakthrough curves, it was not possible - when using these best-fit parameter values - also to reproduce the measured tracer deposition profile in the specimen. Therefore, we consider it as very risky to inversely model only a measured breakthrough curve; several concepts may give - more or less - the same result with acceptable best-fit parameter values but some (or even all) of these models might fail if further information, such as tracer deposition in the HCP, is considered.

3.2.2. Modelling results for the iodide experiments no. 5 and 6

3.2.2.1. No-sorption case

Both breakthrough curves were fitted to equation (3.1.14) using the procedure outlined in more detail in sub-section 3.1. In two subsequent fits we adjusted the only free parameter D_e to diffusion-sorption profiles using the measured data from the first 50 and, subsequently all data available, to a total of 84 days. In a first attempt we tried to model the measured data with a concept entirely neglecting sorption.
When compared to the fits for chloride breakthrough, the quality of the fits is now much better.

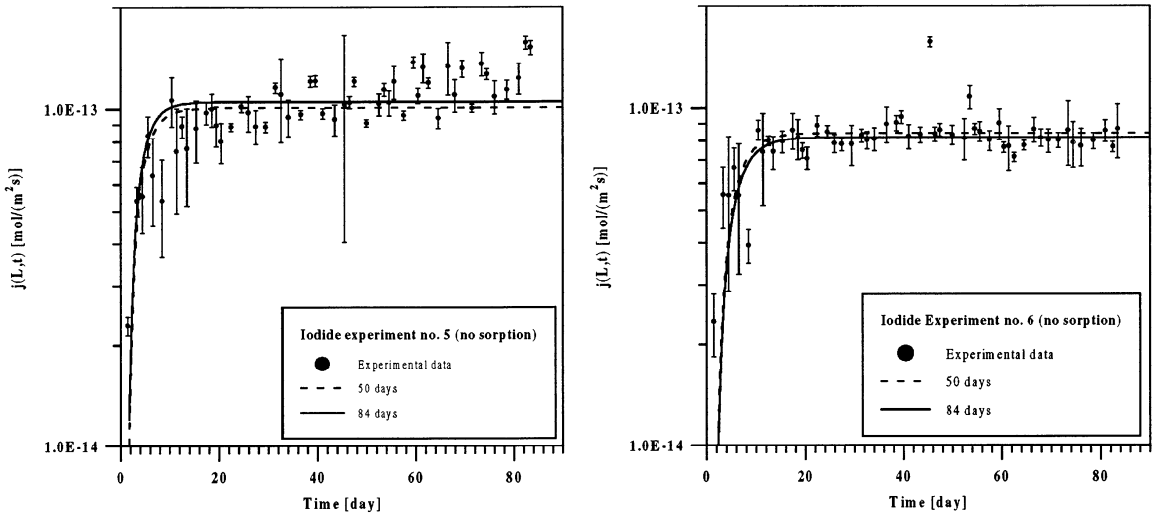

Figure 3.2.2.1.-1: Comparative plot of the experimental data and theoretical breakthrough curves for the diffusive iodide flux for both experiments. Shown are the best-fit curves neglecting sorption at all and using experimental data from the first 50 and 84 days respectively, as indicated in the legends. (The higher averaged flux for experiment no. 5 is considered to be the effect only of slow evolution of the system after about 30 days.)

For experiment no. 5 the model is not able to account for the slow evolution of the diffusive flux. Both fits are quite satisfying, although in the rising edge for experiment no. 6 especially the diffusive flux is underestimated by the model. In the table below we have compiled the best-fit parameter values together with their one-standard deviation errors for both experiments.

		Experiment no. 5		**Experiment no. 6**	
Δt	N	$D_e \cdot 10^{11}$	χ^2_ν	$D_e \cdot 10^{11}$	χ^2_ν
[day]	**[-]**	**[m²/s]**	**[-]**	**[m²/s]**	**[-]**
0-50	33	2.79 ± 0.08	39.864	2.27 ± 0.08	37.544
0-84	53	2.91 ± 0.07	42.940	2.20 ±0.05	27.087

Table 3.2.2.1.-1: The best-fit values extracted for the effective diffusion coefficient D_e together with their one-standard deviation errors, and the minimum values for the reduced χ^2_ν for iodide through-diffusion (experiments no. 5 and 6). For the adjustment, N data triplets were used measured in the time interval Δt.

The values for D_e are roughly an order of magnitude smaller than values obtained from modelling chloride breakthrough. Whether this is a general trend will be shown in further investigations.
Although the concept reproduces the measured iodide breakthrough fairly well an appropriate model should be capable of predicting other observations of the diffusion system, which must be part of the model structure, of course. In our case, such an observable quantity is the amount of tracer deposited in the cementitious material. However, an intercomparison of predicted and measured iodide up-take clearly demonstrates that the concept is completely insufficient to account for the tracer deposition. This can be seen with the help of the following figure showing that the calculated tracer deposition is two orders of magnitude lower than the measurements for both experiments.

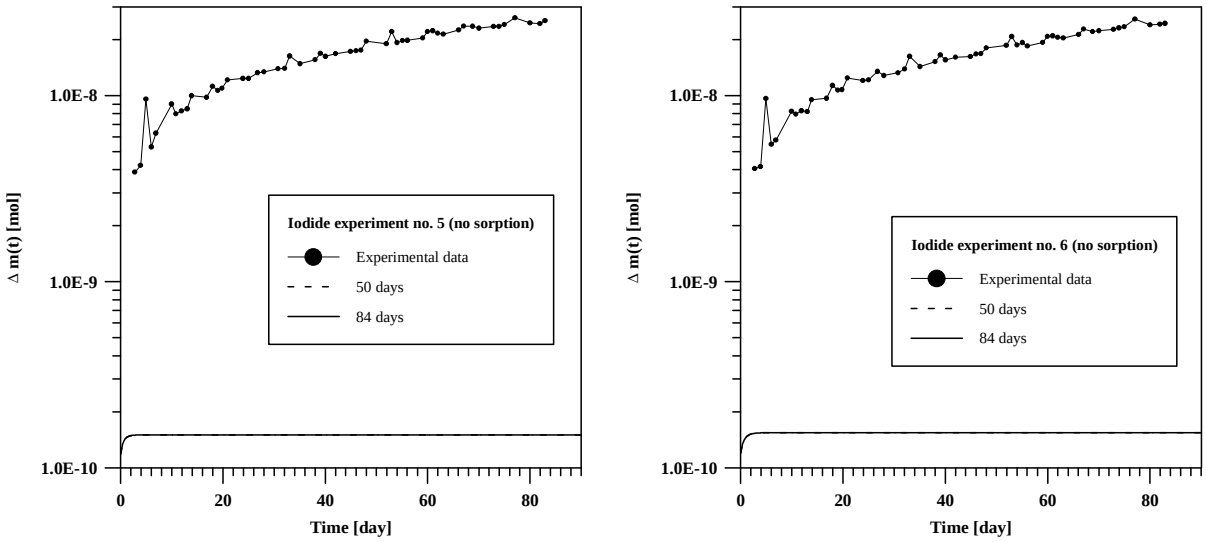

Figure 3.2.2.1.-2: Comparative plot of the experimental data for tracer deposition in the HCP and theoretical curves for both iodide experiments. The calculations are based on the best-fit parameter values from modelling the diffusive flux across the down-stream boundary, entirely neglecting sorption and using experimental data from the first 50 and finally 84 days, as indicated in the legends. The calculations using data from the first 50 and 84 days coincide practically.

An obvious conclusion from the modelling is the following: Having fixed the sample's porosity and adjusted the only free fit-parameter - the effective diffusion constant D_e - it is impossible to reproduce all the measured data concerning diffusive flux and tracer deposition in the HCP. Hence, **at least a further transport mechanism such as e.g. sorption which accounts for the marked iodide up-take by the HCP, is necessary** if we want to reach an appropriate description for iodide-diffusion through cementitious material.

3.2.2.2. Linear sorption case

As a next step we included linear, instantaneous equilibrium sorption of the tracer onto inner surfaces of the HCP. Now an additional fit-parameter - the linear equilibrium sorption distribution coefficient K_d - could be varied.

All the fits look practically identical to those obtained considering no-sorption. Therefore, linear sorption seems to play only a minor role for iodide through-diffusion.

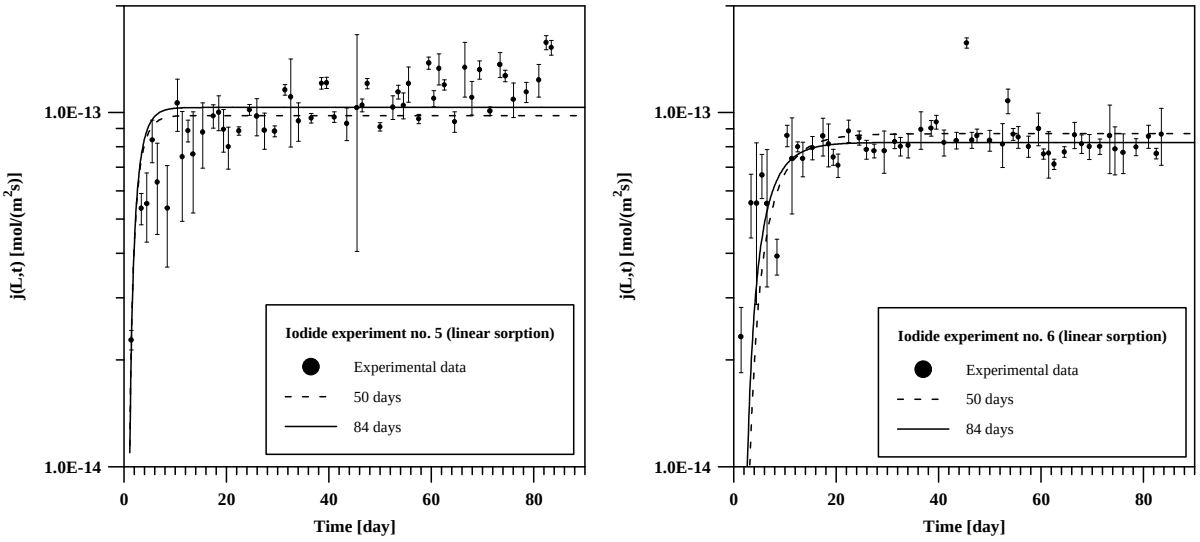

Figure 3.2.2.2.-1: Comparative plots of the experimental data and theoretical breakthrough curves for the diffusive iodide flux in both experiments assuming linear sorption. The best-fit curves using experimental data from the first 50 and 84 days are shown as indicated in the legends.

For **experiment no. 5** the transient phase in the model is only about 10 days, after which the flux is more or less constant. When comparing fit and measurements an obvious conclusion is that the concept over-predicts the diffusive flux in this phase. Moreover, after about 50 days the measurements show a trend to higher flux values which cannot be reproduced by the model. Hence, this model reproduces the data only in a somewhat averaged way neglecting important features of the experiment. The best-fit values for the effective diffusion coefficient are $(2.7 - 2.9) \cdot 10^{-11}$ m^2/s, comparable to values from the previous no-sorption case. Best-fit values for K_d are twice clearly negative. Hence, these are unphysical numbers. This is considered an indication that the concept is not suitable to account properly for the real physical processes involved in this experiment.

The modelling results for **experiment no. 6** look different, despite the fact that both experiments were performed simultaneously in the same glove-box under the same conditions. Here, no general trend to higher flux values after a first fast transient phase can be observed. Therefore, the plateau region of the breakthrough curve is fairly well reproduced, but in the rising edge the diffusive flux seems to be underestimated slightly by the model. The extracted best-fit values for the effective diffusion coefficient are $(2.2 - 2.4) \cdot 10^{-11}$ m^2/s, which are very similar to those from the sister-experiment. Using only data from the first 50 days the K_d-value is $(0.375 \pm 0.234) \cdot 10^{-3}$ m^3/kg ($\alpha \pm \Delta\alpha = 0.921 \pm 0.189$) and which is quite small and with large error bars compared with values from batch experiments. However, when taking all available data into account for fitting this value is reduced to $(0.114 \pm 0.179) \cdot 10^{-3}$ m^3/kg ($\alpha \pm \Delta\alpha = 0.719 \pm 0.148$) with even larger error bars.

		Experiment no. 5			Experiment no. 6		
Δt	N	$D_e \cdot 10^{11}$	$K_d \cdot 10^3$	χ^2_ν	$D_e \cdot 10^{11}$	$K_d \cdot 10^3$	χ^2_ν
[day]	[-]	[m^2/s]	[m^3/kg]	[-]	[m^2/s]	[m^3/kg]	[-]
0-50	33	2.72 ± 0.07	- 0.325 ± 0.037	23.142	2.35 ± 0.10	0.375 ± 0.234	37.454
0-84	53	2.86 ± 0.07	- 0.283 ± 0.046	35.021	2.22 ± 0.06	0.114 ± 0.179	27.554[22]

Table 3.2.2.2.-1: The extracted best-fit values for the effective diffusion coefficient D_e and the volume-based linear sorption equilibrium distribution coefficient K_d together with their one-standard deviation errors and the minimum values for the reduced χ^2_ν for iodide through-diffusion (experiments no. 5 and 6). For the adjustment N data triplets were used measured in the time interval Δt.

The suspicion that the linear sorption model may not be suitable to adequately describe iodide through-diffusion is confirmed if we compare the modelled tracer deposition in the HCP with measurements. This is illustrated with the help of the next figure.

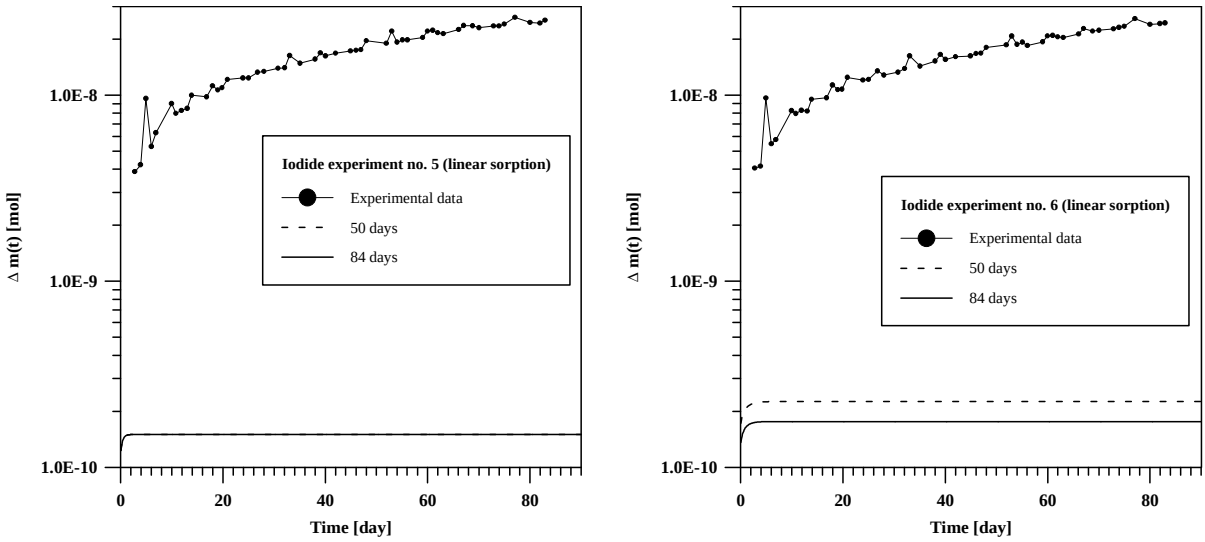

Figure 3.2.2.2.-2: Comparative plots of the experimental data for tracer deposition in the HCP and theoretical curves for both iodide experiments. The calculations are based on the best-fit parameter values from modelling the diffusive flux across the down-stream boundary assuming linear sorption and using experimental data from the first 50 and 84 days, as indicated in the legends. Note that due to unphysical negative K_d-values for experiment no. 5 only the amount of iodide in the liquid phase within the HCP is plotted.

As can be seen, for both experiments - as for the no-sorption case - the model predicts up to two orders of magnitude less iodide deposition in the cementitious material than measured in the experiments. Therefore we have to conclude that the model for iodide deposition in the

[22] Note: Although this value for χ^2_ν is slightly larger than that from the former exercise where sorption was entirely neglected, the minimum value for χ^2 in the present study is smaller and the data are slightly better fitted than in the no-sorption case. This effect on χ^2_ν results from the different degree of freedom of the fit, which is equal to (M - n), i.e., the number of data M minus the number of fit-parameters n.

HCP is completely wrong when it includes only a simple K_d-concept; nevertheless the flux profiles may be reproduced fairly well - especially for experiment no. 6.
Atkinson and Nickerson [1] also reported a discrepancy in the K_d-values obtained in batch sorption and through-diffusion experiments. Their value for α, measured in batch experiments, was about 20 times larger than that from diffusion experiments. They concluded that such a mismatch could not be attributed to the observed non-linearity of the iodide adsorption process. Therefore for iodide diffusion they suggested a porous medium which consists of two types of porosity: one of well-connected pores through which diffusion is fast and a second of connected pore space through which transport may be hindered. If this was the case they continued, then values for α determined in batch experiments would be the true ones rather than values from through-diffusion experiments which relate mainly to the fast diffusion paths. However, with the existing modelling tools we are not in a position to investigate thoroughly whether such a concept is better able to resolve the open questions concerning measured tracer deposition in the HCP.

Further comparison with the results of other studies

Brown et al. [38] modelled diffusion/sorption experiments for some nuclides using the coupled chemical equilibrium and transport code CHEQMATE. Data available include those for iodine diffusion through cement disks of SRCP. They conclude that for this species the model compares well with measurements indicating that the model accounts correctly for the transport processes being involved. Their values for the diffusion coefficient D_p confirm our best-fit values, and their rock capacity factor is roughly by a factor of two larger. However, there are no considerations on tracer up-take in the cement.

Atkinson and Nickerson [39] reported values for the effective diffusion coefficient and the rock capacity factor as functions of the W/C-ratio. For the through-diffusion experiments they used pastes made of Ordinary Portland Cement (OPC) and pushed the diffusion process with a 1M inactive iodide solution at the reservoir side. Their results imply a strong exponential dependency of D_e on the W/C-ratio, but there is no theoretical basis to support such a dependency. Their values for the rock capacity factor α are in general relatively low and cover a range of 0.072 - 1.4 which is consistent with the values of the present study. Due to the unknown porosity and bulk density as a function of the W/C ratio, we are not able to compare their values thoroughly with those from our study.
The same authors [1] present results obtained on SRCP pastes. The W/C-ratio was again 0.40, the porosity $\varepsilon = 0.3$ and their extracted values for D_e and for iodide were of the order of $(0.5 - 1.2) \cdot 10^{-11}$ m^2/s for initial iodide concentrations of 10^{-4} and 1 mol/l, respectively. For α they found values between 0.11 - 1.9. In batch experiments they observed a strong non-linear behaviour of the sorption process.

In a previous study Sarott et al. [6] analysed both iodide experiments neglecting the measurement errors and using a model where linear and - alternatively - non-linear sorption was taken into account. The authors conclude that it was possible to model the diffusion/sorption results successfully by a linear isotherm, and found that almost equally good fits were obtained using a non-linear (Freundlich) isotherm but with exponents larger than unity. They considered such a result to be chemically unrealistic. For D_e they obtained very similar values; for K_d in one case they found a 20 times larger value of $K_d = 2.3 \cdot 10^{-3}$ m^3/kg.

Batch sorption measurements of iodide on concrete were performed by Hietanen et al. [40]. Their traced solution was about 10^{-7} M, hence slightly higher than our reservoir concentration. For concrete they determined K_d-values of $(2.2 \pm 0.2) \cdot 10^{-3}$ m^3/kg and $(7.7 \pm 0.1) \cdot 10^{-3}$ m^3/kg respectively, i.e. rather high values when compared with our best-fit values. On aggregate they measured slightly lower K_d-values.

A further study was performed by Anderson et al. [41] in which diffusion and sorption of caesium and iodide in slag cement paste and concrete was investigated. For iodide with an initial concentration of 10^{-8} M they report relatively high K_d -values of $(16 - 19) \cdot 10^{-3}$ m^3/kg obtained from batch sorption experiments. The diffusion coefficient could not be measured because the low diffusivity and short half-life of the isotope used. Typical W/C-ratios were of the order of 0.35 - 0.40.

Finally one of the authors (Sarott) also measured the K_d for iodide on crushed cementitious material used as diffusion barrier in the through-diffusion experiments. His values were of the order of $350 \cdot 10^{-3}$ m^3/kg, larger by orders of magnitude. In contradiction to Atkinson et al. [1] he could not observe any non-linearity in the sorption process [17].

In the next table we have compiled all values for the diffusion coefficients and for K_d and α for comparison purposes.

Source	C_0	**W/C**	ε	$D_e \cdot 10^{11}$	$D_p \cdot 10^{11}$	$K_d \cdot 10^3$	α
	[mol / l]	[-]	[-]	[m^2/s]	[m^2/s]	[m^3/kg]	[-]
Brown et al. [38]	10^{-6}		0.2	0.46	2.3	0.56	1.2
Atkinson and Nickerson [40]	1 	0.2 0.3 0.4 0.5 0.6 0.7		0.025 0.11 0.41 2.3 6.1 15			 0.43 0.22 0.072 0.52 1.4
Atkinson and Nickerson [1]	1 10^{-4}	0.4 0.4	0.3 0.3	0.74 ± 0.06 0.75 ± 0.09 1.2 ± 0.1 0.5	2.5 2.5 4.0 1.7		0.11 0.31 0.32 1.9
Sarott et al [6]	$3.9 \cdot 10^{-8}$	1.3	0.65	2.7 ± 0.1 2.2 ± 0.1		2.3 ± 0.3 no fit possible	
this study	$(3.61 \pm 0.17) \cdot 10^{-8}$ $(3.71 \pm 0.17) \cdot 10^{-8}$	1.3 1.3	0.63 ± 0.05 0.63 ± 0.05	2.86 ± 0.07 2.22 ± 0.06	4.54 ± 0.45 3.52 ± 0.35	no fit possible 0.114 ± 0.179	0.63 ± 0.05 0.719 ± 0.148
Hietanen et al. [40] (Batch - concrete)	$< 10^{-7}$					2.2 ± 0.2 7.7 ± 0.1	
Anderson et al. [39] (Batch)	10^{-8}	0.35 0.35 0.40				19 16 17	
Sarott [17] (Batch)	$4 \cdot 10^{-10}$-$4 \cdot 10^{-6}$	1.3	0.63 ± 0.05			350	

Table 3.2.2.2.-2: Reported values for the diffusion coefficients, K_d and the rock capacity factor α for various water/cement (W/C) ratios. Most of the results are obtained from through-diffusion experiments on SRCP; those by Atkinson et al. [40] were obtained on OPC and are given for comparison purposes. In the lower part the results from three batch sorption studies were also included. Note that the values from Hietanen et al. are based on concrete.

Taking all together we may conclude:

- In the case of experiment no. 5 the breakthrough curve is only roughly reproduced and the best-fit K_d-values have unphysical - because negative - values.
- For the second iodide experiment the agreement between model and measurements is quite satisfying, but the K_d-values are low and show large error bars.
- The correlations between the two fit-parameters are weak, with values always between 0.38 and 0.64. Hence they are acceptably low.
- The principal deficiencies of the model become obvious when predicted iodide deposition in the diffusion barrier - based on the best-fit parameter values for D_e and K_d - is compared with measurements. In the frame of the model, one to two order of magnitudes less iodide is taken up by the HCP than is really observed.
- Compared to the no-sorption case, there is no essential improvement of the quality of the fits and for the tracer deposition profiles. Hence, having a further free fit-parameter does not result in a better description of the observations.
- The only reasonable conclusion which can be drawn is that this model, too, is not applicable to describe diffusive iodide breakthrough through cementitious material and deposition in the HCP comprehensively.

In their paper Atkinson and Nickerson [1] mention that iodine sorption was found to be more complicated in batch sorption experiments than other nuclides such as caesium and strontium and that the isotherm is significantly non-linear. To elucidate whether the sorption characteristics may be non-linear - indeed - and whether our best-fit values will be consistent with those from Atkinson and Nickerson, we have modelled the experiments assuming, for sorption, a Freundlich isotherm according to equation (3.1.2).

3.2.2.3. Non-linear (Freundlich) sorption case

Both iodide experiments were fitted using only data from the first 50 and 84 days to test the predictive quality of the non-linear sorption model. In order to ensure that a global χ_v^2-minimum was located, we repeated the calculations up to 8 - 15 times with different sets of starting values for the fit-parameters.

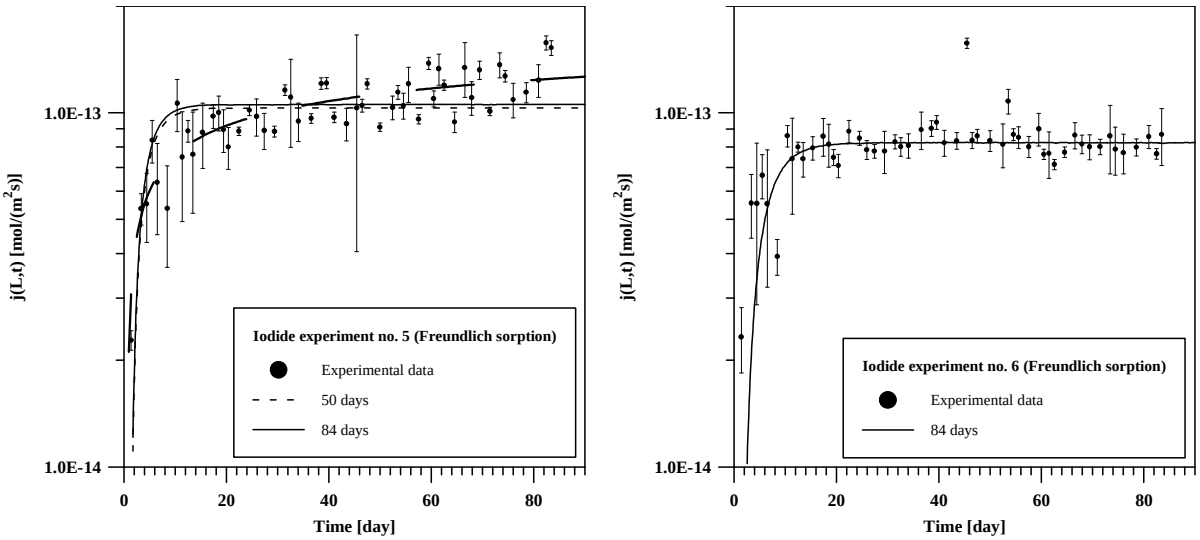

Figure 3.2.2.3.-1: Comparative plots of the experimental data and theoretical breakthrough curves for the diffusive iodide flux and both experiments assuming non-linear (Freundlich) sorption. The best-fit curves using experimental data from the first 50 and 84 days are shown as indicated in the legends. For experiment no. 5 (left figure) the broken line represents a general trend in the measurements which corresponds to neither fit. For experiment no. 6 a fit could not be obtained using data only from the first 50 days.

When compared with the plots from the previous model with linear sorption, the results do not look better. Although, there is now a third freely adjustable parameter (the Freundlich exponent) the calculated breakthrough curves are not reproduced better. For experiment no. 5 the modelled flux at the rising edge is often too small, and the model misses the trend for a continuously increased diffusive flux. This leads to the conclusion that this model, too, is not capable of describing the iodide through-diffusion experiment successfully. For experiment no. 6 no fit could be obtained when using only data from the first 50 days. Both modelling tasks yield values for the Freundlich exponent which are larger than unity with small standard deviations (N_p = 1.25 - 1.96). Similar results obtained from modelling other experiments were interpreted as indications of possible tracer precipitation in the HCP.
Although the values for the Freundlich exponent are larger than unity, the iodide up-take by the HCP's is still clearly underestimated by the model indicating that the model structure must be wrong.

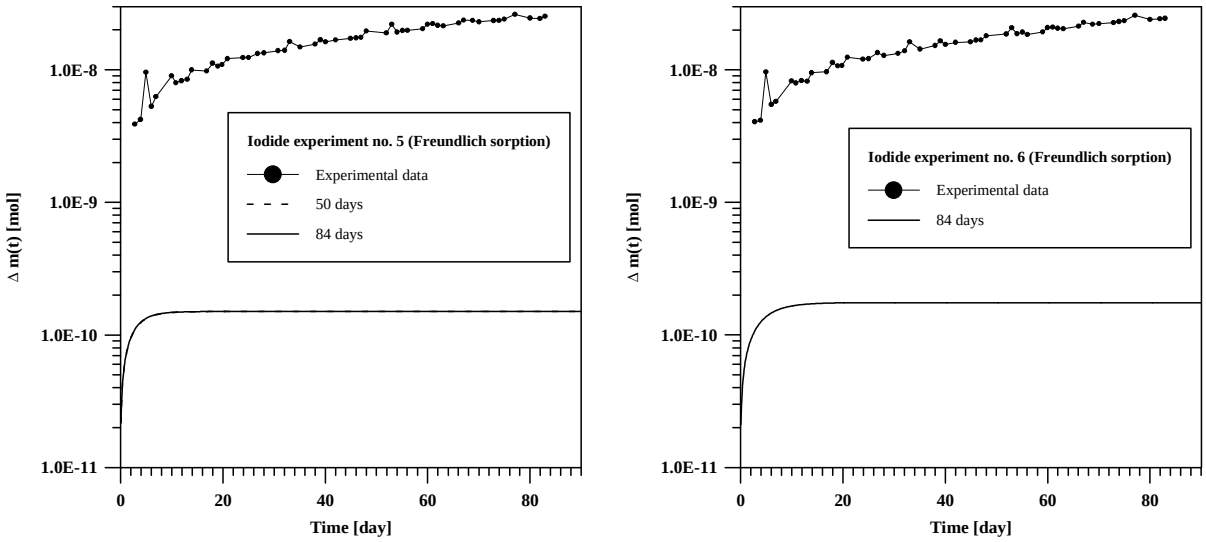

Figure 3.2.2.3.-2 Comparative plots of the experimental data for tracer deposition in the HCP and theoretical curves for both iodide experiments. The calculations are based on the best-fit parameter values from modelling the diffusive flux across the down-stream boundary assuming non-linear (Freundlich) sorption and using experimental data from the first 50 and 84 days as indicated in the legends. For experiment no. 6 no fit could be obtained using only data from the first 50 days.

For experiment no. 5, the best-fit values for K_p are about $(3.0 - 4.2) \cdot 10^{-3}$ $\text{mole}^{1-N_p}\,\text{m}^{3N_p}\,\text{kg}^{-1}$ with unphysically large exponent values of $N_p = 1.8 - 2.0$. As can be seen in the figure above, there is a slightly increased tracer deposition compared to the corresponding calculations made using a linear sorption/diffusion model. However, the general problem of a significant underestimation of the iodide up-take by the HCP remains the same.
Moreover, such a conclusion is supported by the following considerations: Interpreting the correlation matrix a contradictory picture is again obtained. From the formalism, anti-correlations between the two Freundlich parameters are expected; an increased value for K_P should be anticipated by a reduced value for the exponent N_p to obtain the same sorption effect, and both parameters should be correlated to D_e. But the correlations do not follow this scheme. For both experiments frequent anti-correlations between D_e and K_p were obtained. Simultaneously, slightly weaker anti-correlations between D_e and N_p and correlations between K_p and N_p could be observed. These facts are, considered a further indication that the model also has the wrong mathematical structure meaning that the wrong physical process for retardation (instantaneous equilibrium non-linear sorption) is considered.

From these results for experiments no. 5 and 6 we conclude:

- The transient part of the diffusion curve is only roughly reproduced and there are only minor improvements in this part of the breakthrough curve when compared to the linear sorption case.
  The extracted best-fit values for the Freundlich exponent for both experiments are between 1.25 and 1.96; hence, they are unphysically large and violate basic assumptions of the Freundlich isotherm formalism.
- The fit-parameters often show correlations/anti-correlations which do not correspond to the procedure's underlying formalism.

- The modelled iodide deposition in the HCP is orders of magnitude too small, thus clearly demonstrating fundamental deficiencies of the concept.
- Ultimately, this model must be rejected due to its inability to reproduce all the observations with reasonable accuracy and with parameter values consistent to those obtained in alternative experiments.

		Experiment no. 5				**Experiment no. 6**			
Δt	N	$D_e \cdot 10^{11}$	$K_p \cdot 10^3$	N_p	χ^2_ν	$D_e \cdot 10^{11}$	$K_p \cdot 10^3$	N_p	χ^2_ν
[day]	**[-]**	**[m²/s]**	**[*]**	**[-]**	**[-]**	**[m²/s]**	**[*]**	**[-]**	**[-]**
0 - 50	33	2.86 ± 0.09	3.02 ± 0.30	1.96 ± 0.17	43.336	not possible to fit the data			
0 - 84	53	2.92 ± 0.09	4.18 ± 0.10	1.82 ± 0.07	44.559	2.22 ± 0.03	1.52 ± 0.03	1.25 ± 0.02	27.889

Table 3.2.2.3.-1: The extracted best-fit values for the effective diffusion coefficient D_e and the two Freundlich isotherm parameters K_p ([*] = [$mol^{1-N_p} m^{3N_p} kg^{-1}$]) and N_p together with their one-standard deviation errors and the minimum values for the reduced χ^2_ν for both iodide through-diffusion experiments. For the adjustment N data triplets were used measured in the time interval Δt.

3.2.2.4. First-order sorption kinetics - linear/linear case

In a further step we investigated the effect of first-order sorption kinetics according to equation (3.1.3) on the diffusion-sorption profile. The fit-parameters were now the effective diffusion coefficient D_e, the rate for sorption k_s [s^{-1}], and the rate for desorption k_r [s^{-1}]. First, only the data from the first 50 days were used for the fit-procedure to test the predictive quality of the model.

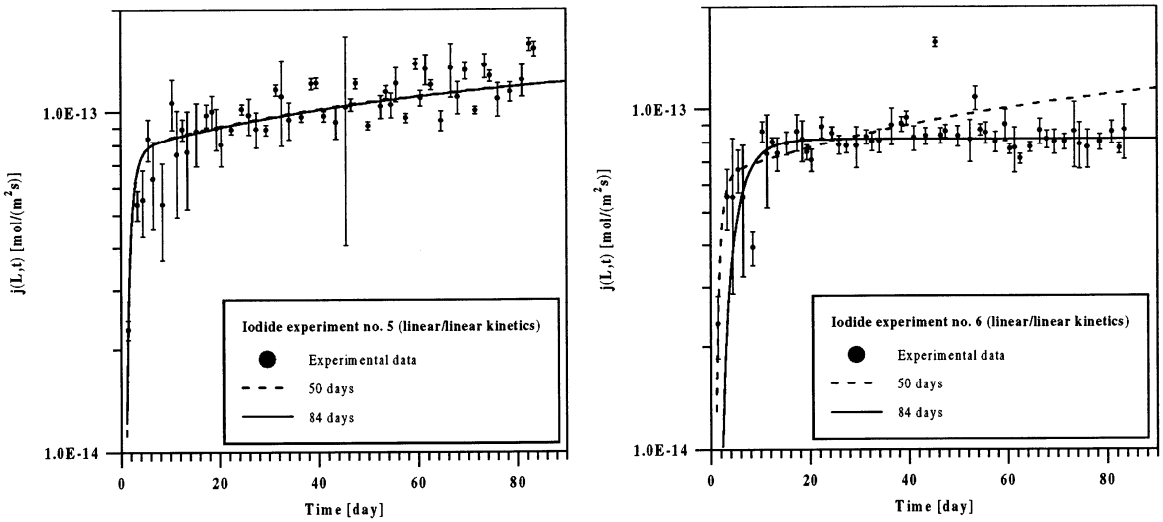

Figure 3.2.2.4.-1: Comparative plot of the experimental data and theoretical breakthrough curves for the diffusive iodide flux and for both experiments when assuming first-order sorption kinetics. Shown are the best-fit curves using experimental data from the first 50 and 84 days as indicated in the legends.

Inspecting the transient part of the diffusion curve of experiment no. 5, we can recognise a better representation of the measurements by this model compared to one with a linear or non-linear sorption isotherm. Correlations between the fit-parameters are relatively large, as a rule, they become smaller when using more and more data for the fit-procedure. Using data from the first 50 days the maximum correlation between D_e and k_s is of the order 0.95; using all available data for the fit this value is decreased to 0.86. All other correlations are clearly smaller when compared to this maximum correlation. Using the data from the first 50 days from experiment no. 6, no near steady-state phase for the diffusive flux is obtained. However, the rising edge of the breakthrough curve is reproduced quite well. Using all available data for the adjustment, the asymptote is reproduced well but in return the model fails to adjust the data below five days successfully. The correlations between the three fit-parameters are clearly smaller than for experiment no. 5.

In the near steady-state where $\frac{dS}{dt} = 0$ holds we can calculate the equilibrium sorption distribution coefficient K_d according to equation (3.2.4). In the table below we have compiled these K_d -values for both experiments together with their standard errors.

		Experiment no. 5	Experiment no. 6
Δt	# of data	$(K_d \pm \Delta K_d) \cdot 10^3$	$(K_d \pm \Delta K_d) \cdot 10^3$
[day]	[-]	[m^3/kg]	[m^3/kg]
0 - 50	33	13.1 ± 3.6	22.8 ± 12.7
0 - 84	53	14.8 ± 4.4	$(29.8 \pm 3.2) \cdot 10^{-8}$

Table 3.2.2.4.-1: The computed K_d-values with 1σ-standard errors according to equation (3.2.4) using measured data in the time interval Δt for the fitting procedure when using first-order sorption kinetics.

The values for K_d are extraordinarily high when compared with those from a diffusion/linear sorption model except for experiment no. 6 when using all available data where sorption is entirely neglected [23]. From modelling we know that such a model, too, is able to approximately reproduce the iodide breakthrough curve. The best-fit values for D_e for experiment no. 5 are $4.3 \cdot 10^{-11}$ m^2/s, which are clearly larger than those obtained from the previous modelling concepts using linear or non-linear sorption isotherms. Experiment no. 6 for D_e with $2.2 \cdot 10^{-11}$ m^2/s again yields a value which is consistent with former modelling tasks. Such a difference in the two values for D_e must be the consequence of not having reached a near steady-state in the case of experiment no. 5.

The failure of this model is illustrated with the help of the reported time history of the iodide up-take by the cement sample.

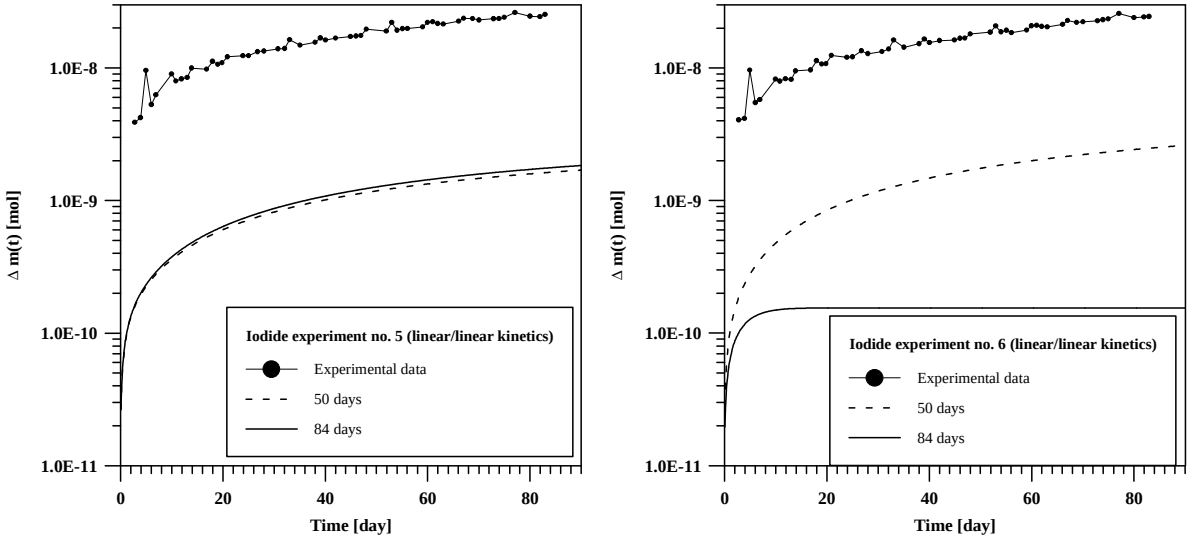

Figure 3.2.2.4.-2: Comparative plots of the experimental data for tracer deposition in the HCP and theoretical curves for both iodide experiments. The calculations are based on the best-fit parameter values from modelling the diffusive flux across the down-stream boundary assuming first-order sorption kinetics and using experimental data from the first 50 and 84 days as indicated in the legends.

[23] This could be an indication for a breakdown in the sample.

In the table below we have compiled all best-fit parameter values together with their one-standard deviations and the minimum value for the reduced χ^2_ν-merit function.

		Experiment no. 5				**Experiment no. 6**			
Δt	N	$D_e \cdot 10^{11}$	$k_s \cdot 10^6$	$k_r \cdot 10^7$	χ^2_ν	$D_e \cdot 10^{11}$	$k_s \cdot 10^6$	$k_r \cdot 10^7$	χ^2_ν
[day]	**[-]**	**[m^2/s]**	**[s^{-1}]**	**[s^{-1}]**	**[-]**	**[m^2/s]**	**[s^{-1}]**	**[s^{-1}]**	**[-]**
0 - 50	33	4.22 ± 0.27	2.97 ± 0.41	1.84 ± 0.40	20.507	4.47 ± 0.69	4.77 ± 1.61	1.70 ± 0.74	32.281
0 - 84	53	4.32 ± 0.24	3.20 ± 0.66	1.75 ± 0.34	24.752	2.20 ± 0.06	$(2.09 \pm 0.14) \cdot 10^{-10}$	5.68 ± 0.10	28.118

Table 3.2.2.4.-2: The extracted best-fit values for the effective diffusion coefficient D_e and the rates for sorption k_s and desorption k_r together with their one-standard deviation errors and the minimum values for the reduced χ^2_ν for both iodide through-diffusion experiments. For the adjustment N data triplets were used measured in the time interval Δt.

The conclusion for this model are as follows:

- The transient phase of the breakthrough curves is better reproduced than with alternative models. The overall quality of the fits is quite good, but the values for the effective diffusion coefficient for experiment no. 5 are by a factor of two larger and those for experiment no. 6 are close to values obtained from previous concepts. The rates for sorption and desorption cannot be discussed because there are no measurements known.
- In the near steady-state, values for K_d can be calculated from the rates for sorption and desorption. For experiment no. 5 these are smaller by a factor of 27 than those obtained from batch sorption experiments. For the second experiment a zero K_d-value was obtained due to the near steady-state region in the breakthrough curve beyond 15 days. This could be an indication for a breakdown in the sample. The amount of iodide up-taken in the HCP for both experiments is at least one order of magnitude too small, and the model is able to reproduce only the general trend of the measurements, not the correct values.
- Taking all together we must conclude that this model, too, is not capable of correctly reproducing and predicting iodide through-diffusion and iodide deposition in the cementitious material; nor does it lead to values for the fit-parameters which are consistent with those obtained from batch experiments.

3.2.2.5. First-order sorption kinetics - non-linear/linear case

Finally, just for completeness, we investigated the effect of first-order sorption kinetics according to equation (3.1.3) with a non-linear forward reaction according to the Freundlich isotherm and a linear desorption reaction. The fit-parameters were the effective diffusion coefficient D_e, the rate for sorption k_s [$mole^{1-N_s} m^{3N_s} kg^{-1}$], the Freundlich exponent N_s [-], and the rate for desorption k_r [s^{-1}].

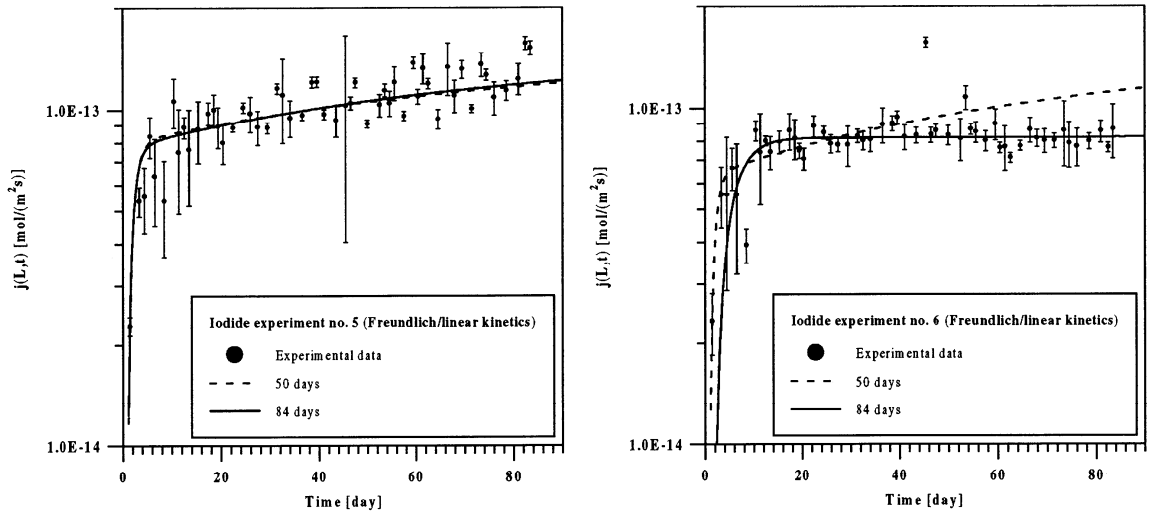

Figure 3.2.2.5.-1: Comparative plot of the experimental data and theoretical breakthrough curves for the diffusive iodide flux and both experiments when assuming first-order non-linear sorption kinetics. Shown are the best-fit curves using experimental data from the first 50 and 84 days as indicated in the legends.

Although a fourth fit-parameter could be adjusted, the increase in the quality of the fits is negligible. The values for D_e are very similar to those from the former concept. The values for the Freundlich exponent are always slightly below unity in clear contradiction to the modelling results where a diffusion/non-linear sorption model was fitted. There, values were always found which are clearly above unity indicating possible tracer precipitation. If desorption is accounted for, these values are reduced to numbers which are consistent with basic assumptions of the Freundlich sorption formalism. As mentioned in sub-section 3.2.2.4. the near steady-state region of experiment no. 6 compels the fit-procedure to neglect sorption entirely. The correlations/anti-correlations between the four fit-parameters were often quite strong and most pronounced between k_s and k_r with values up to -0.94.

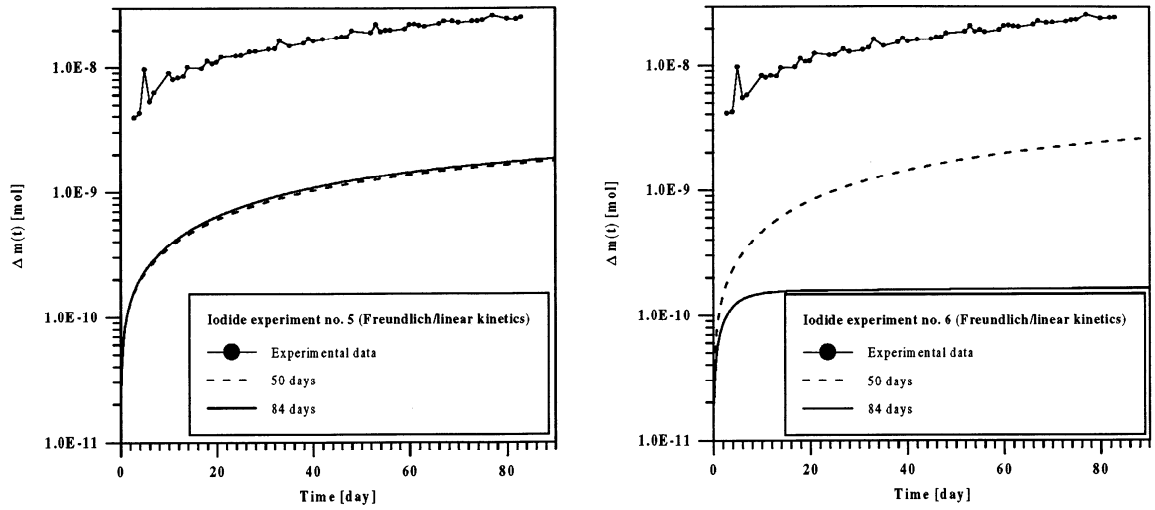

Figure 3.2.2.5.-2: Comparative plots of the experimental data for iodide deposition in the HCP and theoretical curves for both experiments. The calculations are based on the best-fit parameter values from modelling the diffusive flux across the down-stream boundary assuming first-order non-linear sorption kinetics and using experimental data from the first 50 and 84 days as indicated in the legends.

As before, this model is also not able to account for the correct tracer up-take by the HCP. The shape of the deposition profiles shows the correct trend, but the absolute values are at least one order of magnitude too small. Hence, this model, too, fails because it is not able to account for all observations made in simple iodide through-diffusion experiments in a correct way.

In the next table, all best-fit parameter values together with their standard deviations and the minimum value for the reduced χ^2_ν-merit function are compiled.

		Experiment no. 5					**Experiment no. 6**				
Δt	N	$D_e \cdot 10^{11}$	$k_s \cdot 10^6$	N_s	$k_r \cdot 10^7$	χ^2_ν	$D_e \cdot 10^{11}$	$k_s \cdot 10^6$	N_s	$k_r \cdot 10^7$	χ^2_ν
[day]	**[-]**	**[m²/s]**	**[*]**	**[-]**	**[s⁻¹]**	**[-]**	**[m²/s]**	**[*]**	**[-]**	**[s⁻¹]**	**[-]**
0 - 50	33	4.29±0.26	1.30±0.15	0.927±0.023	1.53±0.52	21.039	4.53±1.13	1.43±0.71	0.894±0.073	1.58±0.84	33.403
0 - 84	53	4.35±0.27	1.99±0.35	0.957±0.028	1.69±0.34	25.256	2.22±0.05	$(1.90\pm0.20)\cdot10^{-8}$	1.01±0.11	3.02±0.48	28.741

Table 3.2.2.5.-1: Results from modelling both iodide through-diffusion experiments using a diffusion/first-order non-linear sorption kinetics model. The fit-parameters of the model are the effective diffusion coefficient D_e, the rate coefficient k_s ([*] = [$\mathrm{mol}^{1-N_s}\,\mathrm{m}^{3N_s}\,\mathrm{kg}^{-1}$]), the exponent N_s for sorption and the rate for desorption k_r. The best-fit values are compiled together with their one-standard deviation errors and the minimum values for the reduced χ^2_ν. For the adjustment N data triplets were used measured in the time interval Δt.

3.2.2.6. Conclusions for iodide

1. no sorption case:
   - Fairly good reproductions of the breakthrough curves with consistent values for D_e are obtained, but
   - the model predicts one to two orders of magnitude too little tracer deposition.
   - Therefore at least one further mechanism is necessary to account for the up-taken iodide and, hence
   - the model is not suitable for a comprehensive description of iodide through-diffusion.
2. linear sorption case:
   - The quality of the fitted breakthrough curves is comparable to that of the previous case.
   - The best-fit values for D_e are very similar to those of the no-sorption case, and the values for K_d are very small or even negative.
   - Tracer up-take by the HCP is again up to two orders of magnitude too small, hence
   - the model's retardation mechanism must have another mathematical structure than that of the simple linear sorption isotherm.
3. non-linear (Freundlich) sorption case:
   - For experiment no. 5 only a very rough reproduction of the measured breakthrough curve is obtained; for the second experiment the model fits the data satisfactorily - except for a few data of the rising edge.
   - The values for the Freundlich exponent N_p are always significantly larger than unity which is normally indicative of precipitation reactions.
   - The tracer deposition in the cementitious material is at least one order of magnitude too small , hence
   - this model, too, is inappropriate to model all observations from iodide through-diffusion successfully.
4. first-order kinetics (linear/linear case):
   - This model fits the data in the transient phase of the breakthrough curve much better.
   - The K_d-values obtained from the near steady-state part of the breakthrough curve are higher than those from the linear sorption model but are still too small by a factor 15 to 25 than values from batch sorption experiments. Hence, iodide up-take by the HCP still is significantly too small and consequently
   - the model is inappropriate to reproduce all observations consistently.
5. first-order kinetics (non-linear/linear case):
   - The model yields similarly good reproductions of the measured breakthrough curves as the former model did.
   - The values extracted for the (Freundlich) exponent are slightly below unity, and hence are consistent with the basic assumptions of the Freundlich isotherm formalism, but
   - the calculated tracer up-take is always at least by an order of magnitude too small when compared to measurements.
   - Hence, this model, too, fails because it is not able to reproduce the measured data comprehensively.

None of the five models investigated is able to reproduce all measurements from iodide through-diffusion with parameter values consistent with those from independent experiments.

3.2.3. Modelling results for the caesium experiments no. 7 and 8

3.2.3.1. No-sorption case

Both caesium breakthrough curves were fitted to equation (3.1.14) with the help of the procedure outlined in more detail in sub-section 3.1. In subsequent fits the free parameters were adjusted to diffusion-sorption profiles using the measured data from the first 50 and 87 days respectively, to investigate the predictive power of a given model.
As a first step we tried to model the measured data with a concept neglecting sorption.
The quality of the fits in general is rather poor. The calculated flux profiles do not match the measurements, either in the fast transient phase or in the near steady-state phase where the diffusive flux evolves only moderately. This can be seen in the following figures.

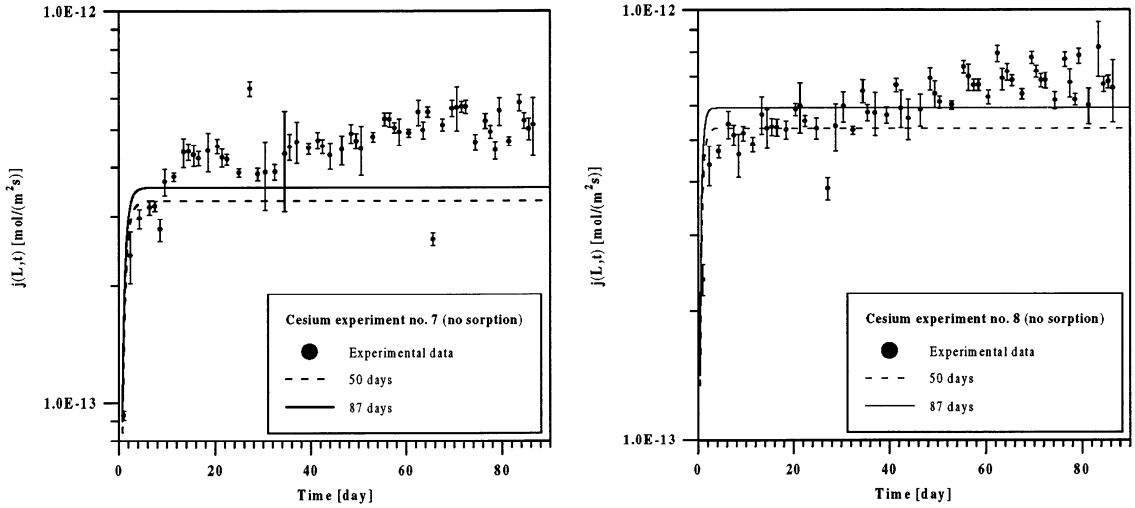

Figure 3.2.3.1.-1: Comparative plot of the experimental data and theoretical breakthrough curves for the diffusive caesium flux for both experiments. Shown are the best-fit curves neglecting sorption and using experimental data from the first 50 and 87 days, respectively as indicated in the legends.

In the table below we have compiled the best-fit parameter values for the effective diffusion constant together with their one-standard deviation errors. Both best-fit values for D_e differ by a factor of 1.6, although the flux profiles of the two experiments are very similar.

		Experiment no. 7		**Experiment no. 8**	
Δt	N	$D_e \cdot 10^{11}$	χ^2_ν	$D_e \cdot 10^{11}$	χ^2_ν
[day]	**[-]**	**[m²/s]**	**[-]**	**[m²/s]**	**[-]**
0 - 50	32	8.61 ± 0.28	114.35	13.9 ± 0.4	27.336
0 - 87	57	9.30 ± 0.31	186.94	15.5 ± 0.4	54.562

Table 3.2.3.1.-1: The extracted best-fit values for the effective diffusion coefficient D_e together with their one-standard deviation errors and the minimum values for the reduced χ^2_ν for both caesium through-diffusion experiments. For the adjustment N data triplets were used measured in the time interval Δt.

It might be that for experiment no. 7 the fit-procedure did not reach the global minimum, although the calculations were repeated several times with different starting values. However, the higher values for the diffusion constant of experiment no. 8 seem to be more reasonable.

In the next figure the amount of caesium taken up by the HCP is plotted versus time. The overall width of the data is considered a measure for the measurement errors of the caesium taken up. Both calculations fall within the same interval and represent the amount of caesium dissolved in the liquid of the connected pore space of the HCP's.

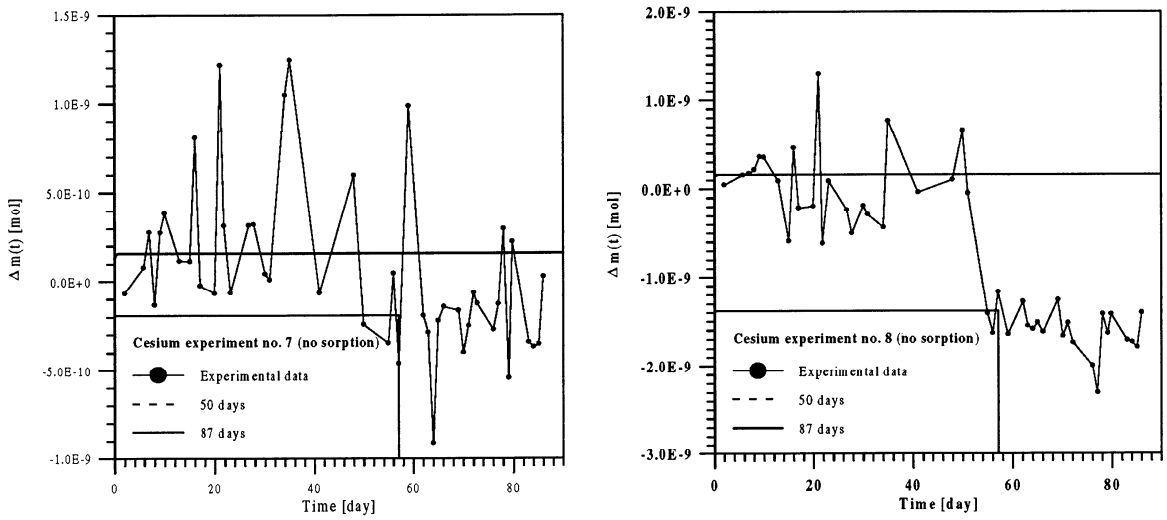

Figure 3.2.3.1.-2: Comparative plot of the experimental data for tracer deposition in the HCP and theoretical curves for both caesium experiments. The calculations are based on the best-fit parameter values from modelling the diffusive flux across the down-stream boundary, neglecting sorption, and using experimental data from the first 50 and 87 days respectively, as indicated in the legends.

Although the model is the most simple one and although the breakthrough curves are only roughly reproduced, the differences between measured and modelled deposition data are still acceptable. A reasonable conclusion is that caesium sorption on such cementitious material might be very low or even negligible; hence, caesium could act as a conservative tracer.
Subsequently we will investigate whether the measured breakthrough curves can be modelled better by including a further retarding mechanism such as sorption in the concept and an agreement between measured and calculated tracer up-take by the cement disks.

3.2.3.2. Linear sorption case

Next we took into account linear, instantaneous equilibrium sorption of the tracer onto inner surfaces of the HCP. The procedure now includes an additional fit-parameter - the linear equilibrium sorption distribution coefficient K_d.

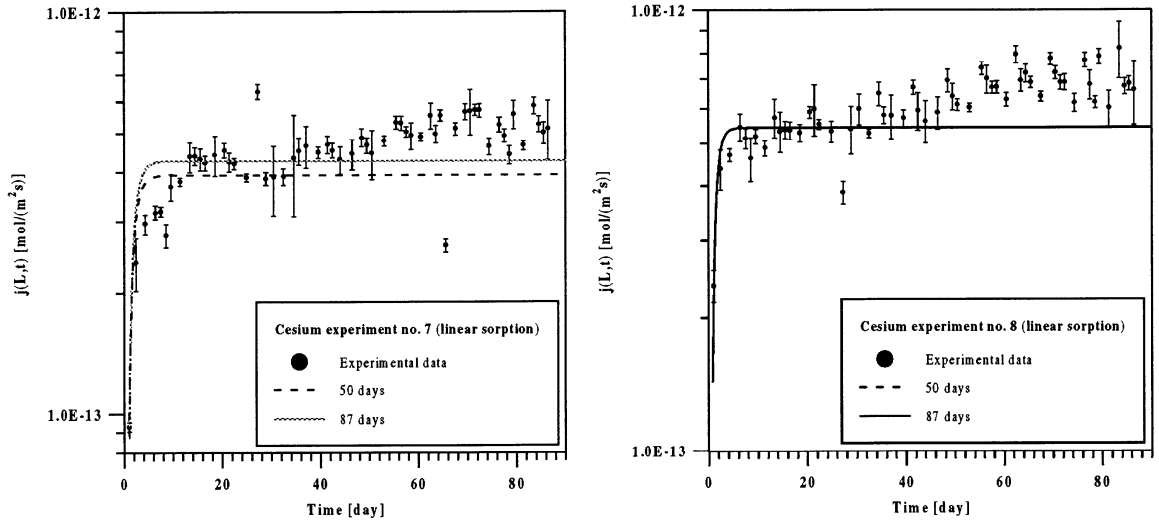

Figure 3.2.3.2.-1: Comparative plot of the experimental data and theoretical breakthrough curves for the diffusive caesium flux and both experiments when assuming linear sorption. Shown are the best-fit curves using experimental data from the first 50 and 87 days, as indicated in the legends.

Accounting for linear sorption increases the calculated diffusive flux for experiment no. 7 slightly, but the reproduction of the measurements remains unsatisfactory. The model predicts a fast transient phase up to about five days followed by a near-steady state. But the flux in the experiment is always increasing and never reaches a constant value. A similar result is obtained for the second experiment; the overall quality of both fits is rather poor. Using all available data for the adjustments instead of a sub-set in the limit 0 - 50 days does not change much. Both best-fit parameter values are slightly larger, but the effect on the calculated breakthrough curve is negligible.

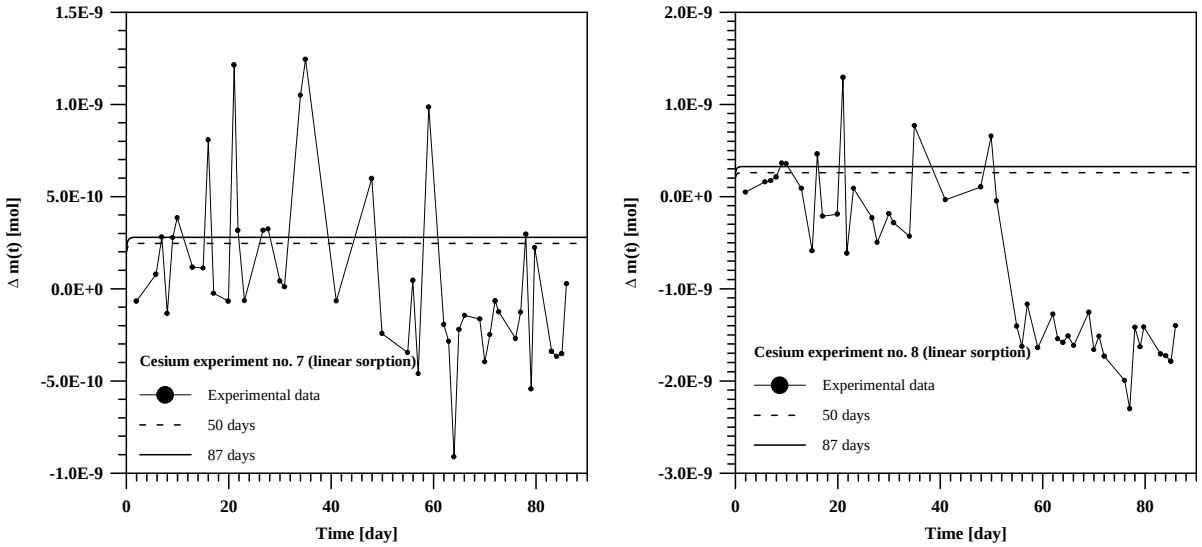

Figure 3.2.3.2.-2: Comparative plots of the experimental data for caesium deposition in the HCP and theoretical curves for both experiments. The calculations are based on the best-fit parameter values from modelling the diffusive flux across the down-stream boundary assuming linear sorption and using experimental data from the first 50 and 87 days respectively, as indicated in the legends.

Due to small but non-vanishing values for K_d the tracer deposition in the HCP are in both cases slightly larger when compared to the former model where sorption processes were neglected at all, but both curves remain consistent with the measurements.
In the table below we have compiled all best-fit parameter values together with their 1σ - standard errors.

		Experiment no. 7				**Experiment no. 8**			
Δt	N	$D_e \cdot 10^{11}$	$K_d \cdot 10^3$	α	χ^2_ν	$D_e \cdot 10^{11}$	$K_d \cdot 10^3$	α	χ^2_ν
[day]	**[-]**	**[m²/s]**	**[m³/kg]**	**[-]**	**[-]**	**[m²/s]**	**[m³/kg]**	**[-]**	**[-]**
0 - 50	32	10.3 ± 0.3	0.445 ± 0.073	0.976 ± 0.076	45.128	14.2 ± 0.3	0.501 ± 0.179	1.02 ± 0.15	21.515
0 - 87	57	11.2 ± 0.4	0.610 ± 0.096	1.10± 0.10	88.313	15.7 ± 0.4	0.838 ± 0.299	1.28± 0.24	46.251

Table 3.2.3.2.-1: The extracted best-fit values for the effective diffusion coefficient D_e, the volume-based linear sorption equilibrium distribution coefficient K_d, and the rock capacity factor α together with their one-standard deviation errors and the minimum values for the reduced χ^2_ν for two caesium through-diffusion experiments. For the adjustment N data triplets were used measured in the time interval Δt.

For comparison purposes we have compiled the values for the apparent diffusion coefficient $D_a = D_e / \alpha$ in the next table for both the no sorption and the linear sorption model. This quantity takes into account the rock capacity factor (α) in order to identify transient processes such as sorption.

	Experiment no. 7				Experiment no. 8			
	no sorption		linear sorption		no sorption		linear sorption	
Time	$D_a \cdot 10^{11}$	α	$D_a \cdot 10^{11}$	α	$D_a \cdot 10^{11}$	α	$D_a \cdot 10^{11}$	α
[day]	[m^2/s]	[-]	[m^2/s]	[-]	[m^2/s]	[-]	[m^2/s]	[-]
0 - 50	13.7 ± 1.2	0.63 ± 0.05	10.6 ± 0.9	0.976 ± 0.076	22.1 ± 1.9	0.63 ± 0.05	13.9 ± 2.1	1.02 ± 0.15
0 - 87	14.8 ± 1.3	0.63 ± 0.05	10.2 ± 1.7	1.10 ± 0.10	24.6 ± 2.1	0.63 ± 0.05	12.3 ± 2.4	1.28 ± 0.24

Table 3.2.3.2.-2: Compilation of the best-fit values for the apparent diffusion coefficient $D_a = D_e / \alpha$ for both caesium experiments, either neglecting sorption processes at all or including linear sorption.

Comparison with the results of other investigations

There are many measurements of caesium on cementitious material. Studies on the leaching behaviour and through- and out-diffusion experiments were performed, accompanied by batch sorption measurements. Therefore many more data are available than for other elements.

Batch sorption experiments were carried out by Hietanen et al. [40] and Atkinson et al. [1]. The first group measured the sorption on crushed concrete, concrete pieces and on crushed sand ballast using two different groundwaters for the tracer solution. The initial caesium concentration was lower than 10^{-7} M. On concrete they found K_d values of $(150 \pm 2) \cdot 10^{-3}$ m^3/kg and $(390 \pm 12) \cdot 10^{-3}$ m^3/kg. Errors are given as one standard deviation. By interpreting autoradiographic experiments they concluded that the sorption of caesium on concrete is mainly onto the aggregates and depends on their mineral composition.

Such a conclusion is supported by measurements by Atkinson et al. where K_d-values were determined on cementitious material of SRCP with various particle sizes and initial concentrations of the traced solution 10^{-2} - 10^{-6} M. They found that the sorption is so weak that the results tend to be imprecise. However, their investigations showed that Cs^+ is sorbed reversibly by cement and the isotherm is linear. They observed that the sorption did not depend on time, particle size and initial tracer concentration used but on the volume of liquid (V_l) to volume of solid (V_s) ratio. They explained that sorption increased with increased V_l / V_s-ratio. Hence, they discussed sorption in terms of the rock-capacity factor α, which is independent of these quantities. Their value for caesium - averaged over all experiments performed for a V_l / V_s-ratio of 15.6 - is:

$$\alpha = 1.4 \pm 0.3.$$

Leach-tests were performed by several groups. One study was done by Atkinson et al. [42] using Ordinary Portland Cement with a water/cement-ratio (W/C) of 0.3. The experiments were made by applying different flow-rates of the leachant; which was always demineralised water at 25°C. They found that leaching could be characterised by only two parameters; one is the apparent diffusion coefficient $D_a = D_e / \alpha$, with α being the rock-capacity factor. They determined for D_a values of the order

$$D_a = (1.4 - 3.5) \cdot 10^{-12}\ m^2/s \text{ and}$$
$$\alpha = 0.26 - 2.5$$

depending on the flow rate, the specimen's surface and the time of exposure to the leachant.

Other leach tests were performed by Plecaš et al. [43] using ^{137}Cs immobilised in cement in concrete containers. For the modelling a simple 1D-diffusion equation was used where the sample was treated as a semi-infinite medium with a constant effective diffusion coefficient. The authors concluded that the leaching process might consist of two different phases with different diffusivities. For a first period up to 150 days they found for

$$D_a(I) = 1.2 \cdot 10^{-11}\ cm^2/d$$

and for the second stage between 150 and 815 days a value of

$$D_a(II) = 8.3 \cdot 10^{-11}\ cm^2/d$$

with $D_a(II) > D_a(I)$. However, no further information on the concrete or the water used are available.

A further leach study was done by Krishnamoorthy et al. [44] on cylindrical OPC cement blocks with a W/C ratio of 0.4. The analysis of the experiments suggested a fast tracer release in the beginning followed by a slow release for a long time period. The diffusion model allowed the determination of values for D_e and α. Astonishingly their values for D_e are very similar to ours; their values for the rock capacity factor, however, are larger by a factor of three. For comparison purposes we have compiled the values for D_e from these authors and the present study in the table below.

Krishnamoorthy et al.		**Experiment no. 5**		**Experiment no. 6**	
$D_e \cdot 10^{11}$ [m^2/s]	α [-]	$D_e \cdot 10^{11}$ [m^2/s]	α [-]	$D_e \cdot 10^{11}$ [m^2/s]	α [-]
16.1 / 17.9	3.05 / 3.61	11.2 ± 0.4	1.10 ± 0.10	15.7 ± 0.4	1.28 ± 0.24

Table 3.2.3.2.-3: Comparison of the best-estimates for D_e and α from Krishnamoorthy et al. [44] and from the present study.

Many more data are available from **diffusion experiments** than from leach tests. Most of them were carried out in equipment very similar to ours using cementitious disks of either OPC or SRPC but with very different W/C-ratios. Therefore it is difficult to compare the numerical values for the transport parameters obtained on diffusion barriers with such different experimental conditions.

Let us start with an early study performed by Anderson et al. [41]. They used disk-like samples of slag cement pastes with a W/C-ratio of 0.35 and 0.40, aged for about 17 and 25 months in the absence of air in a saturated $Ca(OH)_2$-solution. The traced solution had an initial concentration of 10^{-8} M. For the experiments they used different water compositions such as artificial sea water, Baltic sea water, artificial groundwater, and two artificial pore waters. In the table below we have compiled their values for two artificial pore waters with varying composition.

W/C	$D \cdot 10^{14}$ [m^2/s]	$K_d \cdot 10^3$ [m^3/kg]
0.35	6.4 / 7.0	0
0.40	2.3 / 1.7	7

Table 3.2.3.2.-4: Table of the best-estimate parameters for the diffusion coefficient D and K_d (from batch sorption experiments) from Anderson et al. [41].

Their values for D are orders of magnitude smaller than ours whereas their K_d-values cover our range.

Atkinson and co-workers made several efforts to measure and interpret diffusion/sorption profiles of caesium through cementitious materials. A first study was made 1984 [39] when they measured D_e and α for various W/C-ratio. The initial CsCl concentration was 0.1 M. They found that sorption of caesium was very low on OPC-pastes and that the values for D_e changed roughly four orders of magnitude while varying the W/C-ratio from 0.2 till 0.7. In the figure below (left plot) we plotted the values for D_e versus the W/C-ratio taken from Atkinson et al. and those from the present study. Whereas the older data for D_e approximately follow an exponential dependence, those of our study do not match such a scheme.

In the right figure the values of the rock capacity factor are plotted versus the W/C-ratio.

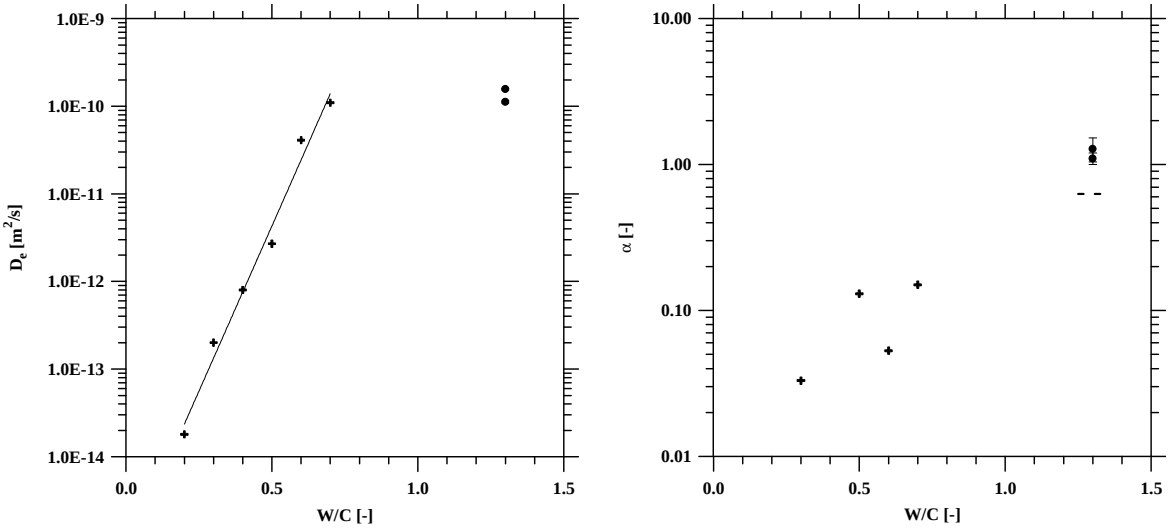

Figure 3.2.3.2.-3: In the left sub-figure the values for the effective diffusion coefficient versus the W/C-ratio are plotted. Values from Atkinson et al. [39] are denoted by a cross, those from our study by dots. The solid line indicates a fitted exponential dependence of D_e(W/C) over about four orders of magnitude. Note, that there is no theoretical basis for such a behaviour.
In the right sub-figure the rock capacity factor α is plotted as a function of the cement/water ratio (the meaning of the symbols is the same as for the left sub-figure). The dashed line below our data indicates a lower limit for α which is equal to the sample's porosity. The error bars represent a 1σ-uncertainty in the values.

In a further study Atkinson and co-workers [1] measured the diffusion/sorption profile of caesium using disk-like samples made of SRCP with a W/C-ratio of 0.4 and a porosity of 0.3. The initial caesium concentration was 10^{-4} M, and from subsequent modelling of the breakthrough curves they determined values for the transport parameters as follows:

$$D_e = 1.8 \cdot 10^{-12}\ m^2/s,$$
$$\alpha = 0.17,$$
$$D_a = D_e / \alpha = 11 \cdot 10^{-12}\ m^2/s,$$

hence the caesium sorption on SRCP can - similarly to the out-come of our study - be considered negligible.

In out-diffusion experiments they clearly diagnosed two distinct diffusion processes from the concentration profiles across the samples: A more rapid diffusion corresponding to a lower value for the rock capacity factor α and a higher apparent diffusion coefficient than for a less rapid diffusion. Their values for caesium are:

Fast process		**Slow process**	
$D_e / \alpha \cdot 10^{12}$ [m^2/s]	α [-]	$D_e / \alpha \cdot 10^{12}$ [m^2/s]	α [-]
4	0.2	0.04	1.7

Table 3.2.3.2.-5: Table of the best-estimate values for the apparent diffusion coefficient D_e / α and the rock capacity factor α for caesium for two distinct diffusion processes. Taken from Atkinson et al. [1].

Muurinen et al. [45] measured the diffusivities and the concentration profiles of caesium in concrete. Like Krishnamoorthy and co-workers they found that the measured profiles follow the theoretical profiles quite poorly. Their conclusion was that the curves seemed to consist of two parts: a slowly and fast diffusing part. For concrete they determined values for the apparent diffusion coefficient D_a and measured values for K_d on crushed concrete for varying compositions of the concrete and groundwater (salt content: 200 ppm, 8000 ppm).

$D_a \cdot 10^{14}$ [m^2 / s]	K_d [m^3 / kg]
7.5	0.122
5.5	0.179
2.6	0.390

Table 3.2.3.2.-6: Values for the apparent diffusion coefficient and K_d measured on concrete pieces and crushed concrete for varying compositions of the samples and the groundwater used. For further details see Muurinen et al. [45].

These D_a-values are at least three orders of magnitude smaller than our values; the K_d-values, are two to three orders of magnitude larger. The high K_d-values are not comparable to the batch sorption measurements performed by Hietanen et al. [40] but they might be caused, too, by caesium sorption onto the aggregate.

Rudin and Landolt [46] measured the penetration of ^{137}Cs through cementitious materials that could be used for radioactive waste management. Eighteen Portland cement formulations containing various portions of fly ash and other additives were used. Their water to cement

ratio was either 0.33 or 0.43. After slicing and analysing the activity distributions across the samples they concluded that caesium penetrates such cementitious material (100 % Portland cement, 0 % fly ash) to depths of at least 12 mm within a 308 days period. Lowering the W/C-ratio results in lower caesium penetration because migration in a hardened cement paste is reduced due to the fact that the number of large capillary pores is reduced as the W/C-ratio is decreased.

Johnston and Wilmot [2] investigated the contaminant transport properties and retardation capabilities of several cement-based grout materials. Diffusion of caesium was studied in cement pastes of SRPC partially blended with various amounts of silica fume (for comparison purposes we only mention the data obtained on samples of pure cement without any portion of silica fume). All experiments were conducted using a simulated saline ground-water solution with pH of 12.5. Distribution coefficients were determined by conventional equilibrium batch methods.

W/C [-]	Density [kg/m^3]	Porosity [-]	$K_d \cdot 10^3$ [m^3/kg]	$D_a \cdot 10^{13}$ [m^2/s]
0.35	2430	0.181	0.12 ± 0.05	3.7
0.25	2450	0.113	0.12 ± 0.05	1.6

Table 3.2.3.2.-7: Measured and calculated parameter values from Johnston and Wilmot [2].

There K_d-values are a factor of 4 - 7 smaller than ours. However, Johnston and Wilmot interpreted these low values for the distribution coefficient as likely to be the effect of the high ionic strength of the saline solution.
The values for the apparent diffusion coefficient match well the measurements for D_e by Atkinson et al. [39] -see also left plot of Figure 3.2.3.2.-3. A direct comparison with our best-fit values can be questioned due to the completely different porosities.

A first evaluation of the caesium data was made in 1992 by Sarott et al. [6] neglecting individual errors of the measurements and fitting $m(t)$ instead of $j(t)$. At that time the following best-fit values for D_e and K_d were determined.

	Sarott et al. [6]		present study	
	$D_e \cdot 10^{10}$ [m^2/s]	$K_d \cdot 10^3$ [m^3/kg]	$D_e \cdot 10^{10}$ [m^2/s]	$K_d \cdot 10^3$ [m^3/kg]
Experiment no. 7	1.4	5	1.12 ± 0.04	0.610 ± 0.096
Experiment no. 8	1.9	6	1.57 ± 0.04	0.838 ± 0.299

Table 3.2.3.2.-8: Comparison of the best-fit parameter values from an earlier study performed by Sarott et al. [6] and the present study.

Finally we also mention the results and conclusions of Albinsson et al. [3]. In their study they investigated among other tracers the diffusion of Cs through different types of concrete in

contact with pore water. For the solid phase they used concrete pastes of either Standard Portland Cement (SPC) or of Sulphate Resistant Cement (SRC). For the following we will restrict the discussion only to those results where no further ballast and additives for the preparation of the samples were used. The samples were aged in pore water (the pH of the concrete pore water was 13.1 - 13.4) and then used for the diffusion measurements. Caesium diffusion into the solid phase took place for about 0.7 yr. After this period the samples were ground; in each grinding a layer of about 0.1 and 0.7 mm was removed and then the activity was measured. In addition autoradiograms were taken after every second grinding showing the activity distribution and penetration of the tracer in the samples. For caesium they determined the following values for the apparent diffusion coefficient after a contact time of 231 days:

Concrete	$D_a \cdot 10^{13}$ **[m^2/s]**
SPC	0.79
SRC	1.0

Table 3.2.3.2.-9: Values for the apparent diffusion coefficient for caesium on concrete pastes of Standart Portland Cement (SPC) and Sulphate Resistant Portland Cement (SRC). Taken from Albinsson et al. [3].

Hence, their values for D_a are similar to the results of [2].

3.2.3.3. Non-linear (Freundlich) sorption case

For both caesium experiments two further fits were carried out using only data from the first 50 and 87 days and accounting for non-linear sorption according to the Freundlich isotherm. In order to ensure that a global χ^2-minimum was located, we repeated the calculations up to 10 - 140 times with different sets of starting values for the fit-parameters.

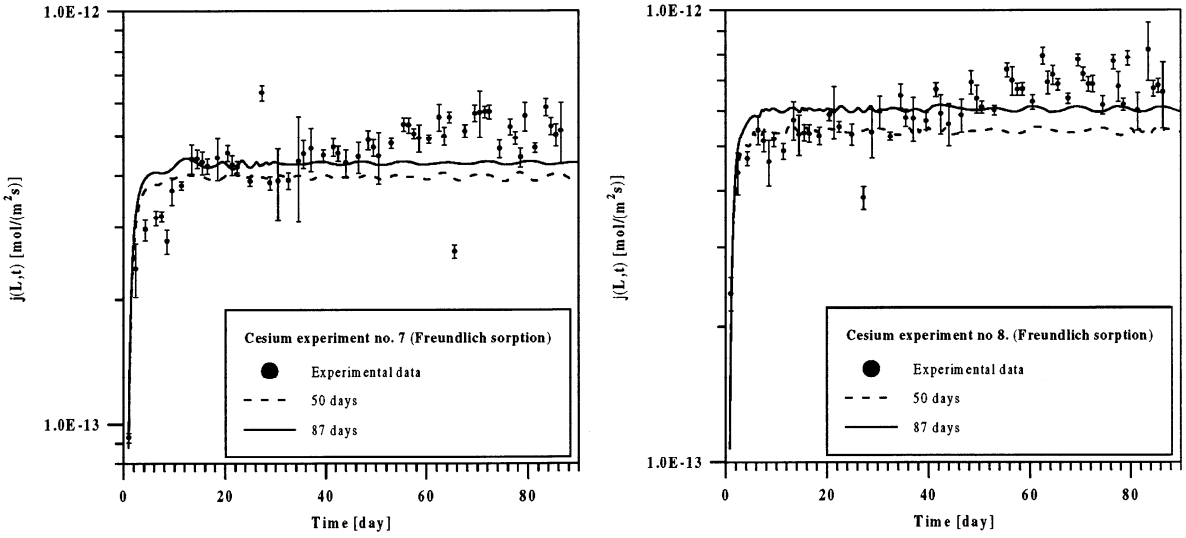

Figure 3.2.3.3.-1: Comparative plots of the experimental data and theoretical breakthrough curves for the diffusive caesium flux for both experiments when assuming non-linear (Freundlich) sorption. Shown are the best-fit curves using experimental data from the first 50 and 87 days, as indicated in the legends. (The wiggles in the calculated breakthrough curves are an artefact of the numerical algorithm only.)

The reproduction of the breakthrough curves is as poor as in the linear sorption case. When comparing the graphical representations of the calculations with those from the former exercise one can hardly see an improvement. Although having now a third freely adjustable parameter (the Freundlich exponent) the calculated breakthrough curves are not better. The leading edge where the modelled flux is - as a rule - too large and the lack of a trend toward a slightly increased diffusive flux leads to the conclusion that this model, too, is not capable of describing the nickel through-diffusion experiments. All modelling tasks yield values for the Freundlich exponent which are slightly lower than unity with small standard deviations (N_p = 0.9 - 0.95, with 1σ uncertainty in the last digit).

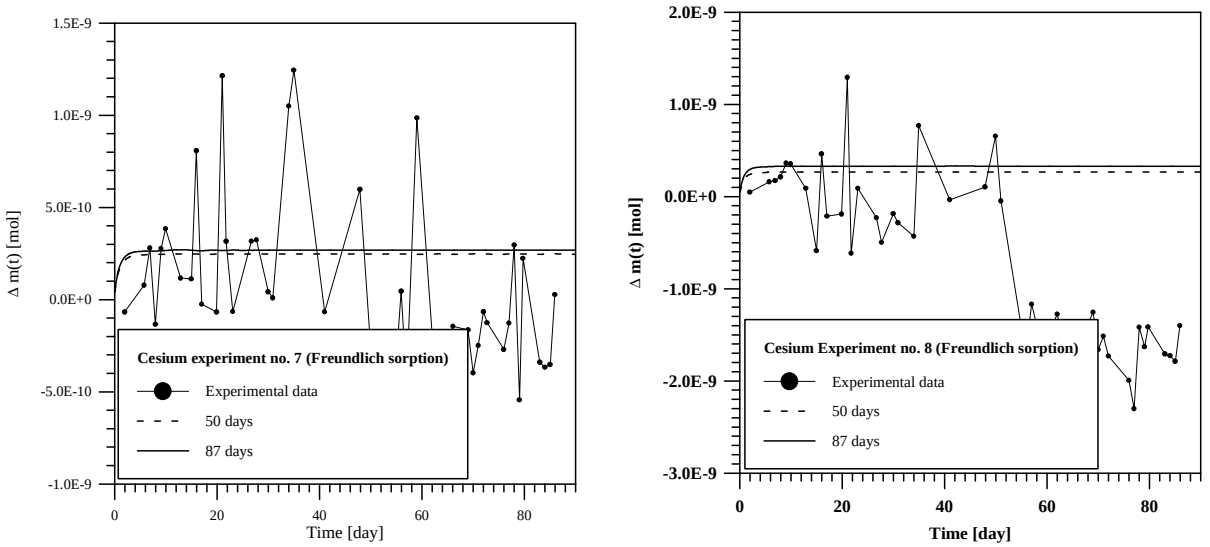

Figure 3.2.3.3.-2: Comparative plots of the experimental data for tracer deposition in the HCP and theoretical curves for two caesium experiments. The calculations are based on the best-fit parameter values from modelling the diffusive flux across the down-stream boundary assuming non-linear (Freundlich) sorption and using experimental data from the first 50 and then 87 days, as indicated in the legends.

The calculated tracer deposition curves are practically identical to those from the former exercise and they do not contradict the measurements. The (anti-)correlations between the fit-parameters are rather small with values between 0.4 - 0.8 for correlations between D_e and K_p, and they allow no further conclusions concerning the adequacy of the present model.

		Experiment no. 7				**Experiment no. 8**			
Δt	N	$D_e \cdot 10^{11}$	$K_p \cdot 10^{3}$	N_p	χ^2_v	$D_e \cdot 10^{11}$	$K_p \cdot 10^{3}$	N_p	χ^2_v
[day]	**[-]**	**[m²/s]**	**[*]**	**[-]**	**[-]**	**[m²/s]**	**[*]**	**[-]**	**[-]**
0 - 50	32	10.4 ± 0.1	0.270 ±0.001	0.952 ± 0.003	40.495	14.2 ± 0.1	0.178 ±0.001	0.896 ± 0.002	20.975
0 - 87	57	11.2 ± 0.1	0.320 ± 0.001	0.948 ± 0.002	83.280	15.8 ± 0.1	0.514 ± 0.001	0.952 ± 0.002	44.809

Table 3.2.3.3.-1: The extracted best-fit values for the effective diffusion coefficient D_e and the two Freundlich isotherm parameters K_p [*] = [$\mathrm{mol}^{1-N_p}\mathrm{m}^{3N_p}\mathrm{kg}^{-1}$] and N_p together with their one standard deviation errors and the minimum values for the reduced χ^2_v for two caesium through-diffusion experiments. For the adjustment N data triplets were used measured in the time interval Δt.

Our conclusions based on these results are the following:

- The transient part of the diffusion curve is only very roughly reproduced, and there are no further improvements in this part of the breakthrough curve when compared to the linear sorption case.
  The extracted best-fit values for the Freundlich isotherm seem to be reasonable and do not violate basic assumptions of the Freundlich isotherm formalism.
- The modelled caesium deposition curves in the HCP are in the range of the measurements.
- However, although a third freely adjustable parameter is available, also this extended model cannot account correctly for the trend in the diffusive flux to higher values at later times.

3.2.3.4. First-order sorption kinetics - linear/linear case

In a further step we investigated the effect of first-order sorption kinetics according to equation (3.1.3) on the diffusion-sorption profile. In our concept we first fixed the exponent to unity. The fit-parameters were now the effective diffusion coefficient D_e, the rate for sorption k_s [s^{-1}], and the rate for desorption k_r [s^{-1}]. As before in a series of subsequent fits data from the first 50 and then 87 days were used for the fitting procedure.

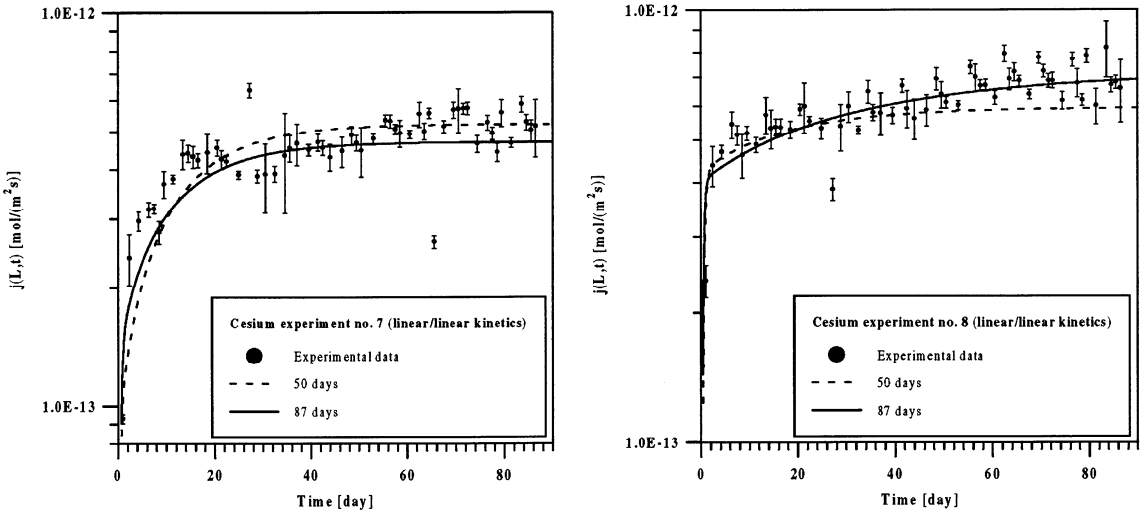

Figure 3.2.3.4.-1: Comparative plot of the experimental data and theoretical breakthrough curves for the diffusive caesium flux and experiments no. 7 and 8 when assuming first-order sorption kinetics. Shown are the best-fit curves using experimental data from the first 50 and 87 days, as indicated in the legends.

Inspecting the fast transient part of the diffusion curve we can recognise a much better representation of the measurements by the model compared to a concept with a linear or non-linear sorption isotherm. Whereas the modelled breakthrough curves for experiment no. 7 evolve smoothly, those of experiment no. 8 are quite “edgy” in accordance to the measured data. For both experiments it is necessary to use the full dataset for the fitting procedure to obtain good representations of the data. This is an indication that both experiments never reached a steady-state.

The final best-fit values for D_e are in the range of (12 - 19) $\cdot$ 10^{-11} m^2/s and are therefore slightly larger than those obtained from the previous modelling concepts using linear or non-linear sorption isotherms. Correlations/anti-correlations between the fit-parameters become smaller when using more data for the adjustment and asymptotically reach values of e.g. $R_{1,3}$ = -(0.8 - 0.9) for D_e and K_p.

		Experiment no. 7				Experiment no. 8			
Δt	N	$D_e \cdot 10^{11}$	$k_s \cdot 10^6$	$k_r \cdot 10^7$	χ^2_ν	$D_e \cdot 10^{11}$	$k_s \cdot 10^6$	$k_r \cdot 10^7$	χ^2_ν
[day]	[-]	[m^2/s]	[s^{-1}]	[s^{-1}]	[-]	[m^2/s]	[s^{-1}]	[s^{-1}]	[-]
0 - 50	32	13.6 ± 0.4	28.5 ± 0.7	23.5 ± 1.8	58.675	15.6 ± 0.6	5.18 ± 1.48	7.40 ± 2.45	20.590
0 - 87	57	12.3 ± 0.4	16.2 ± 1.0	18.5 ± 1.5	82.867	18.9 ± 1.1	11.6 ± 1.2	4.42 ± 1.41	21.877

Table 3.2.3.4.-1: The extracted best-fit values for the effective diffusion coefficient D_e and the rates for sorption k_s and desorption k_r together with their one-standard deviation errors and the minimum values for the reduced χ^2_ν for caesium through-diffusion. For the adjustment N data triplets were used measured in the time interval Δt.

In the table below we have compiled the hypothetical K_d -values, where the diffusion system would be in a steady-state, together with their 1σ-standard errors for both experiments.

		Experiment no. 7	Experiment no. 8
Δt	# of data	$(K_d \pm \Delta K_d) \cdot 10^3$	$(K_d \pm \Delta K_d) \cdot 10^3$
[day]	[-]	[m^3/kg]	[m^3/kg]
0 - 50	34	9.83 ± 1.12	5.68 ± 2.53
0 - 100	68	7.10 ± 0.93	21.3 ± 7.4

Table 3.2.3.4.-2: The computed K_d -values according to equation (3.2.4) with 1σ-standard errors using measured data in the time interval Δt for the fitting procedure when applying first-order sorption kinetics.

In the linear-sorption case values for K_d were obtained of the order of (0.45 - 0.85) · 10^{-3} m^3/kg only. In the frame of the present kinetics model the steady-state values were roughly one order of magnitude larger indicating an increased caesium up-take by the HCP. This can also be recognised in the comparison of calculated and measured tracer up-take.

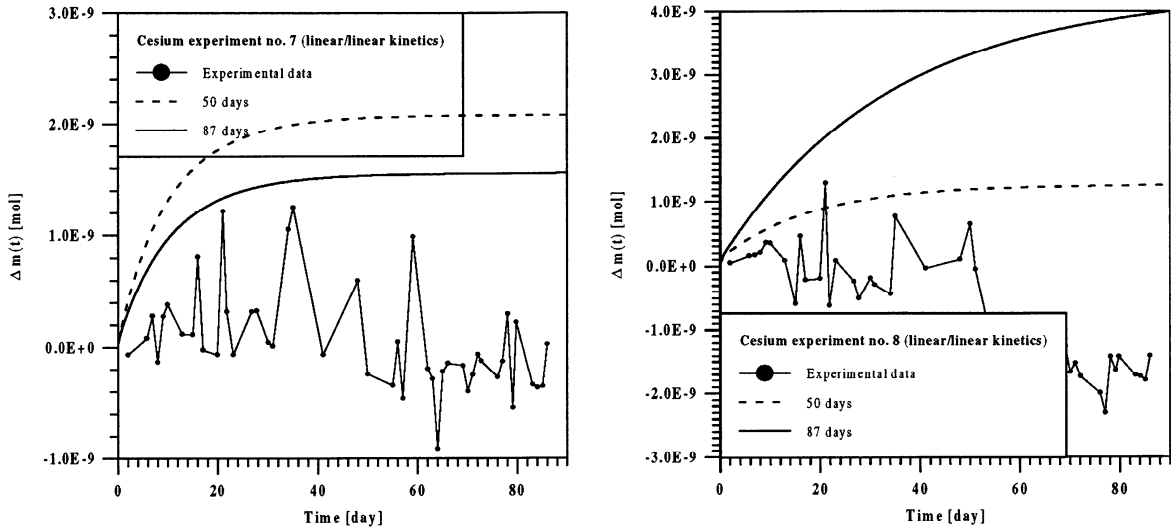

Figure 3.2.3.4.-2: Comparative plots of the experimental data for tracer deposition in the HCP and theoretical curves for both caesium experiments. The calculations are based on the best-fit parameter values from modelling the diffusive flux across the down-stream boundary assuming first-order sorption kinetics and using experimental data from the first 50 and then 87 days, as indicated in the legends.

From this figure we can see that the model accounts for a much too strong tracer up-take by the solid phase - an effect which clearly remains contradictory to the measurements. Although the model fits the breakthrough curves very well and much better than previous models did, it fails to account correctly for all the observations.

3.2.3.5. First-order sorption kinetics - non-linear/linear case

Finally we investigated - just for completeness - the effect of first-order sorption kinetics according to equation (3.1.3) where now the forward reaction is non-linear in terms of the Freundlich isotherm and the desorption reaction is linear. The fit-parameters were now the effective diffusion coefficient D_e, the rate for sorption k_s [$mole^{1-N_s} m^{3N_s} kg^{-1}$], the Freundlich exponent N_s [-], and the rate for desorption k_r [s^{-1}]. Again, in a series of subsequent fits data from the first 50 and 87 days were used for the fit-procedure.

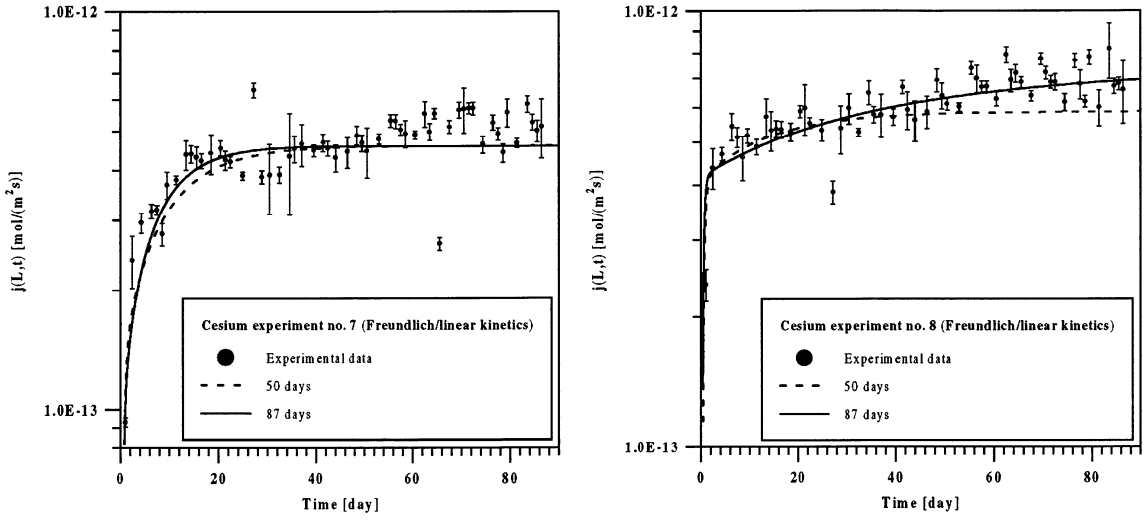

Figure 3.2.3.5.-1: Comparative plot of the experimental data and theoretical breakthrough curves for the diffusive caesium flux for experiments no. 7 and 8 when assuming first-order non-linear sorption kinetics. Shown are the best-fit curves using experimental data from the first 50 and then 87 days, as indicated in the legends.

Although a fourth fit-parameter can be adjusted, the increase in the quality of the fits is only very moderate when compared with the results of the former model.

		Experiment no. 7					**Experiment no. 8**				
Δt	N	$D_e \cdot 10^{11}$	$k_s \cdot 10^6$	N_s	$k_r \cdot 10^7$	χ^2_ν	$D_e \cdot 10^{11}$	$k_s \cdot 10^6$	N_s	$k_r \cdot 10^7$	χ^2_ν
[day]	**[-]**	**[m^2/s]**	**[*]**	**[-]**	**[s^{-1}]**	**[-]**	**[m^2/s]**	**[*]**	**[-]**	**[s^{-1}]**	**[-]**
0 - 50	32	12.0 ± 1.4	0.0987±0.0072	0.568 ± 0.023	16.8 ± 4.1	34.638	15.4 ± 0.6	0.981±0.154	0.849 ± 0.032	9.33 ± 1.39	20.616
0 - 87	57	12.0 ± 0.4	2.29 ± 0.15	0.815 ± 0.027	29.9 ± 11.4	62.816	19.4 ± 1.5	0.307 ± 0.092	0.682 ± 0.022	3.22 ± 1.18	21.861

Table 3.2.3.5.-1: Results from modelling both caesium through-diffusion experiments using a diffusion/first-order non-linear sorption kinetics model. The fit-parameters of the model are the effective diffusion coefficient D_e, the rate coefficient k_s [*] = [$mol^{1-N_s} m^{3N_s} kg^{-1}$], the exponent N_s for sorption, and the rate for desorption k_r. Compiled are the best-fit values together with their one-standard deviation errors and the minimum values for the reduced χ^2_ν. For the adjustment N data triplets were used measured in the time interval Δt.

The values for the effective diffusion coefficient are nearly the same as from former models; however, the values of the two rate constants are now different and are up to one order of magnitude smaller. The best-fit values for the Freundlich-exponent are always less than unity but show a non-uniform behaviour. For experiment no. 7 the non-linearity of the forward reaction is dumped when using the full dataset for the adjustment. For experiment no. 8 the non-linearity becomes greater, i.e. smaller values for the exponent. A similar inconsistency between the two experiments can be observed for the rate coefficient for sorption k_s: a near zero value for experiment no. 7, when using a reduced dataset for the fitting procedure, and which becomes greater when using all data. But experiment no. 8 shows a trend to lower parameter values when using more data for the adjustment. The fourth fit-parameter k_r, too, shows an analogously inconsistent behaviour. Therefore we assume that this model, too, has not the capability to describe the caesium breakthrough curves correctly and with consistent values for the fit-parameters.
Such an assumption of the principal deficiencies of the given model is corroborated when inspecting the tracer deposition curves and comparing them with measurements. Again, as for the former model, the theory predicts too high values for tracer up-take by the cementitious material.

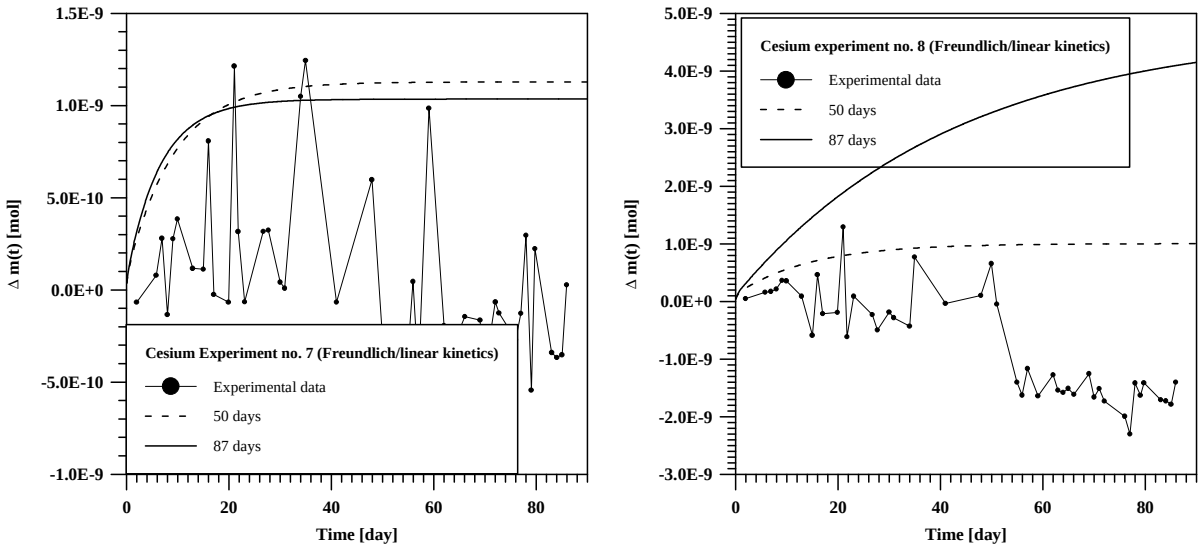

Figure 3.2.3.5.-2: Comparative plots of the experimental data for caesium deposition in the HCP and theoretical curves for both experiments. The calculations are based on the best-fit parameter values from modelling the diffusive flux across the down-stream boundary assuming first-order non-linear sorption kinetics and using experimental data from the first 50 and 87 days, as indicated in the legends.

3.2.3.6. Conclusions for caesium

- The most simple concept where sorption is neglected at all is able to reproduce the breakthrough curves in a very rough and averaged way only. The extracted best-fit parameter values for D_e are consistent with literature data, and the reproduction of the observed time-history for the tracer deposition in the HCP is acceptable.
- Using a more complex model where sorption is included either as a linear or non-linear (Freundlich) isotherm does not improve the quality of the fits. The best-fit parameter values again are reasonable, but nevertheless both models fail to successfully reproduce the observed trend in the breakthrough curves toward increased fluxes for greater times.
- More complex models where first-order sorption kinetics is included yield much better reproductions of the breakthrough curves but seriously overestimate the tracer up-take by the HCP. Hence, such concepts have to be rejected because they are not able to predict all measurements correctly.
- Due to the small tracer up-take by the cementitious material we assume that caesium indeed acts as a nearly conservative tracer. This is corroborated by the fact that the simple model yielded only very small values for K_d in the range of $(0.45 - 0.85) \cdot 10^{-3}$ m^3/kg.
- A trend to higher values for the diffusive flux for greater times is indicative for further (unknown) transport mechanisms which presently are not included in any of our models.

3.2.4. Modelling results for the nickel experiment no. 5 - 8

3.2.4.1. No-sorption case

The breakthrough curves were fitted to the left hand side of equation (3.1.14) with the help of the procedure outlined in more detail in sub-section 3.1. In a series of subsequent fits we adjusted the free parameters to diffusion-sorption profiles using the measured data from the first 50, 100, 200, ... etc. days.

As a first step we tried to model the measured data neglecting sorption entirely.
The quality of the fits in general was very poor: for the slope of the flux profiles unreasonable values were always obtained, and the transient part of the diffusion curve especially was crudely reproduced. Due to the lack of agreement between measurements and theory we do not present comparative plots of the experiments; hence, we do not discuss the extracted best-fit values for D_e. In sub-section 3.2.1.1., for chloride as a representative example, an illustration of these facts is already given.

	Experiment no. 5			**Experiment no. 6**			**Experiment no. 7**			**Experiment no. 8**		
Δt	N	$D_e \cdot 10^{11}$	χ^2_ν	N	$D_e \cdot 10^{11}$	χ^2_ν	N	$D_e \cdot 10^{11}$	χ^2_ν	N	$D_e \cdot 10^{11}$	χ^2_ν
[day]	**[-]**	**[m²/s]**	**[-]**	**[-]**	**[m²/s]**	**[-]**	**[-]**	**[m²/s]**	**[-]**	**[-]**	**[m²/s]**	**[-]**
0-50	33	0.553±0.052	206.62				34	0.478±0.035	162.12			
0-100	65	0.717±0.058	367.20	65	1.07±0.06	181.72	68	0.536±0.041	222.84	68	0.735±0.055	297.01
0-200	130	0.838±0.055	403.23				137	0.677±0.046	286.05			
0-300	198	0.967±0.052	444.08	198	1.49±0.06	226.27	201	0.827±0.049	350.66	201	1.10±0.06	412.96
0-405							266	0.956±0.050	381.92			
0-441	291	1.09±0.05	451.69									
0-500				331	1.73±0.05	206.38				281	1.22±0.06	402.56
0-700				389	1.80±0.05	197.19				309	1.24±0.06	383.77
0-834										328	1.26±0.05	373.13
0-994				430	1.83±0.05	191.95						

Table 3.2.4.1.-1: The extracted best-fit values for the effective diffusion coefficient D_e together with their one-standard deviation errors and the minimum values for the reduced χ^2_ν for nickel through-diffusion (experiments no. 5 - 8). For the adjustment N data triplets were used measured in the time interval Δt.

An obvious conclusion which can be drawn is the following: Having fixed the sample's porosity and adjusted the only free fit-parameter - the effective diffusion constant D_e - it is impossible to reproduce the measured data, meaning that **at least a further transport mechanism, which accounts for nickel-retardation, such as e.g. sorption, is necessary** if we want to arrive at an acceptable mathematical description of the measured nickel-diffusion profiles.

3.2.4.2. Linear sorption case

Next we took into account linear, instantaneous equilibrium sorption of the tracer onto inner surfaces of the HCP. The procedure now includes an additional fit-parameter - the linear equilibrium sorption distribution coefficient K_d.

From the best-fit values obtained from modelling **experiment no. 5** we can conclude that the diffusion process may be in a steady-state phase after roughly 200 days. This is a value which is something larger compared to the estimated 150 days when looking at Figure 2.3.1.-1 where the diffusive flux is plotted versus time. However, an inspection of the transient part of the diffusion-sorption curve shows that this part of the measured data is only roughly reproduced by the model and the flux is significantly too small during this period. Using more and more measurements for the adjustment of the fitting parameters both values increase monotonically also reducing the correlation between the two parameters from values of 0.98 to 0.75. The best-fit value for the effective diffusion coefficient is about $D_e \approx 2.5 \cdot 10^{-11}\ \mathrm{m^2/s}$. This is in excellent agreement with the estimated value from the considerations made in sub-chapter 2.3.1. and is comparable to literature data [6], though for different nuclides. However, the value for the K_d is only $(35-37) \cdot 10^{-3}\ \mathrm{m^3/kg}$ ($\alpha \approx 27-29$) and is therefore too small by a factor of about eight compared to values obtained in static batch sorption experiments [17]. In the following Figure 3.2.4.2.-1 we have plotted the best-fit curves for all four experiments together with the measured data.

The system studied in **experiment no. 6** seems to reach steady-state in about 250 days because the best-fit values of the parameters are - more or less - constant after that time. However, as seen from experiment no. 5, the transient part of the diffusion curve is modelled quite badly. The failure of the model to satisfactorily reproduce the data in the transient phase implies that the representation of the retarding mechanism by a linear sorption isotherm is crude. Such a conclusion is supported by the fact that the best-fit values for K_d range from (25 - 27) $\cdot$ 10^{-3} $\mathrm{m^3/kg}$, again a factor of about eight too small when compared with batch sorption measurements. The best-fit value for the effective diffusion constant D_e is about 2.5 $\cdot$ 10^{-11} $\mathrm{m^2/s}$ and corresponds to that of experiment no. 5 when keeping in mind that the duration of experiment no. 6 was twice of that of the former experiment. The correlation between D_e and K_d weakens from 0.89 when using data only from the first 100 days to 0.64 when using all available measurements for the adjustment.

The series of calculations for **experiment no. 7** implies that the system is not in steady-state at all. The best-fit parameter values of the series change continuously, and also the transient phase of the diffusion curve is only crudely reproduced. This “not reaching a steady-state phase” is supported by our former investigations in sub-section 2.3.3 where a nearly 38 % increase in the flux in the interval between 100 and 405 days was recognised with the help of a simple linear regression of the data. However, the best-fit values for D_e are roughly 15% smaller than those from experiments no. 5 and 6, yet they remain reasonable. The K_d-values are (20 - 25) $\cdot$ 10^{-3} $\mathrm{m^3/kg}$ being also a factor of ten too small compared to values from batch sorption experiments. Consistent with the former experiments the correlation between the two fit-parameters weakens strongly when more and more data are used.

At first sight one could believe that **experiment no. 8** is in steady-state after approximately 100 days. However, we know from former considerations (see also sub-section 2.3.4 in this context) that this is not the case: the diffusive flux increases about 21 % during this period.

Including the measurements beyond 100 days results in slightly larger best-fit values for both parameters. The extracted diffusivity D_e = (2.2 - 2.3)$\cdot 10^{-11}$ m^2 / s is close to values determined from data from the other nickel experiments; the values for the K_d = 19.4$\cdot 10^{-3}$ m^3 / kg are - again - roughly an order of magnitude too small when compared to values from batch sorption experiments. Again the correlation between the two freely adjustable parameters weakens to values of 0.55 when using all available measurements.

The next figure shows a graphical comparison of measured data and calculated flux profiles for all four experiments.

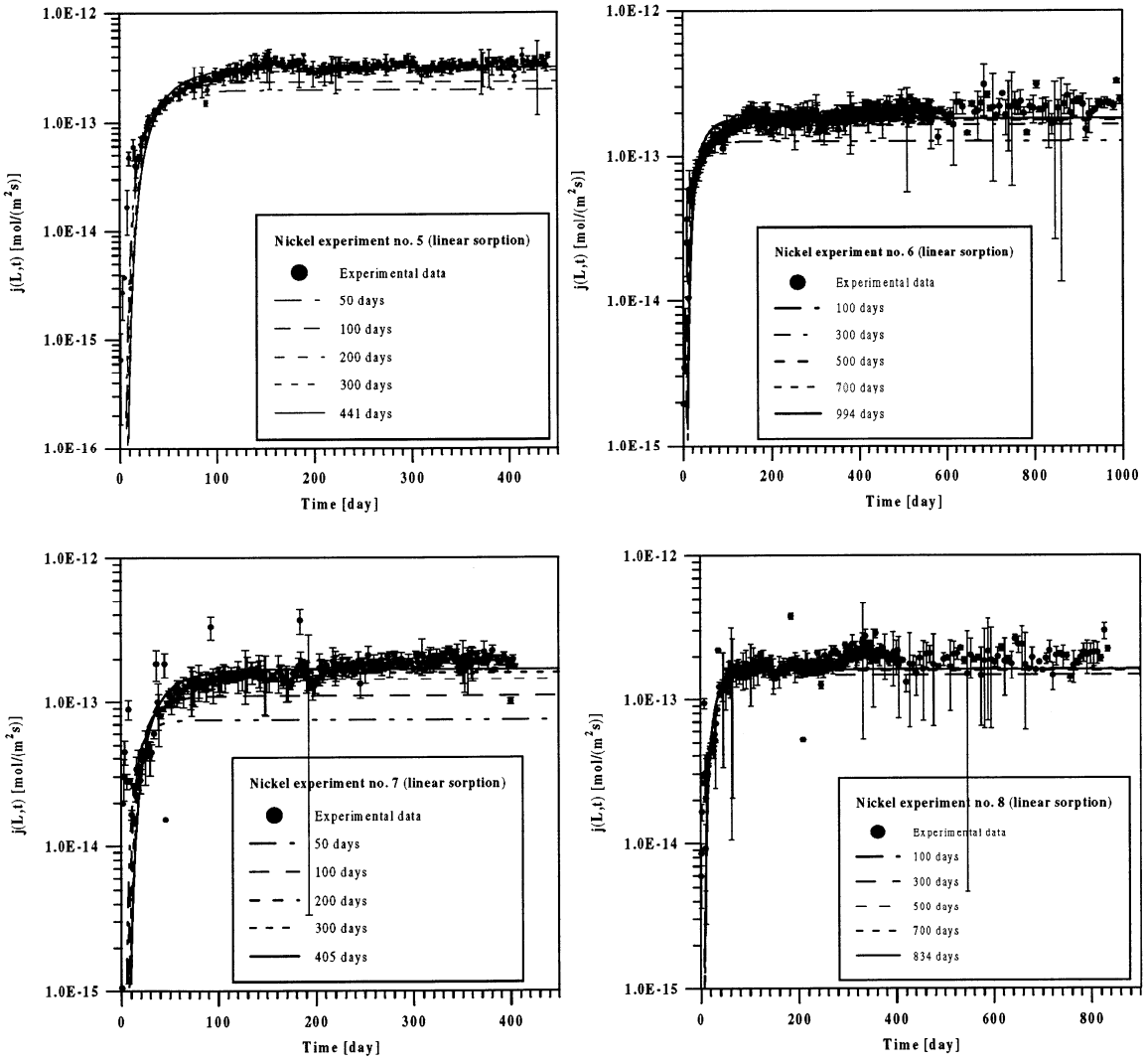

Figure 3.2.4.2.-1: Comparative plot of the experimental data and theoretical breakthrough curves for the diffusive nickel flux and experiments no. 5 - 8 when assuming linear sorption. Shown are the best-fit curves using experimental data from the first 50, 100, etc. days as indicated in the legends.

In general the overall reproduction of the measurements by the model is quite satisfactory. However, the model predicts much too low diffusive flux at the rising edge (see for example the plot for experiment no. 5). It appears that near steady-state is reached after roughly 200 days when the extracted best-fit parameter values become more or less constant. But from the considerations in chapter 2.3. we know that this is not the case, except for experiment no. 5

where we diagnosed a near steady-state. There (see also page 67), for experiment no. 5 we roughly estimated a D_e value of $(2.58 \pm 0.20) \cdot 10^{-11}$ m^2/s using data above 150 days. This is confirmed by the fitting procedure which yields a value of $D_e = (2.52 \pm 0.03) \cdot 10^{-11}$ m^2/s.
The suspicion that the linear sorption model does not adequately describe nickel through-diffusion is confirmed if we compare the modelled nickel deposition in the HCP with measurements. This is illustrated with the help of the next figure.

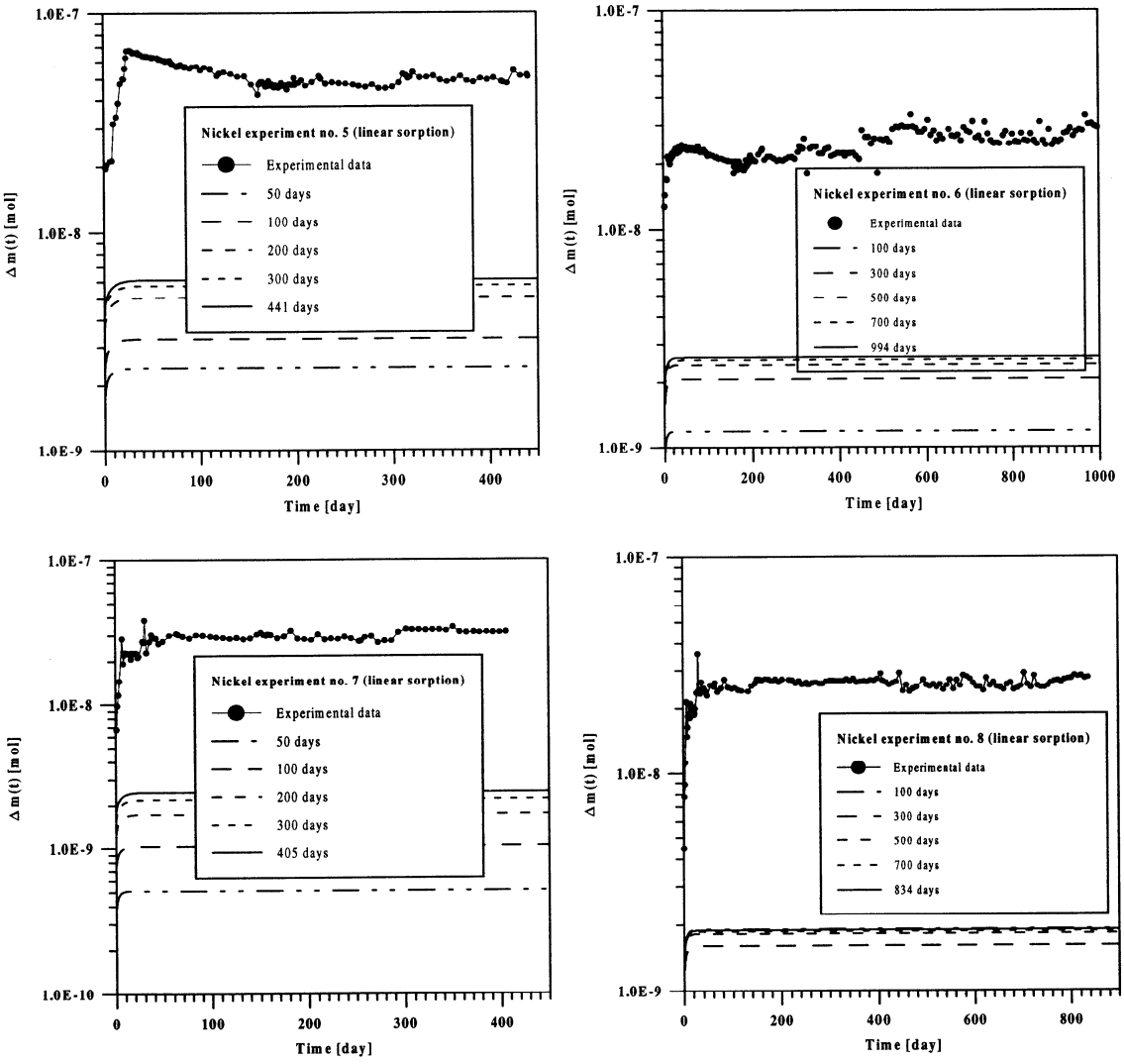

Figure 3.2.4.2.-2: Comparative plots of the experimental data for nickel deposition in the HCP and theoretical curves for all four experiments. The calculations are based on the best-fit parameter values from modelling the diffusive flux across the down-stream boundary assuming linear sorption and using experimental data from the first 50, 100, etc. days as indicated in the legends.

As can be seen for all four experiments the model predicts - by factors from 2 to 7 less nickel deposition in the cementitious material than is measured in the experiments, taking into account that approximately 10^{-8} moles nickel may be sorbed onto the polystyrene of the measurement cell. Therefore we conclude that nickel deposition in the HCP is modelled wrongly using only a simple K_d-concept, though flux profiles were reproduced quite well.
On the next page we have compiled all the best-fit parameter values together with their one-standard deviation errors and the minimum values for the χ^2_ν-merit function for all four experiments.

Comparing the shape of the breakthrough curve and the value for the χ_v^2-merit function for all four experiments it becomes obvious that the fast transient phase of the breakthrough curve of experiments no. 7 and 8 is less well reproduced than that of the other two experiments, which both showing relatively high values for the residuae. However, this is considered to be only the effect of many more outlying data points in the rising edge of experiments no. 7 and 8 which affects the shape of the modelled profile and strongly contributes to the value of the χ_v^2-merit function.

For an ideal steady-state the diffusive flux across the boundary at $x = L$ is independent of retardation mechanisms such as sorption and only allows the adjustment of the effective diffusion constant. Therefore only in the transient part of the diffusion profile processes such as sorption can be recognised. Such sorption processes could also - in principle - be dominated by non-linear concentration-dependent mechanisms.

To elucidate whether the sorption characteristics is maybe non-linear we have modelled the experiments assuming, for sorption, a Freundlich isotherm according to equation (3.1.2).

	Experiment no. 5				Experiment no. 6				Experiment no. 7				Experiment no. 8			
Δt	N	$D_e \cdot 10^{11}$	$K_d \cdot 10^3$	χ^2_v	N	$D_e \cdot 10^{11}$	$K_d \cdot 10^3$	χ^2_v	N	$D_e \cdot 10^{11}$	$K_d \cdot 10^3$	χ^2_v	N	$D_e \cdot 10^{11}$	$K_d \cdot 10^3$	χ^2_v
[day]	[-]	[m^2/s]	[m^3/kg]	[-]	[-]	[m^2/s]	[m^3/kg]	[-]	[-]	[m^2/s]	[m^3/kg]	[-]	[-]	[m^2/s]	[m^3/kg]	[-]
0-50	33	1.54±0.08	13.9±1.3	10.750					34	0.977±0.097	4.39±0.94	81.571				
0-100	65	1.83±0.05	19.1±1.0	15.660	65	1.74±0.04	11.8±0.6	15.571	68	1.42±0.09	9.58±1.09	64.665	68	2.27±0.17	19.6±2.9	120.00
0-200	130	2.30±0.05	30.0±1.3	26.782					137	1.88±0.05	16.7±1.0	43.535				
0-300	198	2.45±0.03	34.3±1.0	22.026	198	2.26±0.03	21.1±0.8	29.049	201	2.09±0.04	21.3±1.0	41.149	201	2.07±0.06	16.4±1.4	128.00
0-405									266	2.20±0.04	24.2±1.0	43.184				
0-441	291	2.52±0.03	36.5±0.8	17.962												
0-500					331	2.43±0.03	24.9±0.7	25.666					281	2.22±0.05	18.7±1.3	109.85
0-700					389	2.48±0.03	26.2±0.7	26.516					309	2.24±0.05	19.2±1.3	102.51
0-834													328	2.26±0.05	19.4±1.3	98.234
0-994					430	2.50±0.03	27.0±0.8	28.817								

Table 3.2.4.2.-1: The extracted best-fit values for the effective diffusion coefficient D_e and the volume-based linear sorption equilibrium distribution coefficient K_d together with their one-standard deviation errors and the minimum values for the reduced χ^2_v for nickel through-diffusion (experiments no. 5 - 8). For the adjustment N data triplets were used measured in the time interval Δt.

3.2.4.3. Non-linear Freundlich sorption case

For all four nickel experiments additional fits were carried out using only data from the first 50, 100, 200, ... etc. days to test the predictive quality of the model. In order to ensure that a global χ^2-minimum was located, we repeated the calculations up to 10 - 140 times with different sets of starting values for the fit-parameters.

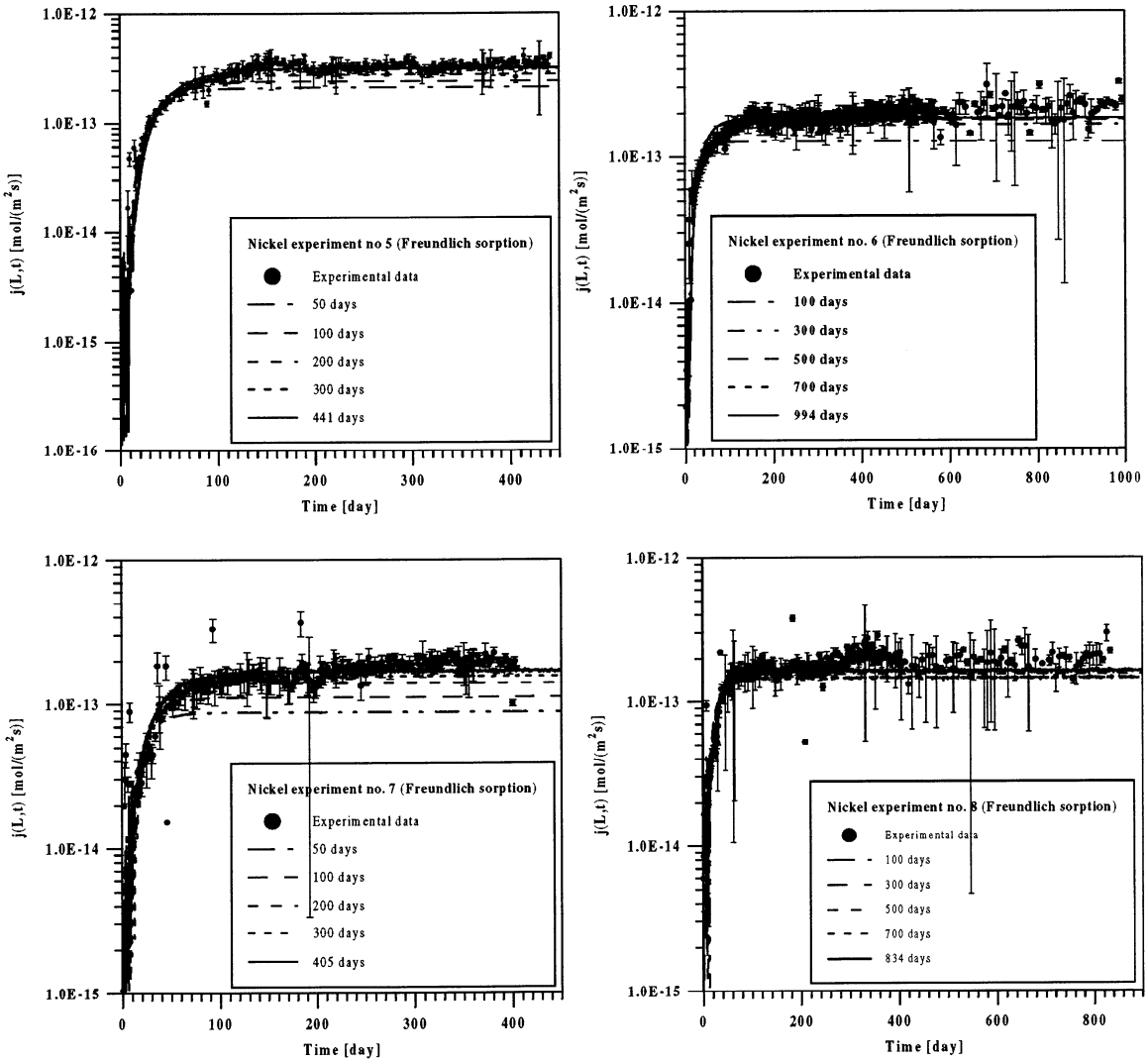

Figure 3.2.4.3.-1: Comparative plots of the experimental data and theoretical breakthrough curves for the diffusive nickel flux and experiments no. 5 - 8 when assuming non-linear (Freundlich) sorption. Shown are the best-fit curves using experimental data from the first 50, 100, etc. days as indicated in the legends.

The reproduction of the breakthrough curves in general is quite satisfactory if one neglects the first attempts where only a part of the available data were used for the adjustments. After about roughly 200 days the changes in the modelled breakthrough curves are negligible in the plots but not in the numerical values for the fit-parameters. There, the values for, e.g., the Freundlich coefficient may change significantly. When comparing the graphical representations of the calculations with those from the former exercise one can hardly see an improvement. Although a third freely adjustable parameter (the Freundlich exponent) is now available the calculated breakthrough curves are not better. Lack of agreement at the rising

edge where the modelled flux is - as a rule - too small and the lack of a slightly increased diffusive flux lead to the conclusion that this model, too, is not capable of describing successfully the nickel through-diffusion experiments. All four modelling tasks yield values for the Freundlich exponent which is larger than unity with small standard deviations (N_p = 1.05 - 1.14, with 1σ uncertainty in the last digit). Similar results were already obtained from modelling other experiments and were interpreted as indications of a possible tracer precipitation in the HCP.

For experiments no. 5 and 6 the values for the Freundlich coefficient are asymptotically of the order (40 - 60) $\cdot$ 10^{-3} $\text{mole}^{1-N_p}\,\text{m}^{3N_p}\,\text{kg}^{-1}$. Together with the values for the exponent which is, as already mentioned, somewhat larger than unity, we expect a slightly increased tracer deposition when compared to the model where only linear sorption was included.

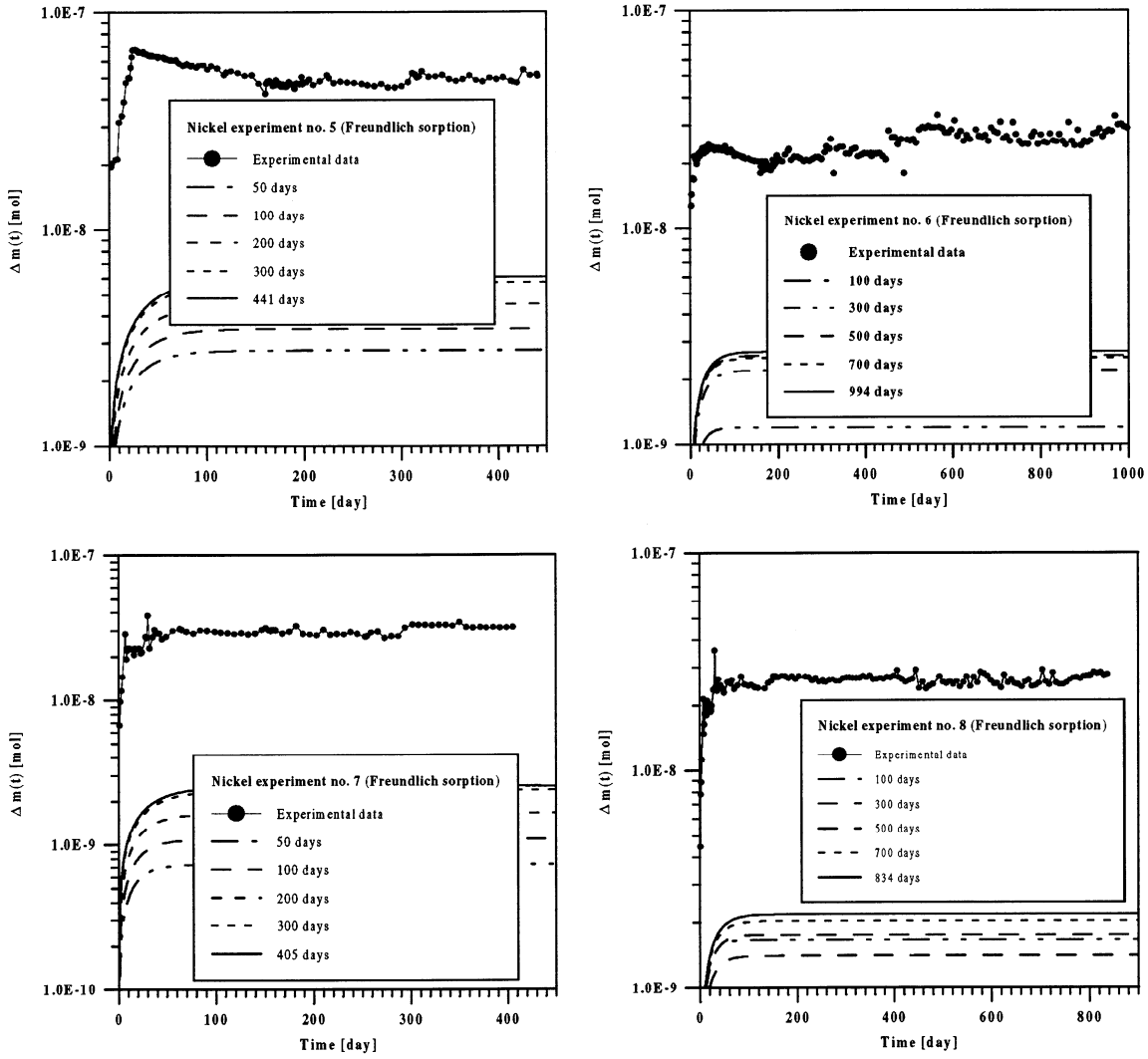

Figure 3.2.4.3.-2: Comparative plots of the experimental data for tracer deposition in the HCP and theoretical curves for all four nickel experiments. The calculations are based on the best-fit parameter values from modelling the diffusive flux across the down-stream boundary assuming non-linear (Freundlich) sorption and using experimental data from the first 50, 100, etc. days as indicated in the legends.

For experiment no. 7 and 8 the best-fit values for K_p are, once more, larger by a factor of two; hence, they are about (90 - 105) $\cdot$ 10^{-3} $mole^{1-N_p} m^{3N_p} kg^{-1}$ with values for the exponent of N_p = 1.14. As can be seen in the figure above, there is - indeed - a slightly increased tracer deposition compared to the corresponding calculations made using a linear sorption diffusion model. However, the general problem of a significant underestimation of the nickel up-take by the HCP remains the same.
The conclusion that the model is incorrect is supported by the following considerations: Interpretation of the correlation matrix also gives a contradictory picture. From the formalism, anti-correlations between the two Freundlich parameters are expected; an increased value for K_p should be accompanied by a reduced value for the exponent N_p, and both parameters should be correlated to D_e. But the correlations do not follow this scheme. For all four experiments anti-correlations between D_e and K_p were often obtained. Simultaneously, slightly weaker anti-correlations between D_e and N_p and correlations between K_p and N_p could be observed. These facts are considered a further indication that this model, too, has the wrong mathematical structure meaning that the wrong physical process for retardation (instantaneous equilibrium non-linear sorption) is considered.

Reasonable conclusions based on these modelling results of experiments no. 5 - 8 are the following:

- The transient part of the diffusion curve is only roughly reproduced, and there are only minor improvements in this part of the breakthrough curve and when compared to the linear sorption case.
- The extracted best-fit values for the Freundlich isotherm for experiments no. 7 and 8 show a trend toward relatively high values.
  For all experiments the coefficient varies within a factor of two, but the exponent is always between 1.05 and 1.14; hence, it is unphysically large and violates basic assumptions of the Freundlich isotherm formalism.
- The fit-parameters often show correlations/anti-correlations which do not correspond with the procedure's underlying formalism. This is considered as a further indication of an inappropriate model structure.
- The modelled nickel deposition in the HCP is too low by factors thereby clearly demonstrating fundamental deficiencies of the concept.
- Hence, even with a third freely adjustable parameter is available, this extended model cannot resolve the discrepancy between the measured K_d-values obtained from independent batch sorption and diffusion experiments; while simultaneously having reasonable physical values for the sorption isotherm parameters and correctly accounting for the tracer deposition in the cementitious material.
- Ultimately, this model, too, fails due to its inability to reproduce all the observations with reasonable accuracy.

	Experiment no. 5					Experiment no. 6					Experiment no. 7					Experiment no. 8				
Δt	N	$D_e \cdot 10^{11}$	$K_p \cdot 10^3$	N_p	χ^2_v	N	$D_e \cdot 10^{11}$	$K_p \cdot 10^3$	N_p	χ^2_v	N	$D_e \cdot 10^{11}$	$K_p \cdot 10^3$	N_p	χ^2_v	N	$D_e \cdot 10^{11}$	$K_p \cdot 10^3$	N_p	χ^2_v
[day]	[-]	[m^2/s]	[*]	[-]	[-]	[-]	[m^2/s]	[*]	[-]	[-]	[-]	[m^2/s]	[*]	[-]	[-]	[-]	[m^2/s]	[*]	[-]	[-]
0-50	33	1.62±0.01	36.9±0.1	1.08±0.01	9.2051						34	1.13±0.01	16.9±0.1	1.09±0.01	70.566					
0-100	65	1.86±0.01	32.9±0.1	1.05±0.01	13.137	65	1.72±0.01	22.7±0.1	1.06±0.01	13.254	68	1.44±0.01	21.5±0.1	1.07±0.01	51.008	68	2.70±0.01	50.0±0.1	1.10±0.01	48.436
0-200	130	2.14±0.01	45.9±0.1	1.05±0.01	24.420						137	1.79±0.01	34.0±0.1	1.07±0.01	29.389					
0-300	198	2.41±0.01	61.7±0.2	1.06±0.01	17.626	198	2.26±0.01	40.5±0.2	1.05±0.01	25.276	201	2.02±0.01	62.6±0.1	1.09±0.01	25.613	201	1.92±0.01	61.1±0.1	1.14±0.01	109.61
0-405											266	2.12±0.01	105±1	1.14±0.01	29.207					
0-441	291	2.45±0.01	59.4±0.1	1.05±0.01	14.963															
0-500						331	2.41±0.01	48.4±0.1	1.06±0.01	22.049						281	2.24±0.01	43.3±0.1	1.08±0.01	95.911
0-700						389	2.45±0.01	47.3±0.2	1.06±0.01	23.743						309	2.32±0.01	97.6±0.1	1.14±0.01	85.417
0-834																328	2.26±0.01	92.1±0.1	1.13±0.01	83.530
0-994						430	2.48±0.01	55.8±0.1	1.06±0.01	25.187										

Table 3.2.4.3.-1: The extracted best-fit values for the effective diffusion coefficient D_e and the two Freundlich isotherm parameters K_p [*] = [$mol^{1-N_p} m^{3N_p} kg^{-1}$] and N_p together with their one-standard deviation errors and the minimum values for the reduced χ^2_v for nickel through-diffusion (experiments no. 5 - 8). For the adjustment N data triplets were used measured in the time interval Δt.

3.2.4.4. First-order sorption kinetics case - linear/linear case

As a further step we investigated the effect of first-order sorption kinetics according to equation (3.1.3) on the diffusion-sorption profile. In our concept sorption may be - in principle - non-linear and desorption linear; however, to avoid a further free fit-parameter and taking into consideration the results from the previous calculations assuming non-linear Freundlich sorption, we - first - fixed the Freundlich exponent to unity. The fit-parameters were now the effective diffusion coefficient D_e, the rate for sorption k_s [s^{-1}], and the rate for desorption k_r [s^{-1}]. In a series of subsequent fits data from the first 50, 100, ... etc. days were used.

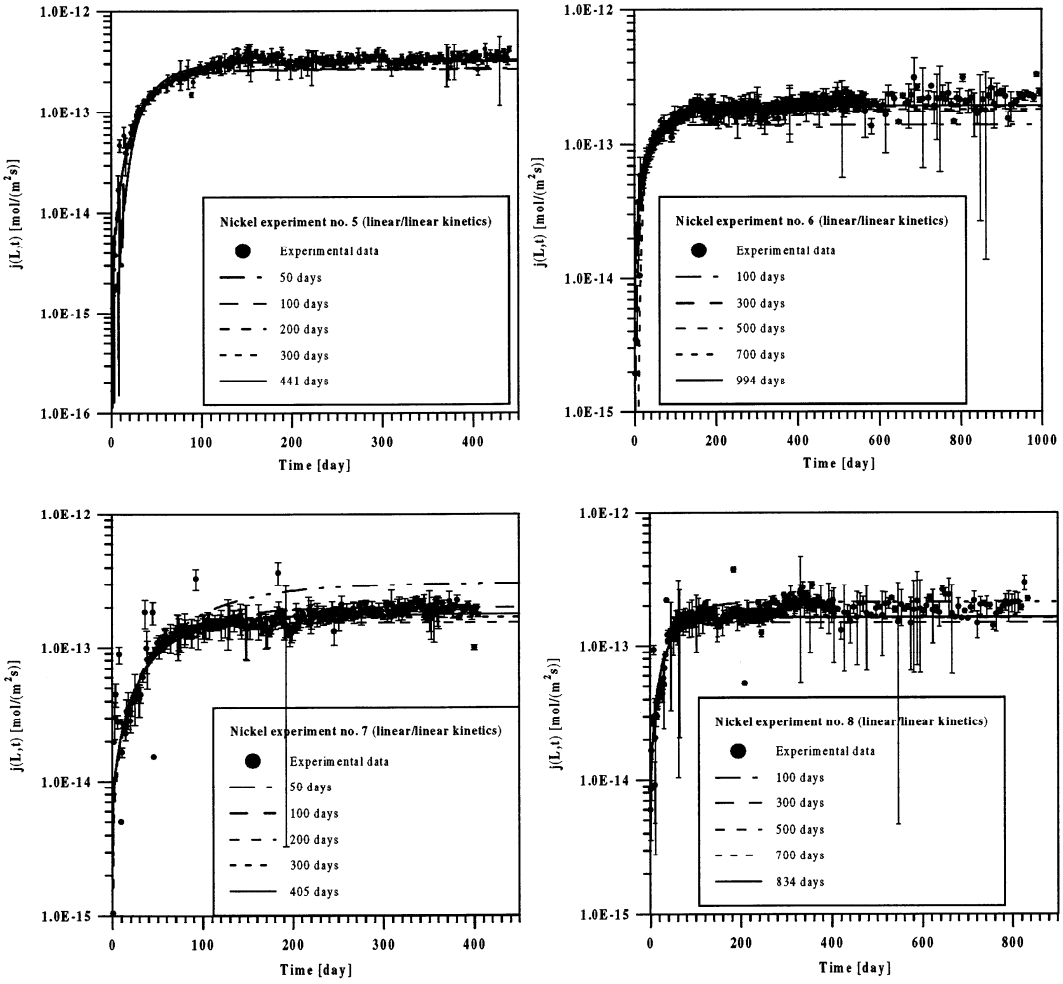

Figure 3.2.4.4.-1: Comparative plot of the experimental data and theoretical breakthrough curves for the diffusive nickel flux and experiments no. 5 - 8 when assuming first-order sorption kinetics. Shown are the best-fit curves using experimental data from the first 50, 100, etc. days as indicated in the legends.

Inspecting the transient part of the diffusion curve, we can recognise a better representation of the measurements by this model than by a model with a linear or non-linear sorption isotherm. As in the previous case (Freundlich sorption case) the parameters show similar, but not understandable, correlations or anti-correlations. As a rule they become smaller when using more and more data for the fit-procedure and are asymptotic to values from 0.62 (for experiment no. 6) to 0.93 (for experiment no. 5).

In the near steady-state, where $\frac{dS}{dt} = 0$, we can calculate the equilibrium sorption distribution coefficient K_d according to equation (3.2.4): In the table below we have compiled these K_d-values together with their standard errors for all four experiments. (For illustration purposes only we have computed K_d-values even when the system clearly was not in a steady-state.) The size of the standard errors is dominated mainly by the uncertainty in the porosity which was assumed to be 0.63 ± 0.05.

	Experiment no. 5		Experiment no. 6		Experiment no. 7		Experiment no. 8	
Δt	# of data	$(K_d \pm \Delta K_d) \cdot 10^3$	# of data	$(K_d \pm \Delta K_d) \cdot 10^3$	# of data	$(K_d \pm \Delta K_d) \cdot 10^3$	# of data	$(K_d \pm \Delta K_d) \cdot 10^3$
[day]	[-]	[m^3/kg]	[-]	[m^3/kg]	[-]	[m^3/kg]	[-]	[m^3/kg]
0 - 50	33	26.2 ± 3.0			34	110 ± 72		
0 - 100	65	25.6 ± 2.3	65	14.9 ± 1.4	68	46.7 ± 7.4	68	43.0 ± 12.9
0 - 200	130	41.4 ± 4.0			137	25.4 ± 2.6		
0 - 300	198	42.0 ± 4.1	198	26.5 ± 2.4	201	33.2 ± 4.2	201	18.2 ± 2.6
0 - 405					266	38.4± 3.4		
0 - 441	291	42.8 ± 4.9						
0 - 500			331	32.7 ± 2.8			281	22.6 ± 2.4
0 - 700			389	33.8 ± 2.7			309	23.7 ± 3.3
0 - 834							324	23.8 ± 3.5
0 - 994			430	33.7 ± 3.1				

Table 3.2.4.4.-1: The computed K_d-values with 1σ-standard errors according to equation (3.2.4) using measured data in the time interval Δt for the fitting procedure when using first-order sorption kinetics. The values in the shaded area are given just for comparison purposes; there the diffusion process in the model is still evolving rapidly and the diffusive flux has certainly not reached a (near) steady-state.

The best-fit values for D_e are finally $(2.3 - 2.6) \cdot 10^{-11}$ m^2/s and therefore are very similar to those obtained from the previous modelling concepts using linear or non-linear sorption isotherms. Experiment no. 5 - 7 yield asymptotic K_d-values of only (34 - 43) · 10^{-3} m^3/kg, whereas for experiment no. 8 a K_d-value of only 24 · 10^{-3} m^3/kg was obtained. We do not have a reasonable explanation for such a low value for this experiment. As stated earlier, there are no other data known concerning values for the effective diffusion coefficient and sorption parameters for nickel - except from [17]. These batch experiments for nickel yield values for K_d of the order of 220 · 10^{-3} m^3/kg which are roughly by a factor of five to nine larger. Therefore we conclude that this concept also fails to resolve the obvious discrepancies in these different K_d-values.

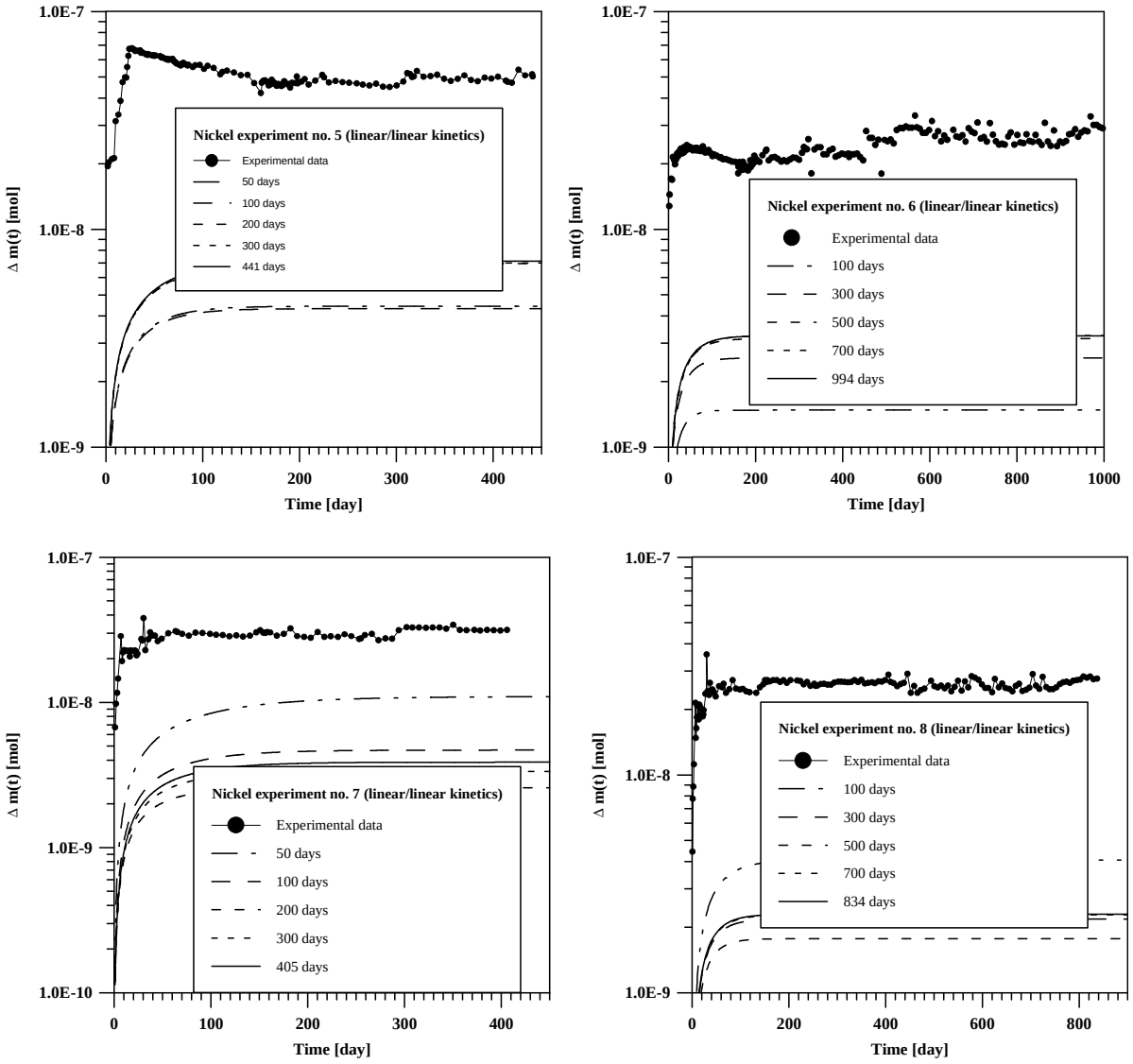

Figure 3.2.4.4.-2: Comparative plots of the experimental data for nickel deposition in the HCP and theoretical curves for all four experiments. The calculations are based on the best-fit parameter values from modelling the diffusive flux across the down-stream boundary assuming first-order sorption kinetics and using experimental data from the first 50, 100, etc. days as indicated in the legends.

For comparison purposes we have compiled, in table 3.2.4.4.-2, all best-fit parameter values together with their standard deviations and the minimum value for the χ^2-merit function. From the results from inverse modelling of the four nickel through-diffusion profiles no. 5 - 8 we conclude:

- The transient phase is now much better reproduced than when using alternative models. The overall quality of the fits is quite good, and the values for the effective diffusion coefficient are close to those obtained from former concepts. The rates for sorption and desorption cannot be discussed because there are no measurements known.

- In the near steady-state values for K_d can be calculated from the rates for sorption and desorption which are about 25% higher than those obtained with the help of the former diffusion/linear sorption model. Hence, also the amount of up-taken nickel in the HCP is larger by this factor but is still significantly too small to reproduce the measured nickel deposition curves.
- The fit-procedure very often yielded illogical correlations between two of the three parameters.
- Taking all together we must conclude that this model, too, is not capable of correctly reproducing and predicting nickel through-diffusion, of nickel deposition in the cementitious material nor is it capable of determining values for the fit-parameters which are consistent with those obtained from batch sorption experiments.

	Experiment no. 5					Experiment no. 6					Experiment no. 7					Experiment no. 8				
Δt	N	$D_e \cdot 10^{11}$	$k_s \cdot 10^4$	$k_r \cdot 10^6$	χ^2_v	N	$D_e \cdot 10^{11}$	$k_s \cdot 10^4$	$k_r \cdot 10^6$	χ^2_v	N	$D_e \cdot 10^{11}$	$k_s \cdot 10^4$	$k_r \cdot 10^6$	χ^2_v	N	$D_e \cdot 10^{11}$	$k_s \cdot 10^4$	$k_r \cdot 10^6$	χ^2_v
[day]	[-]	[m^2/s]	[s^{-1}]	[s^{-1}]	[-]	[-]	[m^2/s]	[s^{-1}]	[s^{-1}]	[-]	[-]	[m^2/s]	[s^{-1}]	[s^{-1}]	[-]	[-]	[m^2/s]	[s^{-1}]	[s^{-1}]	[-]
0-50	33	2.07±0.10	0.996±0.047	3.08±0.19	8.9435						34	3.99±1.60	0.956±0.598	0.703±0.104	25.673					
0-100	65	2.04±0.05	0.975±0.027	3.09±0.08	11.778	65	1.89±0.03	0.673±0.014	3.66±0.14	8.6188	68	2.59±0.12	0.555±0.026	0.963±0.121	16.512	68	2.94±0.56	0.567±0.103	1.07±0.24	48.419
0-200	130	2.55±0.05	1.02±0.05	2.00±0.04	12.611						137	2.00±0.04	0.467±0.015	1.49±0.07	12.705					
0-300	198	2.56±0.03	1.02±0.03	1.97±0.09	10.008	198	2.37±0.03	0.905±0.028	2.77±0.07	15.000	201	2.19±0.03	0.446±0.023	1.09±0.09	12.600	201	2.06±0.06	0.363±0.014	1.62±0.17	109.38
0-405											266	2.31±0.03	0.441±0.009	0.931±0.021	17.847					
0-441	291	2.57±0.02	1.03±0.05	1.95±0.12	8.8342															
0-500						331	2.52±0.02	0.887±0.013	2.20±0.04	12.623						281	2.24±0.05	0.391±0.017	1.40±0.07	95.310
0-700						389	2.56±0.02	0.567±0.019	1.36±0.02	11.398						309	2.26±0.05	0.380±0.028	1.30±0.11	89.052
0-834																328	2.27±0.05	0.396±0.021	1.35±0.15	85.394
0-994						430	2.57±0.02	0.732±0.025	1.76±0.04	15.898										

Table 3.2.4.4.-2: The extracted best-fit values for the effective diffusion coefficient D_e and the rates for sorption k_s and desorption k_r together with their one-standard deviation errors and the minimum values for the reduced χ^2_v for nickel through-diffusion (experiments no. 5 - 8). For the adjustment N data triplets were used measured in the time interval Δt.

3.2.4.5. First-order sorption kinetics - non-linear/linear case

Finally, as a learning exercise and for completeness, we investigated the effect of first-order sorption kinetics according to equation (3.1.3) where the forward reaction is non-linear according to the Freundlich isotherm and the desorption reaction is linear. The fit-parameters were the effective diffusion coefficient D_e, the rate for sorption k_s [$\text{mole}^{1-N_s}\text{m}^{3\,N_s}\text{kg}^{-1}$], the Freundlich exponent N_s [-], and the rate for desorption k_r [s^{-1}]. Again, in a series of subsequent fits, data from the first 50, 100, ... etc. days were used for the fit-procedure.

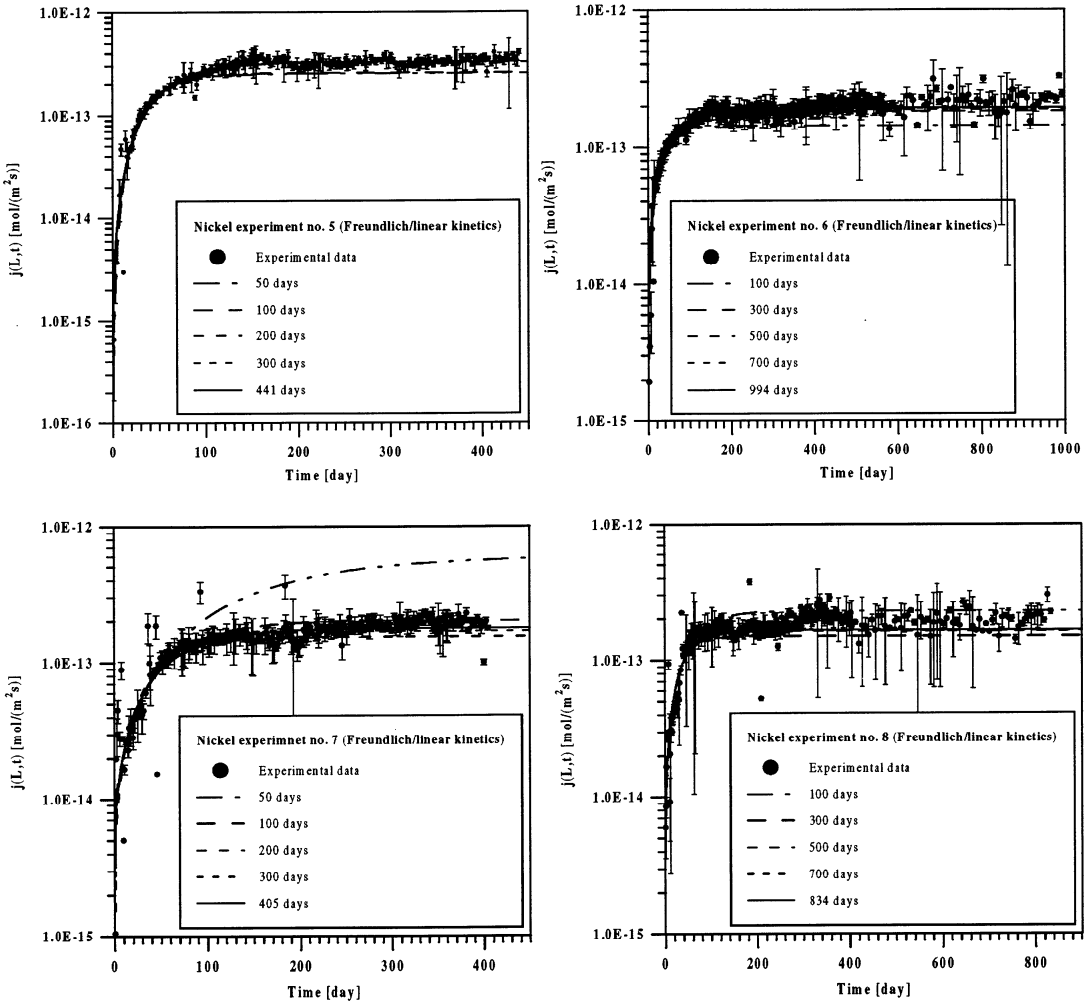

Figure 3.2.4.5.-1: Comparative plot of the experimental data and theoretical breakthrough curves for the diffusive nickel flux and experiments no. 5 - 8 when assuming first-order non-linear sorption kinetics. Shown are the best-fit curves using experimental data from the first 50, 100, etc. days as indicated in the legends.

Although a fourth fit-parameter could also be adjusted, the increase in the quality of the fits is negligible. The values for D_e are of the order of $(2.3-2.6)\cdot 10^{-11}\ \text{m}^2/\text{s}$ and coincide with those from the former concept.

This alternative model too, is not able to account correctly for an increased tracer deposition in the cement. This can be seen with the help of the following figure where the deposited tracer mass versus time for all four experiments is plotted. In general the deposited tracer mass

is at least by a factor too small. Hence, although once more, fairly good reproductions of the breakthrough curves are obtained, the tracer deposition in the cement is modelled incorrectly.

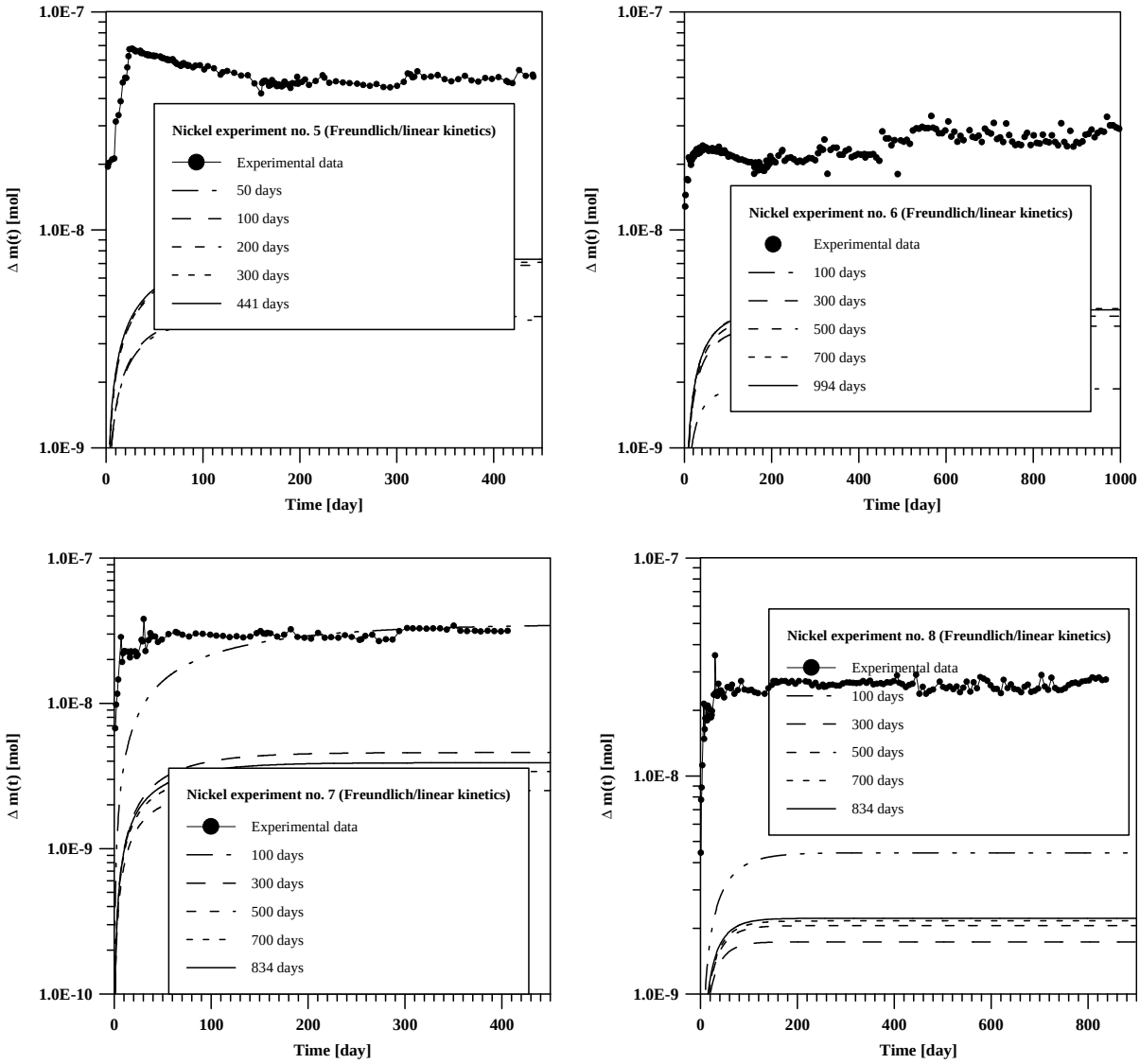

Figure 3.2.4.5.-2: Comparative plots of the experimental data for nickel deposition in the HCP and theoretical curves for all four experiments. The calculations are based on the best-fit parameter values from modelling the diffusive flux across the down-stream boundary assuming first-order non-linear sorption kinetics and using experimental data from the first 50, 100, etc. days as indicated in the legends.

On the next page, all best-fit parameter values together with their standard deviations and the minimum value for the reduced χ^2_ν-merit function are compiled.

	Experiment no. 5						Experiment no. 6					
Δt	N	$D_e \cdot 10^{11}$	$k_s \cdot 10^4$	N_s	$k_r \cdot 10^6$	χ^2_ν	N	$D_e \cdot 10^{11}$	$k_s \cdot 10^4$	N_s	$k_r \cdot 10^6$	χ^2_ν
[day]	[-]	[m^2/s]	[*]	[-]	[s^{-1}]	[-]	[-]	[m^2/s]	[*]	[-]	[s^{-1}]	[-]
0-50	33	1.96±0.12	0.495±0.039	0.944±0.020	3.13±0.22	8.7056						
0-100	65	2.00±0.06	0.500±0.071	0.946±0.018	2.98±0.26	11.714	65	1.96±0.07	3.52±0.21	1.17±0.02	2.42±0.07	5.8591
0-200	130	2.53±0.05	1.19±0.18	1.01±0.02	2.14±0.15	12.686						
0-300	198	2.56±0.03	1.06±0.20	1.01±0.02	1.90±0.20	10.097	198	2.50±0.03	4.25±0.14	1.19±0.01	1.25±0.12	7.5105
0-405												
0-441	291	2.57±0.02	2.22±0.13	1.06±0.01	2.30±0.08	8.7759						
0-500							331	2.59±0.02	2.71±0.72	1.15±0.03	1.00±0.03	7.0747
0-700							389	2.62±0.02	6.15±0.09	1.22±0.01	1.04±0.08	9.1278
0-834												
0-994							430	2.64±0.02	4.11±0.19	1.18±0.01	1.04±0.06	12.260

	Experiment no. 7						Experiment no. 8					
Δt	N	$D_e \cdot 10^{11}$	$k_s \cdot 10^4$	N_s	$k_r \cdot 10^6$	χ^2_ν	N	$D_e \cdot 10^{11}$	$k_s \cdot 10^4$	N_s	$k_r \cdot 10^6$	χ^2_ν
[day]	[-]	[m^2/s]	[*]	[-]	[s^{-1}]	[-]	[-]	[m^2/s]	[*]	[-]	[s^{-1}]	[-]
0-50	34	7.86±0.58	0.775±0.135	0.920±0.008	0.416±0.050	24.082						
0-100	68	2.62±0.11	0.090±0.004	0.862±0.005	0.701±0.028	16.613	68	3.14±0.39	0.072±0.017	0.840±0.013	0.701±0.121	48.113
0-200	137	2.00±0.09	0.185±0.021	0.933±0.010	1.25±0.14	12.722						
0-300	201	2.21±0.03	0.615±0.030	1.02±0.01	1.18±0.09	12.632	201	2.06±0.08	0.098±0.010	0.900±0.014	1.31±0.15	109.69
0-405	266	2.30±0.03	0.726±0.058	1.04±0.01	1.03±0.05	17.888						
0-441												
0-500							281	2.23±0.07	0.054±0.008	0.848±0.017	1.05±0.13	95.468
0-700							309	2.26±0.05	0.054±0.004	0.849±0.014	0.991±0.145	89.152
0-834							328	2.28±0.05	0.148±0.027	0.926±0.018	1.16±0.13	85.598
0-994												

Table 3.2.4.5.-1: Results from modelling all four nickel through-diffusion experiments using a diffusion/first-order non-linear sorption kinetics model. The fit-parameters of the model are the effective diffusion coefficient D_e, the rate coefficient k_s [*] = [$mol^{1-N_s} m^{3N_s} kg^{-1}$], and the exponent N_s for sorption as well as the rate k_r for desorption. Compiled are the best-fit values together with their one-standard deviation errors and the minimum values for the reduced χ^2_ν. For the adjustment N data triplets were used measured in the time interval Δt.

3.2.4.6. Conclusions for nickel

1. From modelling all four nickel through-diffusion profiles using a concept neglecting such retarding mechanisms as e.g. sorption we conclude:
   - To obtain an acceptable fit of the measured flux data only it is clearly necessary to include a further transport mechanism which accounts for nickel-retardation in the diffusion curve.
2. From modelling including linear sorption we conclude:
   - The transient phase of all four experiments (experiments no. 5 - 8) is only roughly reproduced by the concept, because the diffusive flux is underestimated significantly. However, the transient phase of the diffusion curve is especially influenced by retarding mechanism, and the simple linear sorption isotherm obviously does not sufficiently cover all the mechanisms involved in the nickel diffusion.
   - For experiment no. 5 attainment of a steady-state phase is suggested by the model, in good agreement with the experimental data. A corresponding conclusion could be drawn from the modelling of experiment no. 6, but there a continuous flux increase can be seen in the measurements. For experiments no. 7 and 8 the model implies that these systems have never reached a steady-state phase during the whole observation period of one year; consistent with the data.
   - The best-estimate values for the two fit-parameters are for the effective diffusion constant D_e in the range of $(2.2-2.5)\cdot 10^{-11}$ m^2 / s, and for K_d in the interval of $(19-37)\cdot 10^{-3}$ m^3 / kg. Such values for D_e seem reasonable and are comparable to literature data. But those for K_d are roughly an order of magnitude too small when compared to values obtained in batch-sorption experiments.
   - From this fundamental lack of agreement between theory and measurements, we conclude that this concept (linear sorption case) is not appropriate to describe the nickel diffusion profiles.
3. Including non-linear Freundlich sorption did not improve the quality of the fits, although the minimum values for the χ^2-merit function were slightly better than those from the former linear sorption model. But this is considered to be an effect of the third freely adjustable parameter only.
   - No significant improvement in matching the transient phases of the break-through curves could be achieved.
   - The values for the Freundlich exponent are in all cases larger than unity violating fundamental assumptions of a non-linear exchange formalism; hence, they are unphysical in the frame of the concept.

- In addition, the parameters very often show illogical correlations to each other, a further indication that the mathematical description of the diffusion process is not adequate. This concept therefore has no special advantage over the linear sorption model, and the empirical principle of parsimony ("every theoretical element has to express an empirical phenomenon") obliges us to also discard the underlying ideas of this concept.

4. From an extended model including first-order sorption kinetics we conclude:
   - The concept allows a fairly good representation of the transient phase of the breakthrough curve, and the best-estimates for $D_e = (2.3\text{-}2.6)\cdot 10^{-11}$ m^2/s are the same as those from former exercises. However, the extracted K_d-values are (24-43) $\cdot$ 10^{-3} m^3/kg, roughly an order of magnitude smaller than values from batch experiments.
   - As in the Freundlich isotherm case, illogical parameter correlations were obtained which are considered an indication of an inadequate model structure.
   - Therefore, we conclude that this concept also fails to successfully model the nickel-diffusion measurements. The model describes the diffusion profile very well but leads to K_d-values entirely incompatible with the batch-sorption measurements. It is a nice example where the theory matches the breakthrough data satisfactorily but, when additional information from other independent experiments is considered, incompatibilities between the models and the experimental data are clearly demonstrated.

5. Finally we tried to model the measurements using a first-order sorption kinetics model where the forward reaction is non-linear according to the Freundlich isotherm and the backward reaction is linear.
   - From a numerical point of view these gave the best fits of the breakthrough curves but resulted partially in unphysically high values for the Freundlich exponent or in illogical correlations between the fit-parameters. As in all former cases, nickel deposition, was too small by factors when compared with measurements.
   - Therefore, this model, too, obviously fails to adequately describe the diffusion of nickel through cementitious material.

In summary, it is certain that none of the five different concepts is able to describe the relevant transport mechanisms consistently with regard to all available observations and to measurements from independent experiments.

At this point the question arises of whether our basic assumptions are in principle wrong or whether any of them have to be modified to arrive at a model which is able to explain the obvious deficiencies of the present concepts. Let us remember the basis of our models:

- We assumed for the modelling that an REV does exist. Because we are not interested in the microscopic distribution of the tracer, we average relevant quantities over the size of the REV to arrive at a macroscopic (averaged) transport equation.

- The porous medium was considered as macroscopically uniform (homogeneous) and isotropic so that a 1D-diffusion model would be appropriate with a transport coefficient which is constant in time and space.
- For the diffusion equation we specified a suitable initial (3.1.10) as well as two boundary conditions according to expressions (3.1.11) and (3.1.12).
- As the only retardation mechanism we assumed was sorption onto pore surfaces which we described by a (non-)linear, reversible, instantaneous equilibrium, isotherm formalism, or by a first-order kinetics equation.

With respect to the REV: We are not able to describe nickel diffusion in detail, on a molecular level, either due to the lack of knowledge of the geometrical aspects or due to the impossibility of writing an exact mathematical description of all relevant physical/chemical processes between the solid phase and the diffusing nickel species. Therefore, we still assume the existence of an REV and also that the averaging procedure may be appropriate; otherwise we could stop the modelling here.

A medium is called homogeneous with respect to a certain property, if that property is independent of the location within the medium; it is called isotropic, if that property is independent of the direction within the medium.
On a macroscopic scale the samples are considered to be homogeneous, because a detailed inspection [22] shows no micro-fractures or fissures. The grain size is commonly much smaller than 50 μm and there are only a few macro-pores with a size larger than 20 μm; micro-pores seem to be uniformly distributed. However, a few places can be recognised where portlandite precipitation occurred, and these often show stream-flow like patterns. A few cement lenses with diameters up to 50 - 100 μm are uniformly distributed. This analysis considers both disturbances as having no essential influence on homogeneity of macroscopic properties such as porosity, capillarity and the degree of hydratation.
Inhomogeneities could be taken into account in the models by spatial-dependent transport parameters. However, due to the lack of detailed physical data, the enlarged numbers of fit-parameters and, hence, due to tremendously increased numerical problems, such a procedure is not feasible.
There is no information on which to judge the degree of isotropy of the samples. Only with the help of additional experiments which would specifically investigate the tensor characteristics of D_e could further information on possible anisotropy of the samples be obtained. Such observations would consist of subsequent measurements of the particle flux diffused by targets sliced at different angles from the cylindrical cementitious samples. However, to get an appropriate answer to such a question is not our primarily aim and cannot be investigated easily with the present equipment.
Lastly, we consider all the samples as macroscopic, i.e. on a scale larger than 50 μm homogeneous and isotropic, keeping in mind that, maybe, these assumptions might be wrong.

Let us now discuss the initial and boundary conditions used for the modelling. As an initial condition it was assumed that the sample was free of tracer; this assumption cannot be tested, because no nickel compounds were used for the production of the HCP's. According to equation (3.1.14) the diffusive flux across the boundary at the low-concentration side is proportional to C_0, hence, possible fluctuations in the flux are directly proportional to fluctuations in C_0. Such fluctuations in C_0 are reported to be less than $\pm$ 10 %. Fluctuations at the low-concentration side were always less than $2 \cdot 10^{-6}$ mol / m^3 or less than 3 - 5 % of the tracer concentration at the

reservoir side. With such values these fluctuations are much smaller than those at the other boundary and are considered - for the modelling - to be negligibly small. From these considerations we conclude that the failures of the different modelling concepts are not due to inappropriate initial and boundary conditions.

We considered sorption the only retarding mechanism. Starting with the most simple linear sorption isotherm with instantaneous equilibrium we proceeded to the more complex non-linear (Freundlich) sorption. In a further step we investigated the influence of first-order sorption kinetics on tracer breakthrough. In principle, we have accounted for the most obvious sorption ansatzes. Of course, we could introduce more complex sorption formalisms such as a two-site (Langmuir) sorption isotherm, or we could investigate the effect of precipitation and dissolution with the help of - say - a net sink/source term in the formalism. However, there is no experimental evidence of such processes, and also the corresponding parameter values are absent. Generally, more complex concepts for the retarding mechanisms would - in our opinion - inadmissibly increase the numbers of fit-parameters with all the numerical consequences already mentioned.

To obtain further information about homogeneity and the sorption mechanisms involved without destroying the sample we could change the boundary condition at the high-concentration side. If the reservoir solution is “instantaneously” replaced by cement pore water, as is already present on the measurement side, we would begin the out-diffusion of the tracer accumulated within the sample. With such a procedure we test the assumption of a linear concentration profile across the sample according to equation (3.2.1) which is based on the idea that the internal pore structure as well as sorption properties are homogeneous. Using the best-fit values of D_e and K_d from modelling diffusion to predict of how the out-diffusion system evolves we could further check, with the help of a simple mass balance, whether the selective up-take is equal to the release of nickel.

3.3. The governing equations for the out-diffusion - linear sorption case

Migration of radionuclides out of a hardened cement paste saturated with pore water is assumed to be dominated only by molecular diffusion due to the low permeability and the absence of fractures. Radionuclides inside the HCP are transferred by molecular diffusion through interstitial water to the surface of the paste and then released to the water on the reservoir sides. We assume that the out-diffusion experiments - like the diffusion experiments - may be well described by a one-dimensional single porosity medium model; hence, we assume that the diffusion coefficient is constant in space and time and is - for simplicity's sake - independent of the tracer concentration. Therefore we conclude that the flux of a tracer out of a porous medium is dependent on the following mechanisms:

- molecular diffusion in the aqueous phase and
- sorption processes on the solid phase surfaces, such as ion exchange, physical and chemical adsorption, filtration, precipitation, etc.;

and on the geometrical aspects such as:

- the pore constrictivity and
- the tortuosity of the hardened cement paste.

The flux $\vec{j}$ [mol m^{-2} s^{-1}] at the interface at $x = 0, L$ is described by Fick's first law:

$$\vec{j} = -D_e \cdot \vec{\nabla} C = -D_e \left. \frac{\partial C}{\partial x} \right|_{x=0,L} \quad , \tag{3.3.1}$$

where $\vec{\nabla} C$ is the concentration gradient. D_e is, in general, a second-rank tensor for the effective diffusion in a porous medium and includes the effects of tortuosity and constrictivity. In the case of an isotropic porous medium the tensor is reduced to a scalar. If the through-diffusion process is in steady-state - meaning constant flux in time across the boundary at the low-concentration side - and if we assume a homogeneous sample, then the concentration gradient within the HCP should be a linear function of space:

$$C(x) = C_0 \left(1 - \frac{x}{L}\right) \text{ with } \frac{\partial C}{\partial x} = -\frac{C_0}{L} \; ; \tag{3.3.2}$$

hence, the steady-state flux j_L is given by

$$j_L = D_e \frac{C_0}{L} \quad . \tag{3.3.3}$$

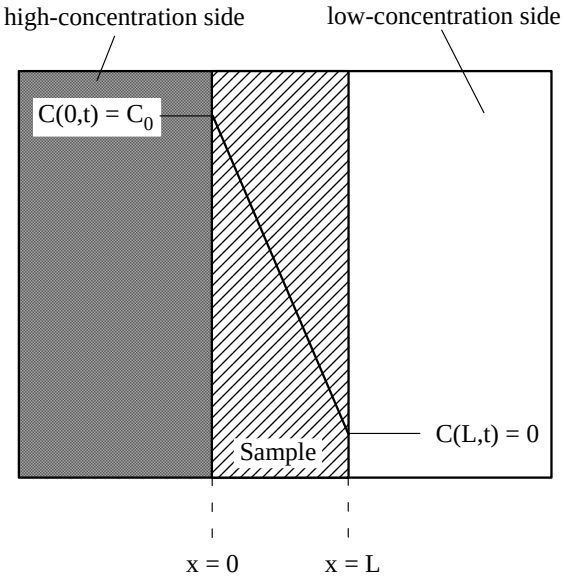

Figure 3.3.-1: Sketch of a cross-section through the diffusion cell and the HCP-diffusion barrier. The solid line across the sample represents the linear tracer concentration profile according to equation (3.3.2) after reaching the steady-state.

To model the out-diffusion with an initial tracer distribution according to equation (3.3.2), the initial tracer concentration C_0 of the high-concentration side has to be replaced "instantaneously" by cement pore water, meaning $C_0 \equiv 0$, and the following diffusion equation has to be solved:

$$\frac{\partial C}{\partial t} = \frac{D}{R}\frac{\partial^2 C}{\partial x^2} = \frac{D_e}{\alpha}\frac{\partial^2 C}{\partial x^2} \quad . \tag{3.3.4}$$

The corresponding boundary conditions are:

$$C(0,t) = C(L,t) = 0 \quad ; t > 0 \quad , \tag{3.3.5}$$

and the initial condition, as already mentioned, is:

$$C(x,0) = C_0\left(1 - \frac{x}{L}\right) \quad ; \; t \le 0 \quad . \tag{3.3.6}$$

To obtain a solution we consider the Fourier sine (Fourier cosine) transformed of *C(x,t):*

$$F_S(C) = \int_0^L C(x,t)\sin\left(n\pi\frac{x}{L}\right)dx \quad , \tag{3.3.7}$$

$$F_C(C) = \int_0^L C(x,t)\cos\left(n\pi\frac{x}{L}\right)dx \quad . \tag{3.3.8}$$

Taking into account the boundary conditions we get for the partial derivatives:

a) $$\int_0^L \frac{\partial C(x,t)}{\partial t}\sin\left(n\pi\frac{x}{L}\right)dx = \frac{\partial}{\partial t}\int_0^L C(x,t)\sin\left(n\pi\frac{x}{L}\right)dx = \frac{\partial}{\partial t}F_s\{C\} = \frac{\partial \tilde{C}}{\partial t} \quad , \tag{3.3.9}$$

$$\int_0^L \frac{\partial C(x,t)}{\partial x}\sin\left(n\pi\frac{x}{L}\right)dx = -\frac{n\pi}{L}\int_0^L C(x,t)\cos\left(n\pi\frac{x}{L}\right)dx = -\left(\frac{n\pi}{L}\right)F_C(C) \quad , \tag{3.3.10}$$

and

b) $$\int_0^L \frac{\partial^2 C(x,t)}{\partial x^2} sin\left(n\pi\frac{x}{L}\right) d\,x = \frac{\partial C(x,t)}{\partial x} sin\left(n\pi\frac{x}{L}\right)\Bigg|_0^L - \frac{n\pi}{L}\int_0^L \frac{\partial C}{\partial x} cos\left(n\pi\frac{x}{L}\right) d\,x$$

$$= -\left(\frac{n\pi}{L}\right)^2 F_s\{C\} - \left(\frac{n\pi}{L}\right)\left[C(L,t) - C(0,t)\right] = -\left(\frac{n\pi}{L}\right)^2 \tilde{C} \quad .$$

(3.3.11)

In the Fourier domain for the partial differential equation (3.3.4) we get

$$\frac{\partial \tilde{C}}{\partial t} = -\left(\frac{n\pi}{L}\right)^2 \frac{D_e}{\alpha}\tilde{C} \quad . \tag{3.3.12}$$

The solution of this ordinary differential equation is:

$$\tilde{C} = \lambda \exp\left(-\left(\frac{n\pi}{L}\right)^2 \frac{D_e}{\alpha} t\right) \quad , \tag{3.3.13}$$

with an integration constant λ which has to be fixed with the help of the initial condition. Therefore we also have to Fourier-sine transform (3.3.6)

$$\int_0^L C_0\left(1-\frac{x}{L}\right) sin\left(n\pi\frac{x}{L}\right) dx = C_0\frac{L}{n\pi} \quad , \tag{3.3.14}$$

hence equation (3.3.13) becomes:

$$\tilde{C} = C_0 \frac{L}{n\pi} e^{-\left(\frac{n\pi}{L}\right)^2 \frac{D_e}{\alpha} t} \quad . \tag{3.3.15}$$

The inverse transformation of equation (3.3.15) yields the requested solution for the tracer concentration in the pore water within the HCP sample:

$$C(x,t) = 2C_0 \sum_{n=0}^{\infty} \frac{1}{n\pi} e^{-\left(\frac{n\pi}{L}\right)^2 \frac{D_e}{\alpha} t} \sin\left(n\pi\frac{x}{L}\right) \quad [24]. \tag{3.3.16}$$

[24] For t = 0 the initial condition is obtained ($\sum_{n=0}^{\infty}\frac{1}{n}\sin(ny) = \frac{(\pi - y)}{2}$; $y = \pi\frac{x}{L}$), and for x = 0, L the boundary conditions are fulfilled.

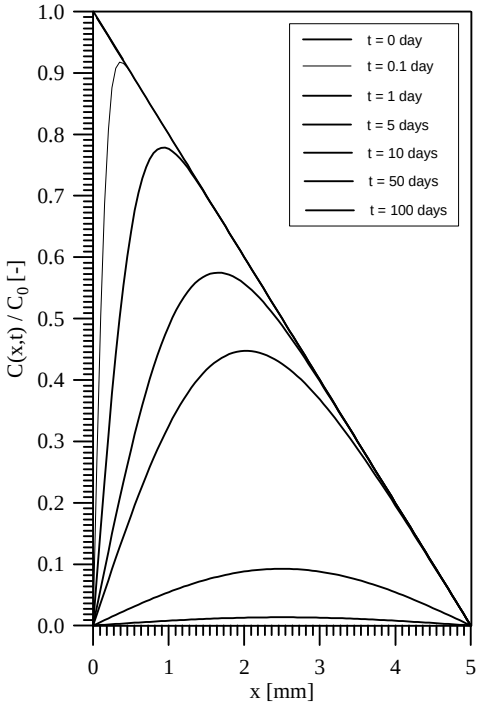

Figure 3.3.-2: Normalised nickel concentration profiles in the pore water across a disk-like cementitious sample considered to be a homogeneous and isotropic porous medium at different times $t_0 < t_1 < t_2 < \ldots$ as indicated in the legend. Starting with a linear concentration profile according to equation (3.3.6) the distribution rapidly decreases and becomes symmetrical. Parameter values used for the calculations are those from the best-fit of nickel through-diffusion experiment no. 7 using a linear isotherm.

As can be seen in the figure, at x = 5 mm the slope is nearly constant for some ten days. Hence, the diffusive flux, which is proportional to the value of the slope, should not change much in this time span. After this period, due to the symmetric tracer profile within the sample, the diffusive flux at x = 0 mm should asymptotically approach that at x = 5 mm.

Because the spatial derivative of equation (3.3.16) is proportional to the flux, we obtain

$$\frac{\partial C(x,t)}{\partial x} = 2C_0 \frac{1}{L} \sum_{n=0}^{\infty} e^{-\left(\frac{n\pi}{L}\right)^2 \frac{D_e}{\alpha} t} \cos\left(n\pi \frac{x}{L}\right) \quad . \tag{3.3.17}$$

Therefore, the absolute value of the diffusive flux at both boundaries is given by:

at x = 0: $$j(0,t) = 2C_0 \frac{D_e}{L} \sum_{n=0}^{\infty} e^{-\left(\frac{n\pi}{L}\right)^2 \frac{D_e}{\alpha} t} = 2 j_L \sum_{n=0}^{\infty} e^{-\left(\frac{n\pi}{L}\right)^2 \frac{D_e}{\alpha} t} \quad , \tag{3.3.18}$$

and at $x = L$: $$j(L,t) = 2C_0 \frac{D_e}{L} \sum_{n=0}^{\infty} (-)^n e^{-\left(\frac{n\pi}{L}\right)^2 \frac{D_e}{\alpha} t} = 2 j_L \sum_{n=0}^{\infty} (-)^n e^{-\left(\frac{n\pi}{L}\right)^2 \frac{D_e}{\alpha} t} \quad [25] \, . \tag{3.3.19}$$

At the beginning, at $t \to 0$, the flux at x = 0 is infinitely large, and at $x = L$ it is equal to j_L. In the limit $t \to \infty$ the ratio of these two fluxes becomes

$$\lim_{t \to \infty} \frac{j(0,t)}{j(L,t)} = -1 \quad . \tag{3.3.20}$$

[25] It holds: $\lim_{x \to 0} \sum_{n=0}^{\infty} (-)^n \exp(-n^2 x) = \frac{1}{2}$ and $\sum_{n=0}^{\infty} (-)^n \exp(-n^2) \cong 0.6503129$.

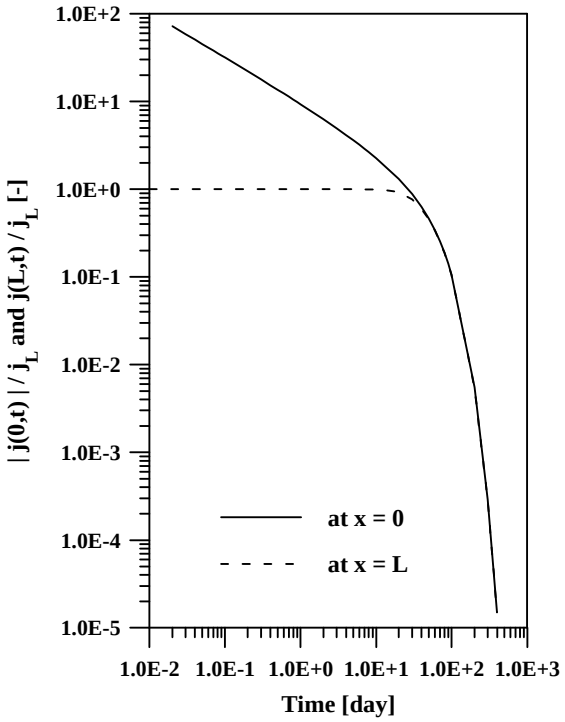

Figure 3.3.-3: The normalised fluxes $|j(0,t)|/j_L$ and $j(L,t)/j_L$ as a function of time. j_L is the steady-state flux at $x = L$ of the preceding through-diffusion phase (for the plot we used the best-fit values for D_e and K_d from inverse modelling the nickel through-diffusion experiment no. 5).

The amount of mass $m(x,t)$ which has (out-)diffused within the sample at position x is:

$$m(x,t) = F \cdot \int_0^t j(x,t')\,dt' = 2C_0\,\alpha F L \sum_{n=0}^{\infty} \frac{1}{n^2\pi^2} \cos\left(n\pi\frac{x}{L}\right)\left[1 - e^{-\left(\frac{n\pi}{L}\right)^2 \frac{D_e}{\alpha} t}\right] \quad , \qquad (3.3.21)$$

where F [m^2] is the cross-sectional area of the HCP accessible for diffusion. At the boundaries we get at $x = 0$:

$$m(0,t) = 2C_0\,\alpha F L\left[\frac{1}{6} - \sum_{n=0}^{\infty} \frac{1}{n^2\pi^2} e^{-\left(\frac{n\pi}{L}\right)^2 \frac{D_e}{\alpha} t}\right] \quad , \qquad (3.3.22)$$

and at $x = L$:

$$m(L,t) = 2C_0\,\alpha F L\left[\frac{1}{12} + \sum_{n=0}^{\infty} \frac{(-)^n}{n^2\pi^2} e^{-\left(\frac{n\pi}{L}\right)^2 \frac{D_e}{\alpha} t}\right] \quad . \qquad (3.3.23)$$

In the limit $t \to \infty$ the amount of diffused tracer becomes:

at $x = 0$: $$m(0, t \to \infty) = \alpha \frac{C_0 F L}{3} \quad , \qquad (3.3.24)$$

and at $x = L$: $$m(L, t \to \infty) = \alpha \frac{C_0 F L}{6} \quad , \qquad (3.3.25)$$

and hence, for the ratio we obtain:

$$\lim_{t\to\infty} \frac{m(0,t)}{m(L,t)} = 2 \quad , \qquad (3.3.26)$$

meaning that in the asymptotic time limit 2 /3 of the total out-diffused mass pass the sample's boundary at $x = 0$ and 1 / 3 that at $x = L$. The total tracer mass in the HCP at the beginning of the out-diffusion experiment is

$$m_{tot} = F \int_0^L \left[\varepsilon C(x) + (1-\varepsilon)\rho S(x)\right] d\,x = F\,L\,\frac{C_0}{2}\alpha \quad . \tag{3.3.27}$$

Using the best-fit parameter values for D_e and K_d obtained by inverse-modelling of the nickel through-diffusion experiments no. 5 and 7 which are compiled for completeness in the table below, the diffusive fluxes across both boundaries according to equations (3.3.18) and (3.3.19) are calculated.

Parameter	**Unit**	**Experiment no. 5**	**Experiment no. 7**
$K_d \cdot 10^3$	[m^3/kg]	36.5	24.2
α	[-]	29.0	19.4
$D_e \cdot 10^{11}$	[m^2/s]	2.52	2.20
$D_a \cdot 10^{13}$	[m^2/s]	8.69	11.3

Table 3.3.-1: Best-fit parameter values for K_d and D_e obtained from inverse modelling of the nickel through-diffusion experiments no. 5 and 7. For comparison purposes also the values for the rock capacity factor α and the apparent diffusion coefficient D_a are listed.

In the next figure the predictions together with the measurements are plotted.

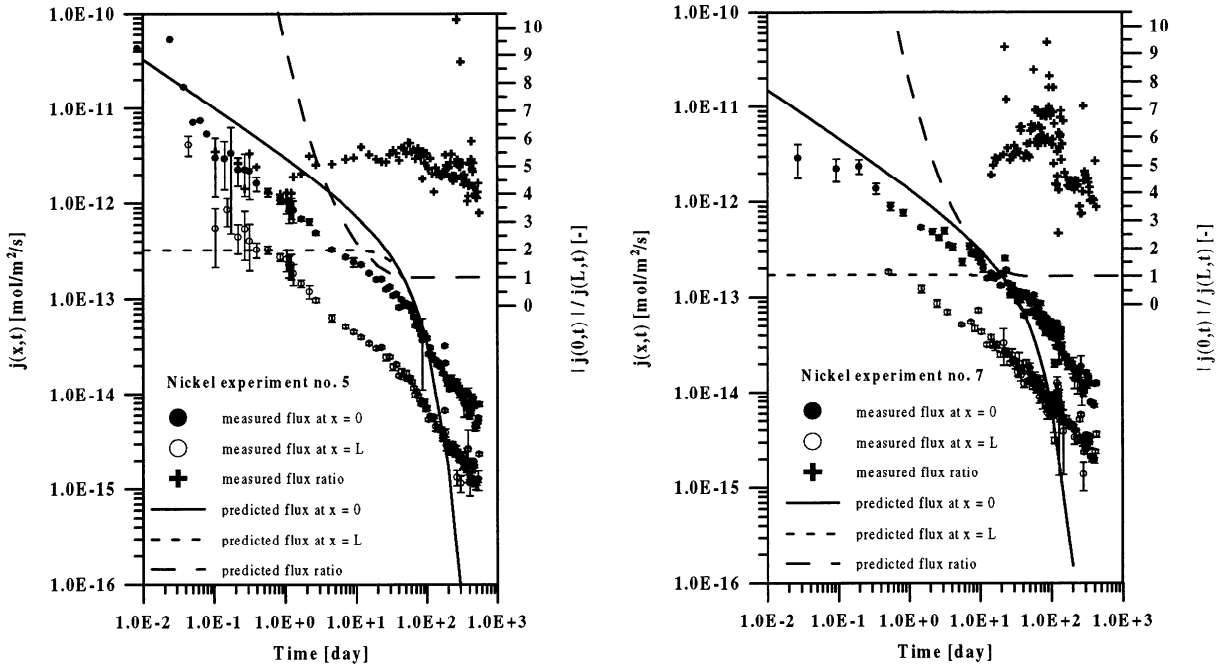

Figure 3.3.-4: Plots of the predicted diffusive fluxes across both boundaries and measurements versus time for both nickel out-diffusion experiments no. 5 (left plot) and 7 (right plot). The solid lines represent the calculated flux at $x = 0$; its corresponding measurements are the filled circles. The dashed lines are $j(L,t)$ and the corresponding measurements are the open circles. In both figures in the right upper corner there is a dashed line predicting the ratio $|j(0,t)| / j(L,t)$ as a function of time (the associated axis is the right one). In the asymptotic limit this relationship should approach unity; the experimental data are represented by crosses.

Both predictions show similar differences to the measurements: Both calculations obtained too high a flux at $x = 0$, a possible indication of a systematic error such as, e.g., too low K_d-values. However, when considering the marked differences between predictions and measurements at the second boundary at $x = L$, the essential deficiencies of the model become evident. Whereas the concept predicts a nearly constant flux for about 20 (for experiment no. 5) and 10 days (for experiment no. 7), the measurements decrease immediately after the start of the out-diffusion. The measured ratio of the fluxes is of the order of 3 to 10 with a trend towards values of about 5. However, the model predicts a fast decrease of the flux ratio within a time span of about 10 days to a value close to unity, but the measurements are larger mostly by a factor of about five. For experiment no. 5 we can observe a clear trend; for experiment no. 7, however, this is not the case. We consider this difference an even stronger indication than the discrepancies between measurements and predicted flux that the basic assumption of a linear, decreasing tracer profile across the cementitious sample due to steady-state diffusion in a homogeneous and isotropic porous medium must be wrong. To study the influence of the K_d-value chosen, two additional calculations for experiment no. 5 were performed with the K_d-value either roughly five times larger than the reference case or equal to zero (see the following figure).

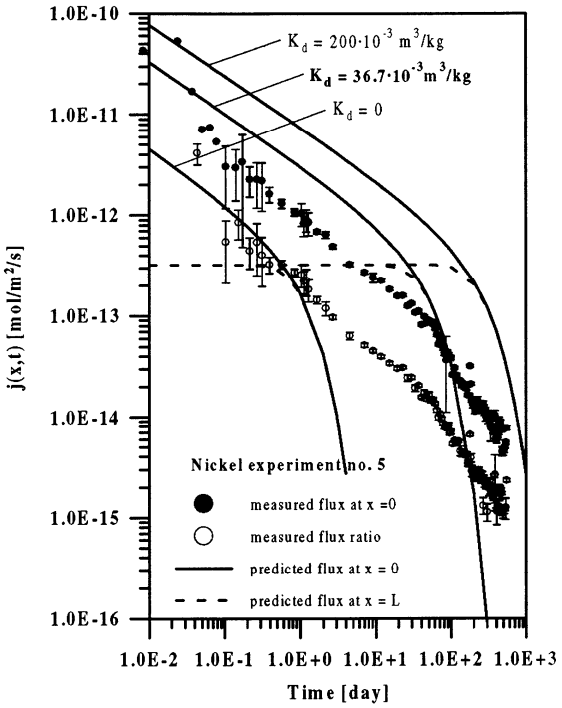

Figure 3.3.-5: Effects of K_d -variation on the flux profiles for the nickel out-diffusion experiment no. 5. The middle K_d-value corresponds to the best-fit value obtained from modelling the through-diffusion experiment no. 5. The other two K_d -values are either by a factor of - roughly - 5 larger or equal to zero as indicated in the figure.
A K_d-value of 0.2 m^3/kg yields a rock capacity factor α of about 156 and an apparent diffusion coefficient D_a of about $0.161 \cdot 10^{-12}$ m^2/s. The corresponding values for $K_d = 36.7 \cdot 10^{-3}$ m^3/kg are: $\alpha = 29.1$ and $D_a = 0.866 \cdot 10^{-12}$ m^2/s; for $K_d = 0$ these values are: $\alpha = 0.63$ (this is equal to the sample's porosity) and $D_a = D_p = 40.0 \cdot 10^{-12}$ m^2/s.

While a smaller K_d-value than that of the best-fit would improve the agreement between modelled flux across the primary boundary at $x = 0$ for a few days only, the predicted decay of the flux profile would start much too early in complete contradiction to the observations. Moreover, at the secondary boundary at $x = L$ the measured time history of the diffusive flux cannot be modelled by any K_d-value.

On the next page a figure shows the prediction for the total diffused masses according to equations (3.3.22) and (3.3.23) together with measurements. In this figure as well the deficiencies of the model become obvious.
In the asymptotic limit the ratio of the diffused masses should approach two. However, both experiments show values of about five, in strong contradiction to the model's prediction. In the figures we can see again the smoothing influence of $m(t)$ which is a cumulative quantity indicating that the value of a single measurement is dependent on the preceding ones.

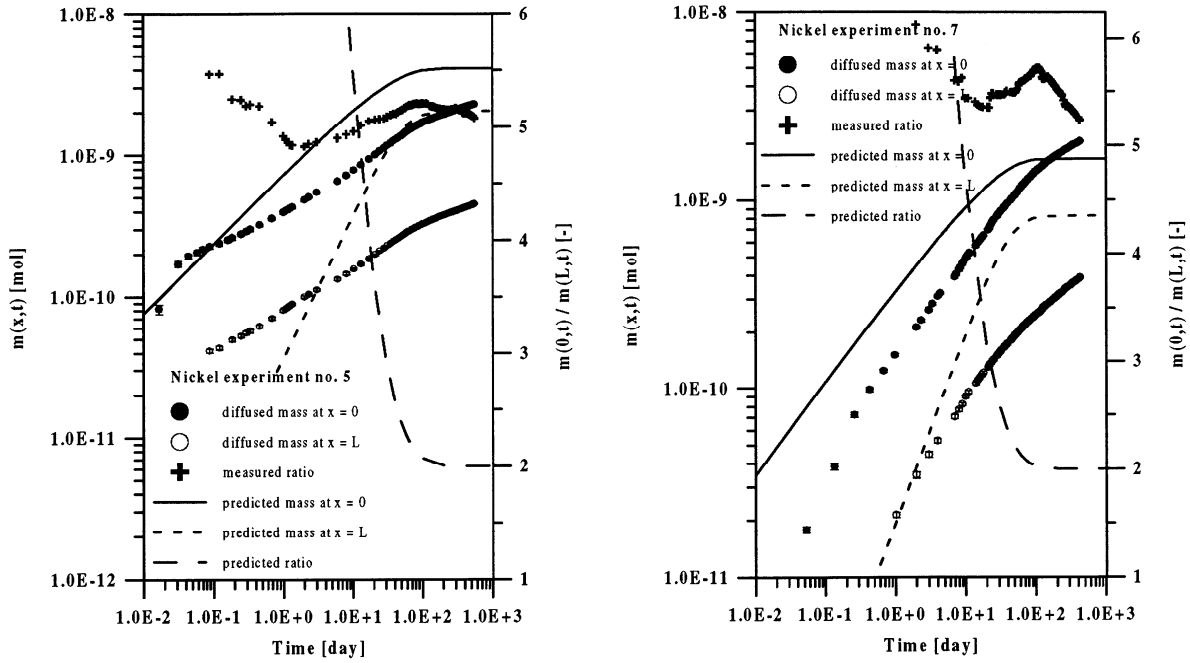

Figure 3.3.-6: Predictions of the total diffused masses versus time and measurements for nickel out-diffusion (experiment no. 5 left and experiment no. 7 right plot). The solid lines represent the calculated total mass which should diffuse across the boundary at $x = 0$, the corresponding measurements are those drawn by filled circles. The dashed lines represent the calculated total diffused mass across the boundary at $x = L = 5$ mm; the corresponding measurements are drawn by the open circles. In the upper part of the figures the calculated ratio $m(0,t) / m(L,t)$ is plotted (the associated axis is the right one); the measured values are represented by crosses.

When the out-diffusion experiment no. 5 was terminated after about 556 days only 45 % of the predicted total nickel had diffused out. For experiment no. 7 this value is 98 % after about 424 days of measurements. The explanation for this marked difference between the two experiments is unknown.

Conclusions

Based on a simple model for diffusion of a tracer out of a disk-like cementitious specimen with high porosity and using the best-fit parameter values for D_e and K_d obtained from inverse modelling of two through-diffusion experiments, the time-history of the diffusive fluxes at both boundaries was predicted. However, the experimental data contradict the concept. In both cases neither their predicted shapes nor their absolute values correspond to the measurements. Especially the predicted ratio of the fluxes $|j(0,t)|/j(L,t)$ which should approach unity after about 10 (20) days is strongly violated. In the previous sensitivity analysis it was shown that no K_d-value is able to save the concept. Hence, we cannot avoid concluding that the underlying assumption of an initial linearly decreasing tracer concentration profile across the sample must be wrong; this being the basic assumption for the model of a homogeneous specimen - the sample has to be considered inhomogeneous.

4. Conclusions and recommendations for future work

Ten through-diffusion and two out-diffusion experiments were performed using four different radiotracers. The experiments went on from two to three months up to three years. Their subsequent modelling was done based on the assumption that the samples were homogeneous, and isotropic and with time-invariant transport properties. We started with the most simple diffusion concept where sorption was completely neglected and proceeded then to more sophisticated models where sorption was either included as linear or non-linear (Freundlich) isotherm or - finally - where first-order sorption kinetics were considered. Some of the models yielded fairly good reproductions of the measured breakthrough curves but - as a rule - with values for the sorption isotherm parameters which were either unphysical or not consistent with measurements from batch sorption experiments. This fact, and mass balance considerations, clearly revealed the deficiencies of all models for all tracers used. Therefore the only reasonable conclusion which can be drawn from the modelling is that the nuclide/cement interaction being involved in through- and out-diffusion experiments cannot be described by a relatively simple diffusion/sorption model for a homogeneous and isotropic porous medium with time-independent properties.
In the following compilation we have summarised our knowledge, conclusions and recommendations for forthcoming work.

- The results of the modelling work clearly demonstrate that the nuclide/cement interaction in major aspects cannot be described correctly when using a relatively simple diffusion/sorption model. None of the concepts, even when including non-linear sorption or first-order sorption kinetics, were able to fit the measurements reasonably well, to yield best-fit parameter values which were consistent with independent measurements; and to account correctly for the tracer mass deposited in the specimen. This failure of the models leads to considerable uncertainty as to which K_d-values should be used in safety assessments. Should these be the much higher values originating from batch sorption experiments which - considering the results of the present study - cannot be considered conservative; or should they be the lower values from the through-diffusion experiments? The study clearly showed that major aspects of the diffusion/deposition process are not understood at all. **Hence, the simple diffusion/sorption model is partially incorrect. If such a model is applied in safety assessments, a careful choice of parameters is thus required, taking these findings into account.**
- It is very common to fit through-diffusion experiments with the help of the backward extrapolation of the breakthrough curve to obtain values for the diffusion coefficient and for the K_d-value of the linear sorption isotherm. Normally, the time history of the accumulated mass $m(t)$, which is the integrated flux across the down-stream boundary, is fitted. Hence, each data point $m_i(t)$ has an accumulated error of all preceding measurements covering finer details of the breakthrough curve. However, we have shown that such a procedure may lead to wrong results and conclusions, e.g. to the erroneous idea that a diffusion experiment has reached steady-state whereas it is still slowly evolving. Moreover, the good quality of such fits might tempt scientists to feel that the nuclide/cement interaction is fairly well described by a simple diffusion/sorption model, but by taking further information into account the inadequacy of such a model becomes obvious. Therefore we strongly recommend to also consider the results from batch-sorption experiments as well as those from mass balance considerations. A further sensitive test for a concept would be the data acquired from out-diffusion experiments. **An appropriate and comprehensive model must be able to account**

correctly for <u>all</u> observations concerning tracer transport through cementitious material!

- One measurement is no measurement, and even two experiments do not sufficiently reduce the statistical uncertainties. For this purpose series of equal experiments should always be performed, even if this requires a much larger effort.
  In our study two or four experiments were performed for each tracer under more or less the same experimental conditions. It turned out, that they often show significant differences in the breakthrough curves and in the extracted best-fit parameter values. In such a case it is extremely difficult for a modeller to arrive at reasonable conclusions. For example, to reduce differences in the experimental set-up, a series of experiments should be based on the same reservoir concentration to guarantee the same up-stream boundary condition. For our experiments the reservoir size was too small by half a litre so that periodically the reservoir concentration had to be adjusted, a procedure which can be easily the source of serious experimental errors. For illustration purposes we refer the reader to sub-chapter 2.1.5. on page 39ff where our experiences adjusting a traced nickel solution due to nickel up-take by the equipment for a blank-measurement are documented. Therefore in new experiments the reservoir volume should be so large that no further adjustments within months would be necessary. With our equipment this could be done with an additional large cavity for the traced solution but - of course - still inside the glove box.
  Blank-value measurements still seem to be unusual in our working field. It should be self-evident that parameter values obtained in experiments without blank-values are nearly worthless. Blank-value measurements shouldn't be done - whenever it is possible - in independent experiments because they show other (unknown) systematic errors. Hence, blank-value measurements should always be part of the real measurements, i.e. under the same conditions as the real experiment and performed in the same equipment. In through-diffusion experiments this could be done with the help of two small platelets of the same material as used for the diffusion cell with a controlled and predefined surface area. Such reference platelets should be inserted on both sides of the diffusion barrier and the activity should be periodically monitored to obtain information on up-taken or released tracer by the equipment's material as a function of time and tracer concentration.

- Especially for chlorine, iodine and caesium it would have been valuable to have undertaken the experiments for longer time in order to investigate carefully whether the experiments had achieved steady-state. In these experiments the diffusive flux and/or the values for the deposited tracer mass in the HCP were still slowly evolving when the experiments were terminated. However, the deviations from steady-state were sometimes only modest and allowed nevertheless to draw reasonable conclusions. The continuous evaluation of the experiments (and <u>not</u> a post-mortem analysis) only allows to estimate the time-span required to reach indeed a near steady-state.

- Our methodology to first do experiments using a conservative tracer such as caesium was correct. However, this should have been checked prior to the through-diffusion experiments with the help of batch-sorption experiments. In a first modelling exercise only the tracer breakthrough curves were analysed, neglecting mass balance considerations along with further experimental aspects of minor priority. Above, we have shown how such a procedure may lead to wrong conclusions. Later on we proceeded with experiments using the much more complex interacting nickel as tracer, a decision which turned out to be wrong. Based on the results and conclusions of our modelling study, we strongly recommend some of the through-diffusion experiments be carefully repeated using really conservative tracers first such as

tritiated water, helium, uranine and caesium. Whether they can indeed be considered to be conservative tracers has to be checked in additional batch sorption experiments prior to the diffusion experiments. If the modelling of the through-diffusion experiments were successful one could then proceed with moderately sorbing tracers etc.

- Activity measurements using a beta-counter are complicated, time-consuming and susceptible to errors. Whenever possible tracers should be used showing γ-lines which can be measured on-line. Of course, the measurement equipment should be calibrated periodically.
- So far the only diffusion experiments carried out were on cementitious specimens in the first degradation phase where the alkalis are still released, hence at high pH. To obtain a comprehensive understanding of all the processes involved, further experiments should be performed also using altered cementitious material in the second and third degradation phase. By varying the porosity of the samples, further information on the geometry factor, hence on constrictivity and tortuosity of the transport pathways, could be gained.
- The processes for reversible or irreversible tracer up-take may show hysteresis meaning that the sorption characteristics may not be the same as for desorption. Such effects could be studied thoroughly in a series of experiments where a through-diffusion phase is followed by an out-diffusion phase etc.
- By varying the sample's thickness further information concerning homogeneity of the specimens and the representative elementary volume (REV) could be obtained.
- So far all disk-like specimens were cut perpendicular to the axes of the cylindrically formed cementitious material. One of the basic assumptions of the study was that the sample's transport properties were considered to be isotropic. However, such an assumption can be questioned, and to study the effects of a possible anisotropy such samples for further diffusion experiments should also be cut in other directions from the cylindrical form.
- There is experimental evidence that the nickel solution is not stable above 10^{-9} M [28]. In new experiments with nickel as tracer the reservoir concentration should therefore be well below such a limit.

For the modelling several different starting points can be considered.

- In the present study all transport parameters are constant in time and space. From previous investigations it is evident that the coefficient for diffusion may not only depend on the temperature but also on the concentration of the components [47]. However, it is an open question whether a concentration-dependent diffusion coefficient can resolve the problems because the tracer concentration is always very low so that effects like ion exclusion in constrictive transport pathways presumably play a negligible role.

- Idemitsu et al. [48] modelled tracer migration in very similar experiments using a double porosity medium concept. The authors considered one possible diffusion pathway to be a fissure with a width of a few microns and with a relatively high diffusion coefficient and a network of submicron pores with a much lower diffusion coefficient where the tracer could penetrate. Due to this additional sink of the porous cement matrix such a model accounts for an increased tracer deposition and results in a much longer transient phase in the breakthrough curve. Until steady-state the penetration profile across the sample would be composed of two parts: a steep slope near the surface on the reservoir side and a gradual slope in the deeper part of the specimen. By slicing the samples and analysing the tracer distribution the basic assumption concerning two different porosities of such a model could be tested.
- With the help of a code such as MCOTAC [49] where transport is coupled to speciation further investigations could be done. This model couples chemical equilibrium, complexation and precipitation/dissolution reactions in porous media and allows the study of the effects of precipitation of secondary phases on the diffusion process, provided that a detailed speciation of the traced solution and the solid phase is available.
- Finally we emphasise that any model development makes sense only if further experimental facts concerning mechanisms involved and tracer distribution in the solid phase become available. We have already mentioned that - to our understanding - in order to perform new and better experiments it is vital to first use real conservative tracers. Having a model which correctly accounts for all the observations, one could then proceed to more complex reacting tracers. Such investigations should consist not only of the breakthrough curves of through-diffusion experiments but should also cover at least:
    - batch sorption experiments to yield information on sorption and desorption,
    - careful mass-balance considerations which are a sensitive test for any model,
    - tracer distribution across the samples to provide information concerning possible alternative transport pathways and/or on the precipitation of secondary phases,
    - out-diffusion experiments which are considered to be a crucial test of the predictive quality of a given model.

Appendix: The analytical solution of the diffusion equation with linear sorption

The partial differential equation to be solved for diffusion and neglecting radioactive decay at all, is of the form:

$$\frac{\partial C}{\partial t} = \frac{D}{R}\frac{\partial^2 C}{\partial x^2} \quad , \tag{A1.1}$$

in the region $0 \le x \le L$. C [mol/m^3] is the tracer concentration in the mobile phase, t [s] means time, x [m] represents the spatial co-ordinate, D [m^2/s] is the diffusion constant, and R [-] is the linear sorption retardation constant. (The only reason for introducing the latter constants in (A1.1) is for the sake of consistency with the formalism developed in chapter 3.)
The initial condition is

$$C(x,t) = 0 \quad ;\forall x; \quad t \le 0 \quad , \tag{A1.2}$$

and the boundary conditions are:

at x = 0: $$C(0,t) = C_0\left[1-\Theta(t-T_L)\right] \quad ;t>0 \quad , \tag{A1.3}$$

and at $x = L$: $$C(L,t) = 0 \qquad ;t>0 \quad ; \tag{A1.4}$$

where $$\Theta(z) = \begin{cases} 0 & ;z \le 0 \\ 1 & ;z > 0 \end{cases} \tag{A1.5}$$

is the Heaviside step function. Here, the Heaviside step function is introduced to obtain a slightly more general solution of the diffusion problem; the consequences in the solution for a restricted transport problem with a constant boundary condition at x = 0 will be obvious. This step-function effect is to change the concentration boundary condition non-continuously from a finite value C_0 [mol/m^3] to a zero value at time $t = T_L$ [s], the tracer release time.

In the Laplace domain equation (A1.1) is given by

$$-\overline{C}(x,0) + p\overline{C}(x,p) = \frac{D}{R}\frac{\partial^2 \overline{C}(x,p)}{\partial x^2} \quad , \tag{A1.6}$$

and taking into account the initial condition it yields:

$$\frac{D}{R}\frac{\partial^2 \overline{C}(x,p)}{\partial x^2} - p\overline{C}(x,p) = 0 \quad . \tag{A1.7}$$

To solve this equation the following ansatz is made:

$$\overline{C}(x,p) = \alpha(p)e^{\gamma(p)x} + \beta(p)e^{-\gamma(p)x} \quad . \tag{A1.8}$$

The second derivative of (A1.8) and the function itself inserted into (A1.7) for $\gamma(p)$ yield:

$$\gamma_{1,2}(p) = \pm\sqrt{\frac{R}{D}p} \quad . \tag{A1.9}$$

To determine $\alpha(p)$ and $\beta(p)$ we make use of both boundary conditions. Therefore we have to Laplace-transform the boundary condition at x = 0:

$$\boldsymbol{L}\left\{C(0,t),t>0\right\}=\boldsymbol{L}\left\{C_0\left[1-\Theta(t-T_L)\right]\right\}=\boldsymbol{L}\left\{C_0\right\}-\boldsymbol{L}\left\{C_0\,\Theta(t-T_L)\right\}$$
$$=\frac{C_0}{p}-\frac{C_0}{p}e^{-pT_L}=\frac{C_0}{p}\left(1-e^{-pT_L}\right)\quad . \tag{A1.10}$$

After some straightforward algebra for $\alpha(p)$ and $\beta(p)$ we get:

$$\alpha(p)=-\frac{C_0}{p}\left(1-e^{-pT_L}\right)\frac{e^{-\gamma(p)L}}{e^{\gamma(p)L}-e^{-\gamma(p)L}}, \tag{A1.11}$$

$$\beta(p)=\frac{C_0}{p}\left(1-e^{-pT_L}\right)\frac{e^{\gamma(p)L}}{e^{\gamma(p)L}-e^{-\gamma(p)L}}\quad . \tag{A1.12}$$

Therefore for the solution of the transport problem in the Laplace domain we get the following expression:

$$\overline{C}(x,p)=\frac{C_0}{p}\left(1-e^{-pT_L}\right)\frac{sinh[\gamma(p)(L-x)]}{sinh[\gamma(p)L]}\quad , \tag{A1.13}$$

the solution $C(x,t)$ being obtained with the help of the inverse Laplace transformation of (A1.13) [50]:

$$\frac{C(x,t)}{C_0}=\left[1-\frac{x}{L}-\frac{2}{\pi}\sum_{n=1}^{\infty}\frac{1}{n}e^{-n^2\pi^2\frac{D}{L^2R}t}\sin\left(n\pi\frac{x}{L}\right)\right]-\Theta(t-T_L)\left[1-\frac{x}{L}-\frac{2}{\pi}\sum_{n=1}^{\infty}\frac{1}{n}e^{-n^2\pi^2\frac{D}{L^2R}(t-T_L)}\sin\left(n\pi\frac{x}{L}\right)\right]. \tag{A1.14}$$

The first part of equation (A1.14) is the solution for a constant tracer input only; the second part represents the response of the change in the boundary condition , (A1.3) at $t=T_L$.

.

Acknowledgements

We would like to thank all colleagues from the waste management laboratory (LES) for their interest in these investigations and helpful discussions. Special thanks to F.J. Pearson, Jr. for careful review of the manuscript and valuable comments, and B. Baeyens, E. Curti and C. Poinssot for the translations of the abstract. This report was externally reviewed by AEA Technology plc (U.K.). These helpful comments and suggestions have improved the quality of the report considerably. Partial financial support by NAGRA is gratefully acknowledged.

References

[1] **Atkinson, A., Nickerson, A.K.:** "Diffusion and sorption of cesium, strontium, and iodine in water-saturated cement", Nuclear Technology, 81 (1988), 100-113.

[2] **Johnston, H.M., Wilmot, D.J.:** "Sorption and diffusion studies in cementitious grouts", Waste Management, 12 (1992), 289-297.

[3] **Albinsson, Y., Andersson, K., Börjesson, S., Allard, B.:** "Diffusion of radionuclides in concrete and concrete/bentonite systems", in: Fourth International Conference on the Chemistry and Migration Behaviour of Actinides and Fission Products in the Geosphere. Charleston, SC, USA, December 12-17, 1993, 485-491 (1994), R. Oldenbourg Verlag, München, 1994., and Journal of Contaminant Hydrology, 21 (1996), 189 - 200.

[4] **Döhring, L., Görlich, W., Rüttener, S., Schwerzmann, R.:** "Herstellung von homogenen Zementsteinen mit hoher hydraulischer Permeabilität", NAGRA unpublished report, NAGRA, Wettingen, Switzerland, 1994.

[5] **Pandolfo, P., Sarott, F.-A., Spieler, P.:** "Apparatur zur künstlichen Alterung und zur Bestimmung der hydraulischen Leitfähigkeit von Zementstein", PSI-internal report, TM-44-95-02, Villigen, Switzerland, 1995.

[6] **Sarott F.-A., Bradbury, M.H., Pandolfo, P., Spieler, P.:** "Diffusion and adsorption studies on hardened cement paste and the effect of carbonation on diffusion rates", Cement and Concrete Research, 22 (1992), 439-444.

[7] **Sarott, F.-A., Spieler, P., Jakob, A.:** "Diffusion and sorption on hardened cement pastes - I. general description of the experiments", PSI-internal report, TM-44-96-04, Villigen, Switzerland, 1996.

[8] **Sarott, F.-A., Spieler, P., Jakob, A.:** "Diffusion and sorption on hardened cement pastes - II. chloride through-diffusion", PSI-internal report, TM-44-96-05, Villigen, Switzerland, 1996.

[9] **Sarott, F.-A., Spieler, P., Jakob, A.:** "Diffusion and sorption on hardened cement pastes - III. iodide through-diffusion", PSI-internal report, TM-44-96-06, Villigen, Switzerland, 1996.

[10] **Sarott, F.-A., Spieler, P., Jakob, A.:** "Diffusion and sorption on hardened cement pastes - IV. cesium through-diffusion", PSI-internal report, TM-44-96-07, Villigen, Switzerland, 1996.

[11] **Sarott, F.-A., Spieler, P., Jakob, A.:** "Diffusion and sorption on hardened cement pastes - V. nickel through-diffusion", PSI-internal report, TM-44-96-08, Villigen, Switzerland, 1996.

[12] **Sarott, F.-A., Spieler, P., Jakob, A.:** "Diffusion and sorption on hardened cement pastes - VI. nickel out-diffusion", PSI-internal report, TM-44-96-09, Villigen, Switzerland, 1996.

[13] **Sarott, F.-A.: "**Artificial ageing of hardened cement pastes - compilation of experimental data", Paul Scherrer Institute PSI, (private communication).

[14] **Berner, U.:** Paul Scherrer Institute PSI, (private communication).

[15] **Van Loon, L.R., Glaus, M.A.:** "Experimental and theoretical studies on alkaline degradation of cellulose and its impact on the sorption of radionuclides", PSI-Bericht Nr. 98-07, Villigen, Switzerland, 1998 and NAGRA-Technical Report NTB-97-04, Wettingen, Switzerland, 1998.

[16] **Wieland, E., Tits, J., Spieler, P., Dobler, J.P.:** "Interaction of Eu(III) and Th(IV) with sulphate-resisting Portland cement", Mat. Res. Soc. Symp. Proc., Vol. 506 (1998), 573 - 578.

[17] **Sarott, F.-A.:** "Die Sorption von Chlor, Jod, Nickel und Americium an gemörsertem Zementstein (Batch-Sorption)", PSI-internal report, TM-44-96-13, Villigen, Switzerland, 1996.

[18] **Skagius, K., Neretnieks, I.:** "Measurements of cesium and strontium diffusion in biotite gneiss", SKB Technical Report TR 85-15, Stockholm, Sweden, 1985.

[19] **Bradbury, M.H., Green, A., Lever, D., Stephen, I.G.:** "Diffusion and permeability based sorption measurements in sandstone, anhydrite and upper magnesian limestone samples", AERE-11995, Atomic Energy Research Establisment (March 1986).

[20] **Smith, P.A.:** "Modeling of a diffusion-sorption experiment by linear and nonlinear sorption isotherms", Nuclear Technology, 92 (1990), 363-373.

[21] **Salazar, H., Bürki, P.:** "Untersuchung einer Zementprobe Typ CPA 55 HTS (Lafarge, Frankreich)", Projekt-Nr. 2031/66017.547 (Bericht-Nr. MA 88/3601/D), 21. Dezember 1988, Holderbank, CH-5113 Holderbank, Switzerland.

[22] Untersuchungsbericht A-9299-1 des *Labors für Präparation und Methodik* (LPM) vom 25. August 1989. LPM Baustoffprüfinstitut, Tannenweg 1066, CH-5712 Beinwil am See, Switzerland.

[23] **Dewaele, P.J., Reardon E.J., Dayal, R.:** "Permeability and porosity changes associated with cement grout carbonation", Cement and Concrete Research, 21 (1991), 441-454.

[24] **Berner, U.:** "A thermodynamic description of the evolution of pore water chemistry and uranium speciation during the degradation of cement", PSI-Bericht Nr. 62, Paul Scherrer Institute, Villigen, Switzerland, 1990 and NAGRA Technical Report NTB 90-12, NAGRA, Wettingen, Switzerland, 1990.

[25] **Wieland, E.:** Paul Scherrer Institute PSI, (private communication).

[26] **Berner, U.:** Paul Scherrer Institute PSI, (private communication).

[27] **Pearson, F.J., Berner, U.:** "NAGRA thermodynamical data base - I. core data" NAGRA Technischer Bericht NTB 91-17, NAGRA, Wettingen, Switzerland, May 1991 and
Pearson, F.J., Berner, U., Hummel, W.: "NAGRA thermodynamical data base - II. supplemental data 05/92", NAGRA Technischer Bericht NTB 91-18, NAGRA, Wettingen, Switzerland, May 1992.

[28] **Tits, J.**: Paul Scherrer Institute PSI, (private communication, to be published).

[29] **Pilkington, N. J., Stone, N. S.:** "The solubility and sorption of nickel and niobium under high pH conditions", Nirex Report NSS/R186, AEA Technology, Harwell Laboratory, Oxfordshire, OX11 0RA, United Kingdom, 1990.

[30] **Mattigod, S. V., Rai, D., Felmy, A. R., Rao, L.:** "Solubility and solubility product of crystalline $Ni(OH)_2$", Journal of Solution Chemistry, 26, No. 4 (1997), 391 - 403.

[31] **Kaiser, R., Gottschalk, G.:** "Elementare Tests zur Beurteilung von Messdaten", Bibliographisches Institut Mannheim, 1972.

[32] "Bericht zur Langzeitsicherheit des Endlagers SMA am Standort Wellenberg", NAGRA Technischer Bericht NTB 94-06, NAGRA, Wettingen, Switzerland, Juni 1994.

[33] IMSL MATH/- and STAT/LIBRARY, FORTRAN Subroutines for mathematical and statistical applications, Version 1.1 (1989), IMSL Incorporation, Houston, USA.

[34] **Page, C. L., Short, N. R., El Tarras, A.:** "Diffusion of chloride ions in hardened cement pastes", Cement and Concrete Research, 11 (1981), 395 - 406.

[35] **Lambert, P., Page, C. L., Short, N. R.:** "Diffusion of chloride ions in hardened cement pastes containing pure cement minerals", in: The Chemistry and Chemically-Related Properties of Cement, Edited by F. P. Glasser, British Ceramic Proceedings, Shelton, Stoke-on-Trent, No. 35, September 1984, 267 - 276.

[36] **Sposito, G.:** "Derivation of the Freundlich equation for ion exchange reactions in soils", Soil Sci. Soc. Am. J., 44 (1980), 652 - 654.

[37] **Farley, K. J., Dzombak, D. A., Morel, F. M. M.:** "A surface precipitation model for the sorption of cations on metal oxides", Journal of Colloid and Interface Science, 106 (1985), 226 - 242.

[38] **Brown, P. L., Haworth, A., McCrohon, R., Sharland, S. M., Tweed, C. J.:** "Modelling and experimental studies of sorption in the near field of cementitious repository", Mat. Res. Soc. Symp. Proc., Vol. 176 (1990), 591 - 598.

[39] **Atkinson, A., Nickerson, A. K.:** "The diffusion of ions through water-saturated cement", Journal of Materials Science 19 (1984), 3068 - 3078.

[40] **Hietanen, R., Jaakkola, T., Miettinen, J. K.:** "Sorption of cesium, strontium, iodine and carbon in concrete and sand", Mat. Res. Soc. Symp. Proc. Vol. 44 (1985), 891 - 898.

[41] **Andersson, K., Torstenfelt, B., Allard, B.:** "Diffusion of cesium in concrete", in: Scientific basis for nuclear waste management, Moore, J. G. (Editor), Plenum Publ. Corp., New York, Vol. 3 (1981), 235 - 242.

[42] **Atkinson, A., Nelson, K., Valentine, T.M.:** "Leach test characterisation of cement-based nuclear waste forms", Nuclear and Chemical Waste Management, Vol. 6 (1986), 241 - 253.

[43] **Plecaš, I., Peric, A., Kostadinovic, A.:** "The migration of Cs-137 and Co-60 through cementitious barriers applicable to radioactive waste conditioning", Ann. nucl. Energy, Vol. 19 (1992), 507 - 512.

[44] **Krishnamoorthy, T. M., Joshi, S. N., Doshi, G. R.:** "Desorption kinetics of radionuclides fixed in cement matrix", Nuclear Technology, Vol. 104 (1993), 351 - 357.

[45] **Muurinen, A., Rantanen, J., Ovaskainen, R.:** "Diffusivities of cesium and strontium in concretes and in mixtures of sodium bentonite and crushed rock", Mat. Res. Soc. Symp. Proc., Vol. 44 (1985), 883 - 890.

[46] **Rudin, M. J., Landolt, R. R.** in: Roy G. Port (Ed.) - Waste management 90 - Waste Processing, Transportation, Storage and Disposal, Vol. II, p. 125 - 130, Arizona Board of Regents, USA, 1990.

[47] **Matano, C.:** "On the relation between the diffusion-coefficients and concentrations of solid metals (the nickel-copper system)", Japanese Journal of Physics, Vol. 8 (1933), 109 - 113.

[48] **Idemitsu, K., Furuya, H., Tsutsumi, R., Yonezawa, S., Inagaki, Y., Sato, S.:** "Migration of cesium, strontium and cobald in water-saturated concretes", Mat. Res. Soc. Symp. Proc., Vol. 212 (1991), 427 - 432.

[49] **Pfingsten, W.:** "Efficient modeling of reactive transport phenomena by a multispecies random walk coupled to chemical equilibrium", Nuclear Technology, Vol. 116 (1996), 208 - 221.

[50] **Spiegel, M. R.:** "Theory and problems of Laplace transforms", McGraw-Hill Book Company, New York, 1965.